THE

LONDON, EDINBURGH, AND DUBLIN

PHILOSOPHICAL MAGAZINE

AND

JOURNAL OF SCIENCE.

[SEVENTH SERIES.]

FEBRUARY 1928.

XXV. *New Evidence of the Existence of Charges smaller than the Electron.*—(a) *The Micromagnet*; (b) *The Law of Resistance*; (c) *The Computation of Errors of the Method.* *By* FELIX EHRENHAFT, *Dr.Phil., Acting Professor of Physics and Head of Physics Institute III. of the University of Vienna, and* EMANUEL WASSER, *Dr.Phil., of Vienna* *.

§ 1. *Introduction.*

IN a former paper, published in this Magazine †, we have referred to a new method of observations which enables us to demonstrate the nature of single colloidal test bodies moving in gases. This method, which depends upon velocity measurements of a single test body in an inhomogeneous magnetic field, is not only suitable for the determination of the magnetic constants of the observed particles, but can also be applied to the measurement of strong magnetic fields of small dimensions.

If we set, according to Faraday (1848), the susceptibility of vacuum $k=0$, and denote a weak magnetic body as paramagnetic when $k>0$, as diamagnetic when $k<0$, then the energy of a small particle of the volume V in the magnetic field H is $\frac{1}{2}k\mathrm{V}\mathrm{H}^2$. From this results that the force acting on a single particle in the direction of the x axis is $k\mathrm{V}\mathrm{H}\frac{d\mathrm{H}}{dx}$. While in a homogeneous field this force disappears, in an

* Communicated by the Authors.

† F. Ehrenhaft and E. Wasser, Phil. Mag. vol. ii. (July 1926).

inhomogeneous field a paramagnetic test body would be driven to the region of the greater force, a diamagnetic body in the opposite direction. We now wish to examine in this way as small test bodies as possible, and construct for this purpose the suitable magnetic field.

§ 2. *The Micromagnet.*

For the following measurements the circular poles of an Ehrenhaft condenser of the diameter 9 mm. were rebuilt

Fig. 1.

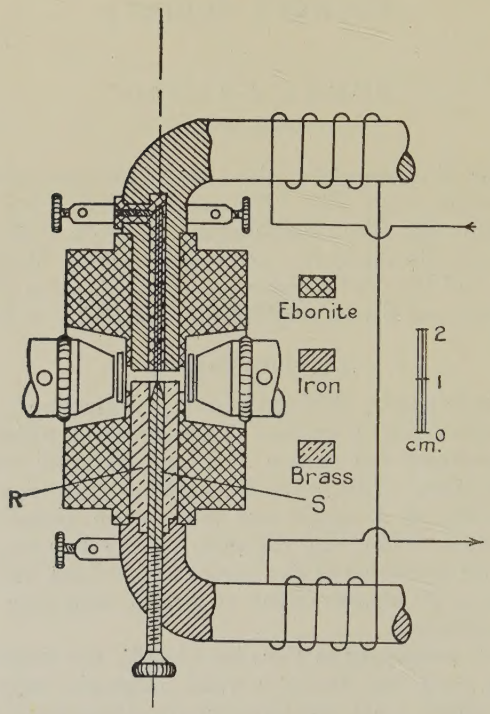

into poles of a strong electromagnet. The upper plate consists of a hollow cylinder of soft iron with an external diameter of 9 mm. and an internal diameter of 2 mm. Into this is introduced an electric insulated solid cylinder of the same iron with a diameter of 1 mm. These cylinders can be brought to various electric potentials. The lower plate ends in a conical iron pin, 2 mm. thick, which has a circular base with a diameter of 1 mm. The pin is surrounded by a mantle of brass with a diameter of 9 mm., so that its base

lies in the same plane as that of the pin. The described condenser plates go over into two iron cores (12 mm. thick, 190 mm. long), each of which is wound with 14 layers of 2-mm. copper wire. An accumulator battery of 120 volts cross-potential and very great capacity furnishes a quite constant current. The number of the ampere turns per 1 cm. is 1080. The two cores are closed by an iron yoke which is insulated from them by leaves of mica. In this way the plates can also be used as an electrical condenser. Four coolers fed with flowing water, two for each core, provide for a sufficient removal of the heat and hold the temperature constant. When the windings are connected with the electrical circuit, there are produced two opposite magnetic poles in the vertical x axis. In this way we get a symmetrical inhomogeneous magnetic field between the plates of an Ehrenhaft condenser, which are at a distance 1·8 mm. apart.

§ 3. *The Measurement of the Micromagnetic Field.*

It is well known that under the influence of a constant force P the velocity v of the test body in a frictional medium is proportional to the force acting. If B denotes the mobility of the test body, then we may write $v = \mathrm{B} \cdot \mathrm{P}$. If P is a function of position, the velocity of the test body will change proportionally to the change in the force. In the following the measurements of the velocities are made over such small regions that the force $\overline{\mathrm{P}}$ in these regions may be regarded as constant, and hence proportional to the velocity $\bar{v}$. If the direction of the magnetic field is the same as that of gravity, and if the test body acquires, under the action of gravity and of the magnetic force, a velocity $\overline{v_m}$ in the frictional medium, then

$$mg \pm k\mathrm{V}\mathrm{H}\frac{d\mathrm{H}}{dx} = \frac{\overline{v_m}}{\mathrm{B}} \cdot \quad . \quad . \quad . \quad . \quad . \quad (1)$$

Here $\overline{v_m}$ is the velocity, H the magnetic intensity, and $\frac{d\mathrm{H}}{dx}$ the gradient of the intensity in a practically very small region in which the force may still be regarded as uniform. The positive sign holds for paramagnetic, the negative sign for diamagnetic bodies. In our case the gradient of the field in the central x axis is in the same direction as gravity. Hence the action of the magnetic field on paramagnetic bodies will be in the direction of gravity, and on diamagnetic bodies in the opposite direction.

In order to undertake the measurement of the inhomogeneous magnetic field, we must first define its geometrical configuration. The observations were made with a microscope objective of the numerical aperture 0·34 and with a Huygens ocular 4. According to this the magnification was 95. This combination of ocular and objective gave a field of vision of a diameter about 2 mm., so that both the plates (distance 1·8 mm.) were still visible. By a scale introduced in the ocular the space between the poles was divided into equal intervals of 9.10^{-3} cm. Of this, only the central part of the scale, 1·08 mm. long, was used for the observations. This central part of the field of vision was divided into 12 intervals. The measurements, however, were made over two intervals at once, as it was found that the velocity under the influence of the magnetic force was sufficiently uniform in this stretch. The magnetic field could therefore be examined over six double intervals of the length of 18.10^{-3} cm., *i.e.* about two-thirds of the space between the poles.

For the purpose of calibration an aqueous solution of 3·01 per cent. $FeCl_3$ was used. It was necessary to hold the concentration as low as possible in order that the susceptibility might not be too high. In this case the velocities in the magnetic field would be very large and difficult to measure, and, furthermore, small susceptibility makes possible a comparison with diamagnetic bodies, most of which have very small susceptibilities. The susceptibility of ferric chloride solution was determined relative to water by repeated measurements, using a large magnet and the buoyancy method. Assuming the value $k=-0{\cdot}77.10^{-6}$ for water, the value $k=1{\cdot}14.10^{-6}$ was found for the 3·01 per cent. $FeCl_3$ solution.

The solution was mechanically sprayed, and upon the test bodies the following measurements were made. Each test body is allowed to fall under the influence of gravity alone, and is repeatedly drawn up again by the electrical field. After ten measurements of the times of fall and rise had been made, the same measurements were repeated in the magnetic field. For the motion in the magnetic field we have the relationship

$$mg+k\mathrm{V}\mathrm{H}\overline{\frac{d\mathrm{H}}{dx}}=\overline{\frac{v_m}{\mathrm{B}}}; \quad \ldots\ldots \quad (2)$$

for the motion under the action of gravity alone the relationship

$$mg=\mathrm{V}\sigma g=\frac{v_f}{\mathrm{B}}, \quad \ldots\ldots \quad (3)$$

where V denotes the volume of the test body. From this follows

$$1+\frac{k}{\sigma g}\cdot\overline{H\frac{dH}{dx}}=\frac{\overline{v_m}}{v_f}. \quad . \quad . \quad . \quad . \quad . \quad (4)$$

From this results that for each interval the mean product of the magnetic intensity into the gradient is

$$\overline{H\frac{dH}{dx}}=\left(\frac{\overline{v_m}}{v_f}-1\right)\cdot\frac{\sigma g}{k}. \quad . \quad . \quad . \quad . \quad (5)$$

If, now, in (5) we give the density the value 1·03 and the susceptibility k the value as above determined, we can compute the value of $\overline{H\frac{dH}{dx}}$ for each interval, and can plot this as a function of position. In the diagram of fig. 2 the

Fig. 2.

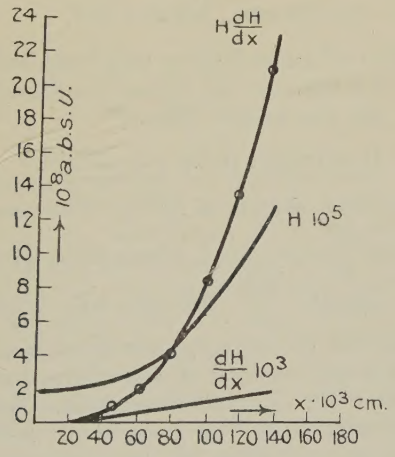

lengths of the intervals measured in 10^{-3} cm. are plotted as abscissæ, the values of $\overline{H\frac{dH}{dx}}$ measured in 10^8 abs. units as ordinates. In the other two curves the ordinates are measured in 10^3 gauss, and $\overline{\frac{dH}{dx}}$ measured in 10^5 abs. units. The marked points show the measured values of $\overline{H\frac{dH}{dx}}$ in the six intervals. In order to determine the values of $\overline{H}$, a cubical parabola was drawn to the points by the method

of least squares. This parabola fits the observed values extremely well. The deviations are all within the region of the errors of observation and are, in mean value, about 1·5 per cent.

Hence the product $\overline{H\frac{dH}{dx}}$ can be written in a form

$$\overline{H\frac{dH}{dx}} = f(x),$$

where $f(x) = ax^3$. For the constant a the value $0{\cdot}856 \cdot 10^{12}$ was obtained.

The equation

$$\overline{H\frac{dH}{dx}} = 0{\cdot}856 \cdot 10^{12} \cdot x^3$$

can easily be integrated. From this results that the magnetic intensity as a function of the position is

$$H = (0{\cdot}428 \cdot 10^{12}x^4 + c)^{1/2}.$$

From the number of ampere turns and from the dimensions of the magnet we have as the initial condition for $c = \overline{H_0}^2$ the value $\sim 4 \cdot 10^6$ abs. units. Hence

$$H = (0{\cdot}428 \cdot 10^{12}x^4 + 4 \cdot 10^6)^{1/2}.$$

This curve is also shown in fig. 2. The quotient of the two ordinates $\overline{H\frac{dH}{dx}}$ and $\overline{H}$ at every point gives the third curve of the diagram $\frac{\overline{dH}}{dx}$. In this way it is possible to examine the nature of the magnetic field in all its details. Here we have a new method of measuring inhomogeneous strong magnetic fields of small dimensions. As can be seen from fig. 2, the intensities run from about 2000 to 13,000 gauss. Of course very close to the point the intensity is still essentially greater, and may even exceed 20,000 gauss.

§ 4. *The Determination of the Magnetic Constants of Small Particles by means of the Micromagnetic Field.*

As the structure of the magnetic field is already known, we can undertake the measurements on other paramagnetic and diamagnetic substances in order to determine their susceptibilities. In the following the results of these researches on several test bodies of selenium and silver are given.

The procedure is here the same as described for $FeCl_3$. If $\overline{v_{m_0}}$ denotes the velocity of a drop of ferric chloride in the magnetic field, and v_f the velocity under the influence of gravity alone in a certain interval, and if, furthermore, $\overline{v_{m_1}}$ and v_{f_1} have the same meaning for a particle of selenium, we get, according to (5), the two equations

$$\left.\begin{aligned} \frac{k_0}{\sigma_0 g} \cdot H\overline{\frac{dH}{dx}} &= \left(\frac{\overline{v_{m_0}}}{v_{f_0}} - 1\right), \\ \frac{k_1}{\sigma_1 g} \cdot H\overline{\frac{dH}{dx}} &= \left(\frac{\overline{v_{m_1}}}{v_{f_1}} - 1\right). \end{aligned}\right\} \quad \ldots \quad (6)$$

As $H\frac{dH}{dx}$, under the assumption made above, has the same value in both cases, there results

$$\frac{k_0}{\sigma_0} : \frac{k_1}{\sigma_1} = \left(\frac{\overline{v_{m_0}}}{v_{f_0}} - 1\right) : \left(\frac{\overline{v_{m_1}}}{v_{f_1}} - 1\right)$$

or

$$\frac{k_1}{\sigma_1} = \frac{k_0}{\sigma_0} \frac{\left(\frac{\overline{v_{m_0}}}{v_{f_0}} - 1\right)}{\left(\frac{\overline{v_{m_1}}}{v_{f_1}} - 1\right)} \quad \ldots \quad (7)$$

In this way, assuming the susceptibility of a calibrating substance as known, the mass susceptibilities of various substances can be determined from velocity measurements alone. Moreover, the advantage of the method is that the magnetic field can be controlled after each measurement; and this we have done in every case. During these measurements we have not only taken care that the electrical current for the exciting of the electromagnet should be as constant as possible, and that the measurement should be carried out on the same spot in the direction of the x axis, but, furthermore, that the particle should not leave the central line of the field of vision. The deviations from the centre, *e. g.* on account of the Brownian movement, could not have been greater than 0·2 mm. In this way we could be assured that the product $H\overline{\frac{dH}{dx}}$ was measured on one and the same spot during the time of observation.

The results of the measurements are given in the following table. In the first and second columns the quotients $\frac{\overline{v_m}}{v_f}$ for the substance in question and that for ferric chloride are shown, measured always in the corresponding interval.

In the third column stand the mass susceptibilities for Ag and Se. The mass susceptibilities agree perfectly well with those for the material in bulk. In particular, the mean values of $\frac{k}{\sigma}$ show quite clearly that the particles actually consist of selenium and silver.

It may further be mentioned that we are here working with red selenium, the mass susceptibility of which has in bulk the value $0{\cdot}117 \cdot 10^{-6}$, which agrees exactly with our value. The value for silver, $\frac{k}{\sigma} = -0{\cdot}20 \cdot 10^{-6}$, comes also within the limits $-0{\cdot}19 \cdot 10^{-6}$ to $-0{\cdot}22 \cdot 10^{-6}$, which have been given by several authors for the susceptibility of silver between 18° and 1100°.

TABLE I.

	T. b.	$(\overline{v_n/v_f})_{Ag}$.	$(\overline{v_m/v_f})_{FeCl_3}$.	$\left(\frac{k}{\sigma}\right) \cdot 10^6$.
Silver.	15. vii. 1926	0·723	2·519	−0·20
	16. „ „ (*a*)	0·907	1·966	−0·22
	16. „ „ (*b*)	0·910	1·966	−0·21
	17. „ „	0·697	2·519	−0·22
	20. „ „ (*a*)	0·615	3·392	−0·18
	20. „ „ (*b*)	0·566	3·392	−0·20
			Mean value	−0·20

	T. b.	$(\overline{v_m/v_f})_{Se}$.	$(\overline{v_m/v_f})_{FeCl_3}$.	$\left(\frac{k}{\sigma}\right) \cdot 10^6$.
Selenium.	31. v. 1926	0·807	2·752	−0·12
	5. vi. „	0·913	1·669	−0·14
	18. „ „	0·835	2·752	−0·10
	24. „ „	0·579	4·980	−0·12
			Mean value	−0·12

§ 5. *Results of the Researches on Single Colloidal Test Bodies at different Gas Pressures.*

Since the nature of the particles in question has been examined by means of the micromagnetic field, we can now complete the proof of the validity of some other assumptions as to normal density and spherical form of the test bodies. These assumptions, it is well known, must be made if we wish to determine the magnitude of the particles according to the law of resistance. With regard to this problem, we may also refer to the above-cited publication. The method

described in this paper enables us to determine, in a purely mechanical way, the constants of the law of resistance by means of velocity measurements on the same test body at different gas-pressures.

This series of researches, which up to the present time has been made on fluid drops and on solid particles of average density, has now been extended to heavy metallic test bodies. Papers prepared in our Institute *, which will shortly be published, show that when suitably produced in the electrical arc, silver and gold particles of constants within the limits of the theoretical derived law of resistance can also be obtained. The observed limits between which the single constants vary are much closer than those theoretically determined. The values of the constants of the law of resistance experimentally found closely agree with the values of the constants found for the substances already tested.

TABLE II.

Substance.	σ.	$A^2\sigma$.	A.	Interval of the radii in 10^5 cm.	$e \cdot 10^{10}$.	n.
Oil	0·93	0·82	0·93	3·59–11·52	4·67	21
$K_4Hg_2I_4$	3·01	3·04	1·00	1·96– 4·21	3·75	7
$BaHgI_4$	3·50	3·90	1·05	1·13– 3·25	3·26	17
Se_I	4·26	4·35	1·01	1·30– 3·72	2·80	26
Se_{II}	„	3·89	0·95	3·19– 5·55	2·56	5
Se_{III}	„	4·02	0·97	1·08– 3·34	1·49	17
Ag.....	10·50	12·15	1·07	1·12– 4·08	1·13	21
Au.....	19·18	19·19	1·00	0·83– 1·80	1·04	24

The above table shows the complete results of all the experiments concerning the validity of the law of resistance for single particles of magnitudes down to $1 \cdot 10^{-5}$ cm. This table is illustrated by fig. 3, which gives the results of measurements of several particles of selenium. The corresponding values of the mean free path of the molecules l and of the velocities u define a straight line the intercepts α and slopes β of which were found by means of the method of least squares. Since for the mobility we have the relation

$$B = \frac{1}{6\pi\mu a}\left(1 + A\frac{l}{a}\right), \quad . \quad . \quad . \quad . \quad . \quad (8)$$

* O. Trauner, *ZS. f. Ph.*; M. Slopkovitzer, *ZS. f. Ph.*

the resulting expressions for the above coefficients, taking the acting forces † into consideration, are

$$\alpha = \frac{2}{9}\frac{g\sigma}{\mu E^*}a^2\,; \quad \beta = \frac{2}{9}\frac{g\sigma}{\mu E^*}.Aa. \quad . \quad . \quad . \quad (9)$$

From these result the values for $A^2\sigma$ and e/A :

$$A^2\sigma = \frac{9}{2}\frac{\mu E^*}{g\sigma}.\frac{\beta^2}{\alpha}; \quad e/A = 6\pi\mu.\frac{\alpha^2}{\beta}. \quad . \quad . \quad (10)$$

Fig. 3.

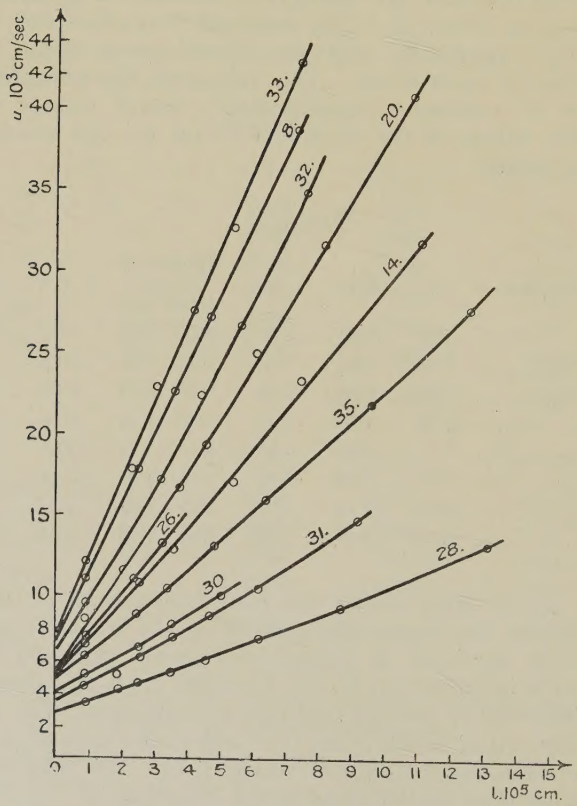

The mean values of $A^2\sigma$ for all materials tested up to the present time are given in Table II. The number of particles used for the computation of the mean values is marked in the table by "n." If we now compare the densities of the materials in bulk, which run from 0·93 (oil) to 19·2 (gold),

† *Cf.* F. Ehrenhaft and E. Wasser, Phil. Mag. *l. c.*

with the products $A^2\sigma$, we notice the proportionality between these two magnitudes. We can illustrate this relationship if we plot in a diagram the densities as abscissæ and $A^2\sigma$ as ordinates. Fig. 4 shows this diagram. The circles mark the values obtained by computation of the arithmetical mean, while the crosses denote the average values of $A^2\sigma$ computed by taking the errors of the measurements into consideration.

The results given below were got by measurements on 140 particles of various densities. The number of single observations used for this purpose was about 32,000. As

Fig. 4.

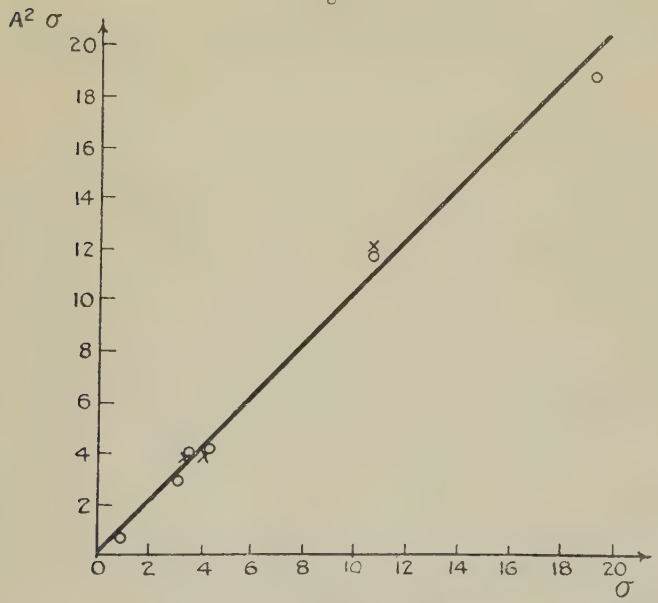

a result of this great number of observations, we may regard the relationship mentioned above as being better established than many well-known laws of physics.

From the proportionality between the densities and the products $A^2\sigma$, as well as from the fact that the products $A^2\sigma$ for one and the same substance show very small deviations from their mean value, the conclusion can be drawn that the single particles produced in various ways have their normal densities and structures. Under this assumption we get the constants A of the law of resistance, which are also shown in Table II. They all lie in the interval 0·93–1·07, and thus show still smaller deviations from each other than is permitted by the limits theoretically computed. The mean

value of all constants A is 1·02, whereof the error is certainly no greater than 0·5 per cent., as very many observations have been used for its calculation.

As the constants A, experimentally determined, prove the validity of all assumptions made for the purpose of the determination of the magnitudes of single test bodies, the charges on these particles can be computed. In each case the smallest charge for each substance is given in Table II. The charges shown there are much smaller than the electron. In particular the value 1.10^{-10} E.S.U. was often found for the gold particles ; and these values can be repeated. These small charges can neither be explained by deviations from the normal structure of the test bodies, nor by errors in the observations, as will be shown in the next paragraph.

§ 6. *The Determination of the Errors of the Experimental Results.*

In a paper which is shortly to appear in the *Zeitschrift für Physik*, E. Wasser gives a computation of the errors of observations according to the evacuation method. For this purpose new measurements were made on selenium particles the magnitudes of which were 1.10^{-5} cm. to 3.10^{-5} cm. Since this critical order of magnitude is characteristic for the determination of small charges, the errors calculated there may be regarded as typical for all other substances.

The averaging of the observations can only be made in accordance with a law which is theoretically well founded. It is well known, theoretically, that for large particles, $\frac{l}{a} \leqslant 1$, the Stokes-Cunningham formula holds in the form as shown by equation (8). For very small particles, however, $\frac{l}{a} \geqslant 1$, the theory gives the relation

$$B = \frac{(A+D)l}{6\pi\mu a^2}. \quad . \quad . \quad . \quad . \quad . \quad (11)$$

An exact theoretical law of resistance should therefore contain both these cases as limits. The empirical formula of Knudsen and Weber * fulfils these conditions, and also closely agrees with the experiment. If, therefore, we wish to take into consideration the curvatures of the lines experimentally found, we are obliged to make use of the formula

$$B = \frac{1}{6\pi\mu a}\left[1 + \frac{l}{a}(A + De^{-C\frac{a}{l}})\right]. \quad . \quad . \quad (12)$$

* M. Knudsen and S. Weber, *Ann. d. Phys.* xxxvi. p. 981 (1911).

According to this, the results of measurements on the selenium particles are first approximated to the linear form of the law of resistance, and the errors resulting from this are calculated in the paper cited. The exponential law is then used for the determination of the sizes and charges of the particles, and the errors in these magnitudes are also computed.

If, on the one hand, we assume the relation between the directly measured values of the mean free path, l, and velocities, u, to be linear, then we can set

$$u_i = \alpha + \beta l_i, \quad . \quad . \quad . \quad . \quad . \quad . \quad (13)$$

where α and β have the meaning given above. Taking the expressions for α and β into consideration, we get

$$A^2\sigma = F(\alpha, \beta, E^*)$$

and

$$e/A = F'(\alpha, \beta). \quad . \quad . \quad . \quad . \quad . \quad . \quad (14)$$

The errors in the products $A^2\sigma$ and quotients e/A are therefore composed of the errors in the values for α, β, and E^*. The errors in the last magnitudes were computed according to the method of least squares †, and give the compound errors for $A^2\sigma$ and e/A shown in Table III.

TABLE III.

T. b. no.	$A^2\sigma$.	$\pm m_{A^2\sigma}\%$.	e/A.	$\pm m_{e/A}\%$.	n.
1	4·338	9·66	1·479	13·94	3
3	4·710	12·64	1·773	24·80	5
8	3·903	2·10	3·669	3·01	6
9	3·390	7·95	1·920	12·27	4
14	3·645	10·23	2·629	17·30	6
15	3·980	8·23	2·531	13·02	7
20	4·518	11·54	2·202	20·14	6
22	4·655	6·95	2·703	11·64	8
24	5·849	7·68	2·874	12·16	6
28	3·498	4·50	2·740	6·43	8
29	4·686	6·46	2·621	9·83	6
30	4·570	5·07	4·130	5·11	4
31	4·168	7·79	2·338	11·40	6
32	4·614	6·25	3·254	9·16	6
33	5·550	7·08	3·550	10·71	6
35	4·22	5·08	3·364	7·62	8
36	3·625	5·00	3·820	4·52	3
Average mean errors.....		7·30		11·35	

† For the extended formulas used in this case we may refer to the paper by E. Wasser.

As may be seen from the above table, the errors run from 2·1 per cent. to 12·6 per cent. for $A^2\sigma$, and from 3·0 per cent. to 24·8 per cent. for e/A. The average errors for these two magnitudes are 7·3 per cent. and 11·3 per cent. The mean value of the products $A^2\sigma$, as well as of the quotients e/A, cannot be calculated according to the formula for an arithmetical mean, for the reason that each observation carries its own error. For the purpose of calculating the mean value, we must therefore regard the value of exactitude of each single observation. Taking this into consideration, we get

$$\overline{A^2\sigma} = 4{\cdot}015\,; \quad \overline{e/A} = 3{\cdot}066\,.\,10^{-10}.$$

The average errors for these two mean values are 1·3 per cent. and 1·8 per cent. respectively *. As the result of measurements on 17 selenium particles, we obtain

$$\overline{A^2\sigma} = 4{\cdot}015 \pm 0{\cdot}053\,; \quad \overline{e/A} = (3{\cdot}066 \pm 0{\cdot}056)\,.\,10^{-10}.$$

In order to determine the absolute values of A, a, and e from the results of observations $A^2\sigma$ and e/A, a further assumption must be made about one of the three magnitudes A, σ, and e. Considering the proportionality between the densities σ and the products $A^2\sigma$ measured on various substances, we may assume for the density its value for selenium in bulk. This assumption enables us to calculate the constants A, the radii of the test bodies a, and their charges e. The corresponding values for these magnitudes are given in Table IV.

By assuming the density σ as an exact figure, the total error in the product $A^2\sigma$ is reduced to the error in A^2. In this way we get the average error of each separate value of the constant A at 3·65 per cent. and the error in the mean value $\overline{A} = 0{\cdot}974$ at 0·66 per cent. Table IV. shows these errors in the constants A as well as the charges e and the radii a. Since the average errors in the charges run from 3·2 per cent. to 23·6 per cent., the majority of the charges is much smaller than the elementary unit $4{\cdot}77\,.\,10^{-10}$ E.S.U.

* There remains the question, how great is the actual variation for the separate values of $A^2\sigma$ and e/A. Above all it is to be considered if this average variation is within the probable error. Should this not be the case, it would be an argument in favour of the presence of real deviations; in fact the e/A vary so much that it is questionable if a mean value is justified. This can, of course, be decided by means of the computation of errors. It is shown in the paper by E. Wasser that these actual variations of the values for e/A are as great as 39·3 per cent., and thus exceed the limits of the average errors in these magnitudes. Accordingly the charges e cannot be regarded as constant.

TABLE IV.

T. b. no.	A.	$\pm m_A\%$.	$a.10^5$ cm.	$\pm m_a\%$.	$e.10^{10}$.	$\pm m_e\%$.
9.....	0·892	3·97	1·08	7·52	1·71	12·90
3.....	1·051	6·32	1·16	13·20	1·86	23·63
15.....	0·966	4·11	1·21	7·90	2·44	13·65
1.....	1·009	4·83	1·25	8·60	1·49	14·75
20.....	1·030	5·77	1·44	11·76	2·27	20·95
8.....	0·957	1·05	1·53	1·91	3·51	3·20
14.....	0·925	5·11	1·66	10·27	2·43	18·03
32.....	1·040	3·12	1·69	5·72	3·38	9·68
33.....	1·141	3·54	1·70	6·60	4·05	11·30
24.....	1·171	3·84	1·91	7·47	3·36	12·76
22.....	1·045	3·47	2·02	6·91	2·82	12·15
36.....	0·922	2·50	2·03	3·74	3·52	5·17
29.....	1·048	3·23	2·06	6·16	2·75	10·34
35.....	0·996	2·54	2·34	4·73	3·35	8·03
31.....	0·989	3·89	2·35	7·23	2·31	12·04
28.....	0·906	2·25	2·92	4·15	2·48	6·81
30.....	1·035	2·53	3·34	4·07	4·27	5·71
Average mean errors ...		3·65		6·93		11·83

Now, the deviations in the charges from the above value cannot be explained by the assumption of the non-validity of the law of resistance, provided this be linear, as has been shown in the above paragraphs.

§ 7. *The Averaging of the Observational Data according to the Exponential Law of Resistance.*

Should the law of resistance be continuous in the interval between the extreme limits mentioned above, then we are obliged to assume a curvature of the (u, l)-lines if the mean free path of the molecules, l, is comparable with the radius a; *i. e.* if $\frac{l}{a} \sim 1$. This dependence of the constants A upon the ratios $\frac{l}{a}$ is given by the empirical formula of Knudsen and Weber, to which we also made reference in our publication cited above.

Considering the acting forces and the formula (12) for the mobility, we get

$$u = \frac{2}{9}\frac{a^2\sigma g}{\mu E^*}\left[1 + \frac{l}{a}(A + De^{-C\frac{a}{l}})\right]. \quad . \quad . \quad . \quad (15)$$

We set $\frac{2}{9}\frac{\sigma g}{\mu E^*} = k$, and make the averaging according to the constants A, D, C and the radius a. For this purpose the above expression for u must be made linear. This can be done by differentiating the equation (15) with regard to the constants A, D, C and the radius a, and by introducing approximate values for these magnitudes. We therefore set

$$A = A_0 + \beta\,; \quad D = D_0 + \gamma\,; \quad C = C_0 + \delta\,; \quad a = a_0 + \alpha.$$

In this way we obtain linear equations of the form

$$\alpha m_i + \beta n_i + \gamma s_i + \delta t_i = r_i. \quad . \quad . \quad . \quad . \quad (16)$$

The minimum condition

$$\Sigma(\alpha m_i + \beta n_i + \gamma s_i + \delta t_i - r_i)^2 = \text{min.} \quad . \quad . \quad (17)$$

gives the normal equations, from which we can calculate the corrections β, γ, δ, α, and from these the averaged values of A, D, C, and a.

This method of computation enables us to determine the radii of the particles, taking the curvatures of the (u, l)-lines into consideration. The measurements made up to the present time allow us only in single cases to make use of the averaging above. In the majority of cases, only six points were measured for each (u, l)-line, which give two surplus equations for the determination of the corrections. This number of equations, however, does not appear to be sufficient for the exact evaluation of the curvature, as the application of the above method of computation to the selenium particles measured in our case has shown. Only in the case of two particles which furnished eight points for the (u, l)-line did we succeed in averaging the observations according to the exponential law of resistance. In all other cases the errors were so great that a curvature of an opposite sign was also probable.

Table V.

T. b. no.	A.	D.	C.	$a \cdot 10^5$ cm.	$e \cdot 10^{10}$ E.S.U.
28	0·860	0·127	3·58	3·02	2·72
35	0·776	0·220	2·38	2·49	4·04
T. b. no.	$\pm m_A$.	$\pm m_D$.	$\pm m_C$.	$\pm m_a$.	$\pm m_e$.
28	0·140	0·085	1·15	0·08	0·21
35	0·133	0·073	0·89	0·07	0·35

The data for these two particles are shown in Table V.

The calculated error for each magnitude stands under the value in question, and is marked by m_A, m_D, m_C, m_a, m_e respectively. If we now compare the values for A, a, and e of the above table with the corresponding values for these two particles as calculated according to the linear form of the law of resistance, we may draw the following conclusions :—

If we take the curvatures of the (u, l)-lines into account, the constants A become smaller ; but also in this case they remain within the theoretical limits. The radii of the test bodies increase by so much as the constants decrease. Accordingly the charges, too, grow ; they do not, however, reach the value of the electron. If we consider the above two examples, we may assert that, on account of the exponential law of resistance, the charges increase by about 10 per cent. to 15 per cent., as against the charges calculated according to the linear formula. This circumstance, however, cannot explain the large deviations of the charges measured in our case from the value of the elementary unit of electricity.

Vienna,
Aug. 6, 1927.

XXVI. *Riemannian Null-Geometry.* *By* J. L. Synge, *Sc.D., F.T.C.D., University Professor of Natural Philosophy, and* A. J. McConnell, *B.A., Lecturer in Mathematics, Trinity College, Dublin* *.

Synopsis.

Part I.—§ 1. Introduction. § 2. Contact of surfaces. § 3. Conjugate cones. § 4. Null-surfaces ; characteristic lines ; geodesic null-lines. § 5. The finite null-cone. § 6. Conditions that a family of geodesic null-lines may constitute a null-surface. § 7. The two null-surfaces passing through an (N−2)-space. § 8. Geometrical solution of $\phi=0$, when ϕ is given over a surface.

Part II.—§ 9. Optical significance of geometrical results. § 10. Reflexion at a moving surface. § 11. Refraction at a moving surface.

§ 1. *Introduction.*

WHEN a non-definite line-element is used in Riemannian geometry, there is introduced an important geometrical entity, the null-cone, which does not exist when the line-element is definite. The present paper is concerned with some aspects of the geometry of the null-cone.

* Communicated by the Authors.

In Part I., which treats of pure geometry, the contact of surfaces at ordinary and double points is discussed. A null-surface is defined as an envelope of null-cones, and its partial differential equation is shown to be

$$\Delta_1\phi \equiv g^{mn}\phi_m\phi_n = 0, \quad (\phi_r = \partial\phi/\partial x^r), \quad . \quad (1.1)$$

while the characteristic lines on a null-surface prove to be geodesic null-lines *. The finite null-cone, formed from all the geodesic null-lines issuing from a point, is shown to be a null-surface. It is proved that through an arbitrary subspace of (N—2) dimensions there pass two null-surfaces, formed from geodesic null-lines issuing from the points of the subspace, two directions being defined at each point. The duality of the solution of (1.1), when the value of ϕ is given arbitrarily over a surface, is then evident.

Part II. deals with the application of the geometrical results to optics. The propagation of light in space-time being defined by a generalized Huyghens's construction, the history of a light wave in space-time is a null-surface. The history of a light-ray, defined as a characteristic on the history of a wave, is therefore a geodesic null-line. By regarding the wave, instead of the ray, as fundamental, we are able to discuss reflexion and refraction at a moving surface. The results are applicable to the general theory of relativity, but it is hoped that the generality of method may also be of some value in the discussion of other problems.

Part I.

§ 2. *Contact of surfaces.*

Let there be a manifold V_N with a coordinate system $(x^1, x^2, \ldots, x^N)$. Let S_{N-1} be a surface immersed in V_N, and let P and Q be two points on this surface. Let Q approach P along any curve on the surface, and let η^r be quantities proportional to $(x^r)_Q - (x^r)_P$ in the limit as Q tends to P. Any such vector η^r is said to be a *tangent* to the surface at P, and the totality of tangent vectors constitute the *tangent element* at P. If the equation of the tangent element is of the form

$$a_m\eta^m = 0, \quad . \quad . \quad . \quad . \quad . \quad . \quad (2.1)$$

* Equation (1.1) will be found in von Laue's 'Relativitätstheorie,' ii. p. 149 (1921), where he develops the theory of the propagation of electromagnetic waves of evanescent wave-length. He also derives the equations of the light-rays from this equation. Here, however, we are concerned with the geometrical aspect.

we say that P is an *ordinary* point. If the equation of the tangent element is of the form

$$a_{mn}\eta^m\eta^n = 0, \quad . \quad . \quad . \quad . \quad . \quad . \quad (2.2)$$

then P is a *double* point; and so on. Equation (2.1) defines the *elementary tangent plane* at an ordinary point; (2.2) defines the *elementary tangent cone* at a double point.

The contact of surfaces will be defined in terms of the contact of their tangent elements.

Let us consider the intersection of an elementary cone C_{N-1}, given by (2.2), in which without loss of generality we assume a_{mn} symmetrical, with an elementary two-space V_2 given by the equation

$$\eta^r = \alpha\lambda^r + \beta\mu^r, \quad . \quad . \quad . \quad . \quad . \quad (2.3)$$

where α and β are parameters, and λ^r and μ^r are fixed vectors. V_2, in general, cuts C_{N-1} in two vectors. If these two vectors coincide, we say that V_2 touches C_{N-1}, and the common vector is the *vector of contact*. The condition for contact is

$$(a_{mn}\lambda^m\mu^n)^2 = a_{mn}\lambda^m\lambda^n \,.\, a_{pq}\mu^p\mu^q, \quad . \quad . \quad (2.31)$$

and the vector of contact may be written in the form

$$\eta^r = \lambda^r \,.\, a_{mn}\mu^m\mu^n - \mu^r \,.\, a_{mn}\lambda^m\mu^n. \quad . \quad . \quad (2.32)$$

In order that λ^r may be the vector of contact, it is necessary and sufficient that

$$a_{mn}\lambda^m\lambda^n = 0 \quad . \quad . \quad . \quad . \quad . \quad (2.33)$$

and

$$a_{mn}\lambda^m\mu^n = 0. \quad . \quad . \quad . \quad . \quad . \quad (2.34)$$

If λ^r be any vector in C_{N-1} and μ^r any vector satisfying (2.34), then the elementary two-space given by (2.3) touches C_{N-1}, λ^r being the vector of contact. Thus all the elementary two-spaces touching C_{N-1} along λ^r constitute an element of $(N-1)$ dimensions, whose equation is

$$a_{mn}\lambda^m\eta = 0, \quad . \quad . \quad . \quad . \quad . \quad (2.4)$$

and which we shall call *the elementary tangent plane to* C_{N-1} *along the vector* λ^r.

In order that the elementary plane

$$b_m\eta^m = 0 \quad . \quad . \quad . \quad . \quad . \quad . \quad (2.41)$$

may touch the elementary cone

$$a_{mn}\eta^m\eta^n = 0, \qquad (a_{mn} = a_{nm}); \quad (2.42)$$

it is necessary and sufficient that λ^r exist such that (2.33) is satisfied and the elementary planes (2.4) and (2.41) coincide. This is the case if, and only if,

$$a_{mn}\lambda^m = \theta b_n, \quad . \quad . \quad . \quad . \quad . \quad (2.43)$$

where θ is a factor of proportionality. Hence

$$\lambda^m = \theta A^{mn} b_n, \quad . \quad . \quad . \quad . \quad . \quad (2.44)$$

where A^{mn} is the cofactor of a_{mn} in the determinant $|a_{mn}|$, divided by the determinant. Substitution in (2.33) gives the condition for contact

$$A^{mn} b_m b_n = 0, \quad . \quad . \quad . \quad . \quad . \quad (2.45)$$

while the vector of contact is given by (2.44), from which the factor of proportionality may be omitted.

We can now define the contact of surfaces. If a point common to two surfaces is an ordinary point on each, the surfaces are said to touch when their elementary tangent planes coincide. If the common point is a double point on one surface, the surfaces touch when the elementary tangent cone to one surface is touched by the elementary tangent plane to the other. If the common point is a double point on each surface, the surfaces touch when their elementary tangent cones have a common vector, and the elementary tangent planes to the elementary tangent cones along this common vector coincide.

Let a surface be given by

$$\phi(x^1, x^2, \ldots, x^N) = 0. \quad . \quad . \quad . \quad . \quad (2.5)$$

If $\partial\phi/\partial x^r$ do not all vanish at P, then P is an ordinary point, and the elementary tangent plane is

$$\phi_m \eta^m = 0. \quad . \quad . \quad . \quad . \quad . \quad (2.51)$$

If $\partial\phi/\partial x^r$ are all zero, but $\partial^2\phi/\partial x^r \partial x^s$ do not all vanish, then P is a double point, and the elementary tangent cone is

$$\phi_{mn}\eta^m\eta^n = 0, \quad . \quad . \quad . \quad . \quad . \quad (2.52)$$

where ϕ_{mn} is the second covariant derivative of ϕ.

If P is an ordinary point common to $\phi=0$ and $\psi=0$, the condition for contact is

$$\phi_r = \theta\psi_r, \quad . \quad . \quad . \quad . \quad . \quad . \quad (2.6)$$

where θ is a factor of proportionality.

If P is a double point on $\phi=0$ and an ordinary point on

$\psi=0$, the condition for contact is

$$\Phi^{mn}\psi_m\psi_n = 0, \quad . \quad . \quad . \quad . \quad . \quad (2.61)$$

where Φ^{mn} is the cofactor of ϕ_{mn} in $|\phi_{mn}|$, divided by this determinant *.

If P is a double point on $\phi=0$ and $\psi=0$, the condition for contact is that λ^r exist, satisfying

$$\phi_{mn}\lambda^m\lambda^n = 0, \quad \psi_{mn}\lambda^m\lambda^n = 0, \quad . \quad . \quad (2.7)$$

and making the elementary planes

$$\phi_{mn}\lambda^m\eta^n = 0, \quad \psi_{mn}\lambda^m\eta^n = 0 \, . \quad . \quad . \quad (2.71)$$

coincide. Thus we must have

$$\phi_{mn}\lambda^m = \theta\psi_{mn}\lambda^m, \quad . \quad . \quad . \quad . \quad (2.72)$$

where θ is a root of the determinantal equation

$$|\phi_{mn}-\theta\psi_{mn}| = 0. \quad . \quad . \quad . \quad . \quad (2.73)$$

Equation (2.72) shows that the satisfaction of the first of (2.7) implies the satisfaction of the second. Thus, to determine whether the surfaces touch, it will be necessary to solve (2.73) and substitute in the first of (2.7) the values of λ^r obtained from (2.72).

§ 3. *Conjugate cones.*

Let us now introduce a fundamental symmetrical tensor g_{mn}, which is such that the quadratic form $g_{mn}dx^m dx^n$ is not definite. The raising or lowering of indices is effected by means of the fundamental tensor. At every point of the manifold there exists an *elementary null-cone*,

$$g_{mn}\eta^m\eta^n = 0. \quad . \quad . \quad . \quad . \quad . \quad . \quad (3.1)$$

Two vectors λ^r, μ^r are said to be *conjugate* (or *perpendicular*) when they satisfy

$$g_{mn}\lambda^m\mu^n = 0. \quad . \quad . \quad . \quad . \quad . \quad (3.2)$$

If we are given a plane element $b_m\eta^m=0$ at a point, there is one, and only one, vector conjugate to every vector in this element, viz. b^r. If we are given an elementary cone C_{N-1} with the equation

$$a_{mn}\eta^m\eta \; = 0, \quad (a_{mn} = a_{nm}), \quad . \quad . \quad . \quad (3.21)$$

the *conjugate cone* is defined as the elementary surface formed

* The notation $|\phi_{mn}|$, used indifferently for determinant and modulus, is not satisfactory. We suggest the notation $|\phi_{mn}|$ for determinant, retaining the customary $|\phi_{mn}|$ for modulus.

of all the vectors conjugate to the tangent planes of C_{N-1}. The vector conjugate to the tangent plane $a_{mn}\lambda^m\eta^n = 0$ is

$$\xi^r = g^{rm}a_{mn}\lambda^n. \quad . \quad . \quad . \quad . \quad . \quad . \quad (3.3)$$

Hence

$$\xi_r = a_{rn}\lambda^n \quad . \quad . \quad . \quad . \quad . \quad . \quad . \quad (3.31)$$

and

$$\lambda^r = A^{rn}\xi_n, \quad . \quad . \quad . \quad . \quad . \quad . \quad . \quad (3.32)$$

where A^{mn} is defined as in § 2. Substitution in the equation of the cone gives for the conjugate cone the equation, η^r being written instead of ξ^r for the variable vector,

$$A^{mn}\eta_m\eta_n = 0 \quad . \quad . \quad . \quad . \quad . \quad . \quad (3.33)$$

or

$$A_{mn}\eta^m\eta^n = 0. \quad . \quad . \quad . \quad . \quad . \quad . \quad (3.34)$$

It is easily seen that the relation between conjugate cones is reciprocal. For the vector conjugate to the tangent plane to (3 34) along λ^r is

$$\xi^r = g^{rm}A_{mn}\lambda^n, \quad . \quad . \quad . \quad . \quad . \quad . \quad (3.35)$$

and when this value of ξ^r is substituted for η^r in (3.21), that equation is satisfied. Thus *every vector conjugate to a tangent plane of the conjugate cone belongs to the original cone.*

The condition for contact of an elementary plane with a cone may be stated as follows :—*An elementary plane touches a cone if, and only if, the vector conjugate to the plane lies in the conjugate cone.*

If we put $a_{mn} = g_{mn}$, we have $A^{mn} = g^{mn}$ and $A_{mn} = g_{mn}$. Thus *the null-cone is self-conjugate.* The elementary tangent plane to the null-cone along the vector λ^r is

$$g_{mn}\lambda^m\eta^n = 0. \quad . \quad . \quad . \quad . \quad . \quad . \quad . \quad (3.4)$$

We may state the following result :—A*n elementary plane touches the null-cone if, and only if, the plane contains its own conjugate vector ; that vector is then the vector of contact.*

§ 4. *Null-surfaces ; characteristic lines ; geodesic null-lines.*

A *null-surface* is defined as a surface which touches the elementary null-cone at every point. Equivalently, we may say that it is the envelope of an ∞^{N-1} family of elementary null-cones. Hence, putting $A^{mn} = g^{mn}$ and $b_r = \phi_r$ in (2.45), we see that, in order that the family of surfaces

$$\phi(x^1, x^2, \ldots, x^N) = \text{constant} \quad . \quad . \quad . \quad (4.1)$$

may be null-surfaces, it is necessary and sufficient that

$$\Delta_1\phi \equiv g^{mn}\phi_m\phi_n = 0 \quad . \quad . \quad . \quad . \quad (4.2)$$

at every point of the manifold. A surface whose normal at every point is a null-vector is a null-surface *. A surface whose normal at every point lies in the tangent plane is a null-surface.

At every point of a null-surface there exists a vector of contact with the elementary null-cone, given by

$$\lambda^r = \phi^r. \quad . \quad . \quad . \quad . \quad . \quad . \quad . \quad (4.3)$$

Thus every null-surface contains a congruence of lines defined by these vectors. These are *characteristic lines.* Their differential equations will now be found †. By suitable choice of the parameter u along any one of these lines we can make

$$\frac{dx^r}{du} = \phi \quad . \quad . \quad . \quad . \quad . \quad . \quad . \quad . \quad (4.31)$$

Hence, taking the contravariant derivative with respect to u along the line, we obtain

$$\frac{d^2x^r}{du^2} + \left\{ \begin{matrix} r \\ mn \end{matrix} \right\} \frac{dx^m}{du}\frac{dx^n}{du} = \phi^r{}_{,s}\frac{dx^s}{du} = \phi^r{}_{,s}\phi^s. \quad (4.32)$$

Covariant derivation of (4.2) with respect to x^r gives

$$g^{mn}\phi_{mr}\phi_n = 0, \quad . \quad . \quad . \quad . \quad . \quad (4.33)$$

which, since ϕ_{mr} is symmetrical, may be written

$$\phi_{rm}\phi^m = 0. \quad . \quad . \quad . \quad . \quad . \quad (4.34)$$

Thus the last expression in (4.32) vanishes, and the characteristic lines satisfy the equations

$$\frac{d^2x^r}{du^2} + \left\{ \begin{matrix} r \\ mn \end{matrix} \right\} \frac{dx^m}{du}\frac{dx^n}{du} = 0. \quad . \quad . \quad . \quad (4.4)$$

These equations, together with the particular first integral

$$g_{mn}\frac{dx^m}{du}\frac{dx^n}{du} = 0, \quad . \quad . \quad . \quad . \quad (4.41)$$

determine the characteristic lines. We shall follow the usual custom in referring to any solution of (4.4) and (4.41) as a *geodesic null-line*, reserving the name *characteristic* for those cases where the line is considered in relation to the null-surface on which it lies.

* *Cf.* Eisenhart, 'Riemannian Geometry,' p. 41 (1926).

† The work is similar to that of von Laue, *loc. cit.*, but we preserve tensorial form throughout.

If we transform from the parameter u to a general parameter v, (4.4) and (4.41) become

$$\left.\begin{aligned} \frac{d^2x^r}{dv^2} + \left\{ \begin{matrix} r \\ mn \end{matrix} \right\} \frac{dx^m}{dv}\frac{dx^n}{dv} &= \theta \frac{dx^r}{dv}, \\ g_{mn}\frac{dx^m}{dv}\frac{dx^n}{dv} &= 0, \end{aligned}\right\} \quad . \quad . \quad (4.5)$$

where θ is a factor of proportionality. Furthermore, a set of equations in the form (4.5) can always be transformed to (4.4) by transformation of the parameter †. If we put $v=x^N$, and eliminate θ from (4.5), we obtain $(N-1)$ differential equations of the second order for the determination of $x^1, x^2, \ldots, x^{N-1}$ as functions of x^N. Thus a geodesic null-line is uniquely determined when its direction (or the ratios $dx^1 : dx^2 : \ldots : dx^N$) is given at a point.

It may be remarked that, although there is no "distance" along a geodesic null-line, there does exist a privileged group of parameters for which the equations take the form (4.4). If u is any privileged parameter, then all the other privileged parameters are given by

$$w = au+b, \quad . \quad . \quad . \quad . \quad . \quad . \quad (4.6)$$

where a and b are constants. Thus any four points P_1, P_2, P_3, P_4 on a geodesic null-line determine a number,

$$\frac{u_2-u_1}{u_4-u_3}, \quad . \quad . \quad . \quad . \quad . \quad . \quad (4.61)$$

independent of the particular privileged parameter employed, since this fraction is invariant under the transformation (4.6). Ordinary geodesics also possess a privileged group of parameters,

$$w = as+b, \quad . \quad . \quad . \quad . \quad . \quad (4.62)$$

and for them the ratio (4.61) reduces to $P_1P_2 : P_3P_4$.

If we change the fundamental tensor to $g^*_{mn}=\lambda g_{mn}$, where λ is a function of the coordinates, the elementary null-cones are not changed. Thus null-surfaces and the characteristic lines on them remain unchanged. Hence we expect that geodesic null-lines also remain unchanged. We shall show that this is in fact the case, although the privileged parameters are changed. Since $g^{*mn}=g^{mn}/\lambda$, we have

$$\left\{ \begin{matrix} r \\ mn \end{matrix} \right\}^* = \left\{ \begin{matrix} r \\ mn \end{matrix} \right\} + \frac{1}{2\lambda}\left(\delta^r_n \frac{\partial\lambda}{\partial x^m} + \delta^r_m \frac{\partial\lambda}{\partial x^n} - g^{rs}g_{mn}\frac{\partial\lambda}{\partial x^s}\right) \quad . \quad . \quad . \quad (4.7)$$

† *Cf.* Veblen & Thomas, "The Geometry of Paths," Trans. Amer. Math. Soc. xxv. p. 556 (1923).

and hence

$$\frac{d^2x^r}{du^2} + \left\{ \begin{matrix} r \\ mn \end{matrix} \right\}^* \frac{dx^m}{du}\frac{dx^n}{du}$$

$$= \frac{d^2x^r}{du^2} + \left\{ \begin{matrix} r \\ mn \end{matrix} \right\} \frac{dx^m}{du}\frac{dx^n}{du} + \frac{1}{\lambda}\frac{d\lambda}{du}\frac{dx^r}{du} - \tfrac{1}{2}g^{*rs}\frac{\partial\lambda}{\partial x^s}g_{mn}\frac{dx^m}{du}\frac{dx^n}{du}. \quad . \quad . \quad . \quad (4.71)$$

Thus, if a curve satisfies (4.4) and (4.41), it also satisfies

$$\left.\begin{aligned} \frac{d^2x^r}{du^2} + \left\{ \begin{matrix} r \\ mn \end{matrix} \right\}^* \frac{dx^m}{du}\frac{dx^n}{du} = \theta\frac{dx^r}{du}, \quad \theta = \frac{1}{\lambda}\frac{d\lambda}{du}, \\ g^*{}_{mn}\frac{dx^m}{du}\frac{dx^n}{du} = 0, \end{aligned}\right\} \quad (4.72)$$

which are the equations of a geodesic null-line in the form (4.5).

§ 5. *The finite null-cone.*

The totality of geodesic null-lines issuing from a point O form a surface which we shall call *the finite null-cone with vertex* O. It is not evident that a finite null-cone is a null-surface in the sense of our definition. We shall now prove that this is in fact the case.

Fig. 1.

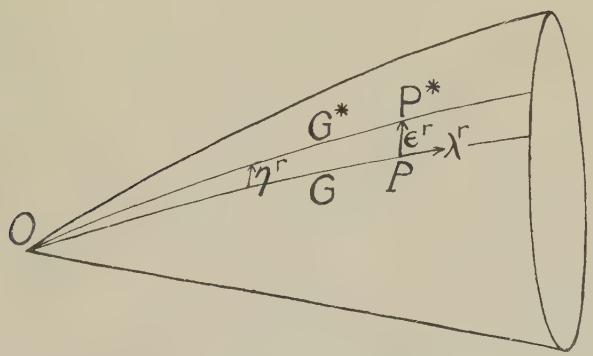

It is required to prove that the finite null-cone touches the elementary null-cone at every point on it, other than the vertex O. Thus, if P be any point on the finite null-cone and G the geodesic null-line passing through O and P, it is required to prove that the vector ϵ^r, drawn from P to any neighbouring point P* of the finite null-cone, is conjugate to the tangent to G at P.

Let G* be the geodesic null-line through O and P* (fig. 1). Having selected a privileged parameter u for G, so that its equations take the form (4.4), it will be possible to choose a privileged parameter u for G* in such a way that the parameters for G and G* have the same value at O and the same value at P and P*. Now, if η^r denote the infinitesimal vector joining any point of G to the point of G* having the same value of the parameter, we have

$$(\eta^r)_P = \epsilon^r, \quad . \quad . \quad . \quad . \quad . \quad . \quad (5.1)$$

and, since G* has a null direction at every point,

$$\left(g_{mn} + \frac{\partial g_{mn}}{\partial x^r}\eta^r\right)\frac{d}{du}(x^m+\eta^m)\frac{d}{du}(x^n+\eta^n) = 0, \quad . \quad (5.2)$$

where x^r denote the coordinates of any point on G. Subtracting the equation

$$g_{mn}\frac{dx^m}{du}\frac{dx^n}{du} = 0, \quad . \quad . \quad . \quad . \quad . \quad (5.21)$$

and retaining only terms of the first order, we obtain

$$g_{mn}\bar{\eta}^m\frac{dx^n}{du} = 0, \quad . \quad . \quad . \quad . \quad . \quad (5.3)$$

where

$$\bar{\eta}^m = \frac{d\eta^m}{du} + \left\{ \begin{matrix} m \\ pq \end{matrix} \right\} \eta_p \frac{dx^q}{du}. \quad . \quad . \quad . \quad (5.31)$$

But from (4.4) we have

$$\frac{d}{du}\left(g_{mn}\eta^m\frac{dx^n}{du}\right) = g^{mn}\bar{\eta}^m\frac{dx^n}{du}, \quad . \quad . \quad . \quad (5.4)$$

and this vanishes by virtue of (5.3). Thus along G we have

$$g_{mn}\eta^m\frac{dx^n}{du} = \text{constant}. \quad . \quad . \quad . \quad . \quad (5.5)$$

But η^r vanishes at O; therefore the constant is zero. Hence at P

$$g_{mn}\epsilon^m\lambda^n = 0, \quad . \quad . \quad . \quad . \quad . \quad (5.6)$$

where λ^r is the tangent vector to G. Thus ϵ^r is the conjugate to λ^r, and we have proved that *a finite null-cone is a null-surface.*

Let S be a null-surface and O a point on it. Let C be the finite null-cone with vertex O. Since S touches C at O, they have a common tangent vector at O, and this vector defines a geodesic null-line G contained in C and also in S,

as a characteristic line (fig. 2). We shall now prove that S *touches* C *at every point of* G.

Let P be any point on G, and let c be the elementary null-cone at P. Then, by the result established above, C touches c at P, the vector of contact being λ^r, the tangent vector

Fig. 2.

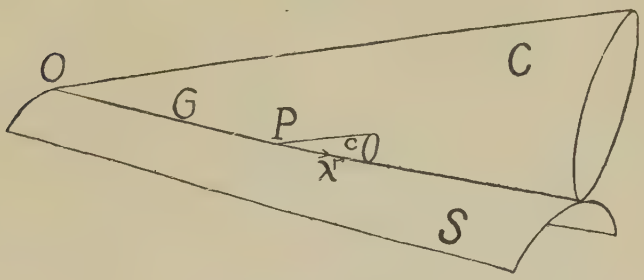

to G. But S also touches c, and has the same vector of contact. Thus the tangent planes to S and C at P coincide, being the tangent plane to c along λ^r; thus the result is established.

§ 6. *Conditions that a family of geodesic null-lines may constitute a null-surface.*

In the case of the finite null-cone we dealt with an ∞^{N-2} family of geodesic null-lines constituting a null-surface. An ∞^{N-2} family of geodesic null-lines picked at random, subject only to a condition of continuity, will not in general form a null-surface. We proceed to investigate the conditions which the family must satisfy.

Let S_{N-1} be a surface cut by the family. Each geodesic null-line cuts a surface in a point, and thus all the points of section form an $(N-2)$-space, Σ_{N-2}. Let the parametric equations of Σ_{N-2} be

$$x^r = x^r(\alpha_1, \alpha_2, \ldots, \alpha_{N-2}). \quad . \quad . \quad . \quad . \quad (6.1)$$

There will be associated with every point of Σ_{N-2} a direction, viz. that of the geodesic null-line passing through it, which we shall denote by ξ^r. Thus

$$\xi^r = \xi^r(\alpha_1, \alpha_2, \ldots, \alpha_{N-2}), \qquad g_{mn}\xi^m\xi^n = 0. \quad . \quad (6.2)$$

The problem before us is the investigation of the conditions controlling the functions in (6.2). The method adopted is similar to that used in § 5. G and G* are two neighbouring

geodesic null-lines, cutting Σ_{N-2} at O and O* (fig. 3). Privileged parameters are chosen, having the same value at O and O*. P and P* are points with equal values of the parameter, and η^r the vector from P and P*. We derive exactly as before

$$g_{mn}\eta^m \frac{dx^n}{du} = \text{constant}. \quad . \quad . \quad . \quad . \quad (6.3)$$

Fig. 3.

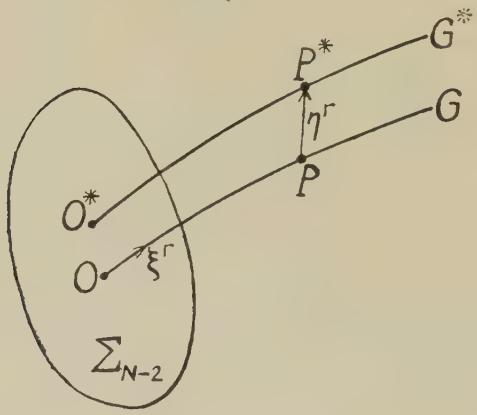

In order that the geodesic null-lines may form a null-surface, it is necessary and sufficient that this constant should vanish all over Σ_{N-2}. Thus all over Σ_{N-2} we must have

$$g_{mn}\eta^m\xi^n = 0. \quad . \quad . \quad . \quad . \quad . \quad . \quad (6.4)$$

for all values of η^r given by

$$\eta^r = \sum_{A=1}^{N-2} \frac{\partial x^r}{\partial \alpha_A} \delta\alpha_A. \quad . \quad . \quad . \quad . \quad . \quad (6.41)$$

Hence at all points of Σ_{N-2} we must have

$$g_{mn}\frac{\partial x^m}{\partial \alpha_A}\xi^n = 0, \quad (A = 1, 2, \ldots, N-2), \quad (6.5)$$

$$g_{mn}\xi^m\xi = 0. \quad . \quad . \quad . \quad . \quad . \quad . \quad . \quad . \quad . \quad (6.51)$$

From (6.5) we derive (N−2) of the ratios $\xi^1 : \xi^2 : \ldots : \xi^N$ as linear functions of the remaining ratio. Substitution in (6.51) gives a quadratic equation for this remaining ratio. Thus at every point of Σ_{N-2} the direction of the geodesic null-line must be one of *two* directions, which are given when Σ_{N-2} is known. These two directions may be called the *characteristic directions associated with any point of* Σ_{N-2}.

They are, in fact, the characteristic directions on the elementary envelope of the $^{N-2}$ family of elementary null-cones having their vertices in Σ_{N-2}.

§ 7. *The two null-surfaces passing through an* $(N-2)$*-space.*

Let Σ_{N-2} be an arbitrary subspace immersed in V_N. From § 6 we see that there are two families of geodesic null-lines passing through Σ_{N-2} and forming null-surfaces. From (6.5) we see that the characteristic directions on these null-surfaces are conjugate to every direction tangent to Σ_{N-2}. Now, the normal at a point on a surface is unique, but the normals at a point on a subspace of $(N-2)$ dimensions form a linear two-space. Thus the characteristic directions at any point lie in the linear two-space normal to Σ_{N-2}. Let λ^r and μ^r be two vectors assigned at every point of Σ_{N-2} and lying in the normal two-space. Then for either of the characteristic directions at any point we may write

$$\xi^r = \alpha\lambda^r + \beta\mu^r, \quad . \quad . \quad . \quad . \quad . \quad (7.1)$$

where α and β are as yet undetermined. Since ξ^r is a null-vector, we have

$$\alpha^2 g_{mn}\lambda^m\lambda^n + 2\alpha\beta g_{mn}\lambda^m\mu^n + \beta^2 g_{mn}\mu^m\mu^n = 0, \quad . \quad (7.2)$$

a quadratic equation for the determination of the ratio $\alpha:\beta$; hence the directions of the characteristic vectors $\xi^r_{(1)}$, $\xi^r_{(2)}$ are determined. The totality of geodesic null-lines drawn in the directions $\xi^r_{(1)}$, $\xi^r_{(2)}$ at all points of Σ_{N-2} constitute the two null-surfaces passing through Σ_{N-2}.

Let it be required to determine the second null-surface passing through the intersection of a surface S_{N-1}, given by $f=$*constant*, and a null-surface, given by $\phi=$*constant*. The characteristic directions at a point in Σ_{N-2}, the subspace of intersection, are given by (7.1), with $\lambda^r=f^r$ and $\mu^r=\phi^r$. But

$$g_{mn}\phi^m\phi^n = 0, \quad . \quad . \quad . \quad . \quad . \quad (7.3)$$

and therefore (7.2) reduces to

$$\alpha^2 g_{mn}f^m f^n + 2\alpha\beta g_{mn}f^m\phi^n = 0. \quad . \quad . \quad . \quad (7.4)$$

This gives as one solution $\alpha=0$, leading by (7.1) to the characteristic direction $\xi^r_{(1)}=\phi^r$, belonging to the given null-surface. The other solution is

$$\frac{\alpha}{\beta} = -2\frac{g_{mn}f^m\phi^n}{g_{mn}f^m f^n}. \quad . \quad . \quad . \quad . \quad . \quad (7.5)$$

Hence the second characteristic direction, belonging to the required null-surface, may be written

$$\xi^r_{(2)} = 2f^r \cdot g_{mn} f^m \phi - \phi^r \cdot g_{mn} f^m f^n, \quad . \quad . \quad (7.6)$$

the sense of $\xi^r_{(2)}$ and the magnitudes of its components being at present of no significance. We note that the two characteristic directions and the normal to the given surface lie in a linear two-space, as is, indeed, also obvious from (7.1), since the normal to S_{N-1} at a point in Σ_{N-2} must lie in the linear two-space normal to Σ_{N-2}.

The second characteristic direction is the second intersection of the null-cone at the point with the linear two-space containing the first characteristic direction and the normal to S_{N-1}.

§ 8. *Geometrical solution of* $\Delta_1\phi = 0$, *when* ϕ *is given over a surface.*

The integrals $\phi = constant$ of the partial differential equation

$$\Delta_1\phi \equiv g^{mn}\phi_m\phi_n = 0 \quad . \quad . \quad . \quad . \quad (8.1)$$

are null-surfaces in the language of this paper. Let it be required to find a function $\phi(x^1, x^2, \ldots, x^N)$ to satisfy (8.1) and to have arbitrarily-assigned values at all points of a surface S_{N-1}. The given subspaces $\phi = constant$ in S_{N-1} are each of $(N-2)$ dimensions; we have seen how to construct the two null-surfaces passing through each such subspace. In this way we obtain two singly-infinite families of null-surfaces. Thus at any point P outside S_{N-1} there are *two* values of ϕ, which are the two values of ϕ on S_{N-1} at the intersections of S_{N-1} with the two null-surfaces (one belonging to each family) passing through P.

If the finite null-cone with vertex P be drawn, the two null-surfaces passing through P touch this cone along two geodesic null-lines. Thus there pass through P two geodesic null-lines such that the two values of ϕ at P are equal respectively to the two values of ϕ at the points where S_{N-1} is cut by these two geodesic null-lines. These two geodesic null-lines may be selected from those forming the finite null-cone by the condition that their directions at the points where they meet S_{N-1} must coincide with one or other of the two characteristic directions associated with each point of the subspace of $(N-2)$ dimensions formed by the intersection of S_{N-1} with the finite null-cone.

If ϕ is constant over S_{N-1}, the method requires modification.

Part II.

§ 9. *Optical significance of geometrical results.*

The subject of geometrical optics deals with rays and phase-waves. It is the limit to which physical optics approximates as the wave-length tends to zero. We wish here briefly to develop a theory of geometrical optics, applicable to the gravitational field of Einstein, and based on a generalization of Huyghens's construction.

We define the mode of propagation of light by the condition that *the history of a light-wave in space-time is an envelope of elementary null-cones.* The history of a light-wave is therefore a null-surface. We define the history of a light-ray as a characteristic line on the history of a light-wave. Our method therefore enables us to deduce from our generalization of Huyghens's construction the well-known equations—(1.1) for the history of a light-wave and (4.4), (4.41) for the history of a light-ray. The optical disturbance from a point-event is the finite null-cone having its vertex at the event, and the histories of the rays are the geodesic null-lines which form the finite null-cone.

It is to be observed that, while this theory is formulated so as to be applicable to the general theory of relativity, all the results of ordinary geometrical optics can be deduced from it by putting

$$g_{mn}dx^m dx^n = d\sigma^2 - \mathrm{V}^2 dt^2, \quad . \ . \ . \quad (9.1)$$

where $d\sigma$ is the spatial line-element and V the velocity of light.

§ 10. *Reflexion at a moving surface.*

The history of a moving body fills up a portion of space-time. That portion is bounded by a surface S_3, which is the history of the surface (in the ordinary sense) of the material body. Let us suppose that a light-wave impinges on the surface. The intersection of the history of the light-wave with S_3 forms a subspace Σ_2 in space-time. Through Σ_2, according to § 7, there pass two null-surfaces, of which one is the history of the incident wave and the other is the history of the reflected wave. The two characteristic directions at any point of Σ_2 belong to the histories of the incident and reflected rays. From the remark at the end of § 7, we see how the history of the reflected ray can be constructed when the history of the incident ray and the normal to the history of the reflecting surface are known.

We may state the law of reflexion in space-time: *The*

histories of the incident and reflected rays and the normal to the history of the reflecting surface lie in an elementary linear two-space. It is impossible to state anything concerning the "angles of incidence and reflexion" in space-time, since the angle between a null-vector and another vector is not defined.

The ratios of the components of a tangent vector to a geodesic null-line indicate the curve in space-time along which light is propagated. The *sense* in which the propagation actually takes place will be indicated by the *signs* of the components of the tangent vector.

Fig. 4.

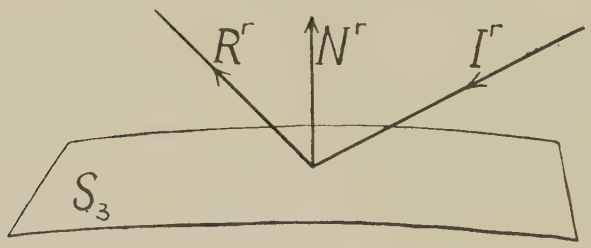

Let us denote by I^r and R^r respectively vectors tangent to the histories of the incident and reflected rays and indicating the senses of propagation of those histories; let N^r be a vector normal to the history of the reflecting surface (fig. 4). Then, instead of (7.6), in which no attention was paid to the sense of $\xi^r_{(2)}$, we write

$$kR^r = 2N^r \cdot g_{mn}I^mN^n - I^r \cdot g_{mn}N^mN^n, \quad . \quad (10.1)$$

where the sign of k is physically determinate.

Now it is evident that, whether N^r be drawn as in the figure or in the reverse direction, we must have

$$N^r = \alpha I^r + \beta R^r, \quad . \quad . \quad . \quad . \quad . \quad (10.2)$$

where α and β have opposite signs. Thus k and $g_{mn}N^mN^n$ must have opposite signs. Remembering that the actual values of the components of R^r have no physical significance, we may write

$$k = -g_{mn}N^mN^n, \quad . \quad . \quad . \quad . \quad . \quad (10.21)$$

and hence

$$R^r = I^r - 2N^r \frac{g_{mn}I^mN^n}{g_{mn}N^mN^n}. \quad . \quad . \quad . \quad (10.3)$$

This is the formula for *reflexion at a moving surface.*

Let us now apply our result to the case of a stationary gravitational field in which x^1, x^2, x^3 are spatial coordinates and x^4 the time. If we understand a range or summation from 1 to 3 when Greek indices are used, such a field is characterized by the equations

$$g_{\mu 4} = 0, \quad \partial g_{mn}/\partial x^4 = 0. \quad . \quad . \quad . \quad (10.4)$$

The spatial line-element is given by

$$d\sigma^2 = g_{\mu\nu} dx^\mu dx^\nu, \quad . \quad . \quad . \quad . \quad (10.41)$$

and the velocity of light by

$$V^2 = -g_{44}. \quad . \quad . \quad . \quad . \quad . \quad (10.42)$$

Fig. 5.

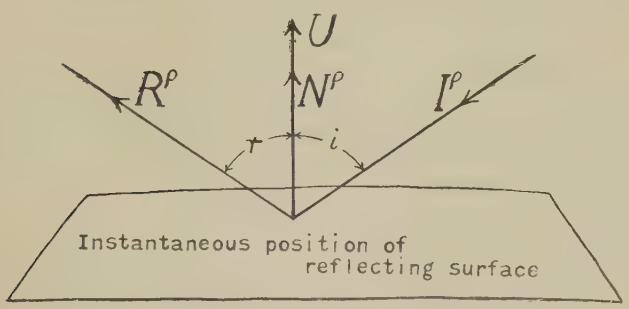

The vectors I^ρ and R^ρ represent the directions of the incident and reflected rays in space. The vector N^ρ is the normal in space to the instantaneous position of the reflecting surface. We shall assume it drawn into the region of incidence (fig. 5) If i and r denote the angles of incidence and reflexion in the ordinary sense, we have

$$\left.\begin{aligned} \cos i &= -g_{\mu\nu} I^\mu N^\nu / [(g_{\rho\sigma} I^\rho I^\sigma)^{\frac{1}{2}} (g_{\theta\phi} N^\theta N^\phi)^{\frac{1}{2}}], \\ \cos r &= g_{\mu\nu} R^\mu N^\nu / [(g_{\rho\sigma} R^\rho R^\sigma)^{\frac{1}{2}} (g_{\theta\phi} N^\theta N^\phi)^{\frac{1}{2}}]. \end{aligned}\right\} \quad (10.5)$$

Since I^r and R^r are null-vectors, we have

$$g_{\rho\sigma} I^\rho I^\sigma = -g_{44} (I^4)^2, \quad g_{\rho\sigma} R^\rho R^\sigma = -g_{44} (R^4)^2. \quad (10.6)$$

Moreover, since x^4 increases along these vectors, I^4 and R^4 are positive. Thus

$$(g_{\rho\sigma} I^\rho I^\sigma)^{\frac{1}{2}} = V I^4, \quad (g_{\rho\sigma} R^\rho R^\sigma)^{\frac{1}{2}} = V R^4. \quad . \quad (10.61)$$

Now, in (10.3) the magnitudes of the components of

I^r and N_r are arbitrary. We may therefore choose them so that I^ρ and N^ρ are unit vectors in space. Then

$$g_{\rho\sigma}I^\rho I^\sigma = 1, \quad g_{\rho\sigma}N\,N^\sigma = 1, \quad . \quad . \quad . \quad (10.62)$$

and hence

$$I^4 = 1/V. \quad . \quad . \quad . \quad . \quad . \quad . \quad (10.63)$$

Thus (10.5) give

$$\cos i = -g_{\mu\nu}I^\mu N^\nu, \quad \cos r = g_{\mu\nu}R^\mu N^\nu/VR^4. \quad (10.7)$$

If dx^1, dx^2, dx^3 denote the infinitesimal displacement in time dx^4 of a hypothetical particle confined to the reflecting surface, we have

$$g_{\mu\nu}dx^\mu N^\nu + g_{44}dx^4 N^4 = 0, \quad . \quad . \quad . \quad (10.71)$$

and, if the displacement of the particle is along the instantaneous normal to the reflecting surface, we have

$$dx^\rho/dx^4 = \theta N_\rho. \quad . \quad . \quad . \quad . \quad . \quad (10.72)$$

Thus, from (10.71),

$$\theta = -g_{44}N^4\,; \quad . \quad . \quad . \quad . \quad . \quad (10.73)$$

and hence, if U denotes the normal velocity of the reflecting surface in the sense of N_ρ,

$$U = -g_{44}N^4, \quad N_4 = U/V^2. \quad . \quad . \quad . \quad (10.74)$$

We deduce

$$\frac{g_{mn}I^m N^n}{g_{mn}N^m N^n} = -\frac{V(V\cos i + U)}{V^2 - U^2}. \quad . \quad . \quad (10.8)$$

Using the first three equations of (10.3), we obtain

$$g_{\mu\nu}R^\mu N^\nu = \frac{V^2\cos i + 2VU + U^2\cos i}{V^2 - U^2}, \quad . \quad (10.81)$$

while the last of (10.3) gives

$$R^4 = \frac{V^2 + 2VU\cos i + U^2}{V(V^2 - U^2)}. \quad . \quad . \quad . \quad (10.82)$$

Thus, substituting in (10.7), we find for the angle of reflexion

$$\cos r = \frac{V^2\cos i + 2VU + U^2\cos i}{V^2 + 2VU\cos i + U^2}$$

$$= \cos i + \frac{2VU\sin^2 i}{V^2 + 2VU\cos i + U^2}. \quad (10.9)$$

Here V is the velocity of light, and U is the normal velocity of the reflecting surface along the normal drawn into the region of incidence.

It must be pointed out that, while (10.3) is believed to be

new and important, (10.9) can be deduced by a direct constructional method by means of the classical Huyghens's construction ; the method presents no difficulties as soon as one is satisfied as to the legitimacy of reducing the problem to that of the incidence of a plane wave on a plane mirror which has a motion of translation in Euclidean space *. The deduction is given here as an example of the general method, which has the advantage of being obviously invariant in character. The result is also valid for a Galileian frame.

§ 11. *Refraction at a moving surface.*

The history of the surface of separation of two media constitutes a surface S_3 in space-time. S_3 divides space-time into two regions, the region of incidence and the region of refraction. Let the null-cones in these regions be respectively

$$g^*_{mn}\eta^m\eta^n = 0, \quad g_{mn}\eta^m\eta^n = 0. \quad . \quad . \quad (11.1)$$

The fundamental tensor is, in general, discontinuous across S_3.

Fig. 6.

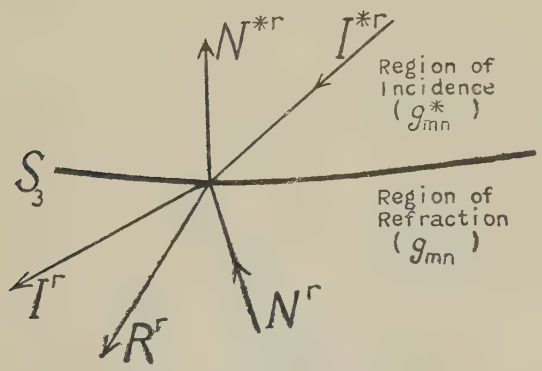

Let a light-wave be incident on the surface of separation. Then the intersection of the history of this wave with S_3 forms a two-space, Σ_2. From each point of Σ_2 there issue four characteristic directions, two in the region of incidence (corresponding to the incident and reflected rays), and two in the region of refraction.

Let $f=0$ be the equation of S_3, and $\phi=0$ the equation of

* A formula equivalent to (10.9), developed in this way for this special case, will be found in Silberstein's 'Theory of Relativity,' p. 89 (1924).

the history of the incident wave. There are two contravariant vectors normal to S_3, viz.:

$$N^{*r} = g^{*rm} f_m, \text{ for the region of incidence ;} \quad (11.2)$$

$$N^r = g^{rm} f_m, \text{ for the region of refraction} \quad (11.21)$$

Similarly the history of the incident wave has two normals at every point where it meets S_3, viz.:

$$I^{*r} = g^{*rm}\phi_m, \text{ in the region of incidence;} \quad (11.22)$$

$$I^r = g^{rm}\phi_m, \text{ in the region of refraction.} \quad (11.23)$$

We shall suppose the sign of ϕ so chosen that I^{*r} indicates the sense of propagation of the incident ray, *i. e.* is directed towards S_3 (fig. 6).

The vectors N^r and I^r are normal to Σ_2 in the region of refraction. Hence (*cf.* (7.1)) the vector R^r, tangent to the history of the refracted ray and indicating its sense of propagation, will be given by

$$kR^r = \alpha N^r + \beta I^r, \quad (11.3)$$

where k is a number whose sign is physically determinate when values have been assigned to α and β, and where the ratio $\alpha : \beta$ is determined by

$$\alpha^2 g_{mn} N^m N^n + 2\alpha\beta g_{mn} I^m N^n + \beta^2 g_{mn} I^m I^n = 0. \quad (11.31)$$

If the roots of this equation are imaginary, there is *total reflexion*. If the roots are real, we have

$$\frac{\alpha}{\beta} = -\frac{g_{mn} I^m N^n}{g_{mn} N^m N^n}\left[1 \pm \left(1 - \frac{g_{pq} I^p I^q \cdot g_{uv} N^u N^v}{(g_{pq} I^p N^q)^2}\right)^{\frac{1}{2}}\right]. \quad (11.4)$$

Now, in the particular case where $g_{mn} = g^*_{mn}$ on S_3, I^r is a null-vector in the region of refraction. Thus (11.4) reduces to

$$\frac{\alpha}{\beta} = -\frac{g_{mn} I^m N^n}{g_{mn} N^m N^n}[1 \pm 1]. \quad (11.41)$$

But in this case there will be no refraction; therefore we require $\alpha = 0$. Thus the minus sign must be taken in (11.41). From continuity this sign must be taken in general in (11.4). Furthermore, in the particular case considered, R^r and I^r must indicate the same sense. Hence we see that the general formula may be written

$$R = I^r - N^r \frac{g_{mn} I^m N^n}{g_{mn} N^m N^n}\left[1 - \left(1 - \frac{g_{pq} I^p I^q \cdot g_{uv} N^u N^v}{(g_{pq} I^p N^q)^2}\right)^{\frac{1}{2}}\right]. \quad (11.5)$$

This is the formula for *refraction at a moving surface.*

We may state the following law of refraction: *The history of the refracted ray and the normals (in the region of refraction) to the histories of the incident wave and the surface of separation lie in an elementary linear two-space.* An analogous theorem holds in the region of incidence.

Let us apply our result to the case of refraction at a moving surface in a stationary gravitational field. We assume

$$g^*_{\mu 4} = g_{\mu 4} = 0, \qquad \frac{\partial g^*_{mn}}{\partial x^4} = \frac{\partial g_{mn}}{\partial x^4} = 0, \quad . \quad (11.6)$$

and, on S_3, the history of the moving surface,

$$g^*_{\mu\nu} = g_{\mu\nu} \quad . \quad . \quad . \quad . \quad . \quad (11.61)$$

Hence we have

$$I^{*\rho} = I^\rho, \qquad N^{*\rho} = N^\rho. \quad . \quad . \quad (11.62)$$

Let the magnitudes of I^ρ and N^ρ be chosen so that

$$g_{\mu\nu} I^\mu I^\nu = 1, \qquad g_{\mu\nu} N^\mu N^\nu = 1. \quad . \quad (11.63)$$

Let V^*, V be the velocities of light in the regions of incidence and refraction respectively. Then

$$V^{*2} = -g^*_{44}, \qquad V^2 = -g_{44}. \quad . \quad . \quad (11.64)$$

Let U be the normal velocity of the moving surface, measured from the region of refraction into the region of incidence, and let us define μ and ν by the equations

$$V^* = \mu V, \qquad U = \nu V. \quad . \quad . \quad . \quad (11.65)$$

Then, as in (10.63) and (10.74) respectively,

$$I^{*4} = 1/V^*, \qquad N^4 = U/V^2 = \nu/V. \quad . \quad (11.66)$$

Now

$$I^4 = g^{44} g^*_{44} I^{*4} = g^*_{44} I^{*4}/g_{44} = \mu/V, \quad . \quad (11.67)$$

and therefore

$$g_{mn} I^m I^n = 1 - \mu^2, \qquad g_{mn} N^m N^n = 1 - \nu^2. \quad . \quad (11.68)$$

Also, since

$$\cos i = -g_{\mu\nu} I^\mu N^\nu, \quad . \quad . \quad . \quad . \quad (11.69)$$

where i denotes the angle of incidence in the ordinary sense (fig. 7), we have

$$g_{mn} I^m N^n = -\cos i - \mu\nu. \quad . \quad . \quad (11.7)$$

Thus we have, as the evaluation of the expression in (11.5),

$$\left\{1-\frac{g_{pq}\mathrm{I}^p\mathrm{I}^q \cdot g_{uv}\mathrm{N}^u\mathrm{N}^v}{(g_{pq}\mathrm{I}^p\mathrm{N}^q)^2}\right\}^{\frac{1}{2}} = \left\{1-\frac{(1-\mu^2)(1-\nu^2)}{(\cos i+\mu\nu)^2}\right\}^{\frac{1}{2}}, \quad (11.71)$$

Fig. 7.

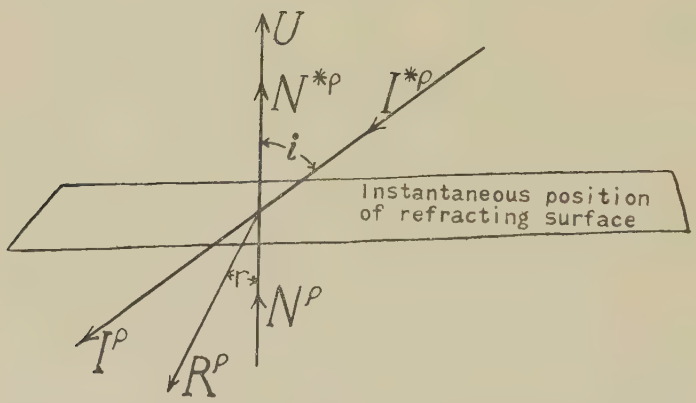

and if we denote this quantity by K, we have, by (11.5),

$$\mathrm{R}^\rho = \mathrm{I}^\rho + \mathrm{N}^\rho \frac{\cos i+\mu\nu}{1-\nu^2}(1-\mathrm{K}), \quad . \quad . \quad . \quad . \quad . \quad . \quad . \quad (11.72)$$

$$\mathrm{R}^4 = \frac{\mu}{\mathrm{V}} + \frac{\nu}{\mathrm{V}}\frac{\cos i+\mu\nu}{1-\nu^2}(1-\mathrm{K})$$

$$= \frac{(\mu+\nu\cos i)-\nu\mathrm{K}(\cos i+\mu\nu)}{\mathrm{V}(1-\nu^2)}. \quad . \quad . \quad . \quad . \quad . \quad . \quad . \quad (11.73)$$

But, if r denotes the angle of refraction in the ordinary sense, we have

$$\cos r = -g_{\mu\nu}\mathrm{R}^\mu\mathrm{N}^\nu/\mathrm{V}\mathrm{R}^4, \quad . \quad . \quad . \quad (11.74)$$

and therefore, by the above equations,

$$\cos r = \frac{-\nu(\mu+\nu\cos i)+\mathrm{K}(\cos i+\mu\nu)}{(\mu+\nu\cos i)-\nu\mathrm{K}(\cos i+\mu\nu)}. \quad . \quad (11.75)$$

This is the formula for refraction at a moving surface in a stationary gravitational field, the quantities μ and ν being defined by (11.65) and K by (11.71).

If $\mathrm{U}=0$, we have $\nu=0$ and

$$\mathrm{K}^2 = 1-\frac{1-\mu^2}{\cos^2 i} = \frac{\mu^2-\sin^2 i}{\cos^2 i}. \quad . \quad (11.8)$$

Equation (11.75) then gives

$$\cos r = \frac{K \cos i}{\mu} \quad . \quad . \quad . \quad . \quad . \quad . \quad (11.81)$$

Hence

$$\sin^2 r = 1 - \frac{K^2 \cos^2 i}{\mu^2} = \frac{\sin^2 i}{\mu^2} \quad . \quad . \quad . \quad (11.82)$$

or

$$\frac{\sin i}{\sin r} = \mu, \quad . \quad . \quad . \quad . \quad . \quad . \quad (11.83)$$

the ordinary formula for refraction at a stationary surface.

XXVII. *On the Constant of Mass Action.*

By R. D. Kleeman, *B.A., D.Sc.**

THE molecules taking part in a gaseous reaction according to a given reaction equation may be divided into two kinds, depending on their behaviour when isolated. One kind does not dissociate, while the other kind dissociates into molecules which themselves do not dissociate. Thus, for example, according to the gaseous reaction expressed by the equation

$$2HI \rightleftarrows H_2 + I_2, \quad . \quad . \quad . \quad . \quad . \quad (1)$$

the iodine and hydrogen molecules when isolated do not dissociate; while the hydrogen iodide molecules when isolated dissociate in part into molecules of hydrogen and iodine. Again, in the case of the reaction expressed by the equation

$$2CO_2 \rightleftarrows 2CO + O_2, \quad . \quad . \quad . \quad . \quad . \quad (2)$$

the carbon dioxide molecules when isolated dissociate in part into molecules of carbon monoxide and oxygen, while molecules of the latter kind on isolation remain unchanged. If the molecules H_2, I_2, and O_2 also dissociate when isolated, this would be expressed by the additional reaction equations

$$I_2 \rightleftarrows 2I,$$

$$H_2 \rightleftarrows 2H,$$

$$O_2 \rightleftarrows 2O.$$

The molecules which now dissociate on isolation are HI, I_2,

* Communicated by the Author.

H_2, O_2, and the molecules and atoms that do not dissociate are CO, I, and H.

It is very important to make a distinction between these two kinds of molecules. Every gaseous reaction would evidently involve both kinds. It will be convenient to distinguish them by names; in this paper the molecules that do not dissociate on isolation will be called sepro-stable, and those that dissociate sepro-unstable molecules.

The sepro-stable molecules when isolated will evidently obey the gas equation, which for our present purpose will be written for one mol in the form

$$v = \frac{RT}{p}, \quad . \quad . \quad . \quad . \quad . \quad . \quad . \quad . \quad (3)$$

where v denotes the volume at the pressure p and absolute temperature T. The sepro-unstable molecules will also obey this equation if there be no change in the number of molecules on dissociation. Hydrogen iodide is a case in point: two molecules on dissociation form a molecule of hydrogen and a molecule of iodine, and thus the pressure would not be altered. On the other hand, if molecules of CO_2 are isolated from a reacting mixture, some of them will dissociate till equilibrium exists between the remaining CO_2 molecules and the dissociation products CO and O_2. The total number of molecules in the end will, however, not be the same as the number of CO_2 molecules isolated in the beginning. Besides, the total number of molecules when equilibrium has been reached will evidently depend on the volume. The resultant mixture will therefore not obey the gas equation, but an equation which for one mol of the original molecules we will write in the form

$$v = \frac{RT}{p} + \Sigma \frac{A_n}{p^n}, \quad . \quad . \quad . \quad . \quad . \quad . \quad (4)$$

where A_n is a function of T. In general it may be said that sepro-stable molecules on being isolated from a reacting mixture obey the gas equation (3), while sepro-unstable molecules obey the equation (4), but that in certain types of sepro-unstable molecules the function A_n is zero.

Let us next consider the constant of mass-action of a reaction between the substances A, B, C, D in equilibrium, proceeding according to the reaction equation

$$aA + bB \rightleftarrows cC + dD, \quad . \quad . \quad . \quad . \quad . \quad (5)$$

where a molecules * of the substance A and b molecules of the

* Meaning gram molecules or mols.

substance B combine to form c molecules of the substance C and d molecules of the substance D, and *vice versâ*. The substances A and B will be supposed sepro-stable and the substances C and D sepro-unstable.

Let us consider two different equilibrium systems of these molecules at the same temperature, obtained by allowing two different mixtures of the reacting substances to come to equilibrium in reservoirs, shown diagrammatically in fig. 1,

Fig. 1.

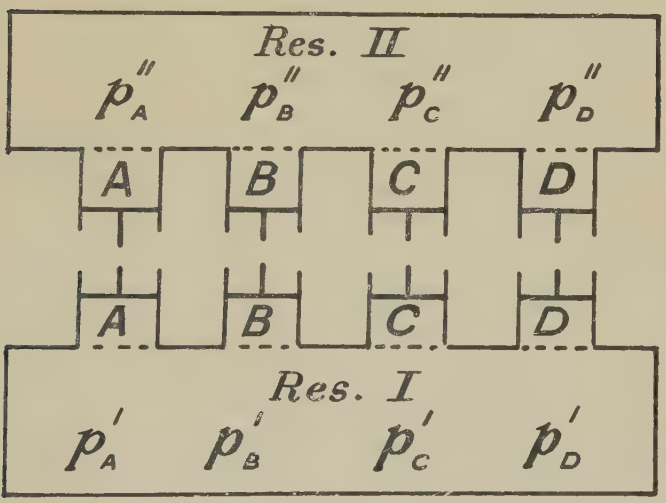

and let these two systems be so large that removal of small quantities of the reacting molecules does not appreciably alter the composition. Furthermore, let us suppose that the vessels are provided with membranes permeable only to molecules A, B, C, and D respectively, in communication with cylinders provided with pistons, by means of which any given component of the mixture may be withdrawn, or added to either system. Now let us:

(*a*) withdraw from reservoir I. a molecules A and b molecules B at the partial pressures p_A' and p_B', at which they are present in the reservoir. The free energy change for this step is evidently zero, since the partial pressures of the substances are not measurably altered.

(*b*) change reversibly the pressure of the two gases to the pressures p_A'' and p_B'', at which they exist in the reservoir II.

The free energy increase of this step is

$$\Delta F_1 = a\int_{p_{A'}}^{p_A''} v\,.\,\partial p + b\int_{p_{B'}}^{p_B''} v\,.\,\partial p = aRT\ln\frac{p_A''}{p_A'} + bRT\ln\frac{p_B''}{p_B'},$$

since these are sepro-stable substances and the gas law (3) is obeyed.

(*c*) introduce the gases into the reservoir II., and since this does not measurably affect the partial pressures, the free energy increase is again zero.

(*d*, *e*, *f*) by a similar series of steps remove c molecules of the substance C and d molecules of the substance D from the reservoir II. and introduce into the reservoir I. The pressures in the cylinders during the process of removing the molecules from the reservoir II. will not be the same as the partial pressures p_C'' and p_D'' in the reservoir, on account of the molecules being sepro-unstable. As soon as a number of molecules C have passed through a permeable membrane into the associated cylinder they dissociate till equilibrium is reached between the undissociated molecules C and the dissociation products, and a similar change takes place with the molecules D. The pressures in the cylinders will therefore be *greater* than the partial pressures in the reservoir, and we will therefore write them $C''p_C''$ and $D''p_D''$, where C'' and D'' are quantities greater than unity. Similarly, when the molecules are transferred into the reservoir I., their pressures in the cylinders will not be equal to the partial pressures p_C' and p_D' in the reservoir but greater, and will be written $C'p_C'$ and $D'p_D'$, where C' and D' are quantities greater than unity.

The total free energy increase during the foregoing operation is

$$\Delta F_2 = c\int_{C''p_C''}^{C'p_C'} v\,.\,\partial p + d\int_{D''p_D''}^{D'p_D'} v\,.\,\partial p = cRT\ln\frac{p_C'}{p_C''} + dRT\ln\frac{p_D'}{p_D''}$$
$$+ cRT\ln\frac{C'}{C''} + dRT\ln\frac{D'}{D''} + c\left[\Sigma\frac{-C_n}{(n-1)p^{n-1}}\right]_{C''p_C''}^{C'p_C'}$$
$$+ d\left[\Sigma\frac{-D_n}{(n-1)p^{n-1}}\right]_{D''p_D''}^{D'p_D'},$$

where, since the substances are sepro-unstable, the equations

$$v = \frac{RT}{p} + \Sigma\frac{C_n}{p^n}$$
$$v = \frac{RT}{p} + \Sigma\frac{D_n}{p^n}$$

are used instead of the gas equation, where C_n is a function of T referring to the substance C, and D_n a function of T referring to the substance D.

The foregoing steps are supposed to be carried out at corresponding times and so slowly that the removed substances are in chemical equilibrium while in the cylinders, and the substances A and B removed from the reservoir I. react in the reservoir II. to replace the substances C and D which have been removed therefrom, which in turn react in the reservoir I. to form the substances A and B. Each step has then been carried out isothermally and reversibly, and the composition of each system is just what it was at the beginning of the process. The total free energy increase is therefore zero, or

$$\Delta F_1 + \Delta F_2 = 0,$$

which becomes, after substituting for ΔF_1 and ΔF_2 and rearranging

$$\begin{aligned} RT \ln \frac{(p_C'')^c (p_D'')^d}{(p_A'')^a (p_B'')^b} = RT \ln \frac{(p_C')^c (p_D')^d}{(p_A')^a (p_B')^b} \\ + \Big[cRT \ln C' + c\Sigma \frac{-C_n}{(n-1)(C' p_C')^{n-1}} \\ - cRT \ln C'' - c\Sigma \frac{-C_n}{(n-1)(C'' p_C'')^{n-1}} \\ + dRT \ln D' + d\Sigma \frac{-D_n}{(n-1)(D' p_D')^{n-1}} \\ - dRT \ln D'' - d\Sigma \frac{-D_n}{(n-1)(D'' p_D'')^{n-1}} \Big]. \quad (6) \end{aligned}$$

If we write X for the expression within the square brackets in this equation and assume that

$$X = 0, \quad . \quad . \quad . \quad . \quad . \quad . \quad . \quad (7)$$

the equation becomes

$$RT \ln \frac{(p_C'')^c (p_D'')^d}{(p_A'')^a (p_B'')^b} = RT \ln \frac{(p_C')^c (p_D')^d}{(p_A')^a (p_B')^b},$$

whence

$$\frac{(p_C'')^c (p_D'')^d}{(p_A'')^a (p_B'')^b} = \frac{(p_C')^c (p_D')^d}{(p_A')^a (p_B')^b}.$$

This equation expresses that if the temperature is kept constant the value of each side is independent of the values

of the partial pressures, and we may accordingly write

$$K = \frac{(p_C)^c (p_D)^d}{(p_A)^a (p_B)^b}, \quad . \quad . \quad . \quad . \quad . \quad (8)$$

where K is a constant at constant temperature which has been called the constant of mass action. If, however, equation (7) does not hold, equation (6) may be written in the form

$$K = \frac{(p_C'')^c (p_D'')^d}{(p_A'')^a (p_B'')^b} = \frac{(p_C')^c (p_D')^d}{(p_A')^a (p_B')^b} e^{X/RT} \quad . \quad . \quad . \quad (9)$$

It is evident that K is now not independent of the values of the partial pressures of the interacting molecules. Since these pressures are fundamentally functions of the independent variables, the volume of the mixture, its temperature, and the masses of the elemental constituents, K is in general also a function of these variables.

It appears, therefore, that in order that in general K be a constant at constant temperature, equation (7) must hold besides equation (6). But there is *à priori* no thermodynamical reason why equation (7) should hold exactly, though it may of course hold approximately in the case of most reactions. In previous investigations of the constant of mass action it has been tacitly assumed, following van't Hoff, that the substances C and D when taken out of the reservoir II. do not dissociate. In that case C′, C″, D′, and D″ would each be unity, and C_n and D_n each zero, giving to X a zero value. But this would assume that on one side of the permeable membranes the molecules C and D may dissociate, while on the other side they do not, which is manifestly an untenable assumption.

It may be suggested that possibly the variables C′, p_C', C″, p_C'', D′, p_D', D″, p_D'' in the expression X identically vanish, and that therefore equation (7) holds. In that case

$$cRT \ln C' + c\Sigma \frac{-C_n}{(n-1)(C'p_C')^{n-1}} = 0$$

separately, and the other similar expressions of X also vanish separately, since each expression contains a different set of variables. On adding $cRT \ln p_C'$ to each side of the equation, it may be written

$$\int v \cdot \partial(C'p_C') = RT \ln p_C' \quad . \quad . \quad . \quad . \quad (10)$$

by means of equation (4). The equation is manifestly absurd, since C′ cannot vanish from the left-hand side independently of p_C'. The expression X cannot therefore

identically vanish, and equation (7) does not hold. It may happen, however, that the value of the integral is not sensitive to variations of C′ from unity upwards over a considerable range, in which case the equation holds approximately. If the same is true for the integral in a similar equation referring to the substance D, equation (7) would hold approximately.

It may also be suggested that possibly equation (7) identically vanishes if C′, C″, D′, D″, C_n, and D_n are expressed in terms of the partial pressures by the help of the mass-action equation (8), and that therefore the latter equation holds. Let us suppose that this is true, though actually it can be shown not to be true in most cases. The constancy of K will then still rest on the assumption expressed by equation (7), which is an assumption, since in general, without introducing assumptions, the equation $V+Z=0$ may be decomposed into the two equations $V+W=0$ and $Z-W=0$ only, where W is an arbitrary function.

But it is likely that in most cases K is approximately a function of the temperature only, as shown by experiment. The reason for this can be given. If the dissociation is small the substances C and D approximately obey the gas laws, and in that case, C′, C″, D′, D″ do not differ appreciably from unity and the quantities C_n and D_n are small, and hence X is small. In that case K is approximately a function of the temperature only. If the dissociation is large the substances C and D will again approximately obey the gas laws, and C_n and D_n will be small as before. The quantities C′, C″, D′, D″ will, however, now be large. The expression involving them may be written

$$c\mathrm{RT}\ln\frac{\mathrm{C}'}{\mathrm{C}''}+d\mathrm{RT}\ln\frac{\mathrm{D}'}{\mathrm{D}''}.$$

Since the number of undissociated molecules available is small the pressure of the mixture may be varied considerably without much further dissociation taking place, and hence we may write $\mathrm{C}'=\mathrm{C}''+x$ and $\mathrm{D}'=\mathrm{D}''+y$, where x and y are quantities which are very small in comparison with C″ and D″ respectively. The foregoing expression therefore becomes

$$c\mathrm{RT}\ln\left(1+\frac{x}{\mathrm{C}''}\right)+d\mathrm{RT}\ln\left(1+\frac{y}{\mathrm{D}''}\right),$$

which is approximately equal to zero. Thus, under these conditions also the constant of mass action is approximately a function of the temperature only. This may therefore also hold for intermediate degrees of dissociation, which is

rendered highly likely from the following considerations: The series $\Sigma \frac{C_n}{p^n}$ in the equation of the substance C is as a whole positive, and its integral $\Sigma \frac{-C_n}{(n-1)p^{n-1}}$ therefore as a whole negative. The quantities $c\mathrm{RT} \ln C'$ and

$$c\Sigma \frac{-C_n}{(n-1)(C'p_C')^{n-1}}$$

will therefore have different signs and may therefore approximately cancel each other. This corresponds to the integral in equation (10) not being sensitive to variations of C'. Similar remarks apply to the terms involving D', C'', and D''.

It must happen, however, in certain cases and under certain conditions, that the constant of mass action varies appreciably with the volume of the mixture and the masses of the elemental constituents. Taking this possibility into account will help to explain many things that have been puzzling the chemist up to the present.

This possibility can also be predicted from purely kinetic considerations. Let us consider, for example, the reaction expressed by equation (2). The chance of two molecules of CO_2 forming two molecules of CO and one of O_2 depends on their chance of encounter. The number of molecules of CO_2 dissociating per sec. per c.c. is therefore given by

$$k_1 C_{CO_2}^2,$$

where C_{CO_2} denotes the concentration of the CO_2 molecules and k_1 the velocity constant of dissociation. But the chance of a molecule of CO_2 getting dissociated may not only depend on its chance of encountering another CO_2 molecule but on its previous encounters with other molecules, or two CO_2 molecules on encountering each other will dissociate only if they have been activated, so to speak, by previous encounters with other molecules. This activation will be expressed by the factor, or activation constant, κ_1 in the foregoing expression, so that the number of molecules dissociating per second is

$$\kappa_1 k_1 C_{CO_2}^2.$$

Similarly, the number of molecules of O_2 and CO forming molecules of CO_2 per second per c.c. is not expressed by

$$k_2 C_{CO} C_{O_2},$$

but by

$$\kappa_2 k_2 C_{CO} C_{O_2},$$

where C_{CO} and C_{O_2} denote the concentrations of the CO and O_2 molecules respectively, and κ_2 the activation constant of a pair of molecules due to encounters with other molecules. When there is equilibrium

$$\kappa_1 k_1 C_{CO_2}^2 = \kappa_2 k_2 C_{CO} C_{O_2}, \quad . \quad . \quad . \quad . \quad (11)$$

whence

$$K = \frac{\kappa_1 k_1}{\kappa_2 k_2}, \quad . \quad . \quad . \quad . \quad . \quad . \quad (12)$$

where K is the constant of mass action. From the kinetic theory of gases it follows that k_1 and k_2, expressing chances of encounter per unit concentration, are functions of the temperature only. But the quantities κ_1 and κ_2 evidently depend on the frequencies of the encounters and their nature, and are therefore functions of the fundamental independent variables the volume of the mixture, its temperature, and the masses of the elemental constituents. Therefore, unless $\kappa_1 = \kappa_2$, K will also be a function of these variables. It may be pointed out that κ_1 and κ_2 contain the whole theory of catalytic action, a subject that will be discussed in detail at some future period.

It may finally be pointed out that if K in general is not a constant but a function of the above-mentioned independent variables, differential equations should exist connecting K with these variables. These differential equations will be given in a subsequent paper.

Schenectady, N.Y., U.S.A.

XXVIII. *The Conductivities of some Dilute Amalgams at various Temperatures.* *By* A. L. Johns, *M.Sc., and* E. J. Evans, *D.Sc., Physics Department, University College of Swansea*.*

Introduction.

THE work described in this paper is a continuation of that carried out by E. J. Williams † and T. I. Edwards ‡, who determined accurately the conductivities of dilute amalgams of cadmium, indium, magnesium, thallium, germanium, antimony, yttrium, cerium, aluminium, and beryllium.

Many investigations have been made on the conductivity of liquid amalgams, notably by Matthiessen and Vogt §,

* Communicated by Prof. E. J. Evans.
† Phil. Mag. Sept. 1925, p. 589.
‡ Phil. Mag. July 1926, p. 1.
§ Phil. Mag. (4) xxiii. p. 171 (1862).

Weber*, and Batelli†, but these observations, in the majority of cases, have been made at comparatively low temperatures, and furthermore the results are not altogether in agreement.

In this research the dilute amalgams investigated were those of germanium, gallium, silver, and copper, and observations were carried out between room temperature and about 300° C. When the metal employed is only soluble to a small extent in mercury, observations could only be made at comparatively high temperatures, but in other cases it was possible to make observations at both high and low temperatures.

One of the main difficulties encountered in these experiments, especially when the solubility of the metal is small, is uncertainty concerning the purity of the specimen. This uncertainty is more pronounced in the case of rare metals, which are difficult to prepare in a state of purity. For this reason, the experiments carried out by Edwards‡ on germanium amalgams were repeated for two concentrations of the metal. The germanium used in these experiments was supplied by Adam Hilger, and had been analysed spectroscopically. The specimen of the rare metal gallium was also obtained from the same source, and, in each case, the metals used in preparing the amalgams were in a high state of purity. The results of the spectroscopic analysis will be given later.

In the case of copper and silver there was no difficulty in obtaining material of a high state of purity.

The results obtained in this investigation will be examined in relation to a theory put forward by Skaupy §.

Let L and η be the conductivity and viscosity respectively of the pure solvent (mercury), and c the concentration of metal dissolved in mercury expressed in gram atoms per 100 gram atoms of mercury.

If ΔL and $\Delta\eta$ be the changes in conductivity and viscosity corresponding to the small concentration c, and putting

$$\frac{1}{L}\frac{\Delta L}{c} = l \quad \text{and} \quad \frac{1}{\eta}\frac{\Delta\eta}{c} = r,$$

Skaupy showed that $l_\infty + r_\infty$ ‖ is of the same order of magnitude for different metals dissolved in mercury. Except in the case of some alkali amalgams, the values of l_∞ are

* *Wied. Ann.* xxiii. p. 470 (1884).

† *Atti Accad. Lincei*, (4) iv. p. 206 (1887).

‡ *Loc. cit.*

§ Skaupy, *Zeit. für Physik. Chemie*, lxviii. p. 560 (1907); *Verh. Deut. Phys. Ges.* xvi. p. 156 (1914); *ibid.* xviii. p. 252 (1916); *Phys. Zeit.* xxi. p. 597 (1920).

‖ l_∞ and r_∞ express the values of l and r for infinite dilution.

approximately the same when different metals are dissolved in mercury, and as the variation of viscosity with concentration is not sufficiently known, especially in the neighbourhood of 300° C., the values of l_∞ for the different amalgams will be discussed in the present paper. Skaupy * also showed, in the case of amalgams in which the change of viscosity is not as great as in the alkali amalgams, that

$$\frac{l_\infty - l}{c}$$

is constant.

Before the work on the amalgams was commenced, preliminary experiments on the electrical conductivity of pure mercury contained in a quartz tube were carried out at various temperatures ranging from 0° C. to about 300° C. The results agreed within experimental error with those already obtained by Williams † and Edwards ‡.

The amalgams employed in this investigation were very dilute, the percentage weight of the metals dissolved in mercury varying from about ·01 to ·1.

In most cases the tube containing the amalgams was open to the atmosphere, but the results for one or two concentrations in the case of silver, gallium, and copper were confirmed by preparing the amalgams and measuring their conductivities in a sealed apparatus containing hydrogen.

Experimental Arrangement.

It is not proposed here to enter into a detailed account of the apparatus and method of using it, as that has already been given by Williams § and Edwards ‖.

The conductivity of an amalgam was determined by measuring the electrical resistance of a fine cylindrical column of it by means of a Callendar and Griffiths bridge in conjunction with a moving-coil galvanometer of high sensitivity. The resistances measured were about 0·6 ohm, and could be determined with an accuracy of ·00005 ohm. This latter quantity was equivalent to a change of temperature of the amalgam column of about ·09° C. at 300° C. The various resistances of the Callendar and Griffiths bridge were all calibrated in terms of the largest resistance by the usual method, and thus the relative values of the bridge resistances were accurately known. These relative values

* *Loc. cit.*
† *Loc. cit.*
‡ *Loc. cit.*
§ *Loc. cit.*
‖ *Loc. cit.*

are sufficient for an accurate determination of the temperature coefficient of resistivity of mercury or of an amalgam. Even for a determination of the absolute value of the resistivity of mercury or of an amalgam at a given temperature, a knowledge of the correct absolute values of the various bridge resistances is not necessary if the standard value (94074×10^{-9}) of the resistivity of mercury at 0° C. be used. This value of the resistivity corresponds to a known value of the resistance of a column of mercury at 0° C., as determined by the bridge. The values of the resistivities of pure mercury at various temperatures previously obtained by Williams and Edwards were again confirmed in preliminary experiments; and, as the resistances of the various amalgams were measured in the same tube and under the same conditions as employed for mercury the absolute values of the resistivities and conductivities of the amalgams could be determined at the same temperature.

The mercury or amalgam was placed in a quartz capillary tube, which opened out at each end into wide limbs at right angles to the capillary. Glass tubes containing mercury and having short pieces of platinum wires sealed into their closed ends fitted into the limbs, and served as leads for the current. This tube and also the special glass apparatus used for determinations in an atmosphere of hydrogen were described in detail by Edwards*.

When the latter apparatus was employed, the resistances of both mercury and amalgam were determined at the same temperature. The resistance of the glass leads was measured separately, and in this way the resistance of a column of mercury or amalgam of constant dimensions was obtained after the application of a small correction for the expansion of the quartz envelope. The resistance measurements at various temperatures were obtained by immersing the tube in a liquid of an appropriate boiling-point. The substances employed were water, aniline, engenol, and diphenylamine. The temperature of each boiling liquid, which was contained in an iron bath, did not remain absolutely constant with continual use, but slowly increased in value with time.

In this way the resistance could be measured at a practically steady temperature, which was determined by a calibrated platinum thermometer placed alongside the capillary. The temperature of the amalgam column corresponding to a given resistance could be determined accurately to within 1/10° C. even at 300° C., and the temperature measurements

* *Loc. cit.* pp. 4–6.

have the necessary accuracy in comparison with those of the resistance.

The main experimental difficulties encountered in the research were caused by thermoelectric currents and the formation of air-bubbles in the capillary, especially at high temperatures. The former difficulty was overcome by keeping the galvanometer arm of the Wheatstone bridge closed, and adjusting the resistances so that there was no change in deflexion on completing the battery circuit. The latter difficulty was overcome by heating the column in an electric furnace to a higher temperature (320° C.) than that at which a determination was made. The tube was then carefully examined by a lens, and if a bubble was observed, the warm amalgam was run through the tube until the bubble was removed. When an amalgam of the desired concentration could be prepared at room temperature, the quartz tube was allowed to cool from the temperature of the electric furnace, and the resistance of the column determined at room temperature. The column was then placed in the liquid heating bath, and the resistance again determined at the high temperature. The tube was then removed from the bath and carefully examined for air-bubbles. The presence of air-bubbles was again tested by redetermining the resistance of the column at room temperature. In general it was found that the resistance of the column returned to its previously determined value. It is, however, of interest to point out that the solution in mercury of the metals employed in this investigation produced a diminution of resistance, whilst the presence of a small air-bubble increased the resistance. The diminution of resistance in the case of very dilute amalgams is small, and great care was exercised in getting rid of all air-bubbles.

Furthermore, in the case of metals like germanium only sparingly soluble in mercury even at 300° C., the column was kept at the boiling-point of diphenylamine for several hours to ensure that the small quantity of metal put into the limbs had completely diffused through the mercury. When this had occurred the resistance of the column became constant.

Calculation of the Conductivities of the Amalgams.

The resistivities of pure mercury at various temperatures, as determined by Williams and Edwards, can be represented by the equation

$$\rho_t = \rho_0(1 + \cdot 0_3 8877\, t + \cdot 0_6 977\, t^2 + \cdot 0_9 19\, t^3)\ *.$$

* Edwards in deducing this equation from his experimental results had corrected for the expansion of quartz.

The above equation also represents the results of the present experiments on mercury within experimental error.

If ${}_aR_t$ be the resistance of the amalgam column of length l and cross-section A at temperature t, and ${}_mR_t$ the corresponding quantity for mercury, then

$$ {}_aR_t = {}_a\rho_t \cdot \frac{l}{A} $$

$$ {}_mR_t = {}_m\rho_t \cdot \frac{l}{A} $$

and

$$ {}_aP_t = \frac{{}_aR_t}{{}_mR_t} \cdot {}_m\rho_t. $$

Thus the resistivity and conductivity of an amalgam at temperature "t" can be calculated from the resistivity of mercury at the same temperature, and the corresponding values of the resistances of the amalgam and mercury at temperature "t."

The percentage probable error in the values of the resistivity and conductivity of mercury and amalgams is estimated to be on the average about ·01.

Since the amalgams of germanium, gallium, and copper employed in these experiments were so very dilute, the values of $\frac{1}{c}\frac{\Delta L}{L}$ and l_∞ given in Table V. cannot claim great accuracy, and errors ranging from about 4 to 8 per cent. depending on concentration are possible on the average. The same is also true for the extremely dilute silver amalgams, but the results for the more concentrated amalgams were determined with greater accuracy.

Experimental Results.

The Electrical Conductivities of dilute Germanium Amalgams.

Edwards * determined the conductivities of four dilute germanium amalgams having concentrations varying from ·0339 to ·0753 at 301·8° C., and also the conductivity of an amalgam having concentration of ·0182 at 250·1° C. He obtained the value 4·7 for $l_\infty \times 10^2$. The solubility of the metal in mercury is comparatively small, and the resistance measurements were consequently carried out at about 300° C. The change of resistance as compared with mercury is small, and the purity of the germanium is therefore a question of

* *Loc. cit.*

primary importance. It was considered advisable to repeat Edwards's observations for two concentrations, employing a specimen of germanium obtained from Messrs. Adam Hilger, Ltd., London. The sample from which the specimen was supplied was subjected by them to spectroscopic analysis. The only foreign line found in the spectrum was a very faint one at 2516 Å.U., indicating the presence of a minute trace of silicon. Chemically a trace of sulphur and a minute quantity of arsenic were recognized, but these substances did not give any lines in the spectrum. These results show that the specimen of germanium employed in the present experiments was in a high state of purity. Some difficulty was experienced in bringing about solution of small pieces of the metal in mercury, even at 300° C. The small pieces of germanium, although lighter than mercury, were found sticking to the sides and bottom of the quartz bulbs at the ends of the capillary, and only a small proportion of the metal had passed into solution. This difficulty was not, however, encountered when the germanium was powdered, and the measured resistance showed a diminution as compared with mercury. The specimen of the metal employed by Edwards was already in the powdered form, and was obtained from Dr. Schuchardt Görlitz.

TABLE I.

Nature of Amalgam.	Temp. in degrees centigrade.	Percentage weight of substance in Mercury.	Concentration "c."	Resistivity of Mercury, $\times 10^8$.	Conductivity of Mercury.	Resistivity of Amalgam, $\times 10^8$.	Conductivity of Amalgam.
Germanium.	299·28	·01226	·0339	12778	7827	12757	7839
	,,	·02503	·0692	,,	,,	12733	7853
Gallium.	301·0	·00764	·0219	12803	7811	12787	7820
	,,	·01427	·0408	,,	,,	12772	7829
	,,	·03299	·0944	,,	,,	12740	7849
	,,	·04497	·1287	,,	,,	12709	7868
*	300·33	·01427	·0408	12793	7817	12764	7835
Copper.	301·76	·01003	·0316	12813	7804	12786	7821
	,,	·02006	·0633	,,	,,	12763	7835
*	,,	·0150	·0473	,,	,,	12776	7827

* These determinations were made in a sealed apparatus containing an atmosphere of hydrogen.

The experimental results are given in Tables I. and V. In Table I. the concentration "c" is expressed in gram atoms per 100 gram atoms of mercury, *i. e.* in atom atoms per cent. approximately. In the fourth column of Table V. are calculated the values of $\frac{\Delta L}{L} \times 10^2$, *i. e.* the increase of conductivity relative to that of mercury at the same temperature multiplied by 100; and in the fifth column the values of $\frac{\Delta L}{L} \times 10^2$ divided by the concentration.

The difference between 4·52 and 4·79 can be accounted for by experimental error, and as the amalgams experimented upon were very dilute, the mean value 4·7 is taken to be equal to $l_\infty \times 10^2$, which is the value of $\frac{1}{c}\frac{\Delta L}{L} \times 10^2$ for infinite dilution.

The Electrical Conductivities of dilute Gallium Amalgams.

As found by Ramsay *, gallium readily amalgamates with mercury, and as the amalgam does not readily oxidise, even at 300° C., measurements of the resistance were carried out n the quartz tube in air.

The metal used in these experiments was supplied by Messrs. Adam Hilger, who also made a qualitative and quantitative spectroscopic analysis of the sample from which the specimen was taken. The foreign elements found were indium (the chief impurity), lead, and possibly silver. The two chief lines of silver were evident in strong spectra only. The quantitative determinations were :—

Indium.....	0·8 per cent.
Lead.....	0·013 per cent.

The conductivities of indium amalgams had previously been determined by Williams †, and it is evident from his values that the small quantity of impurities present in the gallium could not possibly affect the experimental results to any material extent.

The conductivity of gallium amalgam of concentration ·0408 prepared in a sealed apparatus containing hydrogen gas was measured at a temperature of 300·33° C., and the results agreed with those determined in the quartz tube.

* Journ. Chem. Soc. lv. p. 521 (1889).
† *Loc. cit.*

Possible oxidation did not, therefore, affect the experimental results obtained with the quartz tube to any measurable extent.

The results * obtained for four amalgams of concentrations varying from ·0219 to ·129, and also for the amalgam of concentration ·0408 prepared in an atmosphere of hydrogen,

Graph I.—Gallium.

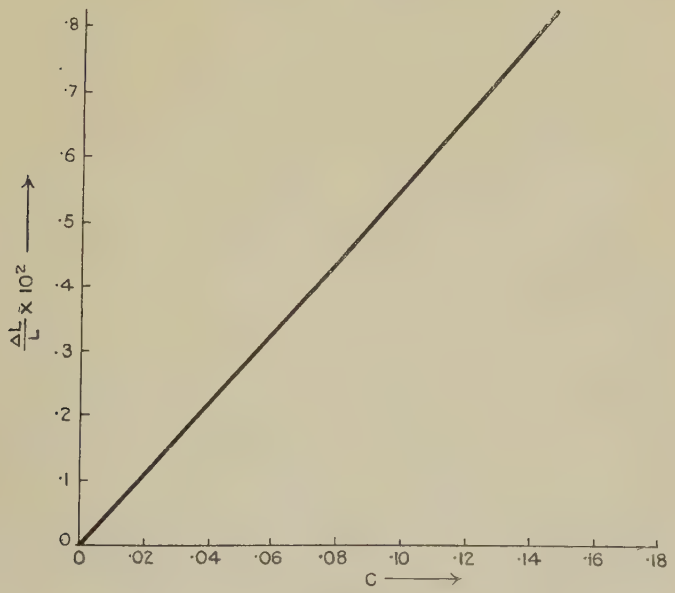

are given in Tables I. and V. The value of $l_\infty \times 10^2$ is taken to be the mean of the values of $\frac{1}{c}\frac{\Delta L}{L} \times 10^2$, which are constant within experimental error. The values of $\frac{\Delta L}{L} \times 10^2$ are plotted against c in Graph I., and the relation between them is a linear one.

The Electrical Conductivities of dilute Copper Amalgams.

The electrical conductivities of copper amalgams have been investigated by Batelli † and Schleicher ‡. Batelli employed

* The authors have not found any reference to work carried out by other investigators on the conductivities of gallium amalgams.

† *Loc. cit.*

‡ *Zeit. Electrochem.* xviii. p. 998 (1912).

amalgams whose atomic composition varied from Cu_1Hg_{127} to Cu_4Hg_{127}, and determined the relative resistance of these amalgams (*i. e.* resistance of amalgam relative to that of mercury at 0° C.) at 13° C. and 100° C. Schleicher measured the electrical resistance of amalgams whose concentrations were much greater than those employed in this investigation, and the results are therefore not comparable with those obtained in the present experiments. The solubility of copper in mercury is very small at room temperature, but increases with rise of temperature. Two dilute amalgams of concentration ·0316 and ·0633 were prepared, and their resistivities determined at about 300° C. The finest electrolytic copper was employed in the preparation of the amalgams, and the measurements were carried out in the quartz tube. Later, a copper amalgam of concentration ·0473 was prepared in an atmosphere of hydrogen, and its conductivity measured at about 300° C. The results are in agreement with those previously obtained with the quartz tube, and are given in Tables I. and V.

The Electrical Conductivity of dilute Silver Amalgams.

The electrical conductivities of silver amalgams have been determined by Matthiessen and Vogt *, Weber †, Batelli ‡, Calvo §, and Parravano and Jovanovich ‖.

Matthiessen and Vogt measured the conductivities of silver amalgams containing from ·01 per cent. to 1·0 per cent. of silver at a temperature of about 13° C. The conductivities were compared with that of a gold-silver alloy, whose conductivity at 0° C. was taken to be 100. The ratio of the conductivities at 15° C. of silver amalgams containing ·1 per cent. and ·01 per cent. of silver, as determined in the present experiments, is 1·0068, whilst the value of the ratio as calculated from Matthiessen and Vogt's measurements is 1·0059. Weber in his investigations deals with more concentrated amalgams than those studied in the present experiments. A. Batelli also employed amalgams of greater concentrations. He measured the relative resistances of silver amalgams (*i. e.* relative resistance with respect to mercury at 0° C.) at 13° C. and 100° C., using amalgams whose atomic composition ranged from Ag_1Hg_{400} to Ag_1Hg_{50}.

* *Loc. cit.* † *Loc. cit.* ‡ *Loc. cit.*

§ A. R. Calvo, 'Ion,' ii. p. 409 (1910).

‖ N. Parravano and G. Jovanovich, *Gazz. Chim. Ital.* xlix. p. 16 1919).

A. R. Calvo * found for very dilute amalgams containing from ·0015 per cent. to ·06 per cent. of silver, that between 0° C. and 20° C. the electrical resistance is a linear function of the concentration. For higher temperatures the resistance-concentration graph is a curve concave to the concentration axis. Parravano and Jovanovich† measured the conductivities of amalgams very rich in silver, the percentage of mercury varying from 0 to 14. In the present experiments the electrical resistances of silver amalgams of concentrations ranging from ·018 to ·186 have been determined. The resistance of each amalgam contained in the quartz tube was measured at three temperatures, viz. at room temperature, 100° C., and about 300° C., and for one amalgam of concentration $c = ·186$ the resistance was measured at two temperatures between 100° C. and 300° C. Finally, a silver amalgam of concentration ·0743 was prepared in an atmosphere of hydrogen, and its conductivity measured at room temperature and at 300° C. The results are in agreement with those previously obtained, when the measurements were carried out in the quartz tube. The amalgams of various concentrations were prepared from the purest silver obtainable, and the experimental results are given in Tables II., III., IV., and V.

Table III. shows the variation of the average temperature coefficient of resistivity of silver amalgam of concentration $c = ·186$ as the temperature difference is increased. The average temperature coefficient of resistivity increases as the temperature difference increases, but the values are less than the corresponding ones in the case of pure mercury.

The values of $\frac{\Delta L}{L}$, the increase of conductivity relative to that of mercury at the same temperature, have also been calculated. For the same concentration the value of $\frac{\Delta L}{L}$ increases with temperature.

The values of the average temperature coefficient of resistivity of amalgams of various concentrations between 15° and 100° C. are given in Table IV., and the results show that this average temperature coefficient diminishes as the concentration increases.

* *Loc. cit.*
† *Loc. cit.*

TABLE II.

Nature of Amalgams.	Temp. in degrees centigrade.	Percentage weight of Silver in Mercury.	Concentration "c."	Resistivity of Mercury, $\times 10^3$.	Conductivity of Mercury.	Resistivity of Amalgam, $\times 10^3$.	Conductivity of Amalgam.
	15	·00995	·0185	9535	10488	9527_5	10496
	,	·02017	·0375	,,	,,	9519	10505
	,,	·03012	·0560	,,	,,	9513	10512
	,,	·03978	·0739	,,	,,	9505_5	10520
Silver.	,,	·05499	·1022	,,	,,	9498	10528
	,,	·06500	·1208	,,	,,	9489	10538
	,,	·08503	·1580	,,	,,	9480	10548_5
	,,	·10001	·1859	,,	,,	9463	10568
*	18·05	·03997	·0743	9561	10459	9531	10492
	100	·00995	·0185	10336	9675	10325	9685
	,	·02017	·0375	,,	,,	10315	9695
	,,	·03012	·0560	,,	,,	10306	9703
	,,	·03978	·0739	,,	,,	10296	9712
Silver.	,,	·05499	·1022	,,	,,	10283	9725
	,,	·06500	·1208	,,	,,	10268	9739
	,,	·08503	·1580	,,	,,	10252	9754
	,,	·10001	·1859	,,	,,	10231	9774
Silver.	303	·00995	·0185	12831	7793_5	12810_5	7806
	,,	·03012	·0560	,,	,,	12775	7828
	300·5	·03978	·0739	12795	7816	12721	7861
	,,	·05499	·1022	,,	,,	12707	7870
Silver.	,,	·06500	·1208	,,	,,	12697	7876
	,,	·08503	·1580	,,	,,	12678	7888
	,,	·10001	·1859	,,	,,	12664	7897
	300·9	·01966	·0366	12801	7812	12762_5	7835_5
*	300·33	·03997	·0743	12793	7817	12720	7862
	15	·10001	·1859	9535	10488	9463	10568
	100	,,	,,	10336	9675	10231	9774
Silver	188·47	,,	,,	11320	8834	11204	8925
	266·89	,,	,,	12325	8114	12199	8198
	300·5	,,	,,	12795	7816	12664	7897

* These determinations were made in a sealed apparatus containing an atmosphere of hydrogen.

TABLE III.

Silver Amalgams of Concentration ·1859.

Temperature, $t°$ C.	Resistivity of Mercury, $\times 10^8$.	Resistivity of Amalgam, $\times 10^8$.	Average temperature coefficient of resistivity of Mercury from 15° C. to $t°$ C., $\times 10^4$.	Average temperature coefficient of resistivity of Amalgam from 15° C. to $t°$ C., $\times 10^4$.	$\frac{\Delta L}{L} \times 10^2$.
15·0	9535	9463	—	—	·763
100·0	10336	10231	9·883	9·548	1·023
188·47	11320	11204	10·792	10·606	1·030
266·89	12325	12199	11·617	11·478	1·034
300·5	12795	12664	11·976	11·848	1·036

TABLE IV.

Silver Amalgams.

Concentration "c."	Average temperature coefficient of resistivity of Amalgams from 15° to 100° C., $\times 10^4$.	Concentration "c."	Average temperature coefficient of resistivity of Amalgams from 15° to 100° C., $\times 10^4$.
·0185	9·841	·1022	9·723
·0375	9·838	·1208	9·658
·0560	9·807	·1580	9·581
·0739	9·784	·1859	9·548

The relation between the electrical resistance (which is proportional to the resistivity) and the concentration "c" at 15° C. and 100° C. is shown in Graph II. At these temperatures the relation is almost linear. The same result is also obtained if the electrical resistance is plotted against concentration at 300·5° C.

Graph III. gives the relation between $\frac{\Delta L}{L} \times 10^2$ and "c" at 15° C., 100° C., and 300° C. The graphs for 15° C. and 100° C. are straight lines, showing that for the comparatively dilute silver amalgams examined the increase of conductivity relative to mercury at the same temperature is proportional to the concentration. This result is, however, not obtained at 300°C.

Graph II.—Silver.

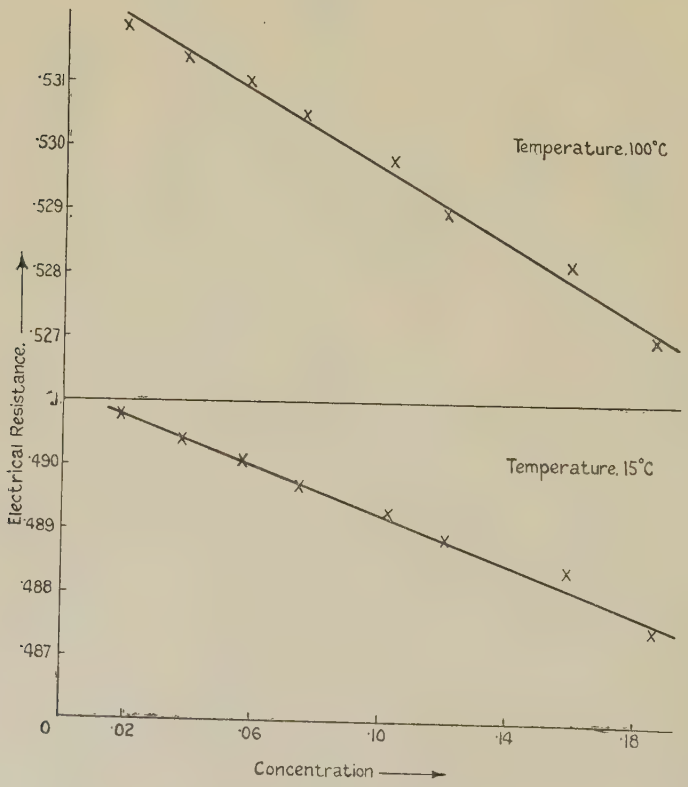

Discussion of Results.

For purposes of discussion, the results obtained for all the amalgams examined have been collected in Table V. The meanings of the various quantities tabulated have, in most cases, been previously explained. The sixth column gives the value of "l" for infinite dilution: *i. e.*, the value of the

increase of conductivity relative to the conductivity of mercury at the same temperature divided by the concentration when the latter is very small. According to Skaupy's theory, which has been referred to previously, the value of $H_\infty = l_\infty + r_\infty$ should be of the same order of magnitude for different metals dissolved in mercury. The values of r_∞ at 15° C., 100° C., and 300° C. are not known for amalgams of

GRAPH III.—Silver.

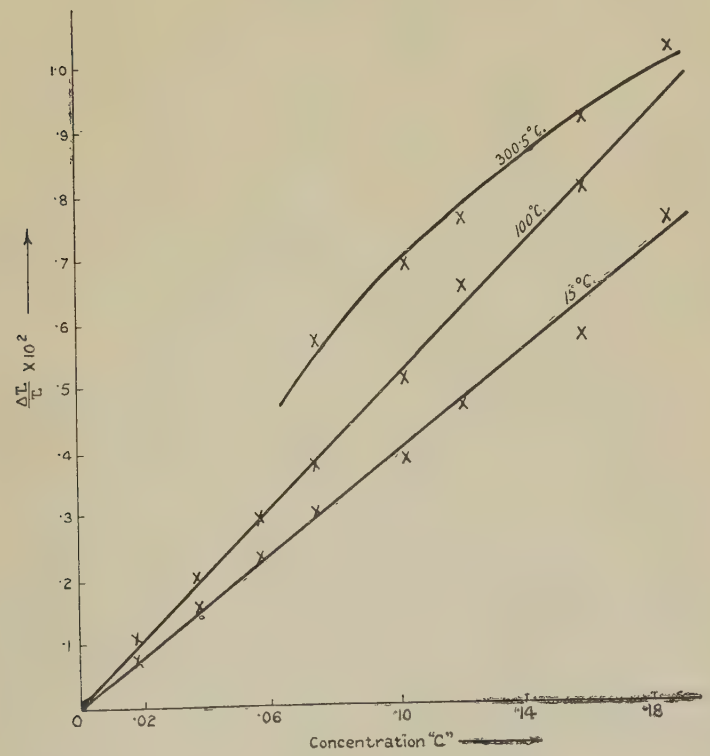

the concentrations employed in the present experiments, and consequently the values of l_∞ for the different amalgams are considered. It is seen that for germanium, gallium, and copper the values of l_∞ vary from $4{\cdot}7 \times 10^{-2}$ to $6{\cdot}5 \times 10^{-2}$, and the mean value of l_∞ obtained for germanium in the present experiments is in good agreement with the value $(4{\cdot}7 \times 10^{-2})$ previously determined by Edwards *.

* *Loc. cit.*

TABLE V.

Nature of Amalgam.	Temperature in degrees centigrade.	Concentration "c."	$\frac{\Delta L}{L}\times 10^2$.	$\frac{1}{c}\frac{\Delta L}{L}\times 10^2 = l\times 10^2$.	$l_\infty \times 10^2$.
Germanium.	299·23	·0339	·153	4·52	4·7
	,,	·0692	·332	4·79	
Gallium.	301·0	·0219	·115	5·25	5·5
	,,	·0408	·230	5·64	
	,,	·0944	·487	5·20	
	,,	·1287	·730	5·67	
	300·33	·0408	·230	5·64	
Copper.	301·76	·0316	·218	6·90	6·5
	,,	·0633	·397	6·27	
	,,	·0473	·295	6·24	
Silver.	15	·0185	·0763	4·12	4·0
	,,	·0375	·162	4·32	
	,,	·0560	·229	4·09	
	,,	·0739	·305	4·13	
	,,	·1022	·381	3·73	
	,,	·1208	·477	3·95	
	,,	·1580	·577	3·65	
	,,	·1859	·763	4·05	
	18·05	·0743	·316	4·25	
Silver.	100·0	·0185	·103	5·57	5·3
	,,	·0375	·207	5·52	
	,,	·0560	·289	5·16	
	,,	·0739	·382	5·17	
	,,	·1022	·517	5·06	
	,,	·1208	·661	5·47	
	,,	·1580	·816	5·17	
	,,	·1859	1·023	5·50	
Silver.	303·0	·0185	·162	8·74	
	,,	·0560	·443	7·91	
Silver.	300·5	·0739	·577	7·81	9·0
	,,	·1022	·691	6·76	
	,,	·1208	·768	6·36	
	,,	·1580	·921	5·83	
	,,	·1859	1·036	5·57	
	300·9	·0366	·301	8·23	
	300·33	·0743	·577	7·77	
Silver.	15·0	·1859	·763	4·05	
	100 0	,,	1·023	5·50	
	188·47	,,	1·030	5·54	
	266·89	,,	1·034	5·56	
	300·5	,,	1·036	5·57	

The values of $\frac{1}{c}\frac{\Delta L}{L} \times 10^2$ were determined at about 303° C., and were found to be constant within experimental error at different concentrations. The mean value of $\frac{1}{c}\frac{\Delta L}{L} \times 10^2$ for each amalgam was therefore taken to be the value of l_∞ for that amalgam. In the case of silver, the values of $\frac{1}{c}\frac{\Delta L}{L} \times 10^2$ were determined at 15° C., 100° C., and at about 300° C. At 15° C. and 100° C, the values of this quantity were practically constant, and l_∞ was taken to be the mean value. In this way it was found that l_∞ is $4{\cdot}0 \times 10^{-2}$ at 15° C., and $5{\cdot}30 \times 10^{-2}$ at 100° C. At about 300° C., however, the value of $\frac{1}{c}\frac{\Delta L}{L} \times 10^2$ decreases with increasing concentration, and varies from 8·74 at the concentration ·0185 to 5·57 at the highest concentration ·1859. The value of $l_\infty \times 10^2$ at 300·5° C. as deduced from a graph in which $\frac{1}{c}\frac{\Delta L}{L} \times 10^2$ is plotted against concentration is 9·0.

According to Skaupy's theory, the value of $\frac{H_\infty - H}{c}$ should be constant, and if the variation of viscosity with concentration be neglected, the expression $\frac{l_\infty - l}{c}$ should be constant. According to this relation, the greater the value of the concentration the smaller the value of l; and this is in agreement with the results obtained at the high temperature.

The values of $(l_\infty - l) \times 10^2$ are plotted against concentration in graph IV., and the relation between the two quantities as approximately a linear one. It is, however, important to point out that the values of $l = \frac{1}{c}\frac{\Delta L}{L}$ are difficult to determine with the necessary accuracy, for a perfectly satisfactory verification of the relation $\frac{l_\infty - l}{c} = \text{constant}$. The values of l obtained for silver amalgams of concentrations examined in this investigation increase with rise of temperature, and in this respect agree with results previously obtained by Edwards * for thallium amalgams. This increase in the

* *Loc. cit.*

value of l at high temperature may possibly be due both to an increase of electron concentration with rise of temperature, and also a diminution in viscosity under the same conditions. It is hoped that accurate measurements of the conductivities

GRAPH IV.

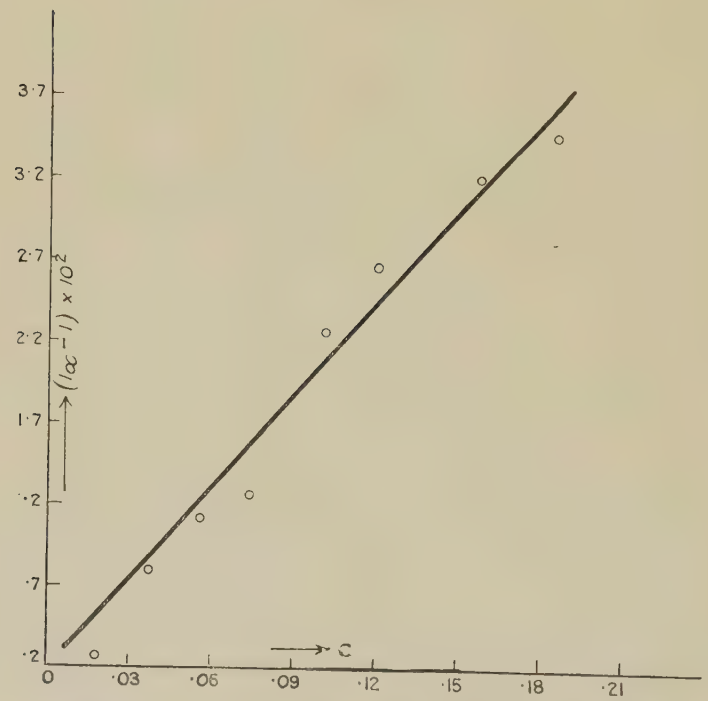

and viscosities of dilute amalgams at various temperatures will throw further light on the nature of conduction in amalgams. The results obtained for the amalgams examined in the present work show that the values of l_∞ are of the same order of magnitude in all cases.

SUMMARY.

1. The conductivities of dilute amalgams of germanium gallium, silver, and copper have been determined. The conductivities of germanium, gallium, and copper amalgams of different concentrations were measured only at about 300° C., but the conductivities of silver amalgams of various concentrations were determined at 15°, 100° C., and at about

300° C. In the case of silver amalgam of concentration $c = \cdot 186$ the conductivity was also measured at 184·4° C. and 266·8° C.

2. The average temperature coefficient of resistivity between 15° C. and various higher temperatures of silver amalgam of concentration ·186 was found to increase as the temperature difference increased. The values were less than the corresponding ones in the case of pure mercury.

3. The values of the average temperature coefficient of resistivity of silver amalgams of various concentrations between 15° and 100° C. showed a diminution as the concentration increased.

4. In the case of dilute germanium, gallium, copper, and silver amalgams (at 0° and 100° C.) examined it was found that the increase of conductivity relative to the conductivity of mercury at the same temperature was practically proportional to the concentration. This, however, was not found to be the case for silver amalgams at about 300° C.

5. It was found that the increase of conductivity relative to the conductivity of mercury divided by the concentration (when the latter was extremely small) was of the same order of magnitude for all the amalgams examined.

The authors wish to thank Mr. Frank Homeyard for his valuable assistance in the construction of the apparatus.

XXIX. *The Angular Velocity of a Rigid Body.* *By* E. A. Milne, *F.R.S., Beyer Professor of Applied Mathematics in the University of Manchester* *.

1. *The Usual Treatment.*

CONSIDER a rigid body in motion about some fixed point. The fundamental property of the motion is that it can be described by a certain vector, which is called the angular velocity of the body.

It is customary in treatises on dynamics † to deduce this property by considering first the finite displacement of a rigid body, secondly the infinitesimal displacement of a rigid

* Communicated by the Author.

† *E. g.* Whittaker, 'Analytical Dynamics,' Chap. I. Routh, 'Elementary Rigid Dynamics,' Chap. V. Lamb, 'Higher Mechanics,' Chap. V. Appel ('Mécanique Rationelle,' Chap. II.) gives, however, an analytical method which deals with the body in motion.

body. It is proved that if a body suffers two rotations about given axes passing through a fixed point, then the final position of the body is independent of the order in which the rotations occur, provided these are "infinitesimal." It is proved further that the resultant rotation may be described by a vector which is the vector sum of the vectors representing the separate rotations. From the fact that the result of *successive* small rotations is equivalent to a rotation represented by the vector sum of the small rotations, it is inferred by proceeding to a limit that a rigid body in continuous motion can be regarded as possessing *simultaneously* angular velocities whose vector sum gives the instantaneous angular velocity of the body. This is also expressed by saying that angular velocities may be compounded according to the vectorial law.

2. *Criticism.*

There seem to the writer to be certain difficulties about this procedure. The essence of the theory of small displacements is that they are *successive*. It is not clear how it is ever possible from this theory to derive a result concerning *simultaneous* motions. Moreover, if we use the ordinary theory of infinitesimal displacements, we do not, in fact, know where the body is after two such displacements unless the order is specified. The difficulty is scarcely overcome by the process of letting an interval δt tend to zero: the displacements remain successive, and are never simultaneous. It could probably be overcome by introducing the notion of simultaneous displacements, by displacing the rigid body in a frame of reference which is itself being displaced as a rigid body. The final position of the rigid body would then be unique, even for finite displacements. The necessary theory would, however, be somewhat different from the usual theory of displacements.

The following treatment avoids these difficulties. It begins with the rigid body actually in motion, and avoids any reference to the theory of displacements or any passage to the limit. After a few years' experience of teaching it to students, the author feels that it may be of interest to other teachers. Even if the above-mentioned objections are not considered weighty, the theory may be held to have the æsthetic advantage of not deducing properties of bodies in motion from the properties of bodies at rest. It involves only elementary vector analysis.

We use the notations $\mathbf{A} \cdot \mathbf{B}$ and $\mathbf{A} \wedge \mathbf{B}$ to denote respectively the scalar and vector products of two vectors A and B.

We need the results

$$(\mathbf{A} \wedge \mathbf{B}) . \mathbf{C} = (\mathbf{B} \wedge \mathbf{C}) . \mathbf{A} = (\mathbf{C} \wedge \mathbf{A}) . \mathbf{B}, \quad . \quad \text{I.}$$

$$(\mathbf{A} \wedge \mathbf{B}) \wedge \mathbf{C} = -\mathbf{A}(\mathbf{B} . \mathbf{C}) + \mathbf{B}(\mathbf{C} . \mathbf{A}), \quad . \quad . \quad \text{II.}$$

together with the elementary distributive theorems etc. of vector analysis.

3. *The Existence Theorem for the Angular Velocity of a Rigid Body.*

Consider a rigid body in motion about a fixed point O. Let P denote any point of the body, and let $\mathbf{r}$ denote the vector distance OP. We use the symbol $\dot{\mathbf{r}}$ to denote the velocity of P. The theorem in question is :

There exists a unique vector Ω *which is such that the velocity of any point of the body is given by the relation*

$$\dot{\mathbf{r}} = \Omega \wedge \mathbf{r}. \quad . \quad . \quad . \quad . \quad . \quad . \quad . \quad . \quad (1)$$

Proof.—Let P_1 be any definite point of the rigid body. Let P_2 be a second point, such that OP_2 is not perpendicular to the velocity of P_1. Let $\mathbf{r}_1$ and $\mathbf{r}_2$ be the vectors representing OP_1 and OP_2. ($\mathbf{r}_2 . \dot{\mathbf{r}}_1 \neq 0$.) The necessary and sufficient conditions of rigidity are

$$\mathbf{r}_1^2 = \text{constant},$$

$$\mathbf{r}_2^2 = \text{constant},$$

$$(\mathbf{r}_1 - \mathbf{r}_2)^2 = \text{constant}.$$

Differentiating these with respect to the time, we have

$$\mathbf{r}_1 . \dot{\mathbf{r}}_1 = 0, \quad . \quad . \quad . \quad . \quad . \quad . \quad (2)$$

$$\mathbf{r}_2 . \dot{\mathbf{r}}_2 = 0, \quad . \quad . \quad . \quad . \quad . \quad . \quad (3)$$

$$(\mathbf{r}_1 - \mathbf{r}_2) . (\dot{\mathbf{r}}_1 - \mathbf{r}_2) = 0. \quad . \quad . \quad . \quad . \quad . \quad (4)$$

Expanding (4) and using (2) and (3), we have

$$\mathbf{r}_1 . \dot{\mathbf{r}}_2 + \mathbf{r}_2 . \dot{\mathbf{r}}_1 = 0. \quad . \quad . \quad . \quad . \quad . \quad . \quad (5)$$

The relation $\mathbf{r}_2 . \dot{\mathbf{r}}_1 \neq 0$ accordingly implies $\mathbf{r}_1 . \dot{\mathbf{r}}_2 \neq 0$. Moreover, since $\dot{\mathbf{r}}_1$ is perpendicular to $\mathbf{r}_1$ and not perpendicular to $\mathbf{r}_2$, it follows that $\mathbf{r}_1$ and $\mathbf{r}_2$ are not parallel.

Now consider the pair of equations

$$\Omega \wedge \mathbf{r}_1 = \dot{\mathbf{r}}_1, \quad . \quad . \quad . \quad . \quad . \quad . \quad . \quad (6)$$

$$\Omega \wedge \mathbf{r}_2 = \dot{\mathbf{r}}_2. \quad . \quad . \quad . \quad . \quad . \quad . \quad . \quad (7)$$

We propose to show that these have one and only one solution in Ω, *i.e.* that they define a unique vector Ω.

We first show that they have at most one solution. For, if possible, let them have two solutions Ω, Ω'. Then

$$(\Omega-\Omega')\wedge\mathbf{r}_1=0,$$
$$(\Omega-\Omega')\wedge\mathbf{r}_2=0.$$

Hence either $\Omega-\Omega'=0$, or $\Omega-\Omega'$ is parallel both to $\mathbf{r}_1$ and $\mathbf{r}_2$. But $\mathbf{r}_1$ and $\mathbf{r}_2$ are not parallel. Hence $\Omega=\Omega'$.

We now show that they have a solution. Multiply (6) and (7) vectorially by $\dot{\mathbf{r}}_2$ and $\dot{\mathbf{r}}_1$ respectively, and expand the continued vector products by II. We find

$$-\Omega(\mathbf{r}_1\,.\,\dot{\mathbf{r}}_2)+\mathbf{r}_1(\Omega\,.\,\dot{\mathbf{r}}_2)=\dot{\mathbf{r}}_1\wedge\dot{\mathbf{r}}_2. \quad . \quad . \quad . \quad (8)$$
$$-\Omega(\mathbf{r}_2\,.\,\dot{\mathbf{r}}_1)+\mathbf{r}_2(\Omega\,.\,\dot{\mathbf{r}}_1)=\dot{\mathbf{r}}_2\wedge\dot{\mathbf{r}}_1. \quad . \quad . \quad . \quad (9)$$

Add (8) and (9), and use (5). We find

$$\mathbf{r}_1(\Omega\,.\,\dot{\mathbf{r}}_2)+\mathbf{r}_2(\Omega\,.\,\dot{\mathbf{r}}_1)=0. \quad . \quad . \quad . \quad . \quad (10)$$

But $\mathbf{r}_1$ and r_2 are not parallel. Hence if a solution Ω exists, (10) requires that

$$\Omega\,.\,\dot{\mathbf{r}}_1=0 \quad . \quad . \quad . \quad . \quad . \quad . \quad . \quad (11)$$

and

$$\Omega\,.\,\dot{\mathbf{r}}_2=0 \quad . \quad . \quad . \quad . \quad . \quad . \quad . \quad (12)$$

Equation (8) now gives

$$\Omega=-\frac{\dot{\mathbf{r}}_1\wedge\dot{\mathbf{r}}_2}{\mathbf{r}_1\,.\,\dot{\mathbf{r}}_2}, \quad . \quad . \quad . \quad . \quad . \quad (13)$$

since $\mathbf{r}_1\,.\,\dot{\mathbf{r}}_2\neq 0$, and similarly equation (9) gives

$$\Omega=-\frac{\dot{\mathbf{r}}_2\wedge\dot{\mathbf{r}}_1}{\dot{\mathbf{r}}_1\,.\,\dot{\mathbf{r}}_2}. \quad . \quad . \quad . \quad . \quad . \quad (13')$$

These are equal by (5). It is immediately verified that this value satisfies the original equations (6) and (7) on using the conditions of rigidity. Relations (11) and (12) are also satisfied. We have accordingly found the unique solution of (6) and (7). It may be written also in the form

$$\Omega=\frac{\dot{\mathbf{r}}_1\wedge\dot{\mathbf{r}}_2}{\dot{\mathbf{r}}_1\,.\,\mathbf{r}_2}=\frac{\dot{\mathbf{r}}_2\wedge\dot{\mathbf{r}}_1}{\dot{\mathbf{r}}_2\,.\,\mathbf{r}_1}. \quad . \quad . \quad . \quad . \quad (13'')$$

We now consider any third point P, whose vector distance from O is $\mathbf{r}$. We suppose in the first instance that OP does not lie in the plane OP_1P_2. Put

$$\Omega\wedge\mathbf{r}=\mathbf{X}.$$

We propose to show that

$$\mathbf{X}=\dot{\mathbf{r}}.$$

To do this we shall show that

$$\left.\begin{aligned} \mathbf{X}\,.\,\mathbf{r} &= \dot{\mathbf{r}}\,.\,\mathbf{r}, \\ \mathbf{X}\,.\,\mathbf{r}_1 &= \dot{\mathbf{r}}\,.\,\mathbf{r}_1, \\ \mathbf{X}\,.\,\mathbf{r}_2 &= \dot{\mathbf{r}}\,.\,\mathbf{r}_2. \end{aligned}\right\} \quad . \quad . \quad . \quad . \quad . \quad . \quad (1$$

It will then follow that $\mathbf{X}=\dot{\mathbf{r}}$. For otherwise $\mathbf{X}-\dot{\mathbf{r}}$ would be perpendicular to each of $\mathbf{r}$, $\mathbf{r}_1$, and $\mathbf{r}_2$, which is impossible by hypothesis.

The conditions that $\mathbf{r}$ is rigidly connected to O, P_1, and P_2 are

$$\mathbf{r}^2 = \text{constant},$$

$$(\mathbf{r}-\mathbf{r}_1)^2 = \text{constant},$$

$$(\mathbf{r}-\mathbf{r}_2)^2 = \text{constant},$$

which give, on differentiation with respect to the time,

$$\mathbf{r}\,.\,\dot{\mathbf{r}}=0, \quad . \quad . \quad . \quad . \quad . \quad (15)$$

$$\mathbf{r}\,.\,\dot{\mathbf{r}}_1+\mathbf{r}_1\,.\,\dot{\mathbf{r}}=0, \quad . \quad . \quad . \quad . \quad . \quad (16)$$

$$\mathbf{r}\,.\,\dot{\mathbf{r}}_2+\mathbf{r}_2\,.\,\dot{\mathbf{r}}=0. \quad . \quad . \quad . \quad . \quad . \quad (17)$$

We have now, on using (15), (16), and (17), and theorem,

$$\mathbf{X}\,.\,\mathbf{r} = \Omega \wedge \mathbf{r}\,.\,\mathbf{r} = 0 = \dot{\mathbf{r}}\,.\,\mathbf{r},$$

$$\mathbf{X}\,.\,\mathbf{r}_1 = \Omega \wedge \mathbf{r}\,.\,\mathbf{r}_1 = -\Omega \wedge \mathbf{r}_1\,.\,\mathbf{r} = -\dot{\mathbf{r}}_1\,.\,\mathbf{r} = \dot{\mathbf{r}}\,.\,\mathbf{r}_1,$$

$$\mathbf{X}\,.\,\mathbf{r}_2 = \Omega \wedge \mathbf{r}\,.\,\mathbf{r}_2 = -\Omega \wedge \mathbf{r}_2\,.\,\mathbf{r} = -\dot{\mathbf{r}}_2\,.\,\mathbf{r} = \dot{\mathbf{r}}\,.\,\mathbf{r}_2,$$

which establish (14). Hence we have result (1), provided $\mathbf{r}$ does not lie in the plane of $\mathbf{r}_1$ and $\mathbf{r}_2$.

Now let P lie in the plane of P_1 and P_2. Take a neighbouring point P′, vector distance $\mathbf{r}'$, not lying in the plane OP_1P_2. Then

$$\Omega \wedge \mathbf{r}' = \dot{\mathbf{r}}'.$$

As $\mathbf{r}' \to \mathbf{r}$, $\Omega \wedge \mathbf{r}' \to \Omega \wedge \mathbf{r}$, and $\dot{\mathbf{r}}' \to \dot{\mathbf{r}}$. Hence

$$\Omega \wedge \mathbf{r} = \dot{\mathbf{r}}.$$

We have thus established (1) generally. Further, $\Omega\,.\,\dot{\mathbf{r}}=0$. We have thus found a vector Ω satisfying any number of equations of the type $\Omega \wedge \mathbf{r}_n = \dot{\mathbf{r}}_n$; and since each pair of such equations has only one solution by the above, the vector Ω is unique.

When the motion is such that Ω is constant, we have

$$\frac{d}{dt}(\Omega\,.\,\mathbf{r}) = \Omega\,.\,\dot{\mathbf{r}} = \Omega\,.\,\Omega \wedge \mathbf{r} = 0,$$

and hence

$$\Omega\,.\,\mathbf{r} = \text{constant}.$$

In this case the vector $\mathbf{r}$, of constant length, is inclined at a constant angle to the fixed direction of Ω. Moreover,

$$\dot{\mathbf{r}}^2=(\Omega\wedge\mathbf{r})^2=\Omega^2\mathbf{r}^2-(\Omega\,.\,\mathbf{r})^2=\text{constant}.$$

Hence the speed of P is constant. In other words, OP rotates round Ω at a constant speed. The time of a complete revolution is the length of the path of P, which is

$$2\pi\frac{|\,\mathbf{r}\wedge\Omega\,|}{|\,\Omega|},$$

divided by $|\,\dot{\mathbf{r}}\,|$, namely $|\,\Omega\wedge\mathbf{r}\,|$, *i.e.* the time of a complete revolution is $2\pi/|\,\Omega\,|$. For this reason the vector Ω is called the angular velocity of the body round the point O.

4. *Notes on the Proof.*

The idea of the proof *, it will be seen, is that we use the motion of two given points to fix Ω, and then show that the motion of any third point is determined in terms of Ω. We naturally need the complete set of conditions of rigidity, namely those expressing that P_1 and P_2 are rigidly connected with O and with one another, and that P is rigidly connected with O, P_1, and P_2.

For the velocity $\dot{\mathbf{r}}$ of any point we have now the explicit formula

$$\dot{\mathbf{r}}=\Omega\wedge\mathbf{r}=\frac{(\dot{\mathbf{r}}_1\wedge\dot{\mathbf{r}}_2)\wedge\mathbf{r}}{\dot{\mathbf{r}}_1\,.\,\dot{\mathbf{r}}_2}$$

$$=\dot{\mathbf{r}}_1\left(\frac{\mathbf{r}\,.\,\dot{\mathbf{r}}_2}{\dot{\mathbf{r}}_1\,.\,\dot{\mathbf{r}}_2}\right)+\dot{\mathbf{r}}_2\left(\frac{\mathbf{r}\,.\,\dot{\mathbf{r}}_1}{\dot{\mathbf{r}}_2\,.\,\dot{\mathbf{r}}_1}\right).$$

This shows that the velocity of any point P of a rigid body in motion round a fixed point is a linear function of the velocities of any two given points P_1 and P_2 (provided $\mathbf{r}_1\,.\,\dot{\mathbf{r}}_2\neq 0$), *i.e.* that the velocities of all points are parallel to the plane. It is an interesting exercise in vector analysis to prove this result without the intervention of Ω, using only the conditions of rigidity.

The following additional remarks may be of interest.

5. *The Theorem of Relative Angular Velocities.*

Let a rigid body or frame of reference (2) have an angular velocity Ω_2 relative to a frame of reference (1), and let (1) have an angular velocity Ω_1 relative to a frame of reference (0). *Then* (2) *has an angular velocity* $\Omega=\Omega_1+\Omega_2$

* A similar proof, using quaternions, is given by Tait, 'Quaternions' (3rd edition, 1890), p. 288.

relative to (0). For if $\mathbf{r}$ denotes any point, $\mathbf{v}$ its velocity in (0), $\mathbf{v}_2$ its velocity in (2), and $\mathbf{v}_1$ the velocity in (0) of the same point considered as belonging to (1), then we have

$$\mathbf{v}=\mathbf{v}_1+\mathbf{v}_2,$$

$$\mathbf{v}_1=\Omega_1\wedge\mathbf{r},$$

$$\mathbf{v}_2=\Omega_2\wedge\mathbf{r},$$

whence $$\mathbf{v}=(\Omega_1+\Omega_2)\wedge\mathbf{r},$$

and so $$\Omega=\Omega_1+\Omega_2.$$

6. *Angular Velocity independent of Origin of Reference.*

Let a rigid body have an angular velocity Ω round a point O, which is moving with velocity $\mathbf{v}_0$. Let O_1 be any other point, and let the angular velocity round O_1 be Ω_1. *Then* $\Omega=\Omega_1$. For if $OO_1=\mathbf{r}_1$, and $\mathbf{v}_1$ is the velocity of O, then

$$\mathbf{v}_1=\mathbf{v}_0+\Omega\wedge\mathbf{r}_1.$$

But if $\mathbf{r}$ denote any point of the body, $\mathbf{v}$ its velocity,

$$\mathbf{v}=\mathbf{v}_0+\Omega\wedge\mathbf{r}.$$

Put $$\mathbf{r}=\mathbf{r}_1+\mathbf{r}'.$$

Then $$\mathbf{v}=\mathbf{v}_0+\Omega\wedge(\mathbf{r}_1+\mathbf{r}')$$
$$=\mathbf{v}_1+\Omega\wedge\mathbf{r}'.$$

But $$\mathbf{v}=\mathbf{v}_1+\Omega_1\wedge\mathbf{r}'.$$

This is true for all points $\mathbf{r}'$. Hence $\Omega_1=\Omega$.

7. The last two results complete the minimum necessary to describe the most general motion of a rigid body in terms of an angular velocity.

The theorem of relative angular velocities allows us to dispense with the somewhat difficult notion of a body possessing *simultaneously* two or more angular velocities. Such cases can always be reduced to the case of a definite velocity in one frame of reference, together with the angular velocity of that frame of reference in a second frame of reference, and so on. The advantage of this is that each angular velocity can then always be measured in principle by a revolution-counter.

October 1927.

XXX. *On the Capillary Rise of Liquids in Wide Tubes.* *By* Claude H. Bosanquet, *M.A., Dr. Lee's Reader in Physics, Christ Church, Oxford* *.

THE form of the surface of a liquid at rest in a circular tube under the influence of capillary forces is given by the equation :

$$\frac{h}{\alpha} - \frac{\alpha}{r}\sin\phi - \alpha\frac{d}{dr}\sin\phi = 0, \quad . \quad . \quad . \quad . \quad (1)$$

where h is the height above the free surface, ϕ is the angle between the radial tangent and the horizontal, and $\alpha^2 = \frac{T}{\rho g}$. For a plain circular tube and a liquid which wets it, $\phi = 0$ at the axis and $\frac{\pi}{2}$ at the walls.

Lord Rayleigh † gives an approximate relation between h at the axis of the tube and r : –

$$\log_e \frac{h}{\alpha} = -\frac{r}{\alpha} + 0{\cdot}8381 + 0{\cdot}2798\frac{\alpha}{r} + \tfrac{1}{2}\log_e \frac{r}{\alpha}. \quad . \quad (2)$$

This formula is only applicable to very wide tubes $\left(\frac{r}{\alpha} > 6\right)$; he also gives a formula for narrow tubes.

Bashforth and Adams ‡ have attacked the problem of a numerical solution of equation (1). They tabulate corresponding values of ϕ and $\frac{x}{b}$ for various values of a parameter β, where $\frac{x}{b} = \frac{rh}{2\alpha^2}$ and $\beta = \frac{4\alpha^2}{h^2}$ in the notation of this paper. This table extends as far as $\beta = 100$, and in this case where $\phi = 90°$, $\frac{x}{b} = 0{\cdot}31646$, so that $\frac{h}{\alpha} = 0{\cdot}2$ when $\frac{r}{\alpha} = 3{\cdot}1646$.

Sugden § gives a table of values of $\frac{r}{a}$ and $\frac{r}{b}$ for $\phi = 90°$, using the results of Bashforth and Adams. In his notation

* Communicated by the Author.
† Rayleigh, 'Collected Papers,' vi. p. 356.
‡ Bashforth & Adams, 'Capillary Action' (Camb. Univ. Press. 1883).
§ Sugden, Tr. Chem. Soc. 1921, p. 1483.

$a^2=2\alpha^2$. He bridges the gap between the end of the tables and the point where Rayleigh's formula begins to apply by graphical interpolation.

It is the object of the present paper to give the results of some direct computations covering this region.

Method of Calculation.

The method employed, though on the same lines as that of Bashforth and Adams, differed in that the central difference notation was used. This method involves working by successive approximations, but it is so much less laborious than their method that the total time for a computation is considerably reduced, besides which the successive approximations provide useful checks on the accuracy of the arithemetic.

In this notation, if a table of values of y for equal increments of x and their differences be formed as below :—

$$
\begin{array}{lllll}
y_{-2} & & & & \\
 & \Delta^{\mathrm{I}}_{-1\frac{1}{2}} & & & \\
y_{-1} & & \Delta^{\mathrm{II}}_{-1} & & \\
 & \Delta^{\mathrm{I}}_{-\frac{1}{2}} & & \Delta^{\mathrm{III}}_{-\frac{1}{2}} & \\
y_0 & & \Delta^{\mathrm{II}}_{0} & & \Delta^{\mathrm{IV}}_{0}. \\
 & \Delta^{\mathrm{I}}_{\frac{1}{2}} & & \Delta^{\mathrm{III}}_{\frac{1}{2}} & \\
y_1 & & \Delta^{\mathrm{II}}_{1} & & \\
 & \Delta^{\mathrm{I}}_{1\frac{1}{2}} & & & \\
y_2 & & & &
\end{array}
$$

Then

$$
\frac{1}{x_1-x_0}\int_{x_0}^{x_1} y\,dx
$$

$$
=\frac{y_0+y_1}{2}-\frac{1}{24}\left\{(\Delta_0^{\mathrm{II}}+\Delta_1^{\mathrm{II}})-\frac{11}{60}(\Delta_0^{\mathrm{IV}}+\Delta_1^{\mathrm{IV}})\right.
$$

$$
\left.+\frac{191}{5040}(\Delta_0^{\mathrm{VI}}+\Delta_1^{\mathrm{VI}})-\frac{2497}{302400}(\Delta_0^{\mathrm{VIII}}+\Delta_1^{\mathrm{VIII}})+\ldots\right\}. \quad (3)
$$

This series is much more convergent than that used by Bashforth and Adams ; in addition it only uses the even terms in the difference series.

A still more convergent series can be obtained if $\frac{dy}{dx}$ is

known in addition to y. Calling this y' and forming the table as below :—

$$\begin{array}{ccccc} y'_{-1} & & & & \\ & \delta^{\mathrm{I}}_{-\frac{1}{2}} & & & \\ y'_0 & & \delta^{\mathrm{II}}_0 & & \\ & \delta^{\mathrm{I}}_{\frac{1}{2}} & & \delta^{\mathrm{III}}_{\frac{1}{2}}. & \\ y'_1 & & \delta^{\mathrm{II}}_1 & & \\ & \delta^{\mathrm{I}}_{1\frac{1}{2}} & & & \\ y'_2 & & & & \end{array}$$

Then

$$\frac{1}{x_1-x_0}\int_{x_0}^{x_1} y\,dx$$

$$= \frac{y_0+y_1}{2} - \frac{x_1-x_0}{12}\left(\delta^{\mathrm{I}}_{\frac{1}{2}} - \frac{1}{60}\delta^{\mathrm{III}}_{\frac{1}{2}} + \frac{1}{560}\delta^{\mathrm{V}}_{\frac{1}{2}} - \frac{79}{302400}\delta^{\mathrm{VII}}_{\frac{1}{2}} + \frac{1759}{39916800}\delta^{\mathrm{IX}}_{\frac{1}{2}} - \ldots\right). \quad . \quad . \quad (4)$$

A table was constructed showing the values of $\frac{h}{\alpha}$, $\sin\phi$, $\tan\phi$, and $\alpha\frac{d}{dr}\sin\phi$, and the differences of $\tan\phi$ and $\alpha\frac{d}{dr}\sin\phi$ for values of $\frac{r}{\alpha}$ differing by 0·1, using various initial values of $\frac{h}{\alpha}$. Up to the point where the difference between $\sin\phi$ and $\tan\phi$ becomes appreciable, the equation can be written :

$$y - \frac{1}{x}\cdot\frac{dy}{dx} - \frac{d^2y}{dx^2} = 0, \quad . \quad . \quad . \quad . \quad . \quad . \quad (5)$$

and values of $\frac{y}{y_0}$ and $\frac{1}{y_0}\cdot\frac{dy}{dx}$ can be obtained from tables of Bessel functions.

After the table had been started in this way, inspection of the general run of the differences gave approximations for the next value of $\alpha\frac{d}{dr}\sin\phi$ and for the required differences. Using only the first term of the correction series, new values

were obtained for ϕ and $\frac{h}{\alpha}$; substitution of these values in equation (1) gave a new value for $\alpha\frac{d}{dr}\sin\phi$. If this value differed from the original extrapolation, the new values of ϕ and $\frac{h}{\alpha}$ were corrected, but with a little practice it was possible to guess the run of the curve with considerable accuracy.

After extending the table by twenty or so steps in this way, a second approximation was made, using the first to provide the correction terms and the approximations for $\alpha\frac{d}{dr}\sin\phi$. This table was then extended to form a first approximation over a new range of $\frac{r}{\alpha}$, and in this way the accumulation of large errors was avoided. Two approximations over any one range of $\frac{r}{\alpha}$ were always sufficient, the full correction series being, of course, used in the second approximation, though terms beyond the second were never required.

When ϕ approaches $\frac{\pi}{2}$, the differences begin increasing rapidly, and it is more convenient to use $\frac{h}{\alpha}$ as the independent variable, the equation becoming

$$\frac{h}{\alpha}-\frac{\alpha}{r}\sin\phi+\alpha\frac{d}{dh}\cos\phi=0. \quad . \quad . \quad . \quad (6)$$

The change of variable was made approximately at the point where $\phi=\frac{\pi}{4}$, and the curve was continued up to the point where $\phi=\frac{\pi}{2}$.

$\frac{r}{\alpha}$ was worked out for several values of $\frac{h}{\alpha}$, and for purposes of interpolation use was made of equation (5). If the difference between $\sin\phi$ and $\tan\phi$ be neglected, then, if in equation (5) $\frac{dy}{dx}=1$ where $x=\frac{r}{\alpha}$, $\frac{h}{\alpha}=y_0$. It can easily be shown that in the limit where $r=\infty$,

$$\log_e\frac{h}{\alpha}=\log_e y_0-0{\cdot}08087.$$

A curve was drawn showing the relation between

$$\log_{10}\frac{\alpha y_0}{h} - 0{\cdot}03512 \quad \text{and} \quad \frac{\alpha}{r};$$

and since the curve must pass through the origin, it can be used for extrapolation of the correction to larger values of r.

Results.

Five values of $\frac{r}{\alpha}$ were worked out, corresponding to values of $\log_{10}\frac{h}{\alpha}$ differing by 0·5; in addition, two points were taken from Bashforth and Adams's tables. The results are given in Table I.

Table I.

$\frac{r}{\alpha}$.	$\mathrm{Log}_{10}\frac{h}{\alpha}\times 10^{10}$.	$\mathrm{Log}_{10}\frac{\alpha y_0}{h} - 0{\cdot}03512$.
3·0	9·36603	0·00188
3·1	9·32651	0·00227
3·9278	9·0	0·00395
5·1866	8·5	0·00406
6·4294	8·0	0·00346
7·6584	7·5	0·00289
8·8764	7·0	0·00262

The first two values were obtained by interpolation from the tables of Bashforth and Adams, the remainder are new points; the values of $\frac{r}{\alpha}$ are somewhat uncertain in the fourth place, but when the figures in the third column are plotted against $\frac{\alpha}{r}$, the smoothness of the curve shows that the values of $\log_{10}\frac{h}{x}$ are unlikely to be in error by as much as three in the fourth place.

The final results are given in Table II., which extends the table given by Sugden up to a point where the capillary rise is infinitesimal.

TABLE II.

$\text{Log}_{10}\frac{h}{\alpha} \times 10^{10}$.

$\frac{r}{a}$.	0·0.	0·2.	0·4.	0·6.	0·8.	1·0.
3·0	9·3660	9·2870	9·2082	9·1294	9·0505	8·9715
4·0	8·9715	8·8924	8·8132	8·7338	8·6542	8·5746
5·0	8·5746	8·4947	8·4147	8·3345	8·2540	8·1734
6·0	8·1734	8·0927	8·0119	7·9309	7·8497	7·7685
7·0	7·7685	7·6870	7·6054	7·5238	7·4420	7·3601
8·0	7·3601	7·2781	7·1960	7·1138	7·0315	6·9491
9·0	6·9491	6·8666	6·7840	6·7014	6·6187	6·5359
10·0	6·5359	6·4530	6·3700	6·2871	6·2040	6·1208
11·0	6·1208	6·0376	5·9543	5·8711	5·7877	5·7042

XXXI. *A Method of Measuring the Radiant Heat emitted during Gaseous Explosions. By* C. H. JOHNSON, *Ph.D.* (*Chemical Department, University College, London*) *.

THE radiation from flames has long been known to represent a considerable fraction of the total heat of combustion. This radiation lies mainly in the infra-red, with very small amounts in the visible and ultra-violet regions of the spectrum. The percentage of the heat of combustion appearing as radiation is governed by a large number of independent factors, so that its magnitude is very largely determined by the experimental conditions. Thus Callendar (Brit. Assoc. Rep. 1910) found that 16 per cent. of the gross heat of combustion was radiated from a large coal-gas flame burning under the most favourable conditions, whilst small flames radiated much less—2 to 3 per cent. only. The latter figures agree with the earlier results of R. Helmholtz (*Verhandlungen des Vereins zur Beförderung des gewerbfliesses in Prüssen*, lxviii. 1889).

Hopkinson (Proc. Roy. Soc. A, lxxxiv. p. 155, 1910) was responsible for the pioneer work upon measurements of radiant energy emitted during gaseous explosions, and using coal-gas and air in such proportions as to ensure complete combustion, found that the energy radiated during explosion

* Communicated by Prof. W. E. Garner, D.Sc.

and cooling amounted to 22 per cent. of the gross heat of combustion; only 3 per cent. appeared up to the time of attainment of maximum pressure, which must represent roughly that emitted during the period of inflammation. David (Proc. Roy. Soc. A, xcviii. p. 183, 1920) has obtained further data which may be summarized briefly. Hydrogen-air mixtures sustained losses by radiation of 8 to 16 per cent. of the total heat of combustion, depending on the strengths of the mixtures employed; the losses from explosions of coal-gas and air varied between 23 and 26 per cent. It is necessary to emphasize the fact that these figures refer to the radiation emitted both during explosion and during the process of cooling. The percentages emitted up to the time of attainment of maximum pressure were from 0·5 to 1·4 per cent. in the case of hydrogen-air mixtures, and from 3·3 to 7·0 per cent. with coal-gas.

This practically represents the whole of the present-day knowledge of this subject. From the standpoint of the engineering sciences, such data are of great value; but from the point of view of physical chemistry in its endeavour to unravel the problems of mechanism of chemical reaction, and in particular of the part played by radiation from the flame front in "activating" the unburnt gases ahead of the wave, all the above measurements suffer from two vital defects. In the first place the gas mixtures which have been studied are very complex, and in the second place it is impossible to distinguish between the radiation received from the burning gases in the wave-front and the purely thermal emission by the hot products of combustion.

Another important aspect is the recognized dual character of radiant heat: first there is thermal emission, which is emitted from any hot material in thermal equilibrium whatever its state of aggregation; and secondly chemi-luminescence or luminous heat, which may be emitted by flames. It is possible that an appreciable part of the available chemical energy of flames is liberated directly as radiation from the freshly-formed molecules, the latter originally containing more energy associated with the so-called internal degrees of freedom than corresponds to their mean kinetic energy. It is unnecessary to enter into a lengthy consideration of this question; practically every contribution connected with the subject contains an elaborate discussion of the meagre experimental data available.

It is nowadays taken for granted that a gas can radiate by virtue of its temperature, and it is fairly certain that the

greater part of the radiation produced during combustion in engine cylinders is of this type. There are, however, two isolated observations—one due to David and the other to R. Helmholtz—which are frequently quoted in support of the view that a portion of the radiation from flames is of the second type, which it is convenient to call "chemiluminescence." David found that the maximum rate of emission of energy from an exploded mixture of coal-gas and air occurred 0·025 sec. before the attainment of maximum temperature, which may indicate occurrence of chemiluminescence in this explosion.

The second experiment is that by Helmholtz, in which he showed that preheating the gases (coal-gas and air) diminished the intensity of radiation from the flame in spite of the fact that the mean temperature of the flame is raised by the preheating. Helmholtz explained the decreased emission as caused by an increase in the rate of attainment of thermal equilibrium at the higher temperature of the flame. In other words, the supposed chemiluminescence was decreased on preheating the gases on account of the more rapid degradation of the chemical energy into thermal energy by molecular collisions. Reference to the original publication and examination of the diagram of the burner used in the experiments shows that the gases (preheated separately to about 1800° K.) mixed before appearing at the jet. Thus there is no doubt that some chemical combination appeared here, and that consequently there was less reaction in the flame and therefore less energy radiated. Haslam, Lovell, and Hunneman (J. Ind. and Eng. Chem. 1925, p. 272), who successfully verified the result, admit that their experiments were inconclusive for the same reason. While, therefore, it would be untrue to say that there have been no indications of luminescent heat, yet up to the present time no certain demonstration of the phenomenon has been given.

It is in this connexion that the augmentation of the infra-red energy which accompanies the drying of mixtures of carbon monoxide and oxygen is particularly interesting (see Garner and Johnson, Phil. Mag. iii. p. 97, 1927). There can be no doubt that the mean flame temperature in the case of an explosion of dried carbon monoxide and oxygen is lower than when a trace of water is present, since the explosion time is relatively long and the combustion less complete. Yet more than three times as much energy is liberated as radiation from the wave-front in the case of the dried gases. Even supposing there were differences in the modes

of propagation in the two cases, it seems impossible to avoid the conclusion that the extra radiation is luminescent in character. This is probably the first reliable evidence of the existence of "luminescent heat."

It may be well to emphasize here the importance attaching to the design of bomb for use in such investigations. It was anticipated that with a narrow cylindrical bomb the very rapid cooling of the gases would reduce to negligible proportions the amount of radiation emitted by the products of combustion. The analyses of total-radiation curves (see later) confirm this expectation, and prove that to all practical purposes the effective radiation is from the wave-front. This is in very sharp contrast with David's experimental conditions, where at least 90 per cent. of the radiation originates in the hot products of combustion. The bomb used by David has a capacity of about 21 litres, which was 150 times that used in these investigations. In explosions of coal-gas and air, only about 3 per cent. of the gross heat of combustion was received upon the bolometer up to the time of attainment of maximum pressure ; of this, only part originated in the flame. Chemiluminescence, if it occurred, would thus be very largely masked by thermal emission in David's experiments.

Having observed the remarkable sensitiveness of the infra-red spectrum of burning carbon monoxide to traces of water and other catalysts (Garner and Johnson, *loc. cit.*), and having established a relationship between the emission of radiant energy and the speed of propagation of flame, it was necessary to determine the absolute amounts of energy emitted, in order to ascertain whether they were of sufficient magnitude to account for the large variations in explosion velocity. The experiments about to be described were carried out with this end in view.

The problem of calculating the percentage of the heat of combustion appearing as radiation is by no means simple with a bomb such as that used in this work in conjunction with a linear thermopile placed at some distance in front of it.

Experimental.

The explosions were carried out in a cylindrical bomb of phosphor bronze, 36 cm. long and internal diameter 2·4 cm., with a standard mixture of pure carbon monoxide and oxygen in the proportions 2 : 1, ignited by the fusion of 1·5 mm. of thin iron wire. The radiation penetrating a fluorite window

was recorded upon a sensitive quick-acting linear thermopile placed some 30 cm. in front of the window, the thermopile working in conjunction with a Downing galvanometer, critically damped. The movements of the latter instrument were recorded photographically upon a revolving drum, and thus was obtained a series of deflexion-time curves the areas of which were proportional to the amount of heat received by the thermopile. For a full account of the experimental procedure, reference should be made to the published work already referred to.

In order to determine the calorific equivalents of these total radiation records, their areas were compared with that of a "Control Curve" obtained by placing suddenly upon the thermopile a known small quantity of radiation and registering the galvanometer deflexion thus obtained, all other experimental conditions being maintained precisely as when recording radiation from the explosions.

To obtain a Control Curve.

Fig. 1 shows the disposition of the apparatus. The pointolite lamp L is held in position in front of the

Fig. 1.

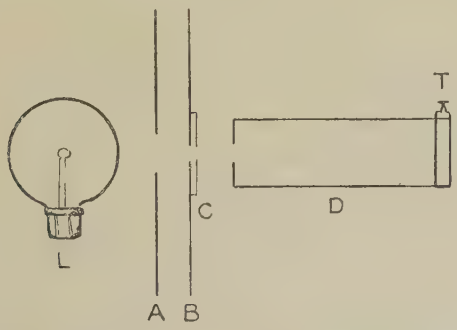

thermopile T, and between them is placed an iron shield A with a circular orifice of 3 cm. diameter, an asbestos board B with an orifice of 1 cm. diameter, and a camera shutter C, mounted with its diaphragm open to about 0·8 cm. The orifices are centrally placed in regard to one another, and of such dimensions that the whole thermopile slit can "see" the glowing point of the pointolite. The thermopile has the same slit-width, and the galvanometer the same sensitivity as in the explosion experiments. It was found that opening and closing the camera shutter caused no deflexion of the galvanometer, provided the lamp was not in circuit. With the camera shutter closed the lamp is turned on (run at a

constant current of 1·25 amps.) and allowed to remain for five minutes before starting the experiment ; several records are then taken with the shutter adjusted to give an exposure of "$\frac{1}{230}$" second. These are the control curves. They were found to be exceedingly reproducible, but the control curve used in the analysis of the explosion record was an average curve obtained by taking means of the ordinates of the individual control curves at corresponding times.

Measurement of the Energy Equivalent of the Control Curve.

There being no standard source of radiant heat available, the problem resolved itself into the measurement of the rate of emission of energy (in absolute units) from a pointolite lamp. The calibration was based upon an experiment by Denning (Phil. Mag. x. p. 270, 1905)), but many modifications were necessary to suit the particular problem in hand. The method is a calorimetric one, the lamp being allowed to illuminate a metal disk of known mass, and the initial rate of rise of temperature determined. It can be shown that the quantity of radiation received by unit area of the disk per second $(R) = \frac{ms}{A}\frac{dT}{dt}$, where m is the mass of the disk, A its area, s the specific heat, and $\frac{dT}{dt}$ (° C./sec.) the initial rate of rise of temperature. The main part of the experiment centres round the measurement of $\frac{dT}{dt}$.

A copper disk, 1 cm. in diameter and 2 mm. thick, is made one junction of a copper-eureka couple, and mounted in an iron tube as shown in fig. 2 ; before mounting, the disk and tube are carefully blacked over a smoky turpentine flame.

Fig. 2.

In explanation of fig. 2, R is the iron tube, N a tight-fitting cork, S, S thin silica tubes, and P and Q are, respectively, fine copper and eureka wires affixed to the copper disk E with a minute amount of solder. The dimensions of the iron tube are very nearly the same as those of the brass tube in front of the thermopile slit (D, fig. 1), and a cardboard disk with an orifice (1·2 × 2 cm.) affixed to the end of the iron tube is exactly similar to the corresponding orifice

in the thermopile tube. The thermopile is removed and the iron tube put in its place, so that the copper disk is in the same vertical plane as previously occupied by the thermopile. Before finally inserting the cork carrying the copper disk it is important to make sure that the tube is aligned in such a way that all parts of the disk can "see" the pointolite, and thus ensure uniform illumination. The other junction of the couple is maintained at constant temperature by immersing in water contained in a Dewar vessel, and the wires are connected to the Downing galvanometer (critically damped). The work consists essentially of two experiments: first, the determination of the rate of change of galvanometer deflexion $\left(\frac{d\theta}{dt}\text{ cm./sec.}\right)$ upon opening the camera shutter with the lamp running at 1·25 amps. (as before); second, the recording of deflexions produced by maintaining the two junctions of the thermocouple at different temperatures; both junctions, in this case, are kept immersed in water in Dewar vessels, the water being stirred by bubbling air through it, and the temperatures measured by means of standardized Beckmann thermometers. The galvanometer deflexions are recorded photographically in both experiments. The $\frac{d\theta}{dt}$ curves are time-marked, and can thus be measured up accurately. In the second case the temperature differences are plotted against deflexions, and $\frac{d\theta}{d\mathrm{T}}$ (cm./° C.) obtained from the slope of the straight-line graph.

Now $\frac{d\theta}{dt} \div \frac{d\theta}{d\mathrm{T}} = \frac{d\mathrm{T}}{dt}$, the inital rate of rise of temperature in ° C. per sec. The mass of the disk is determined, and its mean diameter when blackened measured with the aid of a travelling microscope. Thus all the data necessary for the calculation of R, the quantity of radiation falling on the disk per sq. cm. per sec., has been obtained. The galvanometer sensitivity has to be considerably reduced for this work and the instrument shunted; the only necessary precaution is to ensure that the sensitivity and shunt are the same in both $\frac{d\theta}{dt}$ and $\frac{d\theta'}{d\mathrm{T}}$ experiments. In order to check the accuracy of the method, the whole experiment was repeated with a silver disk in place of the copper. The result with the silver disk was almost precisely the mean of wo obtained with the copper disk.

Calibration of the Camera Shutter.

The pointolite lamp is enclosed in a light-tight box with a small opening, in front of which is placed the camera shutter. A condensing lens (mounted in a tube) focusses the image of the camera diaphragm upon the drum. The method is to take two or three "$\frac{1}{250}$ sec." exposures upon a film with the drum at rest, and then to give "$\frac{1}{250}$ sec." exposures with the drum rotating at a high speed; the film is independently time-marked so that the speed of rotation is readily calculated. From the images thus recorded several things become apparent: first, that even with this short exposure the shutter opens completely and closes instantaneously; a very slight (and not always appreciable) tailing-off in the front of the image indicates that there is sometimes a small lag in the opening process. The maximum error introduced on this account is, however, negligibly small. From the elongation of the image and the speed of rotation of the drum the true time of exposure is easily calculated.

The thermopile line was examined under a low-power travelling microscope, and the discontinuities were found to amount to less than 0·5 per cent. of the total length.

Results.

1. Amount of heat radiated from the pointolite lamp to thermopile per sq. cm. of thermopile surface per second.

Experiment.	Calories/sq. cm./sec.	Mean.
Cu disk	0·0023	
Ag „	0·0024	0·0027
Cu „	0·0026	

2. Exposure time ("$\frac{1}{250}$" second).

Experiment.	Exposure time.	Mean.
1	0·0028	
2	0·0027	0·0028
3	0·0029	
4	0·0027	

3. Effective area of thermopile surface = 0·0574 sq. cm.
Length of thermopile line = 1·13 cm.
Width „ „ „ = 0·504 mm.

CALCULATION.

Energy corresponding to area of control curve
= Energy/cm²/sec. × Area of thermopile surface
× Exposure time
$= 0{\cdot}0024 \times 0{\cdot}0574 \times 0{\cdot}0028.$
$= 3{\cdot}86 \times 10^{-7}$ calorie.

The energy equivalents of all the total radiation records have been estimated from this basic result.

The calorific values of the total-radiation records can be calculated from the product of the energy equivalent of the control curve and the ratio of the areas of the explosion and control curves. The radiation received on the thermopile represents only a minute portion of the total energy radiated during an explosion. The ratio of the energy received on the thermopile to the total radiation is $3{\cdot}519 \times 10^{-7}$. The evaluation of this fraction is a long and complicated process, and is dealt with fully in the appendix to this paper.

There are also several factors that reduce the radiation falling on the thermopile, for which allowance must be made in calculating the true value for the amount of energy radiated during explosion. These are as follows: absorption by the cold carbon monoxide ahead of the wave; absorption and reflexion from the fluorite window; reflexion from the thermopile surface; penetration of the thermopile line due to discontinuities; and absorption by atmospheric moisture and carbon dioxide.

Since the thermopile line cannot "see" the walls of the bomb, reflexion effects do not enter into the problem; the very slight focussing action of the fluorite window is probably negligible. It is not possible to make allowance for absorption of thermal radiation by hot carbon dioxide; the analysis of the radiation curves indicates, however, that practically all the radiation is from the wave-front. The corrections to be applied for the various losses are now considered in detail.

1. *Absorption by Carbon Monoxide.*

The calculation is lengthy, but the steps can be stated briefly:—From data given by Coblentz (Pubns. of Carnegie Inst. No. 35, 1905) the average absorption by carbon monoxide in each of the two regions covered by the emission

bands from the explosion is calculated (Garner and Johnson, *loc. cit.*). From this is computed the average extinction coefficient in both bands, separately, and the emission spectra corrected; the true ratio of emission intensity in the 2·8 μ and 4·4 μ bands of the explosion becomes 1·34 : 1. From this result and the values for the two extinction coefficients is calculated the average extinction coefficient of the cold carbon monoxide in the explosion; the value obtained was 0·000171. From the relation $\frac{E_0}{E} = e^{kpl}$, where l is the length of the column of carbon monoxide, p the partial pressure of the gas, and k the average extinction coefficient, the mean value of $\frac{E_0}{E}$, the ratio of the true to the apparent emission intensity (averaged over the entire length of the bomb), is readily obtained.

The final result showed that 14 per cent. of the total infra-red emission is absorbed by the cold carbon monoxide.

2. *Absorption and Reflexion by the Fluorite Window.*

Coblentz (Pubns. of Carnegie Inst. No. 97, 1908) has found that the extinction coefficient of colourless fluorite is practically constant over the range of wave-lengths between 2 μ and 7 μ.

By experiment it was found that the losses due to these causes for the window used (1·0 cm. thickness) amounted to 14 per cent. of the energy radiated.

3. *Reflexion from the Blackened Thermopile Surface.*

Correction ..... 2 per cent. (Glazebrook's Dict. of Applied Physics.)

4. *Penetration of Thermopile Line and Atmospheric Absorption.*

The losses are negligible.

The total losses therefore represent approximately 30 per cent. of the energy radiated. Thus the radiation curves only register about 70 per cent. of the total energy emitted in the direction of the thermopile. The multiplying factor is therefore 1·43.

Calculation of the percentage of the gross heat of combustion liberated as radiation in an explosion of wet gas mixture, i. e., of standard mixture containing 1·9 per cent. of water-vapour.

Area of curve for wet gas = 4·19 × area of control curve.

∴ Calorific value of wet gas curve = $4{\cdot}19 \times 3{\cdot}86 \times 10^{-7}$ calorie.

Corrected calorific value of wet gas curve* = $4{\cdot}19 \times 3{\cdot}86 \times 10^{-7} \times 1{\cdot}43$ calorie.

Ratio of energy received by thermopile to total energy radiated = $3{\cdot}519 \times 10^{-7}$.

∴ Total energy radiated during wet gas explosion = 6·57 calorie.

Gross Heat of Combustion.

$$2CO + O_2 \rightarrow 2CO_2 + 135{,}400 \text{ calories.}$$

The volume of gas mixture held by the bomb = 164 c.c. (see Appendix). This volume of standard mixture corresponds to a calorific value of 308 calories.

Analyses made upon the gas mixture and upon the products of combustion show that this value needs to be corrected, since in no case is the combustion complete.

Table I.—Gas Analysis.

Description.	Percentage of Mixture unburnt after explosion.	Corrected Gross Heat.
Wet gas	9·0	280 calories.
Dried gas	9·8	278 „
Dried gas + CCl_4 ...	10·0	277 „

The large amount of gas remaining unburnt even in the presence of water-vapour is surprisingly large. Less than 1 per cent. of impurity (probably nitrogen) was detected in the standard mixture. No great accuracy is claimed for the analyses, but a large number were carried out and the results were quite consistent. In any case, the above correction makes little difference to the order of the final result.

Thus percentage of total heat radiated during explosion of wet gas mixture = $\frac{6{\cdot}57 \times 100}{280} = 2{\cdot}3$ per cent.

* Water-vapour of this concentration does not appreciably absorb the energy emitted from the explosion.

Similar calculations have been made in the other cases, and the results are tabulated below.

TABLE II.—Herein are summarized the main results of the research.

Description.	Per cent of Gross Heat of Combustion radiated during explosion.
Wet gas	2·3
Dried gas	8·6
Dried gas+CCl_4 * ...	9·5

It is obvious from the involved nature of the calculations that these percentages can only indicate the order of magnitude of the emission intensities. It is satisfactory that they are in agreement with the results of other similar investigations. Probably a large part of the radiation emitted from an explosion of wet gas mixture is thermal in character; the 6–7 per cent. increase represents the extent of chemiluminescence.

Note. The last two figures should be increased by about 10 per cent. of their values in order to allow for losses by conduction to the parts of the thermopile during the period over which radiation is received upon it. This correction has not been made.

It is at present impossible to take into account the relation of speed of chemical combination to the velocity of propagation of flame, since there appears to be no data relevant to temperature coefficients and velocity constants of the homogeneous reaction between carbon monoxide and oxygen. Assuming a temperature in the neighbourhood of 2500° K. for the explosion wave in wet gas, the loss of an extra 6 or 7 per cent. of the gross heat of combustion from the dried gas mixture may reduce this temperature by 100–150°, and quite apart from other factors which also enter in, such a temperature difference is capable of producing large changes in the velocity of combustion, and hence in the rate of propagation of flame.

* About 1 per cent. by volume of CCl_4. See other publications, *loc cit.*

Appendix.

Calculation of the Fraction of Energy received by the Thermopile of the total amount radiated during an Explosion.

The method is long and somewhat involved, but may summarily be divided into three stages :—

I. By graphical construction, and a drawing to scale, to determine the boundaries of the space within the bomb from which the thermopile, either the whole or part, receives radiation.

II. To determine the average length of thermopile visible from any section of the bomb. Obviously at any section (taken through a plane at right angles to the axis of the bomb) part only will radiate to the whole of the thermopile, and part will illuminate portions of the thermopile.

III. Making use of the general equation obtained in II. to calculate an expression for the fraction of the total radiant energy received upon the thermopile from any section of the bomb, whence the total energy radiated is readily obtained.

Fig. 3.

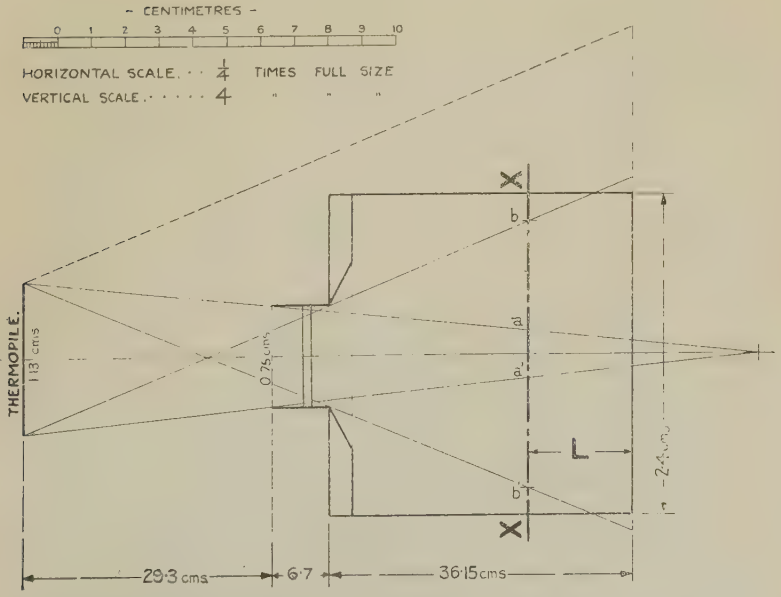

For this work it was necessary to construct accurate drawings to scale, and in II. to obtain a solution by mean

of graphical projections. In this connexion the author is greatly indebted to his friend, E. T. Hutt of the Great Western Railway Co., both for inspiration and for the time spent in making the drawings.

I. The bomb and its relation to the thermopile are drawn to scale in fig. 3. Lines have been drawn from the thermopile to indicate the limits of the effective radiating beam. It is at once apparent from consideration of any length XX at right angles to the length of the bomb and parallel to the thermopile, that only a fraction of it (a, a) "sees" the whole of the thermopile; the parts (ab, $a'b'$) "see" portions only, whilst beyond bb' none of the radiation emitted can be received on the thermopile. From the known dimensions of the diagram and from the properties of similar triangles, it is a fairly simple matter to derive expressions for the lengths aa' and bb' merely involving L, the distance of any section from the end of the bomb, viz.:—

$$aa' = 0{\cdot}012968\,\mathrm{L} - 0{\cdot}19428, \quad . \quad . \quad . \quad . \quad (1)$$

$$bb' = 2{\cdot}6379 - 0{\cdot}0522\,\mathrm{L}. \quad . \quad . \quad . \quad . \quad . \quad (2)$$

II. On account of the fact that the thermopile is rectangular and the orifice of the bomb a cylindrical tube of small bore, the shape of the beam responsible for the radiation falling upon it can only be determined by making orthographic projections at various sections along the bomb. These projections can be contoured in such a way as to show the proportion of the length of thermopile line visible from the different parts of the given sections. Such a contoured projection is reproduced in fig. 4 (6). Details of the construction are now given.

The Method of Projections.

It was convenient to make projections upon a scale eight times the actual dimensions of the bomb. In order to visualize the method, it is helpful to imagine the reverse process of what actually occurs; namely, the illumination of the interior of the bomb by the thermopile line. Then the shadow cast by the outer circular orifice of the small cylindrical tube determines aa' (fig. 3), and that cast by the inner circular orifice bb'. The radii of the shadows cast from the outer and inner orifices can be obtained readily, for any section, from the known dimensions of the small cylindrical

tube, the distances of the thermopile and of the line XX from the window. In this way the following formulæ were obtained :—

Radius of shadow cast by inner orifice,

$$r_i = 0{\cdot}7516 - 0{\cdot}0104\,\mathrm{L}.$$

" " " outer orifice,

$$r_0 = 0{\cdot}92342 - 0{\cdot}12798\,\mathrm{L}.$$

Thus r_i and r_0 can be calculated for any given section.

Fig. 4.

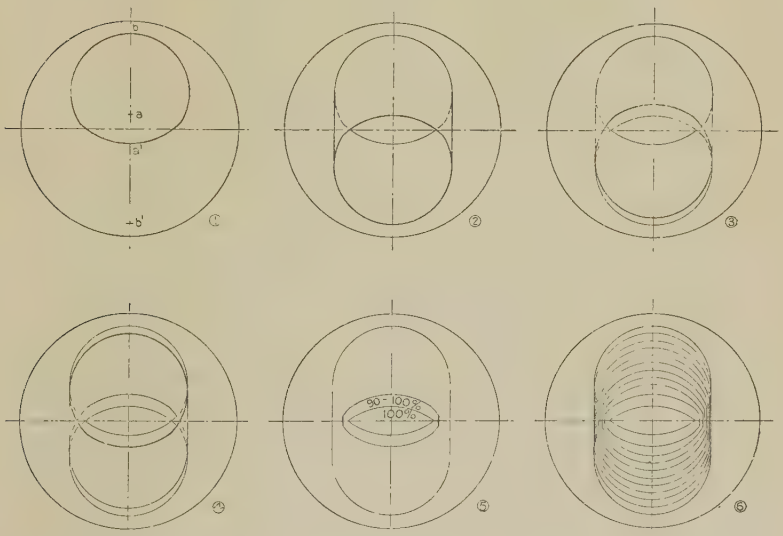

In order to make a contoured projection, the cross-section of the bomb is drawn and rectangular coordinates added ; on the vertical axis the lengths bb', aa' for the given section are set off symmetrically about the centre. Through b the arc of a circle is drawn of radius r_i. Through a' another arc of radius r_0 is drawn to intersect the first. Clearly, the area enclosed by these arcs represents the portion of the given cross-section of the bomb from which the lowest point of the thermopile is visible (fig. 4 (1)). See also fig. 3. This is repeated for b' and a, and thus is obtained the corresponding area for the topmost point of the thermopile. The area included by the overlap of these two outlines gives the portion of the given cross-section of the bomb from which the whole of the thermopile is visible. By drawing the common tangents, an outline (2) is obtained which circumscribes the area from which any fraction whatever of the

thermopile is visible. Any part of the section outside this boundary is invisible from the thermopile and non-effective for the purpose of radiation measurement. In the successive stages of the projection process illustrated in fig. 4, the new construction lines are shown broader than those drawn in preceding stages.

Now consider the similar but slightly more complicated problem of finding the outline of the area within which the thermopile is visible to the extent of 90–100 per cent. In this case a continuous length equivalent to 90 per cent. of the thermopile may be considered to occupy any position along the full length of the thermopile line. First, consider that the 90 per cent. length is measured from the bottom upwards ; as previously, for the full length of the thermopile, the lowest point will again produce the outline (1) in fig. 4, but the topmost point will produce a new outline formed by the intersection of an arc of radius r_0 drawn at a distance p above a, and an arc of radius r_i at a distance q above b'. The distances p and q may be calculated from the diagram in fig. 3 by the method of similar triangles. The area covered by the overlap of these two outlines represents the area of a given cross-section from which the thermopile is at least 90 per cent. visible, in the lower position (3). This process is repeated for the case of the 90-per-cent. length measured from the top downwards, when a similar but inverted outline is obtained as shown in (4). Joining these outlines by vertical straight lines an area is obtained within which 90 per cent. or more of the thermopile line is visible (5).

The quantities p and q are constant for constant decrements of the thermopile length, and thus for 10 per cent. decrements a series of outlines may be obtained, subject, however, to the fact (incidental to the nature of the orifice of the bomb) that r_0 ceases to modify the outlines beyond a certain point. This is easily verified by reference to fig. 3. By repetition of the process the whole of the outline (2) may be contoured. The final result is shown in (6).

The diagram (6) is to be regarded as a contoured map ; it is, in fact, an orthographic projection of a three-dimensional figure with base representing the given cross-section of the bomb and with perpendicular ordinates proportional to the length of thermopile visible from each point in it. Fig. 5 is the projection of another section taken nearer the fluorite window than (6).

In order to obtain the average length of thermopile visible from the given section across the bomb, which from now onwards will be denoted by T, it is necessary to measure

the volume of the three-dimensional figure. This was done by the accurate but laborious method of finding the areas of the separate contours, determining the volume enclosed by each adjacent pair, and summing them. The formula used for calculating the volume enclosed by any two irregular areas A and a separated by a distance d was $v=\frac{d}{3}(A-\sqrt{Aa}+a)$. Since the contours were taken

Fig. 5.

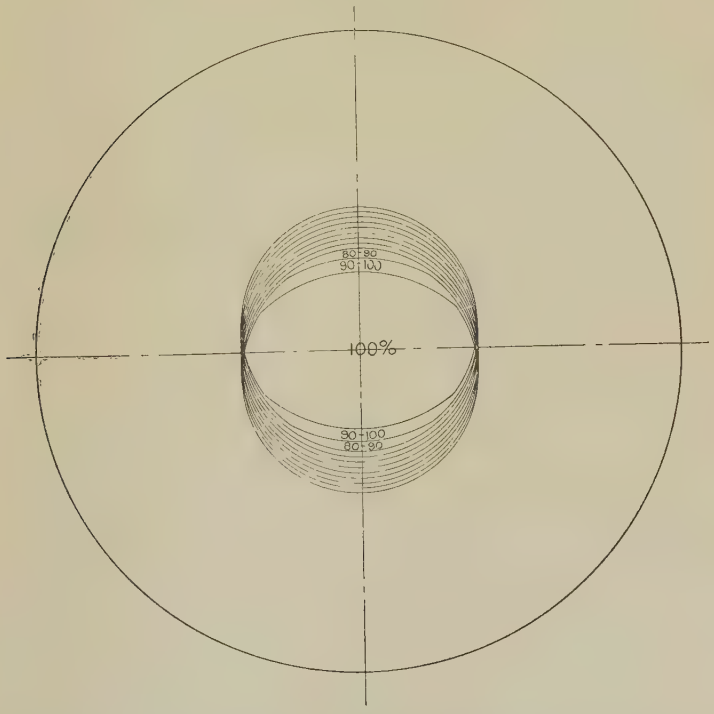

at intervals of 10 per cent., d in the formula is equal to one-tenth of the length of the thermopile line, *i. e.* 0·113 cm. Σv represents the volume of the solid figure V. Then $V \div \frac{\pi D^2}{4}$, where D is the diameter of the bomb, gives the average height to the solid figure, which is the mean value of T for the section considered. Care must be taken when estimating v that due allowance is made for the enlarged scale of the section.

In this way a value of T was obtained at three different sections distant 10, 20, and 30 cm. from the end of the bomb.

From the relation $T=AL^2+BL+C$ the constants A, B, C were evaluated, with the result:

$$T=0{\cdot}0000685\,L^2-0{\cdot}011505\,L+0{\cdot}43370. \quad . \quad (3)$$

From equation (3) it is obvious that when $L=0$, $T=0{\cdot}4337$. T was therefore determined by graphical construction for the section through the extreme end of the bomb, and a value 0·432 obtained. This gives some idea of the accuracy with which the method can be applied, and at the same time proves the general correctness of equation (3).

The justification for assuming an equation of the type $AL^2+BL+C=T$ is that it had previously been found to apply for the imaginary case of a surface thermopile with a circular receiving surface. In this simpler case the contoured projections are made up of a series of concentric circles, the effective beam of radiation within the bomb being conical. If H represents the full diameter of the thermopile surface, D the internal diameter of the bomb, and A and B respectively the values of *aa'* and *bb'*, then it is readily proved that

$$T=\frac{H}{3D^2}(B^2+AB+A^2),$$

or, substituting the values of A and B,

$$T=0{\cdot}0001447\,L^2-0{\cdot}01609\,L+0{\cdot}49098. \quad . \quad . \quad (4)$$

In this particular case of a surface thermopile, T is a mean diameter. Comparison of the T curves obtained from equations (3) and (4) is shown in fig 6. Since with the experimental arrangement the last 4·56 cm. of bomb wall truncate the extreme portions of the *bb'* region, slight corrections are necessary, and are indicated by dotted lines on the curves. The corrections were determined graphically by re-drawing the extreme limits of the *bb'* region on a large scale and, by taking 2 per cent. visibility increments instead of 10 per cent., finding the area cut off by intersection of the bomb walls.

The close resemblance of the curves derived from equations (3) and (4) is rather surprising; the areas enclosed differ only by about 2 or 3 per cent.

III. The next steps in the calculation can be stated summarily as follows:—If the flame-front is considered instantaneously to occupy any particular section of the bomb distant K cm. from the thermopile, it will radiate in a practically uniform manner in all directions, and concentric

spheres proceeding outwards from the flame-front will form surfaces of uniform radiation density. The thermopile can therefore be considered to occupy part of the surface of one of these spheres (radius K cm.), and the fraction of the total energy radiated received by the thermopile is given by the ratio of the area of the thermopile (average length visible × slit-width) to the area of the sphere, $4\pi K^2$. Thus at any

Fig. 6.

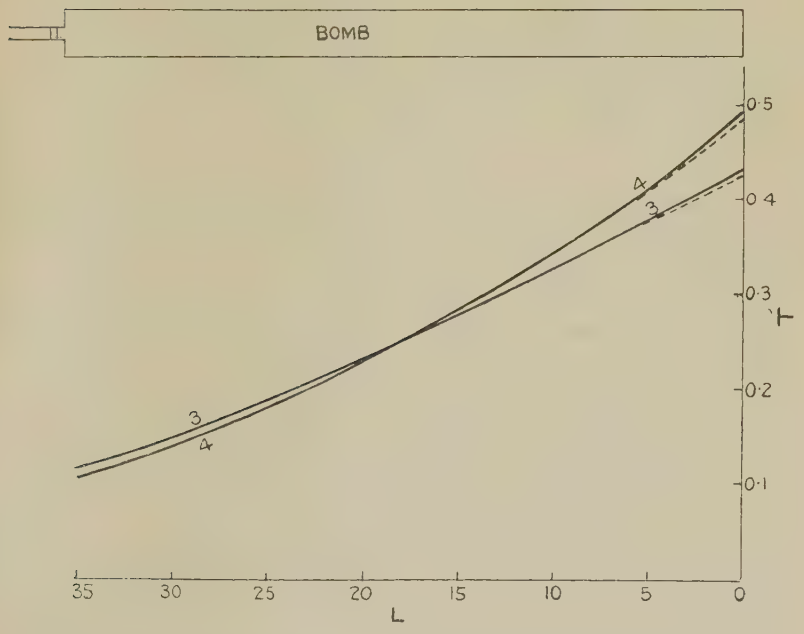

section of the bomb distant K from the thermopile the fraction of the energy received by the thermopile of the total amount radiated $= 4\frac{bT}{4\pi K^2}$, where b is the slit-width.

Note.—Obviously, only the central portion of the thermopile lies in the surface of the sphere of radius K, and moreover, all parts of the wave-front will be distant K cm. from the thermopile, but with the experimental arrangement used, errors introduced on this account are absolutely inappreciable, and neglecting them greatly simplifies the subsequent procedure.

T has already been expressed as a function of L in

equation (3). This can readily be transformed into a function of K, since the thermopile and bomb are fixed in definite relationship to one another. Thus $T=f(K)$, and the above expression becomes

$$\frac{b[f(K)]}{4\pi K^2}.$$

Integration of this expression between the limits imposed by the length of the bomb gives the area enclosed by the curve obtained by plotting values of the above fraction against K. Dividing this area by the length of the bomb, the mean value of the fraction averaged over the length of the bomb is obtained. Thus is calculated the average fraction of the total energy radiated received upon the thermopile.

Calculation.

For the purposes of integration, as has already been pointed out, it is necessary to transform equation (3) from a function of L into a function of K.

When this is done ($L=72{\cdot}15-K$), equation (3) becomes

$$T=0{\cdot}0000685\,K^2+0{\cdot}0016205\,K-0{\cdot}0398. \quad . \quad . \quad (5)$$

$$\frac{\text{Average area of thermopile visible}}{\text{Area of corresponding sphere}}=\frac{bT}{4\pi K^2}$$

$$=\frac{b(\cdot0000685\,K^2+\cdot0016205\,K-\cdot0398)}{4\pi K^2}$$

$$=\frac{b}{4\pi}(\cdot0000685+\cdot0016205\,K^{-1}-\cdot0398\,K^{-2}). \quad (6)$$

From equation (6) can be calculated the fraction of the total energy radiated reaching the thermopile from any section of the bomb.

Integration of (6) gives

$$\frac{b}{4\pi}(\cdot0000685\,K+\cdot0016205\log_e K+\cdot0398\,K^{-1}+C). \quad . \quad (7)$$

The limits of the long cylindrical portion of the bomb between which the integration is to be made are $K=36{\cdot}0$ cm. and $K=72{\cdot}15$ cm. This length also includes a small conical part of the bomb leading from the main portion into the narrow cylindrical tube carrying the fluorite window (see fig. 3). Since no part of the conical neck is visible to the thermopile, it is permissible to treat it as though the transition from the large to the small cylindrical tube was abrupt, provided that allowance is made when estimating the capacity of the bomb for the small extra space assumed to

exist. This method is much less laborious than dealing separately with the small conical space, and perfectly accurate.

Evaluation of equation (7) gives the area enclosed by the $\frac{Tb}{4\pi K^2}$, K curve. Dividing this area by the effective length of the bomb (36·15 cm.), the average fraction of the total radiation received on the thermopile is obtained. The value of this fraction is $3{\cdot}406 \times 10^{-7}$.

The average value of this fraction for the very small cylindrical section between the main bomb tube and the fluorite window is very easily calculated. T is practically constant at 1·10 cm., and the limits of K are 36 and 34·7 cm. The fraction is $3{\cdot}558 \times 10^{-6}$.

The volume of the main cylindrical part of the bomb is 163·5 cc.

The volume of the small cylindrical part of the bomb is 0·57 cc.

By simple proportion, therefore, the fraction of the total radiated energy received by the thermopile, averaged over the entire bomb,

$$= 3{\cdot}519 \times 10^{-7}.$$

The following table is of interest in showing that under the experimental conditions the energy received on the thermopile from any part of the bomb is practically constant.

K.	$\frac{bT}{4\pi K^2}$.
36	$3{\cdot}348 \times 10^{-7}$
40	3·403 „
45	3·431 „
50	3·437 „
55	3·430 „
60	3·414 „
72·15	3·368 „

The above method of calculation has been given at some length, since it may be of use, at any rate in principle, to others engaged upon similar work. A very great simplification is possible if, instead of a linear thermopile, a thermopile with a circular receiving surface or, secondly, a "point" thermopile is used. In these cases no accurate drawings are necessary, since the effective radiating beam within the

bomb is conical in section, and thus the projections (if made) would merely be concentric circles, and the volume of the three-dimensional figure (see text) readily estimated by means of the ordinary formula for the frustrum of a cone. In this connexion reference should be made to equation (4). Unfortunately, a surface thermopile is not suitable for this kind of work, having large thermal capacity, being slow-acting and very susceptible to losses by conduction. A sensitive, single-element, vacuum thermopile (approximating to a "point" thermopile) constructed by Moll is now on the market, and might possibly be adapted for work in the infra-red.

Summary.

When conducting a physico-chemical examination of the radiation from a gaseous explosion, it is very important to discriminate between the emission of radiant energy from the wave-front and that from the hot products of combustion, a point to which little consideration seems to have been given by other investigators. In order to attain the desired result, a long narrow explosion vessel was used in which the rapid cooling of the burnt gases behind the wave reduced to almost negligible proportions the amount of radiation received from that source. A simple method for the calibration of a linear thermopile, necessarily placed at some distance from the bomb, has been described which enabled a quantitative extension of work detailed in other publications to be made.

The effect of water, and incidentally of other catalysts, upon the emission of infra-red radiation from the wave-front in explosions of carbon monoxide and oxygen has proved to be of considerable magnitude. In particular, an additional 7 per cent. of the gross heat of combustion was radiated from a dried gas mixture, in excess of that emitted in the presence of 1·9 per cent. of water-vapour. In future, therefore, no theory designed to explain the action of water in promoting spread of flame through carbon monoxide-oxygen mixtures can be considered complete that does not include the hitherto unrecognized radiation factor.

The author wishes to express his indebtedness to Professor W. E. Garner for helpful criticism and advice during the course of the investigation, to Mr. Allis who constructed the explosion vessel, and to the Department of Scientific and Industrial Research for a maintenance grant.

The Ramsay Laboratories of
Inorganic and Physical Chemistry,
University College, London.

XXXII. *A Study of the Rectification Efficiency of Thermionic Valves at Moderately High Frequencies.* *By* W. E. Benham, *B.Sc.**

Introduction.

THE principle involved in the valve voltmeter due to Moullin † is well known. If a small oscillatory e.m.f. is suitably applied to a thermionic valve, a certain change ΔI in mean anode current takes place. This change in mean anode current is proportional to the square of the amplitude of the input e.m.f., provided this amplitude does not exceed a certain value generally of the order of 1 volt. Calibration of the voltmeter, which may be either of the diode or triode type, is effected by means of measured low-frequency voltages. Suppose, however, that it is suspected that high-frequency voltages will not produce the same value of ΔI as low-frequency voltages of the same amplitude. The calibration would then be subject to correction for frequency. Moullin himself states in his book ‡ that a frequency error of the voltmeter is less than 1·5 per cent. at λ 300 metres, this result being based on measurements with a sensitive electrostatic voltmeter or radio-frequency electrometer. The object of the present paper is to show that for wave-lengths much shorter than λ 300 metres a frequency error is apparent, and to indicate the nature of the frequency variation of ΔI at constant input voltage amplitude. The experiments about to be described consist essentially of measurements on a Moullin diode type voltmeter with a view to investigating the frequency error referred to, the input voltage being measured by means of an electrometer of the suspended needle type. Owing to the large number of variables, the experiments are necessarily very incomplete, and must be regarded as of a preliminary nature only, relative rather than absolute accuracy being aimed at.

Experimental Details.

Various types of valve were tested. In the first experiments the valve was used as a diode.

Referring to the diagram (fig. 1), it will be seen that the grid g is connected externally to the anode a. The filament f was heated by a current supplied by an accumulator e through

* Communicated by Prof. Alfred W. Porter, F.R.S.

† J. I. E. E. lxi. p. 295 (1923).

‡ 'Radio-frequency Measurements' (Griffin), 1926, p. 38.

a variable rheostat r. The source of steady potential E_1 was a high-tension accumulator.

The source of high-frequency oscillations was a valve oscillator covering the range of frequencies from 4·1 to 16·8 megacycles. (N.B. The term megacycle is used throughout this paper to denote 10^6 cycles per second.) The oscillator was calibrated against a standard by a method of harmonics. The coil L had four or five turns only, and was loosely coupled to the oscillator (not shown in the diagram).

The quadrant electrometer Q was a Dolezalek, and served to measure the root mean square value of the high-frequency e.m.f. induced in the coil L; the needle of the instrument was connected to the point A. The condenser C_1 was a blocking condenser of $2\,\mu$ F. capacity, and is needed to isolate the high-tension accumulator, which would otherwise

Fig. 1.—Circuit diagram.

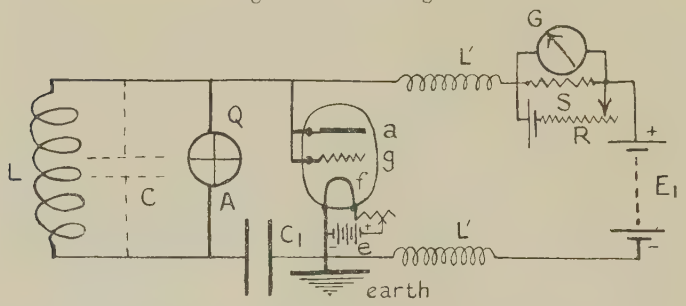

short-circuit. With the frequencies in use, its impedance is always less than 0·04 ohm, so that the voltage drop across it is negligible as far as the high-frequency current through the valve is concerned. The quadrant electrometer can, therefore, be regarded as connected directly across the valve. The electrometer was found to have a capacity of about $0{\cdot}0005\,\mu$ F. This was the only capacity connected across the coil L save that in the valve itself, so its capacity is represented by the dotted condenser C in the diagram.

The rectified component of the current passes through the system G, S, E_2, R, which is adjusted so that there is no current through the galvanometer until the oscillator is brought into play. The shunt S controls the sensitivity of the galvanometer, and makes it sufficiently damped for readings to be taken as quickly as the electrometer itself will allow. The oscillating component is prevented from passing through the galvanometer etc. by air-core chokes L′.

This arrangement confines the high frequency to the left, and the direct currents to the right, in the diagram.

On the high-frequency side of the apparatus all leads were kept short and thick. In view of the importance of ensuring that the valve is subject to the same high-frequency potential as the electrometer, which would not be the case if the leads had an inductance comparable with L or a capacity comparable with C, the valve was mounted near the terminals of the electrometer, and the condenser C_1 was also held very near by means of a wooden stand. The electrometer was at first screened; but this was afterwards found to make no difference, the reason being that stray static potentials have no effect, since the coil L permanently short-circuits the instrument so far as static potentials are concerned.

Sensitivity of Electrometer.

The idiostatically-connected electrometer was connected to sources of steady potential which could be applied in either direction, and the deflexions ϕ on a millimetre scale placed 100 cm. from the instrument were read. The results are recorded in the following table, the last column giving K in the formula $K\phi = V^2$, where K is constant and V is the applied potential in volts, ϕ being in millimetres.

V.	V^2.	Mean ϕ.	K.
26·0	676	97·0	6·97
17·3	299	42·1	6·89
4·0	16	2·2	7·2
2·1	4·4	0·7	6·3

This table shows how insensitive the instrument becomes for low voltages, and it is just the low voltages for which we require to use it. Taking $K = 6{\cdot}9$, we note that for $\phi = 5$ mm. $V = 5{\cdot}9$ volts; for $\phi = 10$ mm. $V = 8{\cdot}3$ volts. In order to get the peak voltage of the corresponding alternating voltages, the above voltages must be multiplied by $\sqrt{2}$, giving 8·3 volts at $\phi = 5$ mm. and 11·7 volts at $\phi = 10$ mm.

Method of Experiment—Outline.

The filaments of the valves were turned on for such time as was necessary for the steady currents to attain constant values. The resistance R was then adjusted to balance out the steady current. The oscillator was then brought into play by completing the plate circuit of the oscillator. The coil L was then coupled sufficiently to the oscillator to deflect the electrometer by a certain amount ϕ read on a millimetre scale. The corresponding deflexion θ of the galvanometer G

was then taken. The oscillator was then cut out and its frequency altered to another value, and the above readings repeated. The zeros of both the electrometer and galvanometer were inclined to change ; but while the change of the former was gradual, and therefore not serious, the changes in the latter were often sudden. This is due to irregularities in the emission from the filament—the well-known Schottky effect *,—and is troublesome when the deflexions are very small, as is the case when measuring small changes in steady current. The trouble caused by these irregularities was to some extent overcome by taking several readings of θ.

In the following series of measurements the input voltage was given several different values at a given frequency. Each of the tables (I. *a–d*) is devoted to a definite frequency. The deflexion ϕ was first adjusted to 1 mm., and the deflexion θ noted as accurately as possible, and then given successively increasing values up to ϕ 1·3 mm., which corresponds to a range of peak voltages from about 3·7 to 13·5 volts. The voltage was then given successively *decreasing* values. The mean value of θ only is shown.

DATA—Marconi R-type Valve.

Filament voltage ..... $e_f = 4{\cdot}0$

Grid / Anode voltage (steady) ..... $E_1 = 26{\cdot}0$

Peak value of input voltage..... $e = 3{\cdot}7 \rightarrow 13{\cdot}5$

Mean anode current ..... $I = 4{\cdot}18$ m. A.

Change in anode current ..... $\Delta I = 0{\cdot}017\theta$ „
(where θ is in cm. deflexion)

TABLE I. (*a*).—N = 15·00.

Electrometer deflexion. ϕ (cm.).	Galvanometer deflexion. Mean θ (cm.).	$\frac{\Delta I}{I}$.	$\frac{1}{\phi}\frac{\Delta I}{I}$.
0·2	0·325	$1{\cdot}24\times10^{-2}$	$6{\cdot}2\times10^{-2}$
0·3	0·5	1·91	6·37
0·4	0·6	2·29	5·73
0·5	0·8	3·05	6·1
0·6	1·025	3·90	6·5
0·7	1·2	4·57	6·53
0·8	1·525	5·8	7·25
0·94	2·05	7·81	8·30
1·0	2·25	8·57	8·57
1·1	2·625	10·0	9·09
1·2	3·075	11·7	9·75
1·3	4·05	15·4	11·85

* *Ann. der Phys.* lvii. p. 541 (1918).

TABLE I. (*b*).—N = 10·89.

Electrometer deflexion. ϕ (cm.).	Galvanometer deflexion. Mean θ (cm.).	$\frac{\Delta I}{I}$.	$\frac{1}{\phi}\frac{\Delta I}{I}$.
0·2 } 0·2 }	0·3375	$1{\cdot}35\times10^{-2}$	$6{\cdot}75\times10^{-2}$
0·3	0·475	1·90	6·33
0·4	0·65	2·60	6·50
0·5	0·825	3·30	6·60
0·6	0·975	3·90	6·50
0·7	1·15	4·60	6·57
0·8	1·425	5·70	7·12
0·9	—	—	—
1·0	1·825	7·30	7·30
1·1	2·15	8·60	7·82
1·2	2·425	9·70	8·08
1·3	2·775	11·10	8·54

TABLE I. (*c*).—N = 8·02.

Electrometer deflexion. ϕ (cm.).	Galvanometer deflexion. Mean θ (cm.).	$\frac{\Delta I}{I}$.	$\frac{1}{\phi}\frac{\Delta I}{I}$.
0·2	0·4	$1{\cdot}57\times10^{-2}$	$7{\cdot}85\times10^{-2}$
0·3	0·55	2·135	7·12
0·4	0·725	2·86	7·15
0·5	0·875	3·45	6·90
0·6	1·05	4·14	6·90
0·7	1·25	4·93	7·04
0·8	1·4	5·52	6·90
0·94	1·85	(7·29)	7·75
1·0	1·85	7·29	7·29
1·1	2·175	8·56	7·78
1·2	2·425	9·56	7·97
1·3	2·7	10·63	8·18

TABLE I. (*d*).—N = 5·02.

Electrometer deflexion. ϕ (cm.).	Galvanometer deflexion. Mean θ (cm.).	$\frac{\Delta I}{I}$.	$\frac{1}{\phi}\frac{\Delta I}{I}$.
0·2	0·425	$1{\cdot}65\times10^{-2}$	$8{\cdot}25\times10^{-2}$
0·3	0·60	2·33	7·77
0·4	0·75	2·91	7·28
0·5	1·0	3·88	7·76
0·6	1·25	4·85	8·08
0·7	1·325	5·14	7·34
0·8	1·575	6·11	7·64
0·94	2·025	7·85	8·35
1·0	2·075	8·05	8·05
1·1	2·4	9·31	8·46
1·2	2·85	11·05	8·21
1·3	3·175	12·32	9·48

On fig. 2 $\frac{1}{\phi}\frac{\Delta I}{I}$ is plotted against ϕ for two frequencies. The result would be horizontal straight lines if rectification took place according to a square law. It will be seen from the curves—

(*a*) That departure from square-law rectification takes place at some value of input voltage amplitude *which is different at different frequencies.*

(*b*) That the rectified current is in general *different at different frequencies* for a given voltage amplitude.

Fig. 2.—Showing relation between rectified current and square of input voltage at two frequencies.

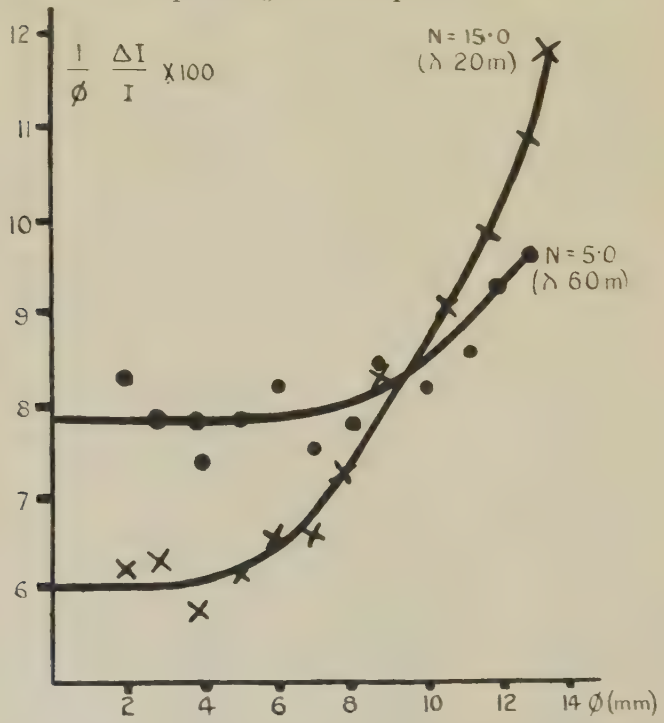

With regard to (*b*), it is to be noted that the frequency variation referred to is independent of the external impedances, and must not be confused with the case in which an oscillatory e.m.f. of given value is supplied to the valve *in series with an external impedance.* In this case (*cf.* Chaffee and Browning, Proc. I. R. E. Am. xv. p. 2, Feb. 1927) a frequency variation arises from the fact that the voltage

across the valve is different at different frequencies. If the voltage across the valve is kept constant, the external impedances have no influence on the rectified current, and any observed frequency variation must be due to the valve itself.

The variation of rectified current with frequency is indicated by fig. 3. The values of $\frac{\Delta I}{I}$ for a given value of

Fig. 3.—Showing the variation of rectified current with frequency at different input voltages.

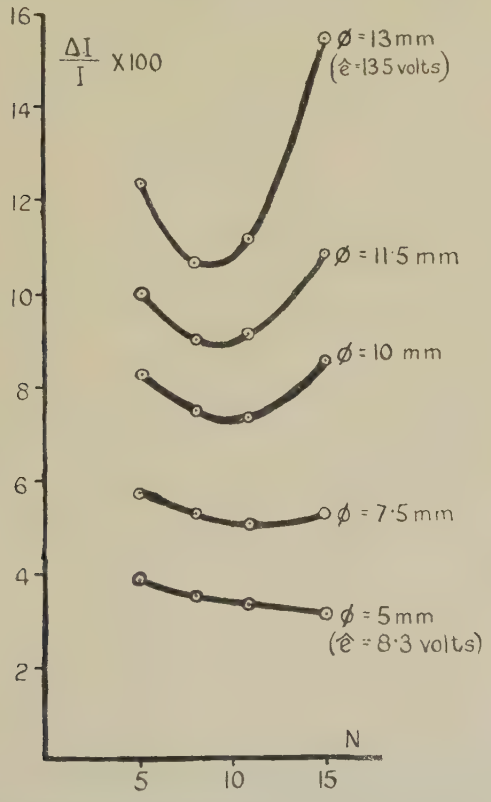

ϕ are smoothed values obtained by plotting a curve having $\frac{\Delta I}{I}$ as ordinates and ϕ as abscissæ. Fig. 3 gives some idea of the increase of input voltage amplitude on frequency variation, but must not be taken as an accurate representation of the variation of rectified current with frequency, as the curves are based on four frequencies only.

Variation of Rectified Current with Frequency for Small Values of Input Voltage Amplitude.

The lowest curve of fig. 3 is of most immediate interest, since the value of ϕ to which it corresponds is low enough to ensure square-law rectification over the greater part of the range $N = 4{\cdot}1 \rightarrow 16{\cdot}9$ mega-cycles. The departure from square-law rectification at $\phi = 5$ mm. is seen from fig. 2 to be in the neighbourhood of 2 per cent. at 15·00 mega-cycles. In order to establish the form of this curve accurately, it is necessary to take measurements at a large number of frequencies. The resulting curves for two valves are shown in figs. 4 and 5. In the case of the Marconi R-type valve,

Fig. 4.—Showing variation of rectified current with frequency at constant (input) voltage amplitude.

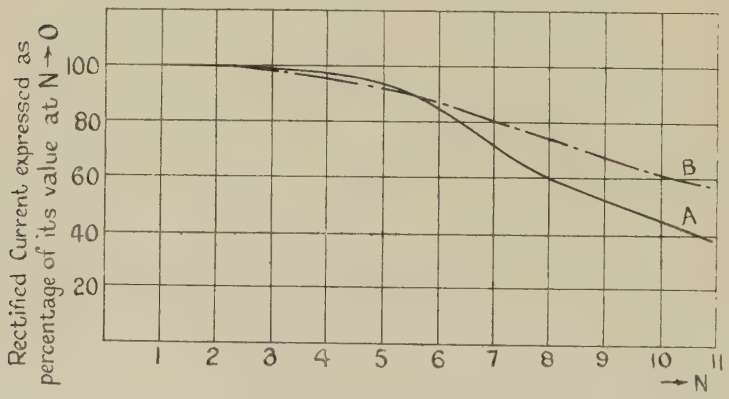

Marconi R-type Valve.

Conditions:—

A. Filament voltage = 4·2.
B. „ „ = 5·0.

For both curves $\acute{e} = 8{\cdot}3$ volts ($\phi = 5$ mm.).
E = 24 „

measurements were made at two filament temperatures. The broken curve B corresponds to a filament voltage of E_f 5·0, the full-line curve to E_f 4·2. Now temperature saturation is approached at a filament voltage of 5 in the case of the valve quoted, so that for this case Langmuir's 3/2 power law is most nearly satisfied. Fig. 5 indicates that the variation is less in the case of a Dutch valve (bright valve, now obsolete), possibly due to the smaller electrode dimensions.

With regard to the upper curves of fig. 3, it appears that the magnitude of the frequency variation is greatly enhanced by increase of input voltage amplitude. For large amplitudes the rectified current arises from a whole series of terms in $\sin npt$, where n is even. The frequency variation of such terms is likely to increase rapidly with n.

It was expected that the anode voltage E would have, for given values of ϕ and E_f, an appreciable effect on the magnitude of the variation. This was not found to be the

Fig. 5.—Showing variation of rectified current with frequency for a Dutch valve.

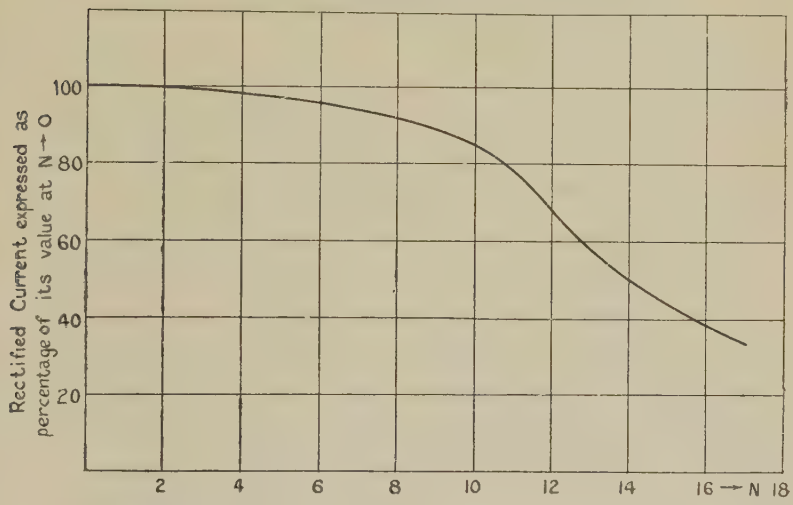

Conditions :—

Filament voltage = 4·0 volts.
$\hat{e}$ = 8·3 „
E = 24 „

case for values of E below that required for voltage saturation, the variation for E=0 being sensibly of the same form and magnitude as the variation for E=24. If the voltage E is increased above voltage saturation value, it becomes necessary to increase E_f in order to obtain a reading at all. The variation is then appreciably diminished, and none could be detected at E 60, E_f 5. The variation must depend on E_f in a very complex manner in view of the crossing of the two curves of fig. 4.

Effect of Gases.

With a view to obtaining information as to the effect of gases a helium-filled valve (Type A.R. 1) was used. Substantially the results were similar to those obtained with gas-free valves, below the critical potential. Above the critical potential enormous frequency variations took place, the change in mean anode current being positive at some frequencies and negative at others; the curves are very unreliable, due to the large amount of ionization. The plate voltage has a very marked effect above the critical potential, inasmuch as increase of plate voltage increases

Fig. 6.—Showing rectified current as function of frequency in case of valve used as a triode and containing helium vapour.

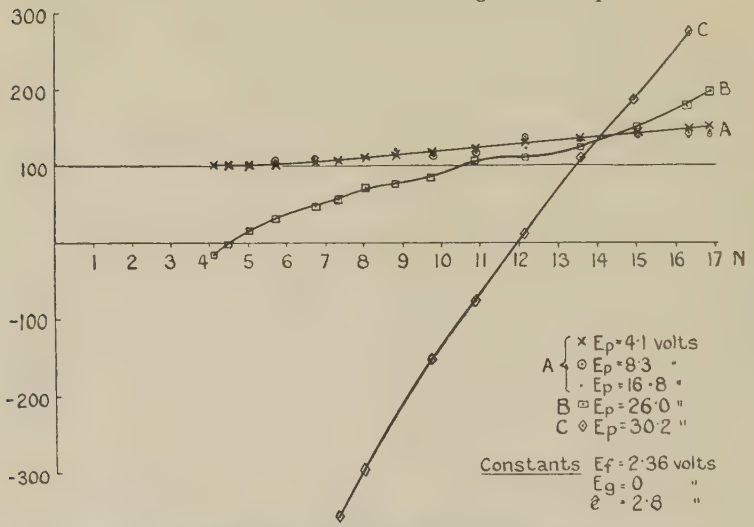

The curve A corresponds to plate potentials E_p *below* the critical potential of helium (=21·4 volts), and represents the rectified current as a percentage of its value at $N \rightarrow 0$. The curves B and C correspond to potentials above the critical potential of helium. The input voltage amplitude ($\hat{e}$=2·8) was the maximum consistent with square-law rectification.

the degree of ionization and therefore the number of slowly-moving ions. The fact that the rectified current changes sign is doubtless due to the fact that two kinds of thermions are present—He^+ and electrons. At low frequencies the observed rectified current is mainly due to He^+ ions. At nigh frequencies these ions become exceedingly sluggish, and the rectified current is again carried mainly by electrons. The curves for this helium valve are shown on fig. 6. The

valve was used as a *triode* in order to diminish the chance of overrunning. The grid was connected through a coupling coil to the filament. It will be seen that the rectified *anode* current *increases* with frequency for a given voltage amplitude between filament and *grid*. The irregularities in the curves obtained for voltages below the critical potential may be due to small traces of ionization. These irregularities did not repeat regularly or in the same place, so that, while the points are shown, the curve drawn corresponds to the average form, which repeated itself. The points × corresponding to $E = 4$ volts lie very nearly on this curve. The curves corresponding to values of E above the critical potential are plotted on the same diagram. The most interesting result to be obtained from fig. 6 is that the curves A, B, and C cross one another at a frequency of 14 megacycles, approximately. The obvious interpretation of this result is that the contribution of the positive ions towards the rectified current is zero at this point.

The presence of gases clearly complicated matters. It would seem as if the observed frequency variation in the absence of gas is in some way due to the inertia of the electrons. The theoretic aspect of this question will be relegated to a subsequent paper.

Summary.

1. Experiments with a diode are described which show that—

(*a*) For a given input voltage amplitude the rectified current is in general different at different frequencies, the frequencies employed in the experiments lying between 4·1 and 16·8 megacycles (λ 73–λ 17·8 metres).

(*b*) The value of input voltage amplitude at which departure from square-law rectification takes place decreases as the frequency is increased.

2. The form of the frequency variation is investigated in detail in the case where the input voltage amplitude is small enough for rectification to take place according to a square law. In this case the rectified current falls off as the frequency is increased, the rate of variation being markedly affected by the filament temperature.

3. Experiments with a helium-filled valve used as a triode show a variation of similar form and magnitude for plate voltages below the critical potential, the variation corresponding, however, to an increase with frequency as

distinct from the decrease with a two-electrode valve. For plate voltages above the critical potential the variation with frequency is much more rapid, doubtless due to the presence of slowly-moving ions; at a certain frequency, depending on the potential, the rectified current is zero, the rectified current due to the space-charge being neutralized by a similar current due to the helium ions. At a higher frequency (about $N = 14$ megacycles) the rectified current is the same as it would be in the absence of helium ions; in other words, there is no rectification due to helium ions in the neighbourhood of this frequency.

In conclusion, the author wishes to thank Prof. E. V. Appleton for the loan of a Helium valve, and the Department of Scientific and Industrial Research for a maintenance grant, with the aid of which this research has been made possible.

XXXIII. *The Problem of a Hidden Polarized Sphere.* *By* Prof. A. Petrowsky, *Hon. Member of Rori (The Russian Society of Radio Engineers)* *.

Contents.

Introduction.

Part I.

§ 1. Differential equations and boundary conditions in the case of a limitless medium.

§ 2. Expression of the electric potential and of the electric force for such case.

§ 3. A polarized sphere in a medium bordered on one side by a plane.

§ 4. Final expression of the electric potential and force.

§ 5. Transformation of the formulæ.

§ 6. A general characteristic of longitudinal electroprofiles.

§ 7. A general characteristic of transversal electroprofiles.

§ 8. Generalization of solving the problem of a hidden sphere.

§ 9. A general characteristic of oblique electroprofiles.

Introduction.

A WIDE application of physics in various regions of knowledge evokes new questions which insistently demand their solution. In this respect geology and mining are in advance, where the spreading of physical methods of investigating the structure of the earth's crust and the quest

* Communicated by the Author.

of useful minerals is daily increasing. It follows, as a matter of course, that the circumstances in which one is obliged to solve physical problems are often so complicated that a mathematical analysis of the question meets with unsurmountable difficulties; in such a case the engineer is assisted by the laboratory and by experimental investigation on models, taking into account the definite demand of similarity. Thus the greater value attaches to the analytical investigation of the simplest cases, especially of those where the question is solved to the end and expressions are obtained in the form of algebraic-trigonometrical formulæ, which give from the first glance a clear conception of the phenomenon.

The examination of one of such simple cases is the subject of the present paper. We shall call it "The Problem of a Hidden Polarized Sphere."

The problem consists in the following :—

All infinite space is divided into two parts by a plane $X O_0 Y$ (fig. 1), and the medium filling the upper part represents a dielectric, whereas the medium filling the lower possesses conductivity.

Fig. 1.—The sphere hidden in a homogeneous isotropic half-space.

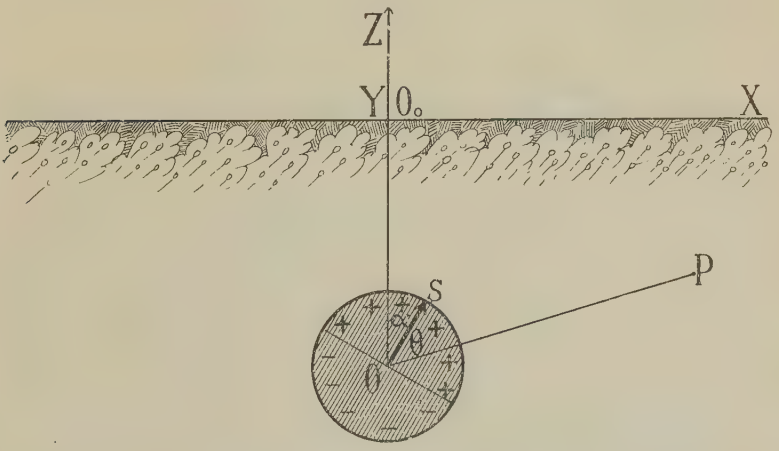

In some region of the lower part an ideally conducting sphere is hid, of a radius r_0, the centre of which O is at the depth h under the plane of division, and is projected on the latter in the point O_0.

By any causes whatever the above-mentioned sphere is polarized—*i. e.*, it develops an electromotive force of its own

which has the greatest value along a certain diameter (axis of polarization), inclined at an angle α to the vertical, and diminishes by cosine law in dependence on the angle θ, which is formed by the given direction and the axis of polarization

$$e = \mathrm{E} \cos \theta. \quad . \quad . \quad . \quad . \quad . \quad . \quad (1)$$

At the same time, in the conducting medium surrounding the sphere a current is formed which spreads over the whole lower part of the space, evoking electric and magnetic effects. It is required to determine whether it is possible, and in what manner, by observing the above-mentioned effects on the plane of division (or near it), to find all elements characterizing the hidden sphere—*i. e.*, the exact situation of O_0, the projection of the centre, the depth of its bed h, and the radius of the sphere r_0.

In solving the question we shall make the following assumptions :—

(*a*) Each of the mediums filling the two parts of the space is homogeneous and isotropic.

(*b*) The bed's depth to the centre of the sphere, h, is considerably greater in comparison with the radius of this sphere r_0.

Part I.

Electric Field of a Hidden Sphere.

§ 1. Let us suppose that the plane of division is absent, and that the whole space is filled with a homogeneous isotropic medium.

Let the right-hand system of coordinates (fig. 2) be disposed so as to place its beginning in the centre of the sphere; the axis $O\zeta$ to correspond in direction with the axis of polarization, viz. of the greatest development of the electromotive force; the axis $O\xi$ to be perpendicular to $O\zeta$ in the plane of the drawing, and the axis $O\eta$ perpendicular to the latter. In such a case, the system being symmetrical in respect of the axis $O\zeta$, we may assume that the electric potential U and all other values are functions of two derivatives only ; for example, of the radius r and the polar angle θ,

$$\mathrm{U} = \mathrm{U}(r, \theta).$$

The value U must satisfy the differential equation of Laplace, which for the considered case will take the form

$$\frac{\partial^2 \mathrm{U}}{\partial r^2} + \frac{2}{r}\frac{\partial \mathrm{U}}{\partial r} + \frac{1}{r^2}\frac{\partial^2 \mathrm{U}}{\partial \theta^2} + \frac{\cot \theta}{r^2}\frac{\partial \mathrm{U}}{\partial \theta} \quad . \quad . \quad . \quad (2)$$

Moreover, this function must be finite, single-valued, and continuous, and must satisfy the following conditions :—

(*a*) For the surface of a sphere it must take the form expressed by the formula (1), namely for

$$r=r_0, \quad U=\frac{E}{2}\cos\theta. \quad . \quad . \quad . \quad . \quad . \quad (3)$$

In fact, the distribution of the electricity over the surface will then be symmetrical, and the difference of potentials in each point will be balanced by the electromotive force.

Fig. 2.—Distribution of the axis of coordinates (vertical and horizontal projections).

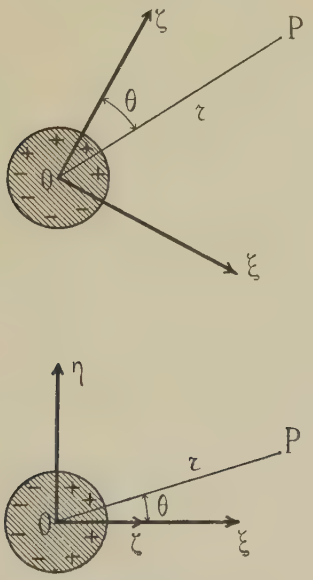

(*b*) For any very distant point of the space it must be reduced to zero. Consequently

$$r=\infty, \quad U=0 \quad . \quad . \quad . \quad . \quad . \quad . \quad (4)$$

§ 2. The solution of these differential equations will be sought in the form

$$U=U'(r)\cos\theta+U''(r), \quad . \quad . \quad . \quad . \quad (5)$$

where $U'(r)$ and $U''(r)$ are unknown functions of the variable r only. Following the method used in my paper "On the Theory of Earth-Currents' Measurement*." we

* Phil. Mag. vol. iii. pp. 50–62 (January 1927).

shall easily find that the function U must have the form

$$U=\left(Ar+\frac{B}{r^2}\right)\cos\theta+\frac{C}{r}+D. \quad . \quad . \quad . \quad . \quad . \quad (6)$$

According as we are dealing with the outer ($r>r_0$) or the inner space ($r<r_0$), we can write two functions of the type (6), though with different arbitrary constants A_{ex}, B_{ex}, C_{ex}, D_{ex} and A_{in}, B_{in}, C_{in}, D_{in}, viz.

$$U_{ex}=\left(A_{ex}r+\frac{B_{ex}}{r^2}\right)\cos\theta+\frac{C_{ex}}{r}+D_{ex}, \quad . \quad . \quad (6')$$

$$U_{in}=\left(A_{in}r+\frac{B_{in}}{r^2}\right)\cos\theta+\frac{C_{in}}{r}+D_{in}. \quad . \quad . \quad (6'')$$

Let us consider the former.

To make it satisfy the condition (a), the following equations must hold :—

$$C_{ex}=D_{ex}=0, \quad . \quad . \quad . \quad . \quad . \quad (7)$$

$$A_{ex}r_0+\frac{B_{ex}}{r_0^2}=\frac{E}{2}. \quad . \quad . \quad . \quad . \quad . \quad (8)$$

Whereas, to make it satisfy the condition (b), it is necessary that

$$A_{ex}=0, \quad . \quad . \quad . \quad . \quad . \quad . \quad . \quad (9)$$

which, on comparison with (8), gives

$$B_{ex}=\frac{Er_0^2}{2}. \quad . \quad . \quad . \quad . \quad . \quad (10)$$

Let us consider the second function (6'').

To make it satisfy the condition (a), it is also necessary that the following equations hold :—

$$C_{in}-D_{in}=0, \quad . \quad . \quad . \quad . \quad . \quad . \quad (11)$$

$$A_{in}r_0+\frac{B_{in}}{r_0^2}=\frac{E}{2}. \quad . \quad . \quad . \quad . \quad . \quad (12)$$

Whereas, to make it remain finite in the centre of the sphere, it is necessary to have

$$B_{in}=0, \quad . \quad . \quad . \quad . \quad . \quad . \quad (13)$$

which, compared with (12), gives

$$A_{in}=\frac{E}{2r_0}. \quad . \quad . \quad . \quad . \quad . \quad (14)$$

Thus we finally have expressions for the electric potential in any outer and in any inner point of the sphere :—

$$U_{ex} = \frac{E_0 r^2}{2r^2} \cos\theta, \quad . \quad . \quad . \quad . \quad . \quad (15)$$

$$U_{in} = \frac{Er}{2r_0} \cos\theta. \quad . \quad . \quad . \quad . \quad . \quad (15'')$$

On translation into Descartes's coordinates, the following expressions have to be substituted for r and θ :—

$$r = \sqrt{\xi^2+\eta^2+\zeta^2}, \quad . \quad . \quad . \quad . \quad . \quad (16)$$

$$\cos\theta = \frac{\zeta}{\sqrt{\xi^2+\eta^2+\zeta^2}}. \quad . \quad . \quad . \quad . \quad . \quad (17)$$

Because of symmetry the electric force in any point of the outer field will lie in the plane passing through the given point and through the axis of polarization ; in particular, if the point lies in the plane of the paper, the electric force will lie in the same plane, and can be transformed into two components : that of the axis directed parallel to $O\zeta$ and the normal one directed perpendicular to $O\zeta$, viz. towards P. They are obtained from functions (15′) and (15″) by means of differentiating according to $-\zeta$ and $-\rho$, and are expressed by

$$(F_\zeta)_{ex} = \frac{Er_0^2}{2} \cdot \frac{3\cos^2\theta - 1}{r^3}, \quad . \quad . \quad . \quad (18')$$

$$(F_\rho)_{ex} = \frac{3Er_0^2}{2} \cdot \frac{\sin\theta\cos\theta}{r^3}. \quad . \quad . \quad . \quad (19')$$

The electric force in a point of the inner field is obtained by the same procedure. It is easy to make certain that it is in all points directed parallel to the direction $-O\zeta$, and is consequently expressed by :

$$(F_\zeta)_{in} = -\frac{E}{2r_0}, \quad . \quad . \quad . \quad . \quad . \quad (18'')$$

$$(F_\rho)_{in} = 0. \quad . \quad . \quad . \quad . \quad . \quad . \quad . \quad (19'')$$

In fig. 3 is graphically shown the distribution of isopotential lines of force in the plane passing through the axis of polarization.

§ 3. It has been supposed so far that the sphere is situated in a limitless medium. In reality its centre is placed at some depth under the earth. In such a case the ascending current lines, when reaching the surface, are forced to curve

and continue their way horizontally. It follows, therefore, that the new function W, which expresses the electric potential, must, in addition to all the above conditions, enumerated under 3, satisfy another condition more, namely:

Fig. 3.—Electric field produced by a polarized sphere in a limitless medium.

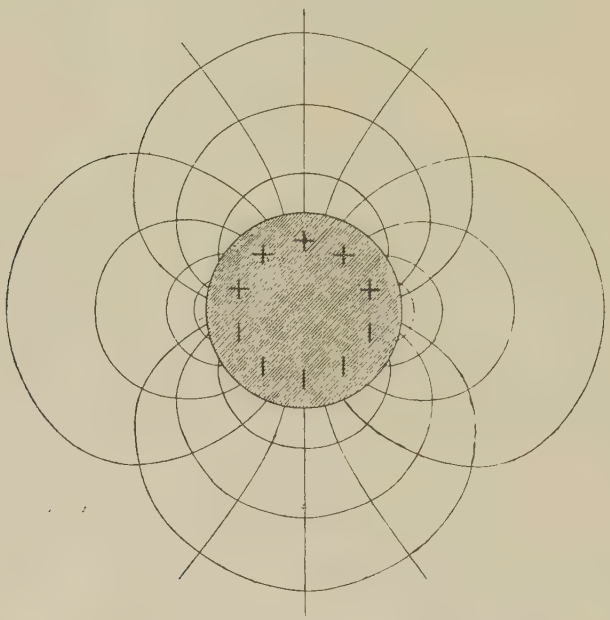

On the parting surface of the two media the electric force must have a tangent component only.

Let us trace a new right-hand system of coordinates (fig. 4) in such manner that its beginning shall be point O_0; in which point the centre of the sphere O is projected on the parting surface. The axis OX shall be directed horizontally either in the plane $O_0O\xi$ or $O_0O\zeta$, passing through the axis of polarization of the sphere; the axis O_0Y horizontally too and perpendicularly to O_0X, whereas the axis O_0Z will be vertically upwards. In such a case the new boundary condition can be expressed by the equation

$$z=0, \quad \frac{\partial W}{\partial z}=0 \quad . \quad . \quad . \quad . \quad . \quad . \quad (20')$$

The function W expressing the electric potential for the

considered case can be found approximately by means of the following consideration.

Let us figure the real electric image of the given sphere O in the plane of parting. It shall be the sphere O′ with radius r_0, situated above the parting surface on the same vertical and at the height h equal to the depth of the centre of the

Fig. 4.—Polarized sphere and its electrical image (vertical and horizontal sections).

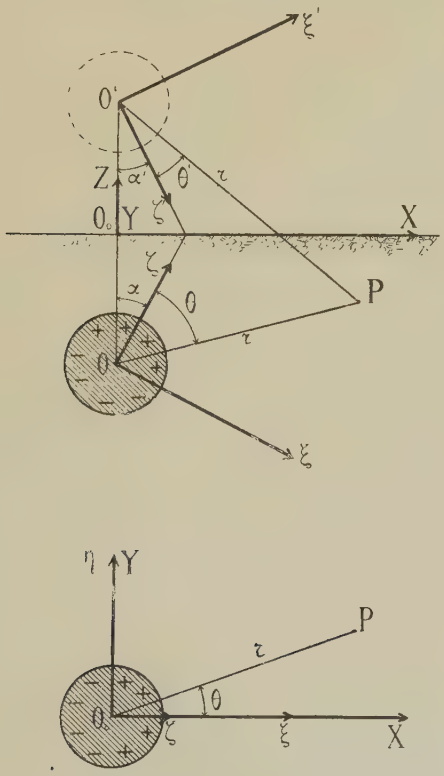

sphere O, polarized in addition according to the cosine law (1) along the line $O'\zeta'$; the latter lies in the plane $OO'Z$ or $OO'\zeta$, and is bent towards $O'O_0$ at the angle $\alpha' = \alpha$.

Should we imagine a third system of coordinates with the axes $O'\xi'$, $O'\eta'$, $O'\zeta'$ which also presents the real image of the system $O\xi$, $O\eta$, $O\zeta$ in the plane of parting, the electric potential produced by the imaginary sphere O′ in any point

P of a uniform, isotropic, limitless medium will obviously be expressed through the formula

$$U'_{ex} = \frac{Er_0^2}{2r'^2}\cos\theta', \quad . \quad . \quad . \quad . \quad . \quad (21')$$

$$U'_{in} = \frac{Er'}{2r_0}\cos\theta', \quad . \quad . \quad . \quad . \quad . \quad (21'')$$

where r' is the distance of the point P to the centre of the sphere O', and θ' is the angle between the direction O'P' and the axis $O'\zeta'$.

The functions (21') and (21'') evidently satisfy all the conditions enumerated under 3.

§ 4. Let us accept the formulæ below for expression of the final potential W in a medium which is limitless on one side and is bordered on the other by the plane $z=0$.

$$W_{ex} = U_{ex} + U'_{ex} = \frac{Er_0^2}{2}\left[\frac{\cos\theta}{r^2} + \frac{\cos\theta'}{r'^2}\right], \quad . \quad (22')$$

$$W_{in} = U_{in} + U'_{in} = \frac{E}{2r_0}\left[r\cos\theta + r_0^3\frac{\cos\theta'}{r'^2}\right]. \quad (22'')$$

It is easy to be convinced that the former satisfies all requirements, including the condition (20), whereas the latter meets them but approximately *. The distribution of the potential within the sphere presenting no practical interest, we may, ignoring the latter circumstance, take the formula (22') for the sought expression of the electric potential created by the polarized sphere situated at some depth under the surface of the plane XO_0Y.

Translating this formula into the coordinates of Descartes, corresponding to the axes X, Y, Z we obtain

$$W = \frac{Er_0^2}{2}\left[\frac{x\sin\alpha + (h+z)\cos\alpha}{[x^2+y^2+(h+z)^2]^{3/2}} + \frac{x\sin\alpha + (h-z)\cos\alpha}{[x^2+y^2+(h-z)^2]^{3/2}}\right], \quad (23)$$

* In the first approximation the coefficient E, standing in the formula (23) and following, is the value of the electric force developed by the sphere; therefore the same expression E is being conserved. In the second approximation it proves to be somewhat lower, namely, instead of E we must put the value A, which is expressed by the formula

$$A = \frac{E}{1+\frac{r_0^2}{8h^2}\left[\frac{\left(1-\frac{r_0}{h}\cos\alpha\right)\cos\alpha + \frac{r_0}{2h}}{\left(1-\frac{r_0}{h}\cos\alpha+\frac{r_0^2}{4h^2}\right)^{3/2}} - \frac{\left(1+\frac{r_0}{h}\cos\alpha\right)\cos\alpha - \frac{r_0}{2h}}{\left(1+\frac{r_0}{h}\cos\alpha+\frac{r_0^2}{4h^2}\right)^{3/2}}\right]}. \quad (24)$$

and on the plane XO_0Y, viz. for $z=0$,

$$W = Er_0^2 \frac{x \sin \alpha + h \cos \alpha}{[x^2+y^2+h^2]^{3/2}}. \quad . \quad . \quad . \quad (25)$$

Fig. 5.—The electroprofile obtained in the plane of polarization.

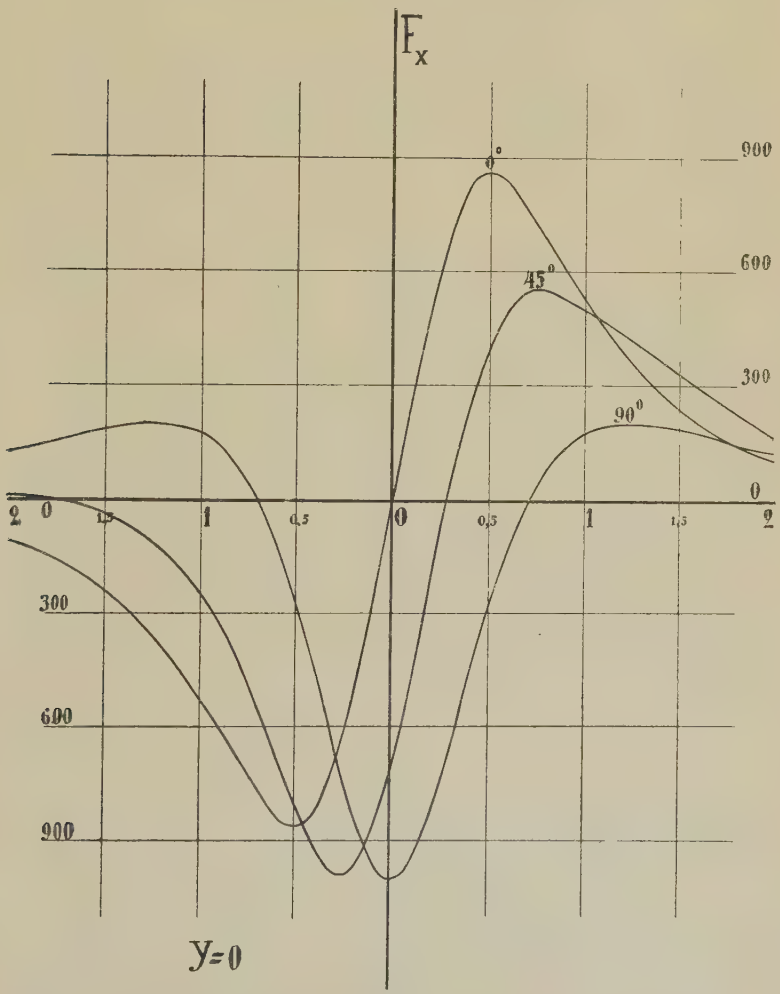

Taking the derivatives of W according to coordinates, we shall find the expressions for respective projections of the electric force too, which on the plane XO_0Y, viz. for

$z=0$, take the form

$$F_x = Er_0^2 \frac{3hx\cos\alpha - (h^2+y^2-2x^2)\sin\alpha}{[h^2+x^2+y^2]^{5/2}}, \quad . \quad (26)$$

$$F_y = Er_0^2 \frac{3(h\cos\alpha + x\sin\alpha)y}{[h^2+x^2+y^2]^{5/2}}, \quad . \quad . \quad . \quad . \quad . \quad (27)$$

$$F_z = 0. \quad . \quad . \quad . \quad . \quad . \quad . \quad . \quad . \quad . \quad . \quad . \quad . \quad (28)$$

§ 5. To get an exact idea of the character of the electro-profile, let us give the graphical representation of the discovered formulæ. For that purpose we introduce the denotations

$$u = \frac{x}{h}, \quad . \quad . \quad . \quad . \quad . \quad . \quad . \quad (29)$$

$$v = \frac{y}{h}. \quad . \quad . \quad . \quad . \quad . \quad . \quad . \quad (30)$$

We have then

(*a*) The electric potential in any point of the plane XO_0Y, possessing the coordinates x and y :

$$W = \frac{Er_0^2}{h^2} \frac{\cos\alpha + u\sin\alpha}{[1+u^2+v^2]^{3/2}}. \quad . \quad . \quad . \quad . \quad . \quad (31)$$

(*b*) The projection of the electric force on the horizontal direction parallel to the plane of polarization of the sphere :

$$F_x = \frac{Er_0^2}{h^3} \cdot \frac{3u\cos\alpha - (1+v^2-2u^2)\sin\alpha}{[1+u^2+v^2]^{5/2}}. \quad . \quad (32)$$

(*c*) The projection of the electric force on a horizontal direction perpendicular to that plane :

$$F_y = \frac{Er_0^2}{h^3} \frac{3(\cos\alpha + u\sin\alpha)v}{[1+u^2+v^2]^{5/2}}. \quad . \quad . \quad . \quad (33)$$

§ 6. In fig. 5 are shown the values of the horizontal projection of the electric force F_x for $y=0$, viz. those obtained when the observer is moving along the axis O_0X (in other words, along the line passing through the horizontal projection of the centre of the sphere and lying in the plane of polarization of that sphere). On the axis of the abscissæ are reckoned the values of u, on the axis of ordinates those of F_x, the coefficient being taken as equal to 1000 $\left(\text{viz. } \frac{Er_0^2}{h^3} = 1000\right)$. The first curve corresponds to the value $\alpha = 0°$ (the axis of polarization of the sphere is running

vertically); the second to the value $\alpha = 45°$ (the axis of polarization is inclined); and the third to the value $\alpha = 90°$ (the axis of polarization is horizontal).

Inspection of fig. 5 leads to the following conclusions: —

1. An electroprofile in a plane of polarization presents in a general case a curve with three numerical maxima, of which two are positive and one negative; besides this the curve has two zero-points, and falls to zero asymptotically when moved from the point where the centre of the hidden sphere is projected.

2. The distribution of the curve of the electroprofile relatively to the projection of the centre of the hidden sphere is not symmetrical:

(*a*) The front zero-point is nearer to the projection of the centre of the sphere than the rear one.

(*b*) The front positive maximum is also nearer than the rear one, and it is greater than the latter.

(*c*) The negative maximum is behind the projection of the centre of the hidden sphere, being nearer to this projection than the front maximum; in absolute value it is greater than either of the positive maxima.

(*d*) In a particular case, when $\alpha = 0°$, *i. e.* in a vertical direction of the axis of polarization, the front zero-point is just above the centre of the hidden sphere, whereas the rear point passes into infinity; at the same time the front positive maximum becomes numerically equal to the negative maximum, and both are placed at a distance from the projection of the centre of the sphere equal to the half of the depth of the sphere's centre; *i. e.*, we have

$$u_m = \pm 0{\cdot}5. \quad . \quad . \quad . \quad . \quad . \quad . \quad (34)$$

The value of each of these two maxima is expressed by the formula

$$F_m = \frac{E r_0^3}{h^3} \cdot \frac{3}{2\,(1{\cdot}25)^{5/2}} = 0{\cdot}859 \frac{E r_0^2}{h^3}. \quad . \quad . \quad (35)$$

The rear positive maximum in the case under discussion is entirely absent.

(*e*) In a particular case, when $\alpha = 90°$, *i. e.* in a horizontal position of the axis of polarization, the front and rear zero-points are placed at distances from the projection of the centre of the hidden sphere equal to

$$u_0 = \pm \frac{1}{\sqrt{2}} = \pm 0{\cdot}707. \quad . \quad . \quad . \quad . \quad (36)$$

Fig. 6.—The electroprofile obtained along a line parallel to the plane of polarization.

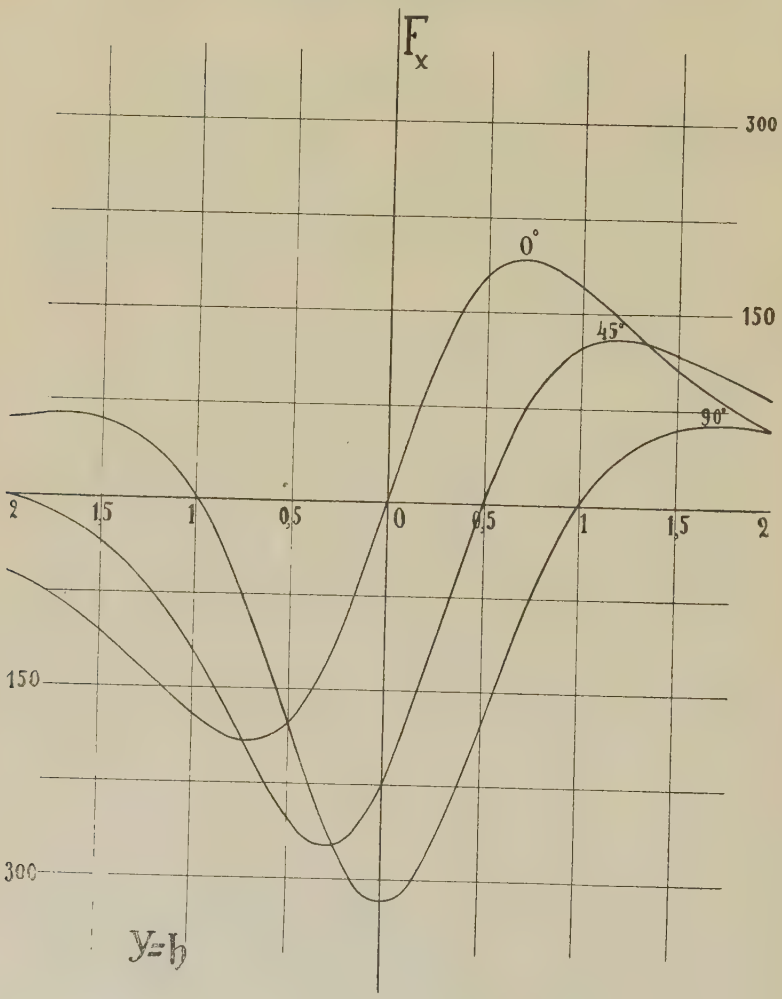

The value of each of them equals

$$F_m = \frac{Er_0^2}{h^3} \cdot \frac{4}{(2\cdot 5)^2 \sqrt{10}} = 0\cdot 202 \frac{Er_0^2}{h^3} \cdot \quad . \quad . \quad . \quad (37)$$

The negative maximum is situated below the very centre of the sphere, and is expressed by the formula

$$F_m = \frac{E r_0^2}{h^3} \quad . \quad . \quad . \quad . \quad . \quad . \quad . \quad (38)$$

On fig. 6 an electroprofile is given, obtained in a survey along the line parallel to the plane of polarization (but not lying in this plane).

From that it is seen :

3. Curves expressing a longitudinal electroprofile in a side dislocation retain the same shape as in a plane of polarization, but zero-points (where there are two) retreat further from the projection of the centre of the sphere ; likewise also do the maxima separate, losing gradually at the same time their sharpness (*i. e.* diminishing numerically).

§ 7. On fig. 7 an electroprofile is represented, obtained along the line perpendicular to the plane of polarization and passing over the centre of the hidden sphere.

From it is seen the following :—

1. The curve expressing the electroprofile has only one zero-point, one positive and one negative maximum ; the curve asymptotically tends to zero the further it moves from the projection of the centre of the sphere.

2. The distribution of a curve of the transversal electroprofile relatively to the projection of the centre of the hidden sphere has a mirror symmetry.

(*a*) The zero-point is always over the centre of the hidden sphere.

(*b*) The maxima are placed at distances from the projection of the centre of the sphere equal to the half of its depth.

$$v_m = \pm \frac{h}{2} . \quad . \quad . \quad . \quad . \quad . \quad . \quad (39)$$

(*c*) The values of the maxima are numerically alike and are expressed as follows :

$$F_m = \pm \frac{48Q}{25\sqrt{5}} \cos \alpha . \quad . \quad . \quad . \quad (40)$$

(*d*) In a particular case, when $\alpha = 0°$, *i. e.* in a vertical direction of the axis of polarization, the transversal electroprofile does not differ from the longitudinal one.

(*e*) In a particular case, when $\alpha = 90°$, *i. e.* in a horizontal

direction of the axis of polarization, the transversal electroprofile is entirely absent ; *i.e.*, the electric force is everywhere equal to zero.

Fig. 7.—The electroprofile obtained along the line perpendicular to the plane of polarization and passing over the centre of the sphere.

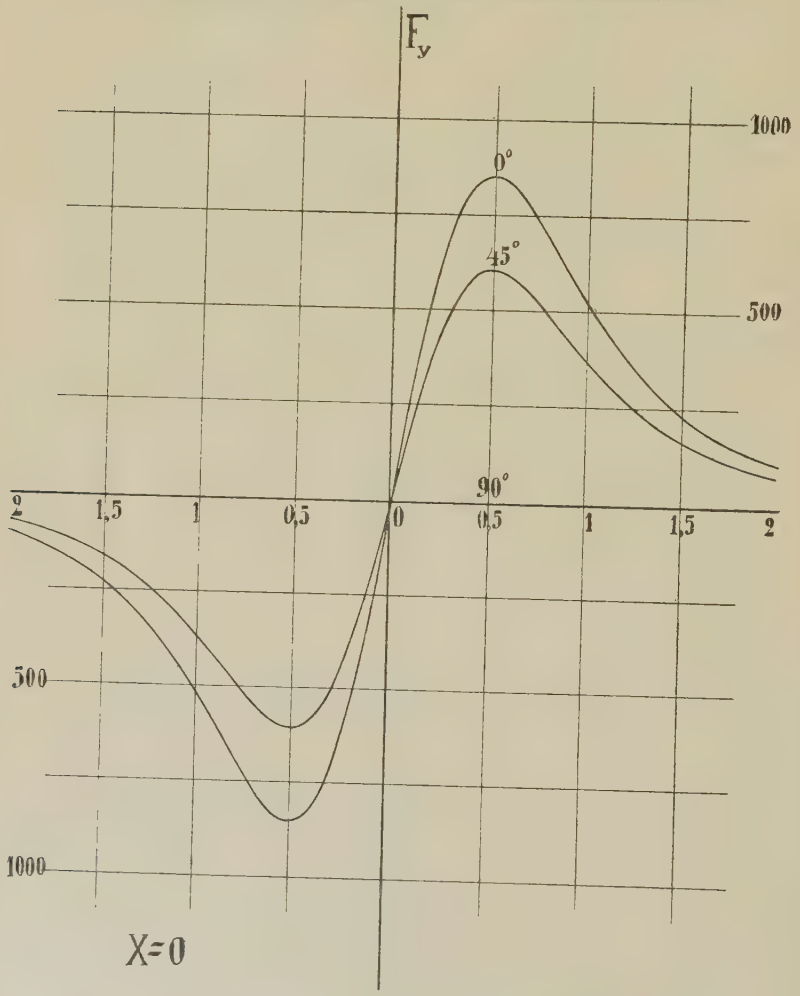

On fig. 8 is given a transversal electroprofile which does not pass over the centre of the hidden sphere.

From this is to be seen :

3. Curves expressing a transversal electroprofile in side displacement do not change their shape, their zero-points

Fig. 8.—The electroprofile obtained along a line perpendicular to the plane of polarization and not passing over the centre of the sphere.

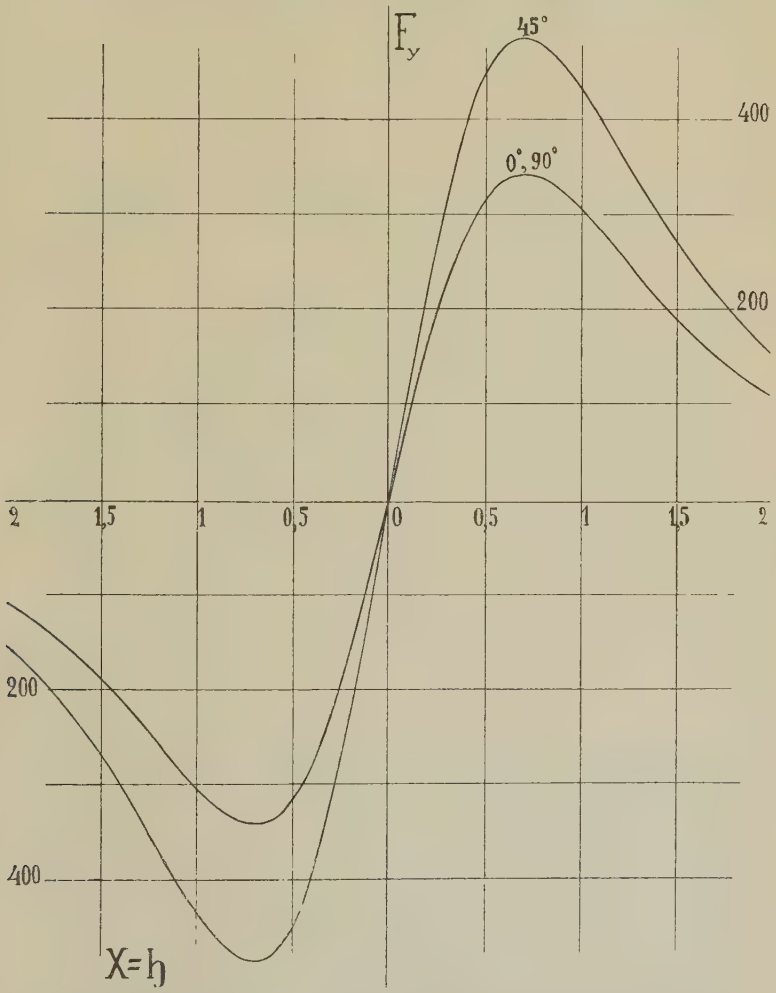

remain in their places, but the maxima gradually separate in different directions and diminish in value the further they are removed from the projection of the centre of the sphere.

§ 8. Let us now suppose that the observer is tracing an electroprofile along the line O_0X', inclined to the line O_0X (and at the same time also to the plane of polarization at the angle ϕ (fig. 9)); and he observes the projection of electric force to the direction O_0X', *i.e.* the value $F_{x'}$, expressing it in the function of coordinates x', y' or in the function of values u', v', connected with x', y' by the following relations:—

$$u' = \frac{x'}{h}, \quad . \quad . \quad . \quad . \quad . \quad . \quad . \quad . \quad (41)$$

$$v' = \frac{y'}{h}. \quad . \quad . \quad . \quad . \quad . \quad . \quad . \quad . \quad (42)$$

Fig. 9.—Distribution of the axis of coordinates in a general case.

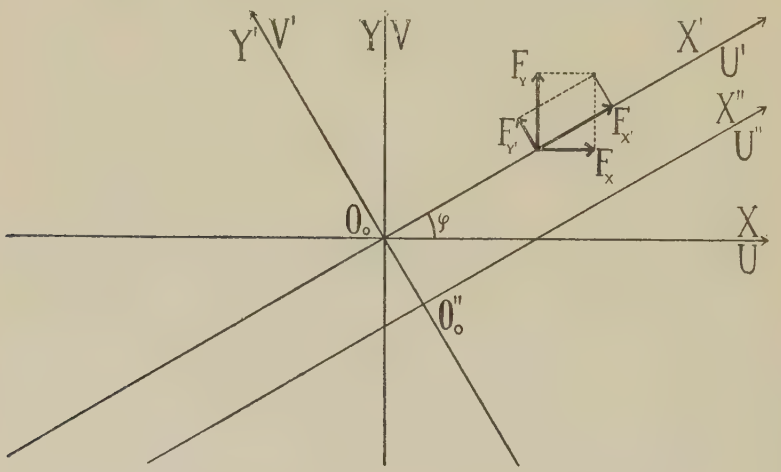

Let us find the expression of the potential and of the electric force in the function of these values. For that purpose we substitute in formula (31) the values u, v by the expressions

$$u = u' \cos\phi - v' \sin\phi, \quad . \quad . \quad . \quad . \quad (43)$$

$$v = u' \sin\phi + v' \cos\phi, \quad . \quad . \quad . \quad . \quad (44)$$

and obtain a formula for the potential W as follows:

$$W = P \frac{\cos\alpha + u' \cos\phi \sin\alpha - v' \sin\phi \sin\alpha}{[1 + u'^2 + v'^2]^{3/2}}. \quad . \quad (45)$$

By differentiating this formula by x' or y', and taking into consideration the relations (41), (42), we obtain the expressions for projections of electric force sought for at the point u', v' along the directions O_0X', O_0Y'.

$$F_{x'} = -\frac{\partial W}{\partial x'} = -\frac{\partial W}{h\partial u'}$$

$$= Q\frac{3u'\cos\alpha - (1+v'^2-2u'^2)\cos\phi\sin\alpha - 3u'v'\sin\phi\sin\alpha}{[1+u'^2+v'^2]^{5/2}}, \quad \ldots \quad (46$$

$$F_{y'} = -\frac{\partial W}{\partial y'} = -\frac{\partial W}{h\partial v'}$$

$$= Q\frac{3v'\cos\alpha + (1+u'^2-2v'^2)\sin\phi\sin\alpha + 3u'v'\cos\phi\sin\alpha}{[1+u'^2+v'^2]^{5/2}}, \quad (47)$$

where

$$Q = \frac{Er_0^2}{h^3}. \quad \ldots \quad (48)$$

§ 9. On fig. 10 an electroprofile is given obtained along the line inclined to the plane of polarization at an angle $\phi = 45°$ and passing through the point O_0 lying over the centre of the hidden sphere.

Examining it, we see the following :—

1. Curves expressing an electroprofile in general have the same shape as in the case of an electroprofile obtained along the line lying in the plane of polarization.

2. Points (2*a*), (2*b*), (2*c*), (2*d*), and (2*e*) enumerated in § 6, corresponding to the above-mentioned curves, retain their meaning also in the given case, but with the following differences:

(*a*) The zero-points are nearer to the point O_0 than in the electroprofile taken along the line lying in the plane of polarization.

(*b*) The maxima are numerically less than in the case of the above-mentioned electroprofile.

(*c*) When $\alpha = 0°$ this diminution is entirely absent; it is the more considerable the nearer α is to 90°.

3. The electroprofile also does not undergo any essential changes in the case when the line of surveying $O_0''X''$, remaining inclined at the same angle ϕ to the plane of polarization, does not pass through the point O_0 lying over the centre of the sphere; such an electroprofile is given on fig. 11.

In this case the following particulars are to be noticed :

(*a*) The zero-points recede from the point O_0—the front one somewhat, the rear one considerably.

Fig. 10.—An electroprofile along the line, inclined to the plane of polarization, but passing through the projection of the sphere's centre.

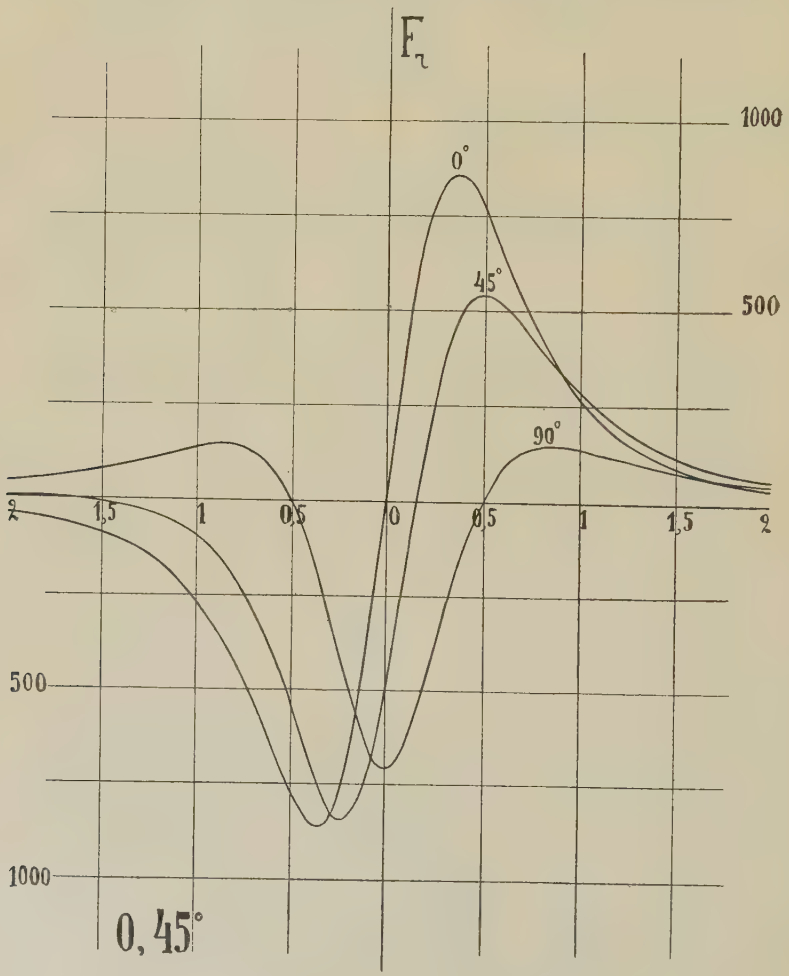

(*b*) The maxima also recede from the point O_0—the front positive maximum and the rear negative one not so quickly as the rear positive maximum ; the numerical values of the

rear maxima diminish ; the numerical values of the front maxima diminish at small angles α and increase at large angles α.

Fig. 11.—An electroprofile along the line, inclined to the plane of polarization, and not passing through the projection of the sphere's centre.

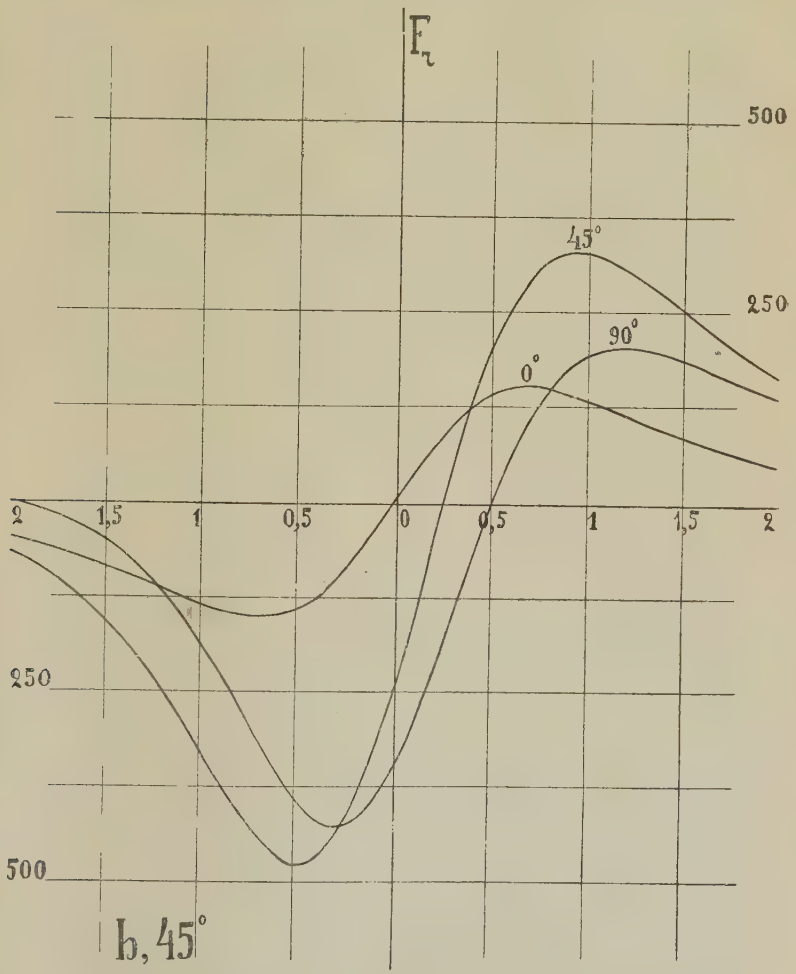

(*c*) At $\alpha = 90°$ the electroprofile loses its symmetry with respect to points O_0 lying above the centre of the bed 0, because the front zero-point remains in its place, whereas the negative maximum shifts back.

XXXIV. *The Crystal Structure of the Isomorphous Sulphates of Potassium, Ammonium, Rubidium, and Cæsium.* By A. Ogg, *M.A., Ph.D., F.Inst.P., Professor of Physics, University of Cape Town* *.

[Plates V. & VI.]

1. THE sulphates of potassium, ammonium, rubidium and cæsium form isomorphous crystals, which belong to the holosymmetric class of the orthorhombic system. The crystallographic characters of this isomorphous series have been very carefully investigated by Tutton †.

The dimensions of the unit cells of potassium, ammonium, rubidium, and cæsium sulphates and the number of molecules per unit cell were determined by Ogg and Hopwood ‡. Each cell contains four molecules. Table I. gives the lengths of the sides of the unit cells in Å.U. (10^{-8} cm.).

Table I.

Crystal.	*a*.	*b*.	*c*.	Axial ratios $a : b : c$.
K_2SO_4	5·731	10·008	7·424	0·573 : 1 : 0·742
$(NH_4)_2SO_4$...	5·951	10·560	7·729	0·563 : 1 : 0·732
Rb_2SO_4	5·949	10·391	7·780	0·572 : 1 : 0·748
Cs_2SO_4	6·218	10·884	8·198	0·571 : 1 : 0·753

The ratio of $b : a$ is very nearly $\sqrt{3} : 1$ or $1 : 0{\cdot}577$. The "c" axis is an axis of pseudohexagonal symmetry. Potassium sulphate shows a marked prevalence of repeated twinning in the form of three individuals interpenetrating to form what appears to be simple hexagonal prisms. Tutton has shown that the other salts of the series frequently twin in the same way. Ogg and Hopwood observed the spectral intensities for the K_α radiation of palladium. I am indebted to Mr. E. N. Grindley, Lecturer, Physics Department of the University of Cape Town, for repeating and extending the observations on potassium and ammonium sulphates for the K_α radiation of molybdenum.

2. Since the intensity of the reflexion of X-rays from any plane depends on the distribution of the scattering power in

* Communicated by the Author.

† 'Crystalline Structure and Chemical Constitution,' by A. E. H. Tutton.

‡ Phil. Mag. xxxii. p. 518 (1916).

a direction perpendicular to that plane, and corrections have to be made for absorption and extinction which are difficult to evaluate, the structure of such crystals has to be determined by a process of trial and error. Atomic arrangements have to be assumed, and then tested by comparing the calculated intensities of the X-ray spectra with the observed intensities. In these crystals, which are orthorhombic, the atoms have, as far as symmetry is concerned, considerable degrees of freedom. The difficulty in such a case is to fix on possible atomic arrangement. The most certain aid to such a selection is that of symmetry. There are 28 space-groups to which these crystals may belong. They are V_h1 to V_h28 in the notation of Schoenflies, or Q_h1 to Q_h28 in the notation of Hilton. Each space-group is characterized by certain internal regularities which cause reflexions from certain planes to have zero intensities *. A comparison of these predicted from the regularities of the space-group with the observed intensities is sufficient to fix the space-group.

The observed spacings of the important planes referred to the spacings of the unit cell given in Table I. were :—

TABLE II.

(100)	halved	(021)	normal
(010)	halved	(110)	normal
(001)	halved	(011)	normal
(111)	normal	(130)	normal

These spectral observations suggest that this isomorphous series of crystals belongs to the symmetry group V_h16, a conclusion which can be tested when the symmetry elements have been placed within the unit cell. This symmetry group contains two reflexion planes, four glide planes, twelve dyad screw axes, and two sets of four centres of symmetry.

3. Elements of Symmetry.

Bradley†, James and Wood ‡, Dickson and Binks§, and Wasastjerna ‖ have shown that in crystals the sulphate SO_4 group forms a tetrahedron with the sulphur atom or ion at the centre of the tetrahedron, and the oxygen atoms or ions at the corners. If we assume this tetrahedral form for the SO_4 group, symmetry and spectral intensities give us at once

* Astbury and Yardley, Phil. Trans. A, cciv. p. 221.
† Phil. Mag. xlix. p. 1225 (1925).
‡ Proc. Roy. Soc. cix. p. 598 (1925).
§ Phil. Mag. ii. p. 114 (1926).
‖ Soc. Scient. Fenn. Comm. Phys. Maths. ii. p. 26.

certain information about the distribution of the symmetry elements and of the SO_4 groups. The two sets of symmetry centres of the V_h16 group form two sets of four-fold points without freedom. The four sulphur atoms cannot, however, be placed at any one of these sets of symmetry centres, because the centre of a tetrahedron with oxygen atoms at the corners cannot be a centre of symmetry. There is, however, another alternative. A point on a reflexion plane with two degrees of freedom is multiplied into four by the action of the symmetry elements. All other points with three degrees of freedom are multiplied into eight by the elements of symmetry. We may say, then, that the sulphur atoms must lie on reflexion planes. It follows that a reflexion plane is a plane of symmetry of the SO_4 group. If the S atom lies on a reflexion plane, two oxygen atoms of the group must also lie on the plane, and two be equidistant from the plane, one being the mirror image of the other in the plane. To fix the position of the SO_4 group three parameters have to be determined, if we assume the dimensions of the tetrahedron constant. The S atom has two degrees of freedom on the plane, and the group may be rotated round an axis perpendicular to the plane.

The spacing of the (100) planes is $a/2$, and the intensities fall off normally for all members of the series, showing that the structure must consist of layers of atoms parallel to (100) with spacings $a/2$. The sulphur atoms will lie in these layers, and since they also lie on reflexion planes, we conclude that the reflexion planes are $(100)_{1/4}$ and $(100)_{-1/4}$, if we take the centre of the unit as the origin of coordinates. Also, since the "c" axis is an axis of pseudohexagonal symmetry, we can settle the positions of the glide planes.

The proposed elements of symmetry, referred to the symmetry centre at the centre of the unit as origin, are:—

Reflexion Planes:

$(100)_{1/4}$, $(100)_{-1/4}$.

Glide Planes:

$(010)_{1/4}$, $(010)_{-1/4}$, Translation $c/2$.
$(001)_{1/4}$, $(001)_{-1/4}$, Translation $a/2$, $b/2$.

Centres of Symmetry:

I. $(0, 0, 0)$, $(\frac{1}{2}, 0, 0)$, $(0, \frac{1}{2}, \frac{1}{2})$, $(\frac{1}{2}, \frac{1}{2}, \frac{1}{2})$.
II. $(0, 0, \frac{1}{2})$, $(\frac{1}{2}, 0, \frac{1}{2})$, $(0, \frac{1}{2}, 0)$, $(\frac{1}{2}, \frac{1}{2}, 0)$.

Dyad Screw Axes:

$(100)_{00}$, $(100)_{1/2\,1/2}$, $(100)_{1/2\,0}$, $(100)_{0\,1/2}$, Translation $a/2$.
$(010)_{0\,1/4}$, $(010)_{0\,-1/4}$, $(010)_{1/2\,1/4}$, $(010)_{1/2\,-1/4}$, Translation $b/2$.
$(001)_{1/4\,1/4}$, $(001)_{-1/4\,-1/4}$, $(001)_{-1/4-1/4}$, $(001)_{1/4\,1/4}$,
Translation $c/2$.

4. The Arrangement of the Atoms.

It has been shown by Bradley* that the distance between S and O centres of the SO_4 group in potassium lithium sulphate crystals lies between 1·5 and 1·6 Å.U. James and Wood† have found that the distance 1·5 gives good agreement with observation for barytes, celestine, and anglesite. The tetrahedral form of SO_4 was assumed as well as the distance S—O 1·5 Å.U., and it has been found that such an SO_4 group fits well with observation.

Since the structure must consist of layers of atoms on reflexion planes parallel to (100), the metallic atoms must lie on reflexion planes. They must consist of two sets of four, and not of one set of eight‡. The environment of the metal atoms may therefore be of two kinds.

A very strong (130) spectrum, a strong (330) spectrum, and the "c" axis being an axis of pseudohexagonal symmetry indicate hexagonal packing or two interpenetrating base-centred structures. Models of SO_4 groups were constructed and built together to satisfy the elements of symmetry, and it soon became clear how the metal atoms would fit into the structure. The atoms were finally adjusted to give as good agreement as possible between the calculated and observed intensities.

If we take the symmetry centre at the centre of the unit as origin, an atom whose coordinates are x, y, z is converted by the elements of symmetry into eight atoms within the unit cell, whose coordinates are :—

$$\pm(x, y, z), \quad \pm(a/2-x, y, z),$$
$$\pm(x, b/2-y, -c/2+z), \quad \pm(-a/2+x, -b/2+y, c/2-z).$$

If the amplitude of the reflected wave due to a given atom is A, when reflexion is taking place in the (hkl) plane, then

* *Loc. cit.*

† *Loc. cit.*

‡ W. L. Bragg and G. B. Brown have found a similar condition for aluminium atoms in chrysoberyl ($BeAl_2O_4$), Proc. Roy. Soc. cx. p. 46 (1926).

the eight corresponding atoms contribute a wave whose amplitude is

$$A\Sigma \cos 2\pi m\left(\frac{hx}{a}+\frac{ky}{b}+\frac{lz}{c}\right),$$

where m is the order of the spectrum.

The summation taken over the eight atoms gives the expression

$$8A \cos 2\pi m\left(\frac{hx}{a}+\frac{h}{4}\right)\cos 2\pi m\left(\frac{ky}{4}+\frac{l+k}{4}\right)$$
$$\cos 2\pi m\left(\frac{lz}{c}+\frac{h+k+l}{4}\right)\cos (h+k+l)\pi.$$

The factor $\cos(h+k+l)\pi$ affects only the sign of the expression. This expression for the amplitude shows that planes of the type (okl), when k and l are not zero, give normal spacings.

Planes of the type (hol) have their spacings halved, when l is odd.

Planes of the type (hko) have their spacings halved, when $(h+k)$ is odd.

Planes of the type (hkl) have normal spacings.

As special cases of the above rules, all pinakoid spacings are halved.

The deductions from the chosen elements of symmetry are in agreement with the observed spacings enumerated in Table II.

In calculating the spectral intensities, Hartree's * values for the scattering functions of potassium and sulphur were used, while for oxygen those of James and Wood † were used. Only general agreement was to be expected.

It was of considerable help in solving the structure to compare the spectral intensities of different members of the series for the same plane, and to observe the effect of the change of the metal atoms. Take, for example, the spectra from the (001) planes. The odd orders are absent. The (002) spectrum of ammonium sulphate is much stronger than the (004) spectrum. The (002) spectrum of potassium sulphate is slightly weaker that the (004) spectrum. The (004) spectrum of rubidium sulphate is the stronger. The (002) spectrum of cæsium sulphate vanishes and the (004) spectrum is very strong. These observations are explained by the proposed structure.

* Phil. Mag. I. p. 289 (1925).
† *Loc. cit.*

In fig. 1 the approximate positions of the atoms of potassium sulphate and the elements of symmetry are projected on to the three principal planes. The atoms are represented by circles of different radii, but these radii are not intended to represent "atomic radii." Since the atoms within the unit lie mostly in two layers parallel to (100), the atoms projected on to the plane (100) have been shaded to distinguish these layers. The white circles represent atoms on

Fig. 1.

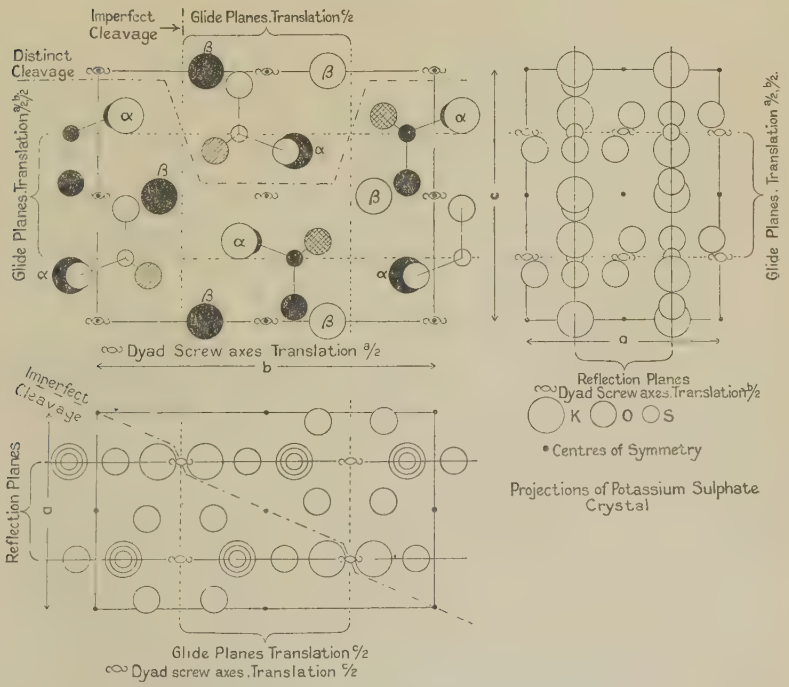

the front plane, and the black circles represent atoms on a parallel plane at a distance $a/2$ behind it. The other shaded atoms lie beween the planes. The SO_4 groups are shown by lines joining the S atoms to the oxygen atoms. One kind of potassium atom is marked α and the other β.

Fig. 2 shows corresponding projections of the atoms of ammonium sulphate. Although we can only locate the NH_4 group as a whole, it is resonable to assume the tetrahedral form of the group with nitrogen at the centre. The

positions of the hydrogen atoms cannot, however, be determined from intensity measurements. Two possible ways of forming the group can be proposed. The nitrogen atom could take up three electrons from the hydrogen atoms to its 2_2 system and become a nitrogen ion with a charge -3, while the fourth hydrogen atom would give up an electron to one of the oxygens of the SO_4 group. The NH_4 group would then consist of a central nitrogen ion with charge -3 surrounded by four ions, each of charge $+1$. The NH_4 group

Fig. 2.

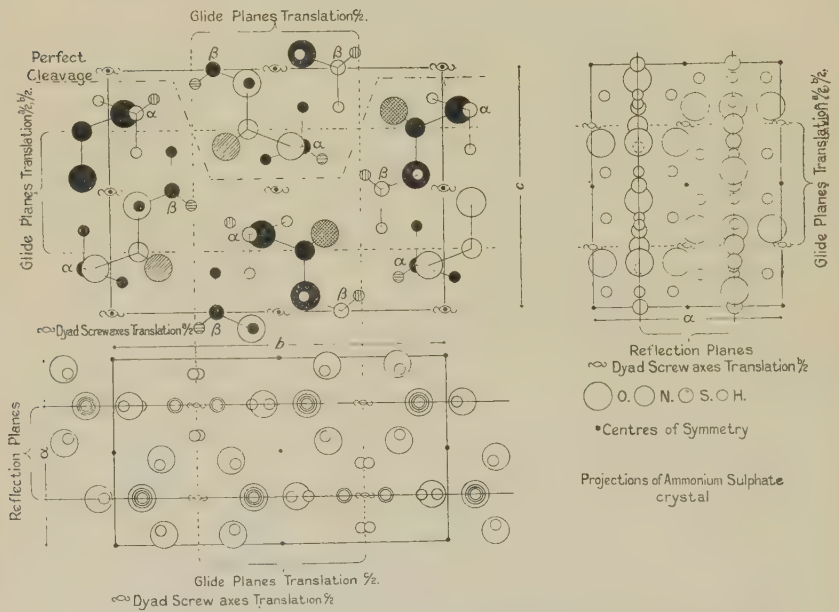

would be equivalent to a polar ion of charge $+1$. The nitrogen atom could, however, in accordance with the suggestion made by Niven * for ammonia, give up four electrons to the four hydrogen atoms to complete their 1_1 systems, and also one electron to one of the oxygen atoms giving a nitrogen ion of charge $+5$, surrounded by four hydrogen ions, each with a charge -1. The orientation of the (NH_4) groups would, however, be different in the two cases. The first alternative in which the positive hydrogen ions would form the connecting-link between the nitrogen and oxygen ions has been adopted.

* Phil. Mag. iii. p. 1315 (1927).

TABLE III.

Crystal.	Atom.	No. in unit cell.	Linear coordinates as fractions of a, b, and c.	Angular coordinates.
K_2SO_4	S	4	0·250, 0·417, 0·250	$\pi/2$, $5/6\pi$, $\pi/2$
	O	4	0·250, 0·417, 0·048	$\pi/2$, $5/6\pi$, $\pi/2-0·404\pi$
	O	4	0·250, −0·443, 0·317	$\pi/2$, $-7/6\pi+0·280\pi$, $\pi/2+0·135\pi$
	O	8	0·037, 0·347, 0·317	$\pi/2-0·416\pi$, $5/6\pi-0·140\pi$, $\pi/2+0·135\pi$
	K_α	4	0·250, 0·417, −0·317	$\pi/2$, $5/6\pi$, $-\pi/2+0·135\pi$
	K_β	4	0·250, 0·317, 0	$\pi/2$, $\pi/2+0·135\pi$, 0
Rb_2SO_4	S	4	0·250, 0·417, 0·250	$\pi/2$, $5/6\pi$, $\pi/2$
	O	4	0·250, 0·417, 0·058	$\pi/2$, $5/6\pi$, $\pi/2-0·384\pi$
	O	4	0·250, −0·447, 0·314	$\pi/2$, $-7/6\pi+0·272\pi$, $\pi/2+0·128\pi$
	O	8	0·044, 0·349, 0·314	$\pi/2-0·412\pi$, $5/6\pi-0·136\pi$, $\pi/2+0·128\pi$
	Rb_α	4	0·250, 0·417, −0·314	$\pi/2$, $5/6\pi$, $-(\pi/2+0·128\pi)$
	Rb_β	4	0·250, 0·310, 0	$\pi/2$, $\pi/2+0·12\pi$, 0
Cs_2SO_4.....	S	4	0·250, 0·417, 0·250	$\pi/2$, $5/6\pi$, $\pi/2$
	O	4	0·250, 0·417, 0 067	$\pi/2$, $5/6\pi$, $\pi/2-0·366\pi$
	O	4	0·250, −0·455, 0·311	$\pi/2$, $-7/6\pi+0·256\pi$, $\pi/2+0·122\pi$
	O	8	0·053, 0·353, 0·311	$\pi/2-0·394\pi$, $5/6\pi-0·128\pi$, $\pi/2+0·122\pi$
	Cs_α	4	0·250, 0·417, −0·311	$\pi/2$, $5/6\pi$, $-(\pi/2+0·122\pi)$
	Cs_β	4	0·250, 0·308, 0	$\pi/2$, $\pi/2+0·116\pi$, 0
$(NH_4)_2SO_4$ ...	S	4	0·250, 0·417, 0·250	$\pi/2$, $5/6\pi$, $\pi/2$
	O	4	0·250, 0·417, 0·056	$\pi/2$, $5/6\pi$, $\pi/2-0·388\pi$
	O	4	0·250, −0 451, 0·315	$\pi/2$, $-7/6\pi+0·264\pi$, $\pi/2+0·130\pi$
	O	8	0·045, 0·351, 0·315	$\pi/2-0·410\pi$, $5/6\pi-0·132\pi$, $\pi/2+0·130\pi$
	N_α	4	0·250, 0·417, −0·315	$\pi/2$, $5/6\pi$, $-(\pi/2+0·130\pi)$
	N_β	4	0·250, 0·311, 0	$\pi/2$, $\pi/2+0·122\pi$, 0

In this case the orientation of the α (NH_4) groups would appear to be fairly certain ; but there are two possible orientations of the β groups consistent with the symmetry and the linkage of hydrogen to oxygen. The one which gives the hydrogen linked to those oxygen which have the closest approach to the metal ions of the other crystals has been taken.

The coordinates of the atoms with the centre of the unit as origin are summarized in Table III. In each case the coordinates of one atom is given, the others being derived from it by the operation of the symmetry elements.

The oxygen environment of the metal atoms is different for the two sets of metal atoms in the structure. In the diagrams one set is marked α and the other β.

The distances between the atomic centres of the metal atoms and oxygen atoms and the number of times any particular measurement occurs are summarized in Table IV.

TABLE IV.

Atomic distance $M_\alpha - O$ in Å.U.

No.	$K_\alpha - O$.	$Rb_\alpha - O$.	$Cs_\alpha - O$.	$(NH_4)_\alpha - O$.
1.....	2·71	2·89	3·10	2·86
4.....	2·89	2·95	3·20	2·91
3.....	3·00	3·12	3·20	3·15
2.....	3·15	3·17	3·28	3·25
1.....	3·50	3·50	3·70	3·60

Atomic distance $M_\beta - O$.

No.	$K_\beta - O$.	$Rb_\beta - O$.	$Cs_\beta - O$.	$(NH_4)_\beta - O$.
4.....	2·71	2·89	3·10	2·86
2.....	2·91	3·01	3·17	3·10
1.....	2·95	3·15	3·30	3·15
2.....	3·10	3·20	3·37	3·20

The distance of closest approach is the same for both kinds, and is

K—O	.....	2·71 Å.U.
Rb—O	.....	2·89 ,,
Cs—O	.....	3·10 ,,
(NH_4)—O	...	2·86 ,,

These atomic distances are in close agreement with the distances suggested by Wasastjerna * for atomic radii with a clear recognition of the fictitious nature of atomic radii. The values were

$$K-O = 1{\cdot}30 + 1{\cdot}35 = 2{\cdot}65,$$
$$Rb-O = 1{\cdot}50 + 1{\cdot}35 = 2{\cdot}85,$$
$$Cs-O = 1{\cdot}75 + 1{\cdot}35 = 3{\cdot}05.$$

Bradley † mentions in his paper on the structure of lithium potassium sulphate that Prof. W. L. Bragg ‡ modified the values originally proposed by him in the manner suggested by Wasastjerna, and proposed the value for

$$K-O = 1{\cdot}34 + 1{\cdot}36 = 2{\cdot}70,$$

which is in very close agreement with the value given above.

The M_β atoms appear to be more closely linked to oxygen than the M_α atoms.

Bradley's structure for $KLiSO_4$ crystals indicates that it is K_α that is replaced by Li.

The closest approach of the metals is

$K_\alpha - K_\beta$	3·55 Å.U.
$Rb_\alpha - Rb_\beta$	3·75 „
$Cs_\alpha - Cs_\beta$	3·95 „
$(NH_4)_\alpha - (NH_4)_\beta$...	3·75 „

The structure of these sulphates is one in which each positive metallic ion is surrounded as closely and as uniformly as possible by negative oxygen ions, perfect freedom of adjustment being prevented by the attachment of the oxygen ions in fours to sulphur to form the sulphate group. The SO_4 groups are in turn surrounded by metallic ions. In potassium sulphate the distances of the potassium atoms, surrounding an SO_4 group, from the nearest oxygen of that group are two at 2·71, five at distances from 2·900 to 3·00, and three at 3·15 Å·U.

5. In potassium sulphate the cleavage (001) is distinct, and the cleavages (010) and (110) are imperfect. In ammonium sulphate the cleavage (001) is perfect. These cleavage planes are indicated in figs. 1 and 2.

* J. A. Wasastjerna, "On the Radii of Ions," Soc. Scient. Fenn. Comm. Phy. Maths. i. p. 38 (1923).

† *Loc. cit.*

‡ "Interatomic Distances in Crystals," Phil. Mag. ii. p. 258 (1927).

Although the ions of such a structure are in equilibrium in electric fields produced by the surrounding ions, it seems probable from the position of the cleavage planes and from the distances of closest approach of the metallic ions to the oxygen ions that one metal ion of each kind belongs to each SO_4 group to form the molecule. Fig. 3 represents the molecule of potassium sulphate as it occurs in these crystals. The potassium, sulphur, and two oxygen atoms

Fig. 3.

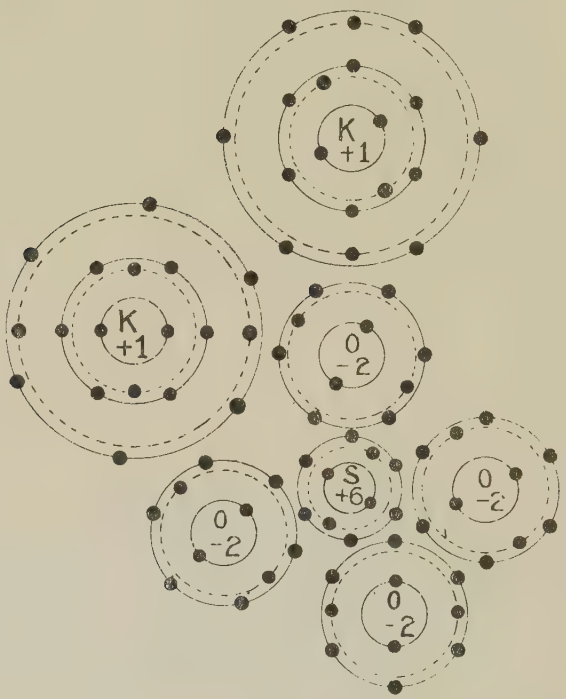

lie in a plane. The other two oxygen atoms, which are equidistant from that plane, are also represented as lying in that plane, and have been displaced to prevent the electron systems from intersecting in the diagram.

6. The crystals of this series show repeated twinning, which results in interpenetrating groups which are almost indistinguishable from simple hexagonal crystals. Fig 4 A

shows a section of such a crystal built from three crystals, I., II., and III.* Figures of characteristic triplets of potassium selenate are given by Tutton †. The external faces of the crystal are the planes p (110) and p' (130). The twinning plane ($1\bar{3}0$) is nearly at right angles to the plane (110). If the re-entrant angles formed by the planes (130) vanish by the growth of the crystal, there results an almost true hexagonal prism terminated by a hexagonal pyramid. Each face is however composed of two halves, which are inclined at a small angle to one another. This inclination can be detected by reflecting light from the face of the crystal.

Fig. 4.

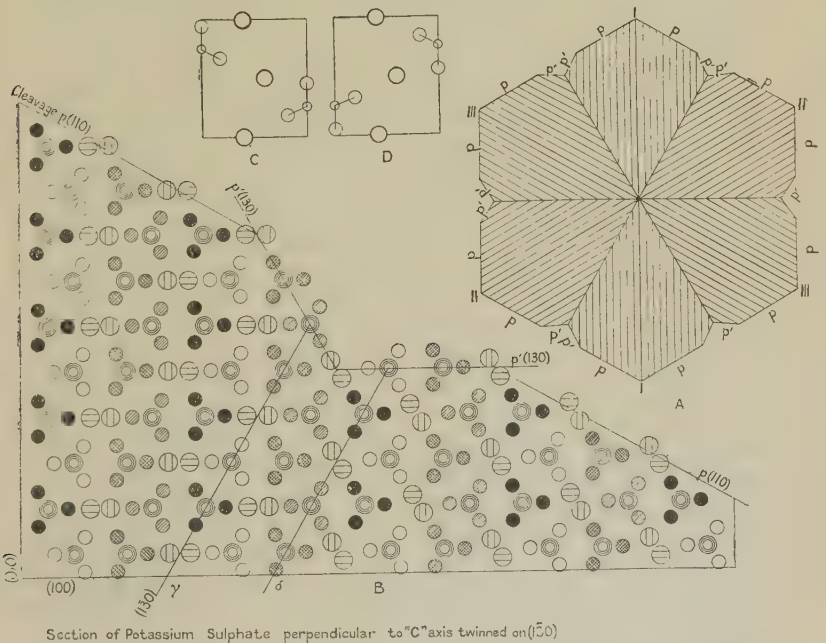

Section of Potassium Sulphate perpendicular to "C" axis twinned on ($1\bar{3}0$)

A twining plane must have special characteristics. The cases hitherto observed show twinning planes to be planes of closely-packed atoms. It must also be such that, if the crystal is built up to this plane, its continuance on the other side of the plane may follow one or more alternatives. One of these is correct and continues the plan of the crystal.

* 'Physikalische Krystallographie,' Groth, p. 406.

† 'Crystalline Structure and Chemical Constitution,' A. E. H. Tutton, p. 93.

The others are not so easy to follow. The plane (130) satisfies these conditions.

Fig. 4 B, which is a section of potassium sulphate perpendicular to the "*c*" axis, explains the process of twinning in these crystals. The figure shows the β-potassium atoms in the projection lying inside a nearly true hexagon of oxygen atoms, which in turn lie inside a larger hexagon of S atoms. These potassium atoms lie in the reflexion planes parallel to (100). Their positions relative to the oxygen atoms are shown in fig. 4 C. If these potassium atoms are rotated through nearly 60° into the plane (130), they would occupy positions relative to oxygen atoms illustrated in fig. 4 D. The crystal would now grow in that direction as the (100) plane of the twin. The potassium atoms might equally well be rotated through nearly 60° in the opposite direction into the plane (130). Arcanite (K_2SO_4) is described in Dana's 'System of Mineralogy' as giving repeated twins on the planes (110) and also on (130) resembling aragonite.

The diagonal of the "hexagon" of S atoms parallel to the plane (100) is slightly longer than that parallel to ($1\bar{3}0$) or (130). The lengths are 6·67 and 6·63 Å.U. The longer direction is the correct direction for the potassium atoms. The section between the lines γ and δ would serve as origin for the growth of either system on each side of it.

7. Models of SO_4 groups were made with spheres of 1·5 cm. diameter to represent both S and O. The distance $S-O=1{\cdot}5$ cm. The K_2SO_4 unit was then constructed with SO_4 models and with spheres of 2·7 cm. diameter to represent K atoms. The radii of these spheres were not intended to represent "atomic radii." A similar model of the $(NH_4)_2SO_4$ unit was made, taking a sphere of 1·5 cm. diameter to represent N and a sphere of 1·0 cm. diameter to represent H. The whole NH_4 group would then lie within a sphere of 1·75 cm. radius.

Two views of the (100) planes of each of these models are given in Pl. V. (figs. 5 A & B) and in Pl. VI. (figs. 6 A & B).

It can be seen from the model that, if ammonium sulphate were to twin like potassium sulphate, not only would the NH_4 group have to be rotated through nearly 60° about an axis parallel to "*c*," but the groups would also have to be inverted; *i. e.*, rotated through 180° about an axis through its centre parallel to "*b*."

Summary.

The structures of the isomorphous sulphates of potassium, ammonium, rubidium, and cæsium have been investigated. The structure is based on a simple orthorhombic lattice having four molecules to the unit cell, and the space-group is V_h^{16}. The positions of the atoms in the structures have been determined. An explanation of the characteristic twinning of these crystals has been given.

In conclusion, I wish to express my thanks to Dr. A. E. H. Tutton, F.R.S., for supplying me with certain crystals for this investigation, to the South African Research Grant Board for some financial assistance, and to Mr. J. A. Linton for skilful assistance in making models and diagrams.

XXXV. *Energy Distribution among Secondary Electrons from Nickel, Aluminium, and Copper.* *By* D. A. Wells, *Assistant Professor of Physics, University of Cincinnati**.

A REVIEW of experimental work indicates that results do not always agree as to the energy distribution of secondary electrons. The highest velocities found by Barber † working with copper correspond to from 2 to 5 volts. The results of McAllister ‡, using practically the same apparatus and continuing the work of Barber, indicate that there are a few electrons reflected or emitted with velocities approaching the velocity of the primary stream. Davisson and Kunsman §, investigating the maximum velocity of secondary electrons from aluminium, platinum, and magnesium, found that secondary electrons with velocities "not appreciably less than that of the primaries proceed from the platinum and magnesium for all bombarding potentials up to the highest investigated in each case, 1000 volts and 1500 volts respectively."

* Communicated by the Author.

† I. G. Barber, "Secondary Electron Emission from Copper and Copper Oxide," Phys. Rev. vol. xvii. pp. 322–338 (1921).

‡ L. E. McAllister, "The Effect of Ageing on the Secondary Electron Emission from Copper Surfaces," Phys. Rev. vol. xix. p. 246 (1922).

§ C. Davisson and C. H. Kunsman, Phys. Rev. vol. xxii. p. 242 (1923).

Description of Apparatus.

Fig. 1 gives a diagram of apparatus and connexions. F, a flat spiral tungsten filament (Coolidge X-ray cathode) heated by means of lead storage-cells, was used as the source of primary electrons. A nickel shield S served as an anode and allowed a narrow beam of primary electrons to fall on *d*, the metal from which secondaries were to be studied. The large disk D, carrying the small disks *d*, could be rotated from the outside by the action of an electromagnet on a short iron bar attached to the extreme end of the axle. The

Fig. 1.

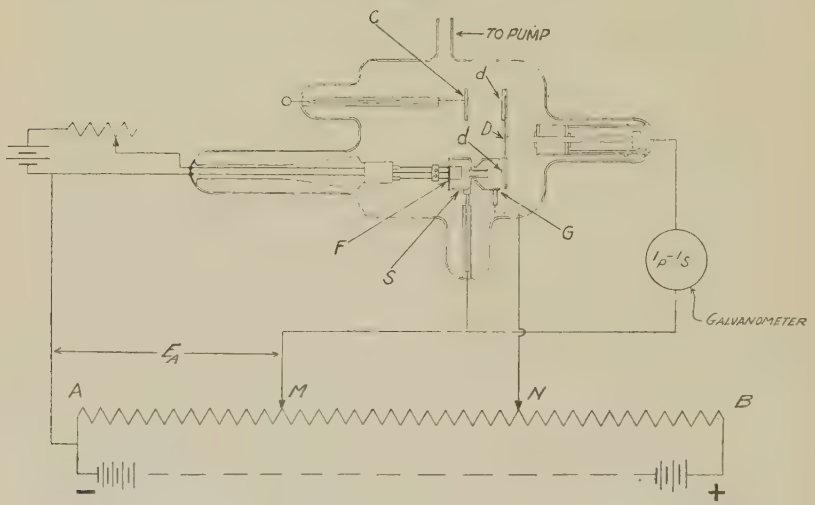

FIGURE 1

APPARATUS AND DIAGRAM OF CONNECTIONS

Faraday cylinder G could be put at any potential with respect to *d* by moving the point N. The primary electrons could be given any desired energy by moving the contact M. From the diagram it may be seen that the galvanometer reads $I_p - I_s$, the difference between the primary current striking and the secondary current leaving *d*. Therefore the complete energy distribution among secondary electrons for a given value of primary accelerating potential E_a may be obtained by moving N from A to B.

The aluminium cathode C was used for bombarding the metals to remove adsorbed gases. The negative terminal of a 7-inch induction coil was connected to this cathode, and

the other terminal to D. When a vacuum just high enough to give a yellow glow had been obtained, the high potential from the coil was applied, and the metal to be investigated was bombarded until the vacuum was of such a degree as to allow no discharge to pass. An iron Langmuir condensation pump, backed by a two-stage rotary oil-pump, was used to maintain the vacuum. Two traps were interposed between the pump and the tube. The one nearest the tube was kept continuously in a freezing-mixture, while the other was filled with coconut charcoal, which, during the first part of the exhaustion, was heated for an hour or more at a temperature of approximately 400° C. and then surrounded by a freezing-mixture.

Experimental Results.

Typical secondary energy-distribution curves for nickel at various primary voltages are shown in fig. 2. The first break

Fig. 2.

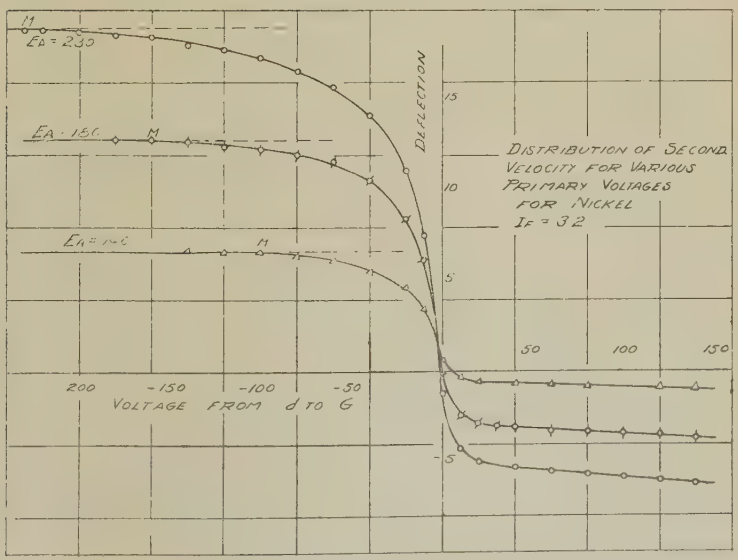

in a curve, shown by the point M where the dotted line becomes tangent to the curve, indicates the maximum energy, expressed in volts, of a perceptible number of secondary electrons emitted for that particular primary voltage. For further decrease in the negative potential of G with respect

to d, more electrons with less energy reach G. When the potential of G with respect to d is zero, practically all secondary electrons have energy enough to reach G. The curve then soon begins to approach saturation as G is made positive with respect to d.

If from the value M, where a curve just begins to break, any other following value is subtracted, it will give the number of secondary electrons having corresponding energies or greater. Repeating this for a number of points to where the voltage of G becomes zero with respect to d, the curve shown in fig. 3 is obtained. This secondary

Fig. 3.

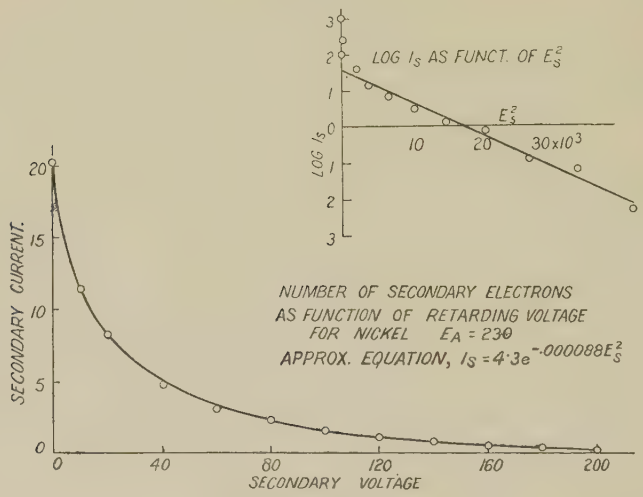

energy-distribution curve has an advantage over the original curve in that it gives directly, for a fixed value of E_a, the number of electrons having a given energy or greater up to the maximum. Values of log I_s plotted as a function of E_s^2 gave (except for the first few points) a straight line, which shows that the curve is closely approximated by the general equation $y = a\,e^{bx^2}$. The actual equation for the curve for nickel where $E_a = 230$ volts is $I_s = 4{\cdot}3\,e^{-{\cdot}000088E^2}$.

A series of curves similar to those of fig. 2 were taken for aluminium and copper, and in each case were found to have the same general form. With this apparatus it is true that secondaries may be emitted from the collector G. However,

in taking the curves of fig. 2 the first electrons from *d* to reach G do so with a velocity equal to zero, and the energy with which the electrons from *d* reach G is never greater than the difference between their energy of emission and the retarding field. Therefore secondary emission from G cannot appreciably affect the energy-distribution curves except for low values of retarding potential.

As mentioned before, the points M (fig. 2), where the curves just begin to break, give the maximum secondary energy for a fixed primary voltage. When values of maximum secondary energy were plotted as a function of primary voltage, for nickel, a straight line was obtained. If the secondary electrons are a result of the atoms absorbing the radiation produced when the primary electrons strike the plate—in other words, if secondary electrons are due to photo-electric effect,—the above graph should be a straight line having a slope of unity. However, the actual slope obtained was 1·34. Data are insufficient to make definite conclusions regarding this.

Conclusions.

In every case the curves indicate that there are a few secondary electrons with energies approaching that of the primary beam. This is shown by the fact that in every case the curves begin to bend while G is still at a high negative potential with respect to *d*. The number having high values of energy is relatively small; indicated by the slight change in slope which first occurs.

The empirical equation found for the curve of fig. 3 is the regular probability equation; and although it does not hold for low values of secondary energy, it indicates that within a certain range the number of electrons having a given energy or greater up to the maximum energy of any being emitted is determined by a law related to the law of probability.

XXXVI. *Metallic Spectra excited by Active Nitrogen.* By J. Okubo *and* H. Hamada. (*From the Laboratory of Physics, Sendai, Japan* *.)

[Plate VII.]

Introduction.

SINCE the discovery of the active modification of nitrogen by E. P. Lewis †, a large number of investigations with a view to find out its real nature have been carried out. Though as the results of the continued experimental work by Lord Rayleigh ‡, A. Fowler §, E. P. Lewis, R. T. Birge ‖, and others many important properties of the gas have come to light, the real nature of its activity still remains obscure. In recent years two different theories to explain this activity have been put forward. The first, advanced by M. N. Saha and N. K. Sur ¶, maintains that active nitrogen is simply nitrogen molecules in the state of excitation, and the contents of its energy are 8·9 volts. If such a molecule collides with other molecules or atoms, parts of its energy can be transferred to those others by the collision of the second kind, as put forward by O. Klein and S. Rosseland ** and confirmed experimentally by J. Franck †† and his students. From the excitation potential of the mercury lines which are excited when active nitrogen is made to act upon this vapour, the energy contents of the nitrogen molecule can be deduced.

The second theory has been put forward by H. Sponer ‡‡, and she is of opinion that the active nitrogen is simply a neutral nitrogen atom. If two nitrogen atoms encounter a neutral metallic atom or molecule, the energy corresponding to the heat of dissociation of a nitrogen molecule can be utilized to excite the neutral atom or molecule, and the spectra of the gas are emitted. From the facts of the peculiar enhancement of the first positive group and the complete lack of the second positive group in the after-glow spectra, H. Sponer concluded that the energy of dissociation is greater than 11·4 volts and smaller than 13 volts, and the

* Communicated by the Authors.

† E. P. Lewis, Astrophys. Journ. xii. p. 8 (1900).

‡ R. J. Strutt, Proc. Roy. Soc. lxxxv. p. 219 (1911); xciii. p. 254 (1917).

§ R. J. Strutt and A. Fowler, Proc. Roy. Soc. lxxxv. p. 377 (1911); lxxxvi. p. 105 (1912).

‖ R. T. Birge, 'Nature,' cxiv. p. 642 (1924).

¶ M. N. Saha and N. K. Sur, Phil. Mag. xlviii. p. 421 (1924).

** O. Klein and S. Rosseland, *Zeit. f. Phys.* iv. p. 46 (1921).

†† J. Franck, *Zeit. f. Phys.* ix. p. 259 (1922).

‡‡ H. Sponer, *Zeit. f. Phys.* xxxiv. p. 622 (1925)

spectral lines of the other gas excited in the after-glow must be lower than 11·4 volts.

Observations on the rate of decay of the after-glow by Angerer * and Rudy † are closely in agreement with the consequences following from Sponer's triple-collision hypothesis, and the experimental results recently published by Ruark, Foote, Rudnick, and Chenault ‡ have also confirmed the same assumption.

As above stated, an exact knowledge of the spectra of various metallic vapours excited by the stream of active nitrogen is very important in throwing light on the real nature of the activity and in other views of chemi-luminescences. We have been investigating, for the last two years, the properties of ionized and excited nitrogen molecules and atoms, and spectroscopic observations of the after-glow and of light-emissions from various metallic vapours under bombardment by active nitrogen have been carefully carried out. The results obtained, as shown in the following paragraph, differ in the case of mercury from that observed by Ruark and others, and other metallic spectra are more fully extended than has been hitherto reported.

Experimental Arrangements.

Various types of discharge-tube were used in this investigation. The one which was mainly used is one similar to that of Strutt and Fowler, also used by R. S. Mulliken § in his researches on the copper iodide spectra. Nitrogen was prepared chemically in the usual manner, from ammonium chloride and sodium nitrite. After passing through a row of purifying and drying tubes the continued stream of nitrogen enters the activating tube, then the activated gas flows into the light-trap of a cranked glass tube, and then into an after-glow tube made of Pyrex glass or fused silica. A small cylindrical side bulb containing the metals under examination connects with the main one, 1 or 2 cm. distant from the connecting part of a light trap, and the bulb is gently heated with a Bunsen burner. The light emitted was always observed end-on through a quartz window at the end of the tube.

The discharge was carried from the secondary coil of an induction coil with a spark-gap and a suitable condenser, and the electrode near the after-glow tube was always

* E. v. Angerer, *Phys. Zeit.* xxii. p. 97 (1921).

† R. Rudy, Phys. Rev. xxvii. p. 110 (1926).

‡ A. E. Ruark, P. D. Foote, P. Rudnick, and R. L. Chenault, J. O. S. A. xiv. p. 17 (1927).

§ R. S. Mulliken, Phys. Rev. xxvi. p. 1 (1925).

earthed. A Hilger quartz monochromator was adapted to serve as a spectrograph by substituting a camera for the telescope.

The Spectra of the After-glow.

In the first place it is necessary to study exactly the light-emissions due to the after-glow itself. Our results were exactly the same as those recorded by Strutt and Fowler, and recently observed by R. C. Johnson and H. G. Jenkins*. The α, β, and γ groups are emitted but the α group are especially enhanced, while traces of the second group of positive bands due to the nitrogen molecules could not be observed, though we endeavoured to expose the photographic plates for more than 60 hours. No one has ever reported the appearance of this group, which contradicts the results obtained by Ruark and his co-operators, and it may be questioned whether their sectored disk operated satisfactorily and perfectly cut out the direct discharge or not. (Pl. VII., *a*.)

Next we went on to the study of the light-emissions from metallic vapours under the bombardment of active nitrogen. All the metallic vapours tried cause deposits as coating of mixtures on the colder parts of the wall of the after-glow tube. The products consist of mixtures of metallic nitrides and of the excess of metal condensed there from vapours.

At the beginning of the experiments the characteristic glow of the metallic vapours appeared very brightly at the places where the metallic vapours met the stream of active nitrogen. It gradually faded out as the coating increased in thickness, and can be explained by the metallic nitrides acting as a poison on the activity of the gas. Other experimental difficulties are that the bulb containing the metals occasionally bursts after the burner has been removed.

We took very great care to prevent the stray discharge from entering the after-glow tube. When the earthing of the electrode near the tube is very good and no metallic clamps are used, no traces of any stray discharge diffuses in the tube. By observing the second positive band, it can be ascertained whether the stray discharge enters or not; but to obtain absolute security a sectored disk of the same kind as that described by R. C. Johnson was used, and confirmed the the fact that our tube was quite free from the stray discharge even when the sectored disk was not placed in the proper position.

* R. C. Johnson and H. G. Jenkins, Phil. Mag. ii. p. 621 (1926).

We have observed metallic spectra under a great variety of conditions. Some plates were exposed for a long time to obtain lines having higher levels of energy, and the results are described in the following paragraph with special remarks.

THE AFTER-GLOW SPECTRA OF METALS.

1. *Mercury.*—As shown in the following table, all the lines excited are arc lines, and the resonance line at λ, 2537 Å., specially enhanced. The highest level of energy appearing in our records was $4d$, corresponding to the excitation potential 9·51 volts. To obtain lines up to this level only four hours were needed, but we could not find any traces of lines higher than those levels of energy even after 100 more hours. On these points there is quite a difference from observations made by Ruark and his co-operators, and we shall discuss this later. Mercury nitrides are black powders and very explosive, as small cracking sounds are heard in the tube and occasionally the explosion was great enough to break the tube. Accompanying these explosions, light of a bluish colour flashed out instantaneously. (Pl. VII., *g*.)

The lines recorded on our plates are :

Obs. Lines.	Class.	Remarks.	Obs. Lines.	Class.	Remarks.
5461	$2p_1$—$2s$		3026–22	$2p_1$—$4d$	
4358	$2p_2$—$2s$		2654–52	$2p_2$—$4d$	
4047	$2p_3$—$2s$				
3341	$2p_1$—$3s$		5791–70 ?	2P—3D 2P—$3d$	Masked by α group.
2894	$2p_2$—$3s$				
2753	$2p_3$—$3s$		4078	$2p_2$—2S	
3663–50	$2p_1$—$3d$		2537	1S—$2p_2$	Very strong.
3132–26	$2p_2$—$3d$				
2967	$2p_3$—$3d$				

2. *Cadmium.*—Cadmium nitrides are dark-grey powders. Ruark failed to photograph lines of this metal and remarked that it destroys the after-glow. We think that in these experimental arrangements the active nitrogen does not collide with the vapour in the concentrated proportions, and the light excited is very feeble. (Pl. VII., *f*.)

Our records are :

Obs. Lines.	Class.	Remarks.	Obs. Lines.	Class.	Remarks.
5086	$2p_1$—$2s$		2982–81	$2p_1$—$4d$	
4800	$2p_2$—$2s$		2881	$2p_2$—$4d$	
4678	$2p_3$—$2s$	[Cd 1S—$2p_2$.	2837	$2p_3$—$4d$	
3253 ?	$2p_1$—$3s$	Masked by	2764	$2p_1$—$5d$	
3133 ?	$2p_2$—$3s$	Masked by	2678 ?	$2p_2$—$5d$	Masked by β
3081	$2p_3$—$3s$	Hg 3132-26.	2640	$2p_3$—$5d$	group 2679.
3614–11	$2p_1$—$3d$		3261	1S—$2p_2$	Very strong.
3468–66	$2p_2$—$3d$				
3404	$2p_3$—$3d$		2288	1S—2P	

3. *Zinc.*—Nitrides of this metal are also dark grey powders. In addition to the lines described by Lewis, we observed many other lines. (Pl. VII., *e*.)

Obs. Lines.	Class.	Remarks.
4811	$2p_1$—$2s$	
4722	$2p_2$—$2s$	
4680	$2p_3$—$2s$	
3072?	$2p_1$—$3s$	Masked by Zn 1S—$2p_2$.
3036	$2p_2$—$3s$	
3018	$2p_3$—$3s$	
2712	$2p_1$—$4s$	
2684	$2p_2$—$4s$	
2670	$2p_3$—$4s$	
3346–45	$2p_1$—$3d$	
3303	$2p_2$—$3d$	
3282	$2p_3$—$3d$	
2801	$2p_1$—$4d$	
2771	$2p_2$—$4d$	
2756	$2p_3$—$4d$	
2609	$2p_1$—$5d$	
2582	$2p_2$—$5d$	
2570	$2p_3$—$5d$	
2516	$2p_1$—$6d$	
2491	$2p_2$—$6d$	
2480	$2p_3$—$6d$	
2463	$2p_1$—$7d$	
2440	$2p_2$—$7d$	
2431	$2p_1$—$8d$	
2408	$2p_2$—$8d$	
2397	$2p_3$—$8d$	[Zn $2p_2$—$8d$.
2409?	$2p_1$—$9d$	Masked by
2387?	$2p_2$—$9d$	Masked by β_2 group 2387.
2139	1S—2P	
4630	2P—4D	
3076	1S—$2p_2$	Very strong.
4293	$2p_2$—2S	

4. *Magnesium.*—The intensity distributions of the lines are exactly similar to those observed previously by Lord Rayleigh and Fowler. In addition to these lines we have observed $2p$—$2s$, $2p$—$4s$, and $2p$—$6d$. Nitrides of this metal need special notice, as some black coatings were produced at the neck of the bulb, while on the wall near the bulb the product was red in colour. After the experiment a cotton-like white compound remains in the bulb, among which crystals of bright golden colour were found; but it is questionable whether these are varieties of magnesium nitrides or not, for the insides of the bulb, made of pyrex glass, are attacked severely by the vapour. The product is very hygroscopic, as it smells as strongly as ammonia gas, in consequence of its absorbing atmospheric moisture. (Pl. VII., *d*.)

Lines observed are listed in the following:

Obs. Lines.	Class.	Remarks.
5184–67	$2p$—$2s$	
3337–30	$2p$—$3s$	
2942–37	$2p$—$4s$	
3838–29	$2p$—$3d$	
3097–91	$2p$—$4d$	
2852–47?	$2p$—$5d$	Masked by Na
2737–32	$2p$—$6d$	2853.
4571	1S—$2p_2$	Very strong.
2852?	1S—2P	Masked by Na 2853.
2783–76	$2p$—$2p'$	Strong.

5. *Sodium.*—Nitrides of this metal are dark grey, and it burns in air. When the metal is heated in the bulb a bright green light column is seen at the neck where the dense vapour meets the stream of active nitrogen, and surrounding this

column broad yellow aureoles diffuse in large volumes. Spectroscopic observation shows the green lines λ 5688–83 Å. strongly at the centre of the column, and at the outside the D line strongly appears, as Lord Rayleigh and Fowler remarked. After several trials it seems that the difference in these colours depends absolutely on the density difference of the vapour, and we shall publish some quantitative investigations of this point in the near future. The glow of this metal is very intense, and nitrides are not so harmful to the activity of gas as that of other metals, and we could not understand why Ruark and his co-operators could not observe any lines in their tube (Pl. VII., *b*). The lines observed are:

Obs. Lines.	Class.	Remarks.	Obs. Lines.	Class.	Remarks.
5890–96	$1s—2p$		5688–83	$2p—4d$	
3302–03	$1s—3p$		4983–79	$2p—5d$	
2853	$1s—4p$		4669–65	$2p—6d$	
2680	$1s—5p$		4498–94	$2p—7d$	
2594	$1s—6p$		4393–90	$2p—8d$	
2544	$1s—7p$		4324–21	$2p—9d$	
2512	$1s—8p$		4277–73	$2p—10d$	
			4242–39	$2p—11d$	
5154–49	$2p—4s$		4216–13 ?	$2p—12d$	
4752–48	$2p—5s$				
4545–42	$2p—6s$				
4423–20	$2p—7s$				

6. *Potassium.*—Nitrides of this metal resemble those of sodium, but it acts as a powerful poison of activity, so it was difficult to obtain sufficient exposure of the plates. Our observations (Pl. VII., *c*.) are :

Obs. Lines.	Class.	Remarks.	Obs. Lines.	Class.	Remarks.
4044–47	$1s—3p$		5832–13	$2p$-$5d$	
3447–48	$1s—4p$		5360–43	$2p$-$6d$	
3217–18	$1s—5p$		5112–97	$2p—7d$	
3102	$1s—6p$	[group 3035.	4965–51	$2p—8d$	
3035 ?	$1s—7p$	Masked by β	4870–56	$2p—9d$	
			4805–91	$2p—10d$	
			4759–46	$2p—11d$	

7. *Thallium.*—Reddish-yellow nitrides are formed. Besides the lines Ruark has reported, $2p—5s$, $2p—7d$, $2p—8d$, and $2p—9d$ were clearly seen. (Pl. VII., *h*.)

Obs. Lines.	Class.	Remarks.	Obs. Lines.	Class.	Remarks.
5350	$2p_1—2s$		3529–19	$2p_1—3\ d$	
3776	$2p_2—2s$		2768	$2p_2—3\ d$	
3230	$2p_1—3s$		2922–18	$2p_1—4\ d$	
2580	$2p_2—3s$		2380	$2p_2—4\ d$	
2826	$2p_1—4s$		2711–09	$2p_1—5\ d$	
2316	$2p_2—4s$		2238	$2p_2—5\ d$	
2666	$2p_1—5s$		2610–09	$2p_1—6\ d$	
2207	$2p_2—5s$		2169	$2p_2—6\ d$	
2586 ?	$2p_1—6s$	Masked by γ group 2596.	2553	$2p_1—7\ d$	
			2517	$2p_1—8\ d$	
			2494	$2p_1—9\ d$	
			2211	Unclassified.	

8. *Calcium.*—The excitation potential of the spark resonance lines of this metal is 9·2 volts, and it is very interesting to ascertain whether these lines appear or not in the after-glow spectra. We have made several attempts to obtain the spectra of this metal, but unfortunately none of the trials was successful, because as soon as the stream of active nitrogen passes through, even in the solid state, it forms nitrides.

9. *Surface Fluorescence of Metals.*—Surface fluorescence was observed when metallic sodium, potassium, magnesium, calcium, and barium were put in the after-glow tube. But it cannot be observed when the surface of pure magnesium is freshly cut with a knife, and it is revealed again after being thrown in the air. Perhaps this phenomenon of the surface fluorescence is intimately connected with the surface conditions of the metal.

Interpretation and Discussion of the Results.

As described in the preceding tables, the metallic spectra excited by active nitrogen are arc lines of the vapours, and no spark lines are observed. It must be remarked that the relative intensities differ from those in the common arcs, and especially that the resonance line $1S—2p_2$ of alkali earth metals is more strongly excited than in other cases. Ruark and others reported that the distribution of intensities did not obey the usual rules of arc, but said nothing about the resonance lines, for they observed accurately only the cases of mercury and thallium.

It will be very worth while to compare our results with the metallic spectra excited by atomic hydrogen in the report recently published by F. L. Mohler *. From his report we can see that the resonance line of sodium and cadmium appeared strongly, very weak and only just observable lines in potassium and mercury, and no lines at all in magnesium and zinc. As the work of dissociation of hydrogen molecule is 4·38 volts, and is so small that it is insufficient to excite the resonance line of mercury, we cannot expect the excitation of lines corresponding to higher levels of energy, but it can be conceived that his results fairly coincide with our cases of nitrogen, and the resonance lines were excited in a comparatively high degree. In other words, it seems that the probability of exciting resonance lines, as triple collisions occur, is comparatively greater than in other cases of excitation.

* F. L. Mohler, Phys. Rev. xxix. p. 419 (1927).

The highest level of energy obtained in our experiments was that of $4d$ of mercury corresponding to the excitation potential 9·51 volts. As above remarked, lines up to this level develop satisfactorily with four hours' exposure, but we could not detect any traces of lines having higher level than this. For example, in mercury the triplets 3026–22, 2654–52 appeared clearly with four hours' exposure, but triplets 2925, 2576, 2464, and 2805–03, 2483–82, 2378 do not appear even with runs of a week's exposure, though the differences in the excitation potentials of the latter are only about 0·14 and 0·32 volt greater than that of the former.

In conflict with our results, Ruark has reported the appearance of series members up to 10·0 volts energy. Of course, the dissociation energy being higher than the excitation potentials of these lines, there are no theoretical objections to this result, but it is very questionable whether these lines can be excited only by the active nitrogen itself or not. We believe that if they had been observed under the conditions as above mentioned, these triplets would not have appeared. It can be stated with certainty that the mercury atom can receive from active nitrogen the energy corresponding to 9·51 volts, but not attain that corresponding to 9·65 volts, and it is smaller than the value expected from Sponer's hypothesis. This discrepancy can be explained after the mechanism of the triple collision has been fully studied.

As the ionization potentials of cadmium, zinc, magnesium, sodium, potassium, and thallium are lower than 9·51 volts, the ionizations of these metallic atoms are theoretically possible. Saha and Sur also pointed out this in connexion with their theory.

Magnesium lines λ 2796 Å. and λ 2803 Å. are intense spark resonance lines corresponding to 12·0 volts, and it is very interesting to see whether these are observable or not; but we could not find them at all. Using titanium tetrachlorides, Jevon* found a few singly ionized titanium lines in the after-glow tube, but his experimental conditions are very complicated and nothing can be deduced as to whether these are due to the atomic nitrogen or not. Thus observations do not tell us that the metallic atoms are ionized in the triple collision. It is very remarkable that from the fact that lines $2p$–$2p'$ of magnesium appear strongly, two electrons may be displaced simultaneously to higher levels of energy.

* W. Jevon, Proc. Roy. Soc. lxxxix. p. 187 (1913).

Lastly, we have carefully examined the band spectra due to formations or decompositions of metallic nitrides, but contrary to the cases of atomic hydrogen, no traces were found, at least in the observed ranges of wave-lengths. As Ruark remarked, from the thermochemical point of view, it is very questionable whether metallic atoms can be excited as the result of the decomposition of metallic nitrides in the after-glow tube.

All the experimental results recently obtained favour Sponer's hypothesis, but no exact explanation of the mechanisms of triple collisions have been hitherto proposed. It is very desirable to attempt some experiments in this direction.

In conclusion, the present writers express their best thanks to the Saito Gratitude Foundation for the expenses of this experiment, which were paid by the Research Fund from the Foundation.

Sendai, Japan.
May 1927.

XXXVII. *On the Diamagnetic Susceptibilities of Gases at Low Pressures.* *By* V. I. Vaidyanathan *.

Abstract.

The Instrument.—The apparatus employed is a modified form of Curie balance of high sensitivity and specially adapted for investigations on weakly magnetic gases. It consists of a thin closed bulb, suspended from the balance-beam in a suitable non-homogeneous field. The gases under investigation surround this bulb. The glass of the bulb is diamagnetic, but it is almost compensated for diamagnetism by enclosing the requisite quantity of air ; so that in a vacuum there is very little magnetic force acting on it at atmospheric temperature. When a diamagnetic gas surrounds the bulb, it is attracted towards the stronger part of the field, causing a twist in the suspension fibre of the balance-beam and *vice versa*. The deflexions give a relative measure of the volume susceptibilities. The balance is enclosed in an air-tight chamber of required shape, into which gases are let in.

Results.—A complete investigation at low pressures showed strict proportionality between pressure and volume susceptibility. The relative values obtained were $-0{\cdot}00092 \times 10^{-6}$, $-0{\cdot}00113 \times 10^{-6}$ and $-0{\cdot}00058 \times 10^{-6}$ for the

* Communicated by Prof. C. V. Raman, F.R.S.

volume susceptibilities of carbon dioxide, argon, and nitrogen respectively at 0° C. and 760 mm. (Air : $0{\cdot}0308 \times 10^{-6}$ at 0° C. and 760 mm.)

Sensitiveness.—A change of volume susceptibility of $0{\cdot}000006 \times 10^{-6}$ in a field of 1400 Gauss corresponds to a deflexion of 1 mm. on a scale at a distance of a metre, and this is much higher than those attained in any previous investigation. The relative values obtained are accurate to within about 5 per cent.

The Susceptibility Balance.

THE instrument* was developed in an investigation by the author on the magnetic susceptibilities of carbon dioxide at low pressures, and is illustrated in fig. 1. It consists essentially of a hollow glass bulb D, which is

Fig. 1.

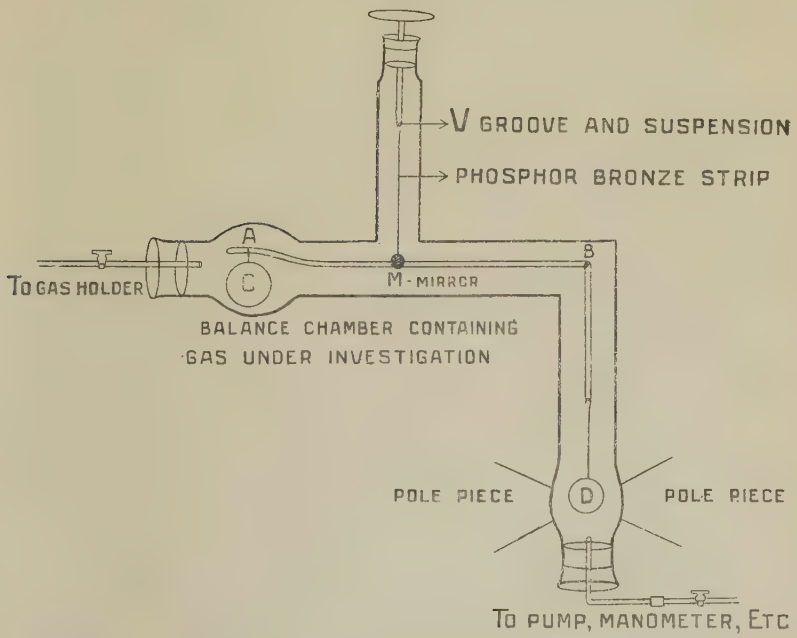

sealed and suspended from one end of a light aluminium bar AB, the latter being suspended by a torsion fibre. The bulb D is blown out of feebly-diamagnetic glass selected by preliminary investigation on various specimens, and this

* Vadiyanathan, Ind. Journ. Phys. vol. i. p. 183 (1926).

diamagnetism is compensated as nearly as possible by enclosing within it the requisite quantity of air. The bulb hangs in a suitable non-homogeneous field between the pole-pieces of an electro-magnet. The bulb C, attached to the other end of the balance, counterpoises the weight of D, and in addition its volume is so adjusted that the hydrostatic buoyancy due to introducing gases into the balance-chamber is completely neutralized. The shape of the balance-chamber is suitably adjusted for the free movement of the balance within it. The chamber is connected to an elaborate arrangement for the introduction of gas and for altering of pressure. M is a galvanometer mirror by which the deflexions of the beam are read by the usual lamp-and-scale arrangement.

When the magnet is excited, the bulb is slightly attracted or repelled in vacuum owing to the imperfection in compensation and temperature fluctuations changing the susceptibility of the contained air. By rotating the torsion head, the balance is so adjusted that the beam lies along the axis of the chamber. Now, if we introduce a diamagnetic gas around the bulb, it apparently becomes more paramagnetic and is drawn towards the stronger part of the field, and on introducing a paramagnetic gas, it becomes diamagnetic to that medium and is repelled. The movement of the bulb D is adjusted to be in a perfectly horizontal plane and at right-angles to the non-homogeneous field, causing a couple in the torsion-fibre of the balance-beam. From the relative deflexions, the volume susceptibility of one gas can be determined if the other is known. The chief difficulty was due to the heating of the coils of the magnet and the consequent rise of temperature. This causes a decrease of the susceptibility of the air used for the compensation of the bulb. To avoid this, only single intervals of pressure were investigated at a time, the next observation for a different pressure being made after a considerable interval. The temperature fluctuations of the atmosphere cause a shift in the zero reading of the spot of light, but do not influence the actual change of deflexion, which alone need be taken account of in the measurements.

Purification of Argon and Nitrogen.

The compressed gas argon, supplied in a cylinder, was purified by passing it in succession through freshly cut phosphorus *, concentrated solution of ferrous sulphate kept

* Hon. R. J. Strutt, Proc. Roy. Soc. A, lxxxv. p. 219 (1911).

cooled in ice, concentrated sulphuric acid, calcium chloride, hard glass tubes containing magnesium, freshly reduced copper heated over a furnace, and a cooling spiral. The stream of gas was maintained for about 15 hours, and 5 litres were collected for subsequent investigations. Nitrogen was prepared by warming a concentrated solution of equi-molar quantities of pure sodium nitrite and ammonium chloride. The purification was effected as in the case of argon, the magnesium tube being substituted by a U-tube containing caustic potash.

Results for Argon.

In the following tables, column I. indicates the pressure p in mm. of mercury between which the measurements are made; II. the corresponding readings of the spot of light; III. the change of pressure; IV. the relative change of deflexion; V. the ratio of the change of deflexion to the pressure; the last column is also a relative measure of susceptibility. The constancy of the ratios in column V. shows that the volume susceptibility is proportional to pressure, and the anomalous behaviour observed by Glaser * is also not found.

TABLE I.

I. p.	II. θ.	III. dp.	IV. $d\theta$.	V. $\frac{d\theta}{dp}$.
0–50	180–188·5	50	8·5	·170
0–86	190–205	86	15	·176
0–176	190–224	176	34	·192
100–196	202–220	96	18	·184
200–300	206–224	100	18	·180
250–540	193–247	290	54	·182
400–500	230–248	100	18	·180
2–500	200–293	500	93	·168
0–250	218–264	250	46	·180
			Mean =	·179

A similar experiment was conducted with pure CO_2 to obtain the value of argon relative to it. The mean value of $d\theta/dp$ for CO_2 was 0·145. Taking the volume susceptibility of CO_2 as $-0{\cdot}00092\times10^{-6}$ at 0° C. and 760 mm.†, this reduces to $-0{\cdot}00113\times10^{-6}$ at 0° C. and 760 mm. for the volume susceptibility of argon.

* Glaser, *Ann. d. Phys.* lxxiv. p. 459 (1924).

† Vaidyanathan, *loc. cit.*

Results for Nitrogen.

TABLE II.

I.	II.	III.	IV.	V.
p.	θ.	dp.	$d\theta$.	$\frac{d\theta}{dp}$.
0–90	273–284	90	11	·122
90–182	283–294	92	11	·120
100–197	271–283	97	12·5	·128
187–273	283–292·5	86	9·5	·109
189–304	270–282	105	12	·113
300–400	282–294	100	12	·120
480–562	277–287	82	10	·121
0–230	260–287	230	27	·118
0–302	255–292	302	37	·120
				Mean = ·119

Over the same regions the change of deflexion corresponding to the change of susceptibility of 1 mm. of air was 5·44 divisions at 30° C. The pressure-changes required in the case of air being of the order of a few mm., these were read with a cathetometer. Taking the volume susceptibility of air as $0{\cdot}0308 \times 10^{-6}$ at 0° C. and 760 mm.*, and performing the necessary calculations, the volume susceptibility of nitrogen is $-0{\cdot}000525 \times 10^{-6}$ at a mean temperature of 29° C. and 760 mm. pressure.

TABLE III.—Susceptibilities.

Gas.	$K_0 \times 10^6$.	$\chi_s \times 10^6$.	$\chi_m \times 10^6$.
N_2	−0·00058	·46	12·9
A	−0·00113	·635	25·3
CO†	−0·0009	·465	20·5

In the above table K_0 is the volume susceptibility observed and reduced to 0° C. and 760 mm., χ_s the specific and χ_m the atomic or molecular susceptibilities.

Sensitiveness and Source of Error.

The relation between the change of deflexion of the balance-beam and of volume susceptibility is

$$c \,.\, d\theta = lv\mathrm{H} \,.\, \frac{d\mathrm{H}}{dx} \,.\, \mathrm{K}g$$

where c denotes the couple per unit twist of the torsion fibre, $d\theta$ the change in the angle of deflexion corresponding to the change $\mathrm{K}g$ of the volume susceptibility of the surrounding medium, l the distance between the point of suspension of

* Také Soné, Phil. Mag. xxxix. p. 305 (1920).

† Vaidyananthan, *loc. cit.*

the beam and the bulb D, v its volume and $H.\frac{dH}{dx}$ a vector. (In the experiment, x is the horizontal axis at right-angles to the field.) From the expression, it is easily seen that the sensitiveness mainly depends on c, l, and v. The advantage secured in the experiment was the possibility of the variation of c. Since the bulb D has practically very little susceptibility at atmospheric temperature and the suspended system is very light, a very sensitive fibre could be employed. v was about 3 c.c., and this was the convenient maximum for the volume, since it had to be suspended within the balance-chamber and oscillate within it without jamming. l was about 11 cm. Since it was the aim to make measurements in small fields, H was not increased beyond 3000 gausses. The retorsion method was found impossible, owing to the mechanical disturbances resulting from the process, but the torsion method was found to be sufficiently accurate. The constancy of the factor $H.\frac{dH}{dx}$ was tested experimentally, and the assumption was found justifiable within experimental errors. The adjustment for hydrostatic buoyancy was tested with a microscope. A series of preliminary experiments were found necessary to select the proper diamagnetic glass, to obtain a thin uniform bulb, to secure the compensation, and to adjust the volume and weight of the counterpoise, making the experimental investigation somewhat difficult and tedious.

Taking the experiment on nitrogen, a change of $0{\cdot}0000066 \times 10^{-6}$ of volume susceptibility corresponds to one division on the scale in a field of 1400 gausses, and this could be easily detected. When a continuous current was running in the magnet for about 6 minutes, a drift of about one division of the spot of light could be observed on the scale, due to various disturbing influences. The current was kept fairly constant with necessary arrangements. Allowing for the maximum effect of the various sources of error, the relative values are accurate to within about 5 per cent.

Comparison of Experimental Data on Diamagnetic Gases.

TABLE IV.—Specific susceptibilities $\times 10^6$.

Gas.	Také Soné *.	Hector †.	Glaser ‡.	Lehrer §.	Author.
CO_2	−0·423	—	−0·43	−0·47 −0·52	−0·48
N_2.....	−·0265	−0·42	−0·26	—	−0·46
A	—	−0·45	—	−0·48 −0·50	−0·64

* Také Soné, *loc. cit.* † Hector, Phys. Rev. xxiv. p. 418 (1926).
‡ Glaser, *loc. cit.* § Lehrer, *Ann. der Phys.* lxxxi. p. 229 (1926).

In the case of argon the value of the susceptibility is 40 per cent. higher than Hector's and 28 per cent. higher than Lehrer's. The values for nitrogen and carbon dioxide are in fair agreement with those of Hector and Lehrer. In investigating argon it was found that the cylinder argon generally supplied contains a large quantity of air, and the purification requires a number of tubes to remove the oxygen and nitrogen. Special attention has been paid to this point. If we substitute the present value in Langevin's formula, after necessary calculations, the mean atomic radius comes out as 1·06 A.U. (approximately), in very close agreement with 1·02 A.U. and 1·43 A.U. obtained from Bragg's determinations and Rankine's viscosity measurements. According to L. Pauling * the calculated value for the gram atomic susceptibility of argon is $21{\cdot}5 \times 10^{-6}$, and according to Dr. Stoner † 30×10^{-6} (the latter is a rough calculation from the ionization potential), while the value obtained in the present investigation is $25{\cdot}3 \times 10^{-6}$.

After the work of the present investigation had been completed, a preliminary note by Hammar ‡ and a paper by Lehrer § appeared in the Proc. N. A. S. and *Ann. der Phys.* respectively, in which they have also found a linear relation between pressure and susceptibility.

In conclusion, I have the greatest pleasure in acknowledging my indebtedness to Prof. C. V. Raman, F.R.S., for suggesting the problem and for taking a deep interest in the work. The work has been carried out in the Physical Laboratory of the Indian Association for the Cultivation of Science.

210 Bowbazar Street, Calcutta (India).
5th May, 1927.

XXXVIII. *The Fine Structure of Mercury Lines.* *By* W. H. McCurdy, *Ph.D.*‖

[Plate VIII.]

NAGAOKA, Sugiura and Mishima ¶ have made an extensive examination of the fine structure of the strong lines of the mercury arc spectrum. They used quartz

* L. Pauling, Proc. Roy. Soc. A, cxiv. p. 181 (1927).
† Stoner, Phil. Mag. iii. p. 336 (Feb. 1927).
‡ Hammar, Proc. N. A. S. xii. p. 594 (1926).
§ Lehrer, *loc. cit.*
‖ Communicated by the Author.
¶ Nagaoka, Sugiura and Mishima, Jap. Journ. of Phys. ii. p. 121 (1923).

Lummer-Gehrcke plates which enabled them to examine the lines in the ultra-violet, which region has, until recently, been little investigated. As a source of radiation they used an Aron's quartz mercury arc, water-cooled to prevent excessive broadening of the lines.

Wood* has repeated their work on the strong line 2537 Å., and has found the earlier results to be incorrect. He has found that the apparent structure of the line may be varied at will by varying the temperature of the arc. Using a carefully cooled Cooper-Hewitt quartz arc and forcing the discharge against the wall of the tube by means of a weak magnetic field, he has found the structure of the line to be entirely different from that given by Nagaoka and his co-workers. He explained the results of the earlier work as due to broadening and self-reversal of the components of the line, the overlapping of the unabsorbed wings accounting for the fact that the number of components found by Nagaoka was not double the number of true components.

In the course of his experiments on Optical Excitation of Mercury Vapour, Wood has observed that one of the components of the line 3650 Å. and also of the line 2967 Å. appears self-reversed under certain conditions. It was therefore considered advisable to repeat Nagaoka's work on these lines, in order to determine whether or not the earlier results were sufficiently reliable to justify attempts to construct the fine structure energy diagrams for mercury.

Apparatus.

A quartz Cooper-Hewitt mercury arc was used as source throughout the work, with the mercury cathode cooled in running water, as shown in fig. 1. The pressure of mercury vapour is controlled by the temperature of the cathode, provided there are no drops of mercury on the sides of the arc; consequently the lines were made sharp by keeping the cathode at a low temperature. This type of arc has the additional advantage of making possible the observation of the arc from the side. It is well known that the width of a spectral line increases as the length of the radiating column is increased, also that the shape of the line is different when the tube is observed end on from the shape when the same tube is observed side on. The long source gives a line with a flat top, and in some cases a reversed or partially reversed line, while the intensity distribution in the case of the tube viewed side on is that given by the probability law. The

* Wood, Phil. Mag. l. p. 761 (1925).

arc was so arranged that the discharge could be thrown against the wall of the tube by means of a magnetic field.

Fig. 1.

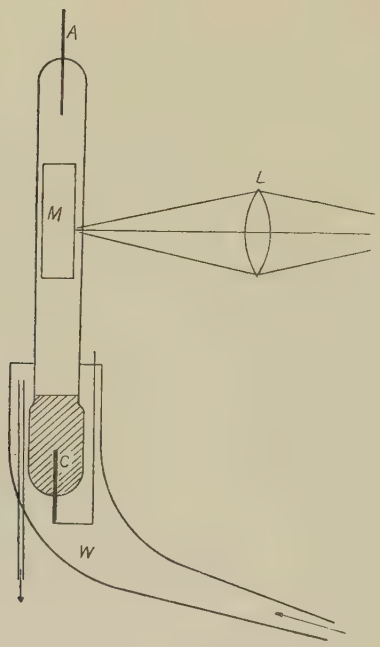

The optical arrangement is shown in fig. 2. The light was polarized before entering the first Lummer-Gehrcke plate by means of the double-image prism P. The two quartz Lummer-Gehrcke plates LG_1 and LG_2 were placed

Fig. 2.

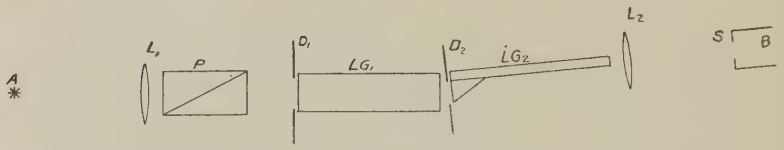

perpendicular to each other as shown, and the light was focussed on the prism of the first plate by the quartz lens L_1. The interference fringes were photographed by means of the large quartz spectrograph B, which served to separate the lines. The slit S was placed at the principal focus of the quartz fluorite lens L_2 as the light is necessarily parallel on

emerging from the interferometer. The photographic plate were placed as nearly as possible perpendicular to the direction of the light from the prism of the spectrograph, which made it possible to obtain approximately square patterns and at the same time circular interference points.

Hammer Special plates were used throughout the work, as they were found to be both fast and clear. Exposure times ranged from $\frac{1}{2}$ to 8 hours.

Fig. 3.

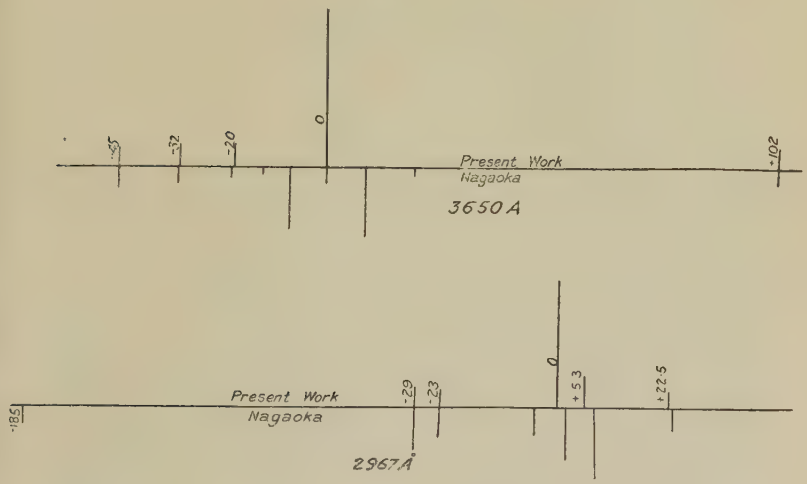

The structures found for the two lines are shown diagrammatically in fig. 3. They are so arranged that comparison with the results of Nagaoka's work is very easy. The components found in the present work are placed above the line, while those found by Nagaoka are placed below.

Discussion of Results.

In the case of the line 3650 Å. the three weak components to the short wave-length side of the main component coincide, within the limits of error of the work, with the corresponding ones measured by Nagaoka, as does also the single one to the long wave-length side. As may be seen in fig. 3, the strong central component is found to coincide with a weak one found by Nagaoka. The two stronger components reported by Nagaoka are not found, however. Exposures taken without the water-cooling on the arc show a

different result. Reproductions of photographs taken with and without water-cooling on the arc are shown in Pl. VIII. (figs. 1 and 2). It may be observed that in the case of a hot arc the central component of the line has become very broad and appears self-reversed. In the case of the cold arc, however, the strong central component appears as an almost circular dot, indicating that within the limits of the apparatus the central component is single, and not multiple as given by the earlier work.

From the above observations it appears probable that the explanation of the results reported by Nagaoka and his co-workers is that they have mistaken a broadened and partially self-reversed line for a group of at least three and probably five components. The two unabsorbed wings of the line and the incompletely absorbed central portion of the line are mistakenly termed three separate components. The two weak components on either side of the central group have not been found in the present work, as may be seen by the plates given in Pl. VIII. (figs. 1 and 2). The only apparent explanation of this is that the excessive broadening of the central component has produced such a broad interference point that it has been mistakenly interpreted as including a weak unresolved component on either side. It is barely possible that these are so weak that they have not appeared in the present work, but this explanation appears improbable considering the relative intensities reported by Nagaoka. It may also be pointed out that the intensity of the main component in the present work is much greater relative to that of the others than is the case in the earlier work. This is apparently further confirmation of the supposed absorption.

As the line 2967 Å. has a place in the energy level diagrams of mercury similar to that occupied by the line 3650 Å., it may be expected to show similar peculiarities. Photographs of the fine structure of this line were also taken with both hot and cold arc. The broadening in the hot arc, however, was so great that it was found impossible to analyse the structure of the line from the plates obtained. Further, the line was so weak that exposures of over eight hours were necessary, using crossed Lummer-Gehrke plates. For this reason the plates were used crossed only to determine the position of the components, and they were used separately for examining the structure in the vicinity of the central component.

The structure of this line in the cold arc, using crossed plates, is shown in Pl. VIII. (fig. 3). This shows the two

components to the short wave-length side of the central group and the single one on the long wave-length side. The weak component reported by Nagaoka at −185 m.Å. does not appear, as it would be expected to almost coincide with one of the stronger components with the particular plates used. Pl. VIII. (fig. 4) shows the structure around the central group. This group is seen to consist of the strong central component, with a weak component on the long wave-length side. The reproduction also shows the other components found with the crossed plates. A diagrammatic representation of the structure of this line is given in fig. 3, contrasted with the structure reported earlier by Nagaoka.

The structure found in the hot arc, using a smaller plate, is shown in Pl. VIII. (fig. 5). This shows the unsymmetrically reversed main component. The asymmetry here is due to the fact that the weak component is not resolved but included in the unabsorbed long wave-wing.

Fig. 3 shows that the two short wave-length components and the single long wave-length one may be made to coincide, within the limits of the work, with the corresponding one reported earlier. The central group, however, is entirely different in the two cases. The explanation appears to be that in the earlier work Nagaoka observed a broadened and partially reversed main component and an incompletely resolved weaker component. The group was mistakenly considered to consist of three separate components of almost equal intensity.

Thus we find that instead of nine components originally reported for the line 3650 Å. there are actually five components, and instead of seven for the line 2967 Å. there are actually six. The separation of these from the main component is given in fig. 3.

Conclusion.

Ruark * has recently attempted to work out the fine structure energy levels of mercury with but limited success. The results of Wood's experiments on the line 2537 Å. and of the present experiments on the lines 3650 and 2967 Å. show the necessity for a complete review of the fine structure of the mercury arc spectrum, although the lines cited are the most liable to be incorrect owing to the difficulties involved in the observations, the first being a principal series line and the others ending on metastable levels. Since the study of fine structure is proving of

* Ruark, Phil. Mag. vol. i. p. 977 (1926).

importance as a tool in the study of atomic structure, it is well that the importance of the source of radiation as well as the reliability of the optical apparatus be realized. The present work shows how unreliable results may prove when care is not taken in selecting a proper source for work with optical apparatus of such high resolving power.

In conclusion, the author wishes to express his most sincere thanks to Prof. R. W. Wood, who first suggested the problem and placed the necessary apparatus at his disposal ; also to the National Research Council for the grant of a Fellowship, which made the work possible.

Johns Hopkins University,
Baltimore, Md.

XXXIX. *Some Approximate Formulæ for the Numerical Integration of Differential Equations. (Analysis and generalization of a method given by* H. T. H. Piaggio.) *By* E. Remes, *Aspirant of the Cathèdre Mathématique, Kieff, Russia* *.

WE shall examine here the case of a single equation,

$$\frac{dy}{dx} = \mathrm{F}(x, y). \quad . \quad . \quad . \quad . \quad . \quad . \quad (1)$$

The approximate determination of an integral curve which passes through the initial point $x=a$, $y=b$, comes, as is well known, to the successive determination of the increments Δy corresponding to the small successive increments Δx. H. T. H. Piaggio has given † a practical method for finding two limits between which Δy must lie.

Considering first the simple case where $\mathrm{F}(x, y)=f(x)$, depending only on x, and assuming that $f''(x)$ keeps the same sign in the interval $(a, a+h)$, we can take as limits of the increment

$$\Delta y = \int_a^{a+h} f(x)\,dx,$$

corresponding to $\Delta x=h$, either of the two pairs of numbers p, q or p, r, where p, q, r measure respectively the following

* Communicated and translated by Prof. H. T. H. Piaggio, M.A., D.Sc., University College, Nottingham.

† Phil. Mag. xxxvii. (1919).

rectilineal areas (see figure) :—

p = trapezium ATUC = $hf(a+\frac{1}{2}h)$
(TU is the tangent at Z) ;
q = trapezium AKZB + trapezium BZMC
= $\frac{1}{4}h[f(a)+2f(a+\frac{1}{2}h)+f(a+h)]$;
r = trapezium AKMC = $\frac{1}{2}h[f(a)+f(a+h)]$.

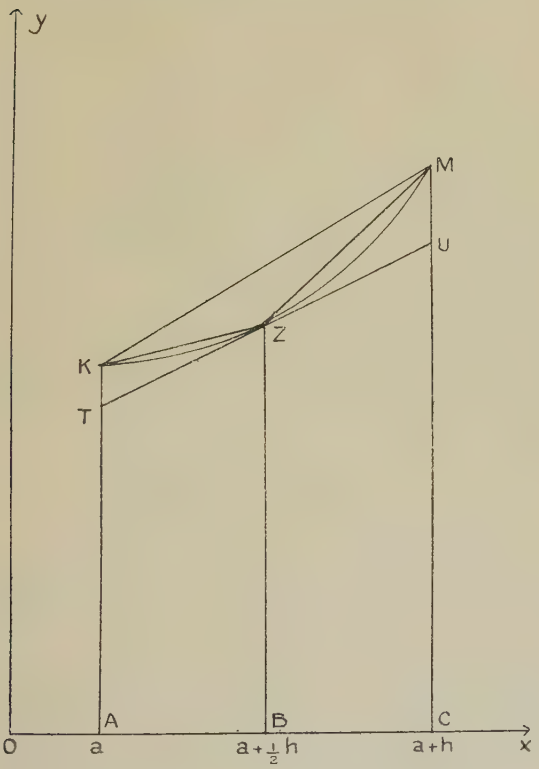

The linear combinations

$$\sigma = \tfrac{1}{3}[3\lambda p+(4-6\lambda)q+(3\lambda-1)r] \quad . \quad . \quad . \quad (2)$$

gives for every value of λ, as is easily verified, the well-known Simpson's Rule, which gives the increment Δy with an error of the 5th order of the small number h. Two particularly remarkable combinations are obtained by putting $\lambda=\frac{1}{3}$ and $\lambda=\frac{2}{3}$, namely

$$\sigma' = \tfrac{1}{3}(p+2q), \quad . \quad . \quad . \quad . \quad . \quad . \quad (3)$$

$$\sigma'' = \tfrac{1}{3}(2p+r). \quad . \quad . \quad . \quad . \quad . \quad . \quad (4)$$

The extension of formulæ (4) and (3) to the general case, where $F(x, y)$ involves y as well as x, leads respectively to the approximate formulæ of Runge * and Piaggio †. But, as there occur in the general case supplementary errors which depend on the approximate evaluation of p, q, r, the total error of these approximate formulæ is generally greater than before, say of the 3rd or 4th order instead of the 5th. To Piaggio is due the idea of using the numbers p and q, each calculated with a suitable upper and lower value so chosen that the signs of the differences $p-\Delta y$ and $q-\Delta y$ are known, as exact limits for Δy. With these he then forms the approximate combination σ'. Generalizing this idea of Piaggio's, we can obviously use in the same manner, as limits for Δy, the two numbers p, r, each calculated with a suitable upper and lower value, and use these to form the approximate combination σ''. We propose now to examine the last two methods of calculation in respect of their precision in order to arrive by combining them to a generalization of Piaggio's method, giving in every case the order of approximation ‡.

We shall assume that the function $F(x, y)$ has, in the neighbourhood of the initial point (a, b), certain continuous partial derivates of some of the lowest orders, which appear in the discussion. We can trace beforehand the curves on which the functions

$$\frac{\partial F}{\partial y}, \qquad \frac{dF}{dx} = \frac{\partial F}{\partial x} + F\frac{\partial F}{\partial y},$$

$$\frac{d^2F}{dx^2} = \frac{\partial^2 F}{\partial x^2} + 2F\frac{\partial^2 F}{\partial x\,\partial y} + F^2\frac{\partial^2 F}{\partial y^2} + \frac{\partial F}{\partial x}\frac{\partial F}{\partial y} + F\left(\frac{\partial F}{\partial y}\right)^2$$

are zero or cease to be continuous, and likewise the curves on which F is equal to ± 1 or becomes discontinuous. Disregarding the case when the integral curve cuts one of these loci of exceptional points, we can obviously assume § that the integral curve is contained in the rectangular

* *Math. Ann.* xlvi. (189).

† *Loc. cit.*

‡ The second form of calculation that we wish to examine depends on the same linear combination σ'' as Runge's method, and these two methods coincide for the trivial case $F(x, y)=f(x)$; but there is certainly an important distinction between them in the general case, for in Runge's method there is no attempt to find exact limits for Δy.

§ Taking y instead of x as independent variable, if $\left|\frac{dy}{dx}\right| > 1$.

domain *

$$a \leq x \leq a+h, \quad b-h \leq y \leq b+h,$$

and that the functions $\partial F/\partial y$, dF/dx, d^2F/dx^2 do not change sign in this domain.

Taking the equation of the integral curve to be $y=\phi(x)$, we shall use the following notation :—

$$x_\alpha = a+\alpha h\,; \quad y_\alpha = \phi(x_\alpha)\,; \quad F_\alpha = F(x_\alpha, y_\alpha)\,; \quad \ldots (\alpha = 0, \tfrac{1}{2}, 1)$$

$$P = hF_{\frac{1}{2}} \quad ; \quad Q = \tfrac{1}{4}h(F_0 + 2F_{\frac{1}{2}} + F_1)\,; \quad R = \tfrac{1}{2}h(F_0 + F_1);$$

$$\Sigma' = \tfrac{1}{3}(P+2Q)\,; \quad \Sigma'' = \tfrac{1}{3}(2P+R).$$

The maximum and minimum values of the function F on the part of the integral curve between the ordinates $x=a$ and $x=a+h$ will be denoted by $\dot{M}$ and $\dot{\underline{M}}$ respectively, while the approximation used instead of these, respectively greater and less than them, by M and $\underline{M}$.

Finally

$$\left.\begin{aligned} \dot{F}_\alpha &= F(a+\alpha h, b+\dot{M}\alpha h)\,; \\ \dot{\underline{F}}_\alpha &= F(a+\alpha h, b+\dot{\underline{M}}\alpha h)\,; \\ \overline{F}_\alpha &= F(a+\alpha h, b+\overline{M}\alpha h)\,; \\ \underline{F}_\alpha &= F(a+\alpha h, b+\underline{M}\alpha h)\,; \end{aligned}\right\} \quad (\alpha = 0, \tfrac{1}{2}, 1)$$

$$\dot{P} = h\dot{F}_{\frac{1}{2}}\,; \quad \dot{\underline{P}} = h\dot{\underline{F}}_{\frac{1}{2}}\,; \quad \overline{P} = h\overline{F}_{\frac{1}{2}}\,; \quad \underline{P} = h\underline{F}_{\frac{1}{2}}\,:$$

with a similar meaning for $\dot{Q}$, $\dot{\underline{Q}}$, $\overline{Q}$, $\underline{Q}$, $\dot{R}$, $\dot{\underline{R}}$, $\overline{R}$, $\underline{R}$.

It is clear that

$$\dot{F}_0 = \dot{\underline{F}}_0 = \overline{F}_0 = \underline{F}_0 = F_0,$$

and that the numbers $\dot{M}$ and $\dot{\underline{M}}$ coincide respectively either with F_1 and F_0, or with F_0 and F_1, according to the sign of dF/dx. It follows that one of the numbers $\overline{M}$, $\underline{M}$ may be taken equal to F_0, and so found immediately. As for the other, we could take for it one of the numbers $F(a+h, b\pm h)$, according to the signs of dF/dx and $\partial F/\partial y$, but to obtain the desired order of accuracy we shall take the value $F(a+h, b+\mu h)$, μ being as follows :

F_0, if $\partial F/\partial y < 0$;

$F(a+h, b+h)$, if $\partial F/\partial y > 0$ and $dF/dx > 0$;

$F(a+h, b-h)$, if $\partial F/\partial y > 0$ and $dF/dx < 0$.

* To fix ideas, we assume $h > 0$.

Hence

$$\overline{P} \geq \dot{P} > P > \dot{P} \geq \underline{P}, \quad \text{if} \quad \partial F/\partial y > 0,$$

but

$$\overline{P} \leq \dot{P} < P < \dot{P} \leq \underline{P}, \quad \text{if} \quad \partial F/\partial y < 0.$$

There are analogous inequalities for Q and for R.

By considering the signs of d^2F/dx^2 and $\partial F/\partial y$ we get four possible cases, in each of which we can indicate limits for Δy, and indeed do so in two different ways. In the first place, using the numbers P and Q, we get:

$$\overline{Q} > \Delta y > \underline{P}, \quad \text{if} \quad d^2F/dx^2 > 0 \text{ and } \partial F/\partial y > 0;$$
$$\underline{Q} < \Delta y < \overline{P}, \quad \text{if} \quad d^2F/dx^2 < 0 \text{ and } \partial F/\partial y > 0;$$
$$\underline{Q} > \Delta y > \overline{P}, \quad \text{if} \quad d^2F/dx^2 > 0 \text{ and } \partial F/\partial y < 0;$$
$$\overline{Q} < \Delta y < \underline{P}, \quad \text{if} \quad d^2F/dx^2 < 0 \text{ and } \partial F/\partial y < 0.$$

The combination Σ' formed with a pair of corresponding numbers $\overline{Q}$, P, or $\underline{Q}$, $\overline{P}$, will be denoted by $\Sigma'(\overline{M}, \underline{M})$.

Secondly, we can use a pair of corresponding numbers $\overline{R}$, $\underline{P}$, or $\underline{R}$, $\overline{P}$ (according to the signs of d^2F/dx^2 and $\partial F/\partial y$) as limits for Δy. The combination Σ'' formed with such a pair will be denoted by $\Sigma''(\overline{M}, \underline{M})$.

We shall now find the order of smallness of the differences $\Delta y - \Sigma'(\overline{M}, \underline{M})$ and $\Delta y - \Sigma''(M, \underline{M})$. As the differences $\Delta y - \Sigma'$, $\Delta y - \Sigma''$ are of the 5th order (taking h as small of the 1st order), we must examine the order of the differences $\Sigma' - \Sigma'(\overline{M}, \underline{M})$, $\Sigma'' - \Sigma''(\overline{M}, \underline{M})$.

Now

$$\Sigma' - \Sigma'(M, \underline{M}) = \{\Sigma' - \Sigma'(\dot{M}, \underline{M})\} + \{\Sigma'(\dot{M}, \underline{M}) - \Sigma'(\overline{M}, \underline{M})\},$$

where $\Sigma'(\dot{M}, \underline{M})$ is what $\Sigma'(\overline{M}, \underline{M})$ becomes when $\overline{M}$, $\underline{M}$ are replaced by $\dot{M}$, $\underline{M}$ respectively; and similarly $\Sigma'' - \Sigma''(\overline{M}, \underline{M})$ may be written as the sum of parts. But if we choose $\overline{M}$ and $\underline{M}$ as above, the differences $\dot{M} - \overline{M}$, $\underline{M} - \underline{M}$ will be of the 2nd order *. Hence the differences $\dot{F}_\alpha - \overline{F}_\alpha$, $\underline{F}_\alpha - \underline{F}_\alpha$ will be of the 3rd order, and consequently $\dot{P} - \overline{P}$, $\underline{P} - \underline{P}$, $\dot{Q} - \overline{Q}$, ... etc. of the 4th order. Thus $\Sigma'(\dot{M}, \underline{M}) - \Sigma'(\overline{M}, M)$ and $\Sigma''(\dot{M}, \underline{M}) - \Sigma''(\overline{M}, \underline{M})$ are also of the 4th order.

* Other ways of choosing $\overline{M}$ and $\underline{M}$ are available, but these may lower the order of mallness of the differences.

It remains to examine the order of the differences $\Sigma'-\Sigma'(\dot{\mathrm{M}}, \dot{\mathrm{M}})$ and $\Sigma''-\Sigma''(\dot{\mathrm{M}}, \dot{\mathrm{M}})$. We shall show that it depends on the sign of the product

$$\frac{\partial \mathrm{F}}{\partial y}\frac{d\mathrm{F}}{dx}\frac{d^2\mathrm{F}}{dx^2} = \Omega(x, y), \quad \text{say.} \quad . \quad . \quad . \quad (5)$$

If $\Omega < 0$, $\Sigma'-\Sigma'(\dot{\mathrm{M}}, \dot{\mathrm{M}})$ is of the 4th order,

$\Sigma''-\Sigma''(\dot{\mathrm{M}}, \dot{\mathrm{M}})$ of the 3rd.

If $\Omega > 0$, the orders are the 3rd and 4th respectively.

Hence the orders of the differences $\Sigma'-\Sigma'(\bar{\mathrm{M}}, \underline{\mathrm{M}})$ and $\Sigma''-\Sigma''(\bar{\mathrm{M}}, \underline{\mathrm{M}})$ are also the 4th and 3rd respectively if $\Omega < 0$, or the 3rd and 4th if $\Omega > 0$.

The proof is a direct application of Taylor's series. Take first the case $\Omega < 0$, and to fix ideas take $\partial \mathrm{F}/\partial y > 0$, $d^2\mathrm{F}/dx^2 > 0$, $d\mathrm{F}/dx < 0$. Using the suffix 0 to denote values at the initial point (a, b), we have *

$$\dot{\mathrm{M}} = \mathrm{F}_0\,; \quad \dot{\mathrm{M}} = \mathrm{F}_1\,;$$

$$\begin{aligned}\Sigma'-\Sigma'(\dot{\mathrm{M}}, \dot{\mathrm{M}}) &= \tfrac{1}{3}(\mathrm{P}+2\mathrm{Q})-\tfrac{1}{3}(\dot{\mathrm{P}}+2\dot{\mathrm{Q}}) \\ &= \tfrac{1}{6}h(\mathrm{F}_1-\dot{\mathrm{F}}_1)+\tfrac{1}{3}h(\mathrm{F}_{\frac{1}{2}}-\dot{\mathrm{F}}_{\frac{1}{2}})+\tfrac{1}{3}h(\mathrm{F}_{\frac{1}{2}}-\dot{\mathrm{F}}_{\frac{1}{2}})\,; \\ \Sigma''-\Sigma''(\dot{\mathrm{M}}, \dot{\mathrm{M}}) &= \tfrac{1}{3}(2\mathrm{P}+\mathrm{R})-\tfrac{1}{3}(2\dot{\mathrm{P}}+\dot{\mathrm{R}}) \\ &= \tfrac{1}{6}h(\mathrm{F}_1-\dot{\mathrm{F}}_1)+\tfrac{2}{3}h(\mathrm{F}_{\frac{1}{2}}-\dot{\mathrm{F}}_{\frac{1}{2}}).\end{aligned}$$

But

$$\begin{aligned}&\tfrac{1}{6}h(\mathrm{F}_1-\dot{\mathrm{F}}_1) \\ &= \tfrac{1}{6}\{\mathrm{F}(x_1, y_1)-\mathrm{F}(x_1, b+h\mathrm{F}_0)\} \\ &= \tfrac{1}{6}h\{y_1-(b+h\mathrm{F}_0)\}\,.\,\partial \mathrm{F}(a+h, b+\theta h)/\partial y \\ &= \tfrac{1}{6}h\left\{\left[b+h\mathrm{F}_0+\frac{h^2}{2}\left(\frac{d\mathrm{F}}{dx}\right)_0+\frac{h^2}{6}\left(\frac{d^2\mathrm{F}}{dx^2}\right)_0+\ldots\right]-(b+h\mathrm{F}_0)\right\} \\ &\qquad\qquad \left\{\left(\frac{\partial \mathrm{F}}{\partial y}\right)_0+h\left(\frac{\partial^2\mathrm{F}}{\partial x\,\partial y}\right)_0+\theta h\left(\frac{\partial^2\mathrm{F}}{\partial y^2}\right)_0+\ldots\right\} \\ &= \frac{h^3}{12}\left(\frac{d\mathrm{F}}{dx}\right)_0\left(\frac{\partial \mathrm{F}}{\partial y}\right)_0+\mathrm{A}h^4+\ldots,\end{aligned}$$

* For simplicity we use infinite series, but it is really sufficient to use finite series with a remainder term, involving only the assumption of the existence and continuity of a few partial derivatives of $\mathrm{F}(x, y)$.

where $0 < \theta < 1$, and

$$A = \frac{1}{36}\left(\frac{d^2F}{dx^2}\right)_0\left(\frac{\partial F}{\partial y}\right)_0 + \frac{1}{12}\left(\frac{dF}{dx}\right)_0\left\{\left(\frac{\partial^2 F}{\partial x\,\partial y}\right)_0 + \theta\left(\frac{\partial^2 F}{\partial y^2}\right)_0\right\},$$

so A is a bounded number depending on h.

Similarly

$$\frac{h}{3}(F_{\frac{1}{2}} - \dot{F}_{\frac{1}{2}}) = \frac{h^3}{24}\left(\frac{dF}{dx}\right)_0\left(\frac{\partial F}{\partial y}\right)_0 + Bh^4 + \ldots;$$

$$\begin{aligned}\frac{h}{3}(F_{\frac{1}{2}} - \dot{F}_{\frac{1}{2}}) &= \frac{h}{3}\{y_{\frac{1}{2}} - (b + \tfrac{1}{2}hF_1)\}\cdot \partial F(a+\tfrac{1}{2}h,\ b+\vartheta h)/\partial y \\ &= \frac{h}{3}\left\{\left[b + \tfrac{1}{2}hF_0 + \frac{h^2}{8}\left(\frac{dF}{dx}\right)_0 + \ldots\right]\right. \\ &\quad \left. - \left[b + \tfrac{1}{2}hF_0 + \frac{h^2}{2}\left(\frac{dF}{dx}\right)_0 + \ldots\right]\right\}\left\{\left(\frac{\partial F}{\partial y}\right)_0 + \ldots\right\} \\ &= -\frac{h^3}{8}\left(\frac{dF}{dx}\right)_0\left(\frac{dF}{\partial y}\right)_0 + Ch + \ldots,\end{aligned}$$

where $0 < \vartheta < 1$, and B, C are bounded numbers.

Hence

$$\Sigma' - \Sigma'(\dot{M}, \underline{M}) = (A + B + C)h^4 + \ldots, \qquad \text{of the 4th order;}$$

$$\Sigma'' - \Sigma''(\dot{M}, \underline{M}) = -\frac{h^3}{6}\left(\frac{dF}{dx}\right)_0\left(\frac{\partial F}{\partial y}\right)_0 + (A + 2C)h^4 + \ldots,$$

of the 3rd order.

Now take the second case, $\Omega > 0$, and to fix ideas take $\partial F/\partial y > 0$, $dF/dx > 0$, $d^2F/dx^2 \geq 0$. We get

$$\dot{M} = F_1; \quad \underline{M} = F_0;$$

$$\Sigma' - \Sigma'(\dot{M}, \underline{M}) = -\frac{h^3}{6}\left(\frac{dF}{dx}\right)_0\left(\frac{\partial F}{\partial y}\right)_0 + \ldots, \text{ of the 3rd order;}$$

$$\Sigma'' - \Sigma''(\dot{M}, \underline{M}) = Dh^4 + \ldots, \text{ of the 4th order.}$$

(D is a bounded number.)

Thus we obtain the following result:—

The error of the approximate formula which uses limits between which Δy must lie is of at least the 4th order of smallness, provided that we choose the special values for $\overline{M}$, $\underline{M}$ specified above, and use the combination $\Sigma'(\overline{M}, \underline{M})$, i. e., *Piaggio's method, in the case $\Omega < 0$, but the combination $\Sigma''(\overline{M}, \underline{M})$,* i. e. *the generalization of Piaggio's method, in the case $\Omega > 0$.*

The often-discussed example of Runge's

$$[dy/dx = (y-x)/(y+x)\,; \quad a = 0,\ b = 1]$$

provides an example of the case $\Omega < 0$. The high degree of precision which the combination $\Sigma'(\overline{M}, \underline{M})$ may give is well shown in Piaggio's paper *.

For the other case, $R > 0$, let us examine the example :

$$dy/dx = 4y/x = F(x, y)\,; \quad a = 1,\ b = 0{\cdot}1,$$

taking the increment $\Delta x = h$ first as 0·1, secondly as 0·01, and thirdly as 0·001. Here

$$\partial F/\partial y = 4/x > 0\,; \quad dF/dx = 12y/x^2 > 0\,;$$
$$d^2F/dx^2 = 24y/x^3 > 0.$$

The exact integral is

$$y = 0{\cdot}1\, x^4 = \phi(x) \quad \text{say,}$$

so that

$$\phi(1{\cdot}1) = 0{\cdot}14641\,; \quad \phi(1{\cdot}01) = 0{\cdot}104060401\,;$$
$$\phi(1{\cdot}001) = 0{\cdot}1004006004001.$$

These exact results enable us to find the degree of precision in the approximate work.

(i.)

$h = 0{\cdot}1\,;$ $\underline{M} = F_0 = 0{\cdot}4\,;$

$$\mu = F(a+h,\ b+h) = 4\times 0{\cdot}2/1{\cdot}1 < 0{\cdot}8;$$
$$\overline{M} = F(a+h,\ b+\mu h) = 4\times 0{\cdot}18/1{\cdot}1 < 0{\cdot}7.$$

$F_0 = 0{\cdot}4\,;$ $\underline{F}_{\frac{1}{2}} = 4\times 0{\cdot}12/1{\cdot}05 > 0{\cdot}457.$

$\overline{F}_{\frac{1}{2}} = 4\times 0{\cdot}135/1{\cdot}05 < 0{\cdot}515\,;$ $\overline{F}_1 = 4\times 0{\cdot}17/1{\cdot}1 < 0{\cdot}619.$

$\underline{P} = 0{\cdot}0457\,;$ $\overline{R} = 0{\cdot}0510\,;$ $\overline{Q} = 0{\cdot}0513).$

$\Sigma''(\overline{M}, \underline{M}) = \frac{1}{3}(2\underline{P}+\overline{R}) = 0{\cdot}0475,$
with an error $-1{\cdot}1\times 10^{-3}.$

$[\Sigma'(\overline{M}, \underline{M}) = \frac{1}{5}(\underline{P}+2\overline{Q}) = 0{\cdot}0494,$
with an error $-3{\cdot}0\times 10^{-3}.$

* Phil. Mag. xxxvii. (1919). [*Translator's note.* I am afraid that this high degree of precision was a lucky accident, due to the values I took for $\overline{M}$, $\underline{M}$. These values were not chosen in the way specified by Mr. Remes.—H. T. H. P.]

(ii.)

$h = 0{\cdot}01$; $\underline{M} = 0{\cdot}4$; $\mu = 0{\cdot}436$; $\overline{M} = 0{\cdot}414$.

$F_0 = 0{\cdot}4$; $\underline{F}_{\frac{1}{2}} = 0{\cdot}405970$; $\overline{F}_{\frac{1}{2}} = 0{\cdot}406249$;

$\overline{F}_1 = 0{\cdot}412436$.

$\underline{P} = 0{\cdot}00405970$; $\overline{R} = 0{\cdot}00406218$; $(\overline{Q} = 0{\cdot}00406234)$.

$\Sigma''(\overline{M}, \underline{M}) = 0{\cdot}00406053$, with an error $-1{\cdot}3 \times 10^{-7}$.

$[\Sigma'(\overline{M}, \underline{M}) = 0{\cdot}0040614\epsilon$, with an error $-1{\cdot}06 \times 10^{-6}$.$]$

(iii.)

$h = 0{\cdot}001$; $\underline{M} = 0{\cdot}4$; $\mu = 0{\cdot}40360$; $\overline{M} = 0{\cdot}40122$.

$F_0 = 0{\cdot}4$; $\underline{F}_{\frac{1}{2}} = 0{\cdot}400599700$; $\overline{F}_{\frac{1}{2}} = 0{\cdot}400602139$;

$\overline{F}_1 = 0{\cdot}401203677$.

$\underline{P} = 0{\cdot}000400599700$; $\overline{R} = 0{\cdot}000400601839$;

$(\overline{Q} = 0{\cdot}000400601989)$.

$\Sigma''(\overline{M}, \underline{M}) = 0{\cdot}000400600413$, with an error $-1{\cdot}3 \times 10^{-11}$.

$[\Sigma'(M, \underline{M}) = 0{\cdot}000400601226$, with an error $-8{\cdot}26 \times 10^{-10}$.$]$

XL. *The Lowest Natural Frequency of Circular Arcs.* *By* J. P. Den Hartog *.

Abstract.

Formulæ are derived for the first and second natural frequencies of a part of a circular ring, hinged or clamped at its ends. It is shown that the type of vibration, in which extension of the fibres occurs, under certain conditions may have a lower natural frequency than any non-extensional type of vibration. The results are given in the form of curves and tables.

THE problem of finding the natural frequencies of vibration of a part of a circular ring has been attacked by Lamb †, who derived the differential equation and solved it for the case

* Communicated by Mr. R. V. Southwell, F.R.S.

† Proc. London Math. Soc. xix. p. 365 (1888).

of small curvatures. The exact integration for the general case of a central angle α having any value between 0° and 360° becomes extremely complicated. In this note the approximate method of Rayleigh-Ritz has been applied for calculating *the lowest* natural frequency of circular arcs subtending any angle, for hinged as well as for clamped ends.

The following notations are used :—

w, v = radial and tangential displacements (fig. 1).
α = the central angle.
R = mean radius.
γ = mass per unit length of the centre line.
EI = rigidity against bending.
k = radius of gyration of the cross-section.
S = cross-sectional area.

Fig. 1

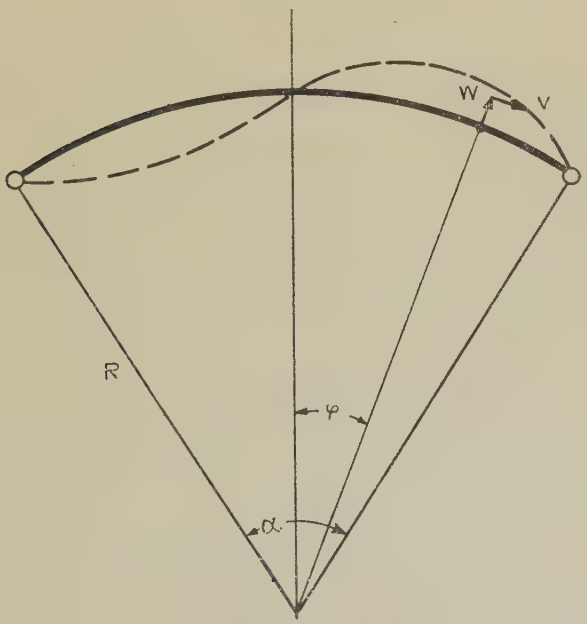

A. Hinged Ends.

The boundary conditions are :—

$$\phi = \pm\frac{\alpha}{2}, \qquad w = v = \frac{d^2w}{d\phi^2} = 0. \quad . \quad . \quad . \quad . \quad (1)$$

We will first consider the non-extensional vibrations, in which case w and v have to satisfy the condition

$$w+\frac{dv}{d\phi}=0. \quad . \quad . \quad . \quad . \quad . \quad . \quad . \quad (2)$$

As a suitable analytical expression for the displacements satisfying (1) and (2) we may take

$$\left.\begin{aligned} w&=\mathrm{A}\sin\frac{2\pi\phi}{\alpha}\sin\omega t,\\ v&=\frac{\mathrm{A}\alpha}{2\pi}\left(\cos\frac{2\pi\phi}{\alpha}+1\right)\sin\omega t. \end{aligned}\right\} \quad . \quad . \quad . \quad . \quad (3)$$

Substituting this in the expressions for the elastic and kinetic energies of the arc,

$$\mathrm{V}=\frac{\mathrm{EI}}{2\mathrm{R}^3}\int_0^\alpha\left\{w+\frac{\partial^2 w}{\partial\phi^2}\right\}^2 d\phi, \quad . \quad . \quad . \quad . \quad (4)$$

$$\mathrm{T}=\frac{\gamma\mathrm{R}}{2}\int_0^\alpha\left\{\left(\frac{\partial v}{\partial t}\right)^2+\left(\frac{\partial w}{\partial t}\right)^2\right\}d\phi, \quad . \quad . \quad (4a)$$

and equating their maximum values, the circular frequency ω is found:

$$\omega^2=\frac{\mathrm{EI}}{\gamma\mathrm{R}^4\alpha^4}\cdot\frac{\alpha^4-8\pi^2\alpha^2+16\pi^4}{1+\cdot075\alpha^2/\pi^2}. \quad . \quad . \quad . \quad (5)$$

For the angle $\alpha=0$ this result coincides with the exact solution for a straight bar, having a node in the middle. For $\alpha=2\pi$ we have a complete ring turning about one hinge, and consequently have zero frequency.

As another assumption satisfying (1) and (2) we take

$$\left.\begin{aligned} w&=\mathrm{A}\left[\frac{\phi}{\alpha}-\frac{40}{7}\left(\frac{\phi}{\alpha}\right)^3+\frac{48}{7}\left(\frac{\phi}{\alpha}\right)\right]\sin\omega t,\\ v&=\alpha\mathrm{A}\left[\frac{3}{28}-\left(\frac{\phi}{\alpha}\right)^2+\frac{20}{7}\left(\frac{\phi}{\alpha}\right)^4-\frac{16}{7}\left(\frac{\phi}{\alpha}\right)^6\right]\sin\omega t, \end{aligned}\right\} \quad . \quad (6)$$

from which in the same manner

$$\omega^2=\frac{\mathrm{EI}}{\gamma\mathrm{R}^4\alpha^4}\cdot\frac{\alpha^4-78\cdot5\alpha^2+1585}{1+\cdot094\alpha^2}. \quad . \quad . \quad . \quad (7)$$

For angles $60^\circ<\alpha<270^\circ$ this will give smaller and therefore better results for ω than (5). From (5) and (7) is deduced

$$\omega=\frac{\mathrm{C}_1}{\mathrm{R}^2}\sqrt{\frac{\mathrm{EI}}{\gamma}}, \quad . \quad . \quad . \quad . \quad . \quad . \quad (8)$$

in which C_1 is to be taken from the following table :—

TABLE I.

α ...	0°	20	40	60	80	100	120	140	160	
C_1...	∞	321	78·5	33·6	17·8	10·65	6·80	4·55	3·14	
α ...	180°	200	220	240	260	280	300	320	340	360
C_1...	2·20	1·56	1·11	·796	·562	·386	·255	·145	·063	0

These values have been calculated from (5) for angles smaller than 60° and larger than 270°; from (6) for angles between 60° and 270°. For small angles α it is more convenient to have the result in the form

$$\omega = \frac{C_2}{l_2}\sqrt{\frac{EI}{\gamma}}, \quad . \quad . \quad . \quad . \quad . \quad . \quad (9)$$

where l is the length of the chord subtending the arc and C_2 has the following values :—

TABLE II.

α ...	0°	20	40	60	80	100	120	140	160	180
C_2...	39·4	38 6	36·7	33·6	29·4	25·1	20·4	16·1	12·15	8·80

This non-extensional type of vibration, in the limit $\alpha = 0$, reduces to the second natural mode of the straight bar (with a node in the middle). The deformation, corresponding to the lowest natural mode of the *straight* bar, which does not have nodes except at the ends, becomes extensional as soon as the bar becomes curved. For small angles α, therefore, the question arises, whether a shape of vibration not fulfilling the condition of non-extensibility (2) may not have a lower period than the one expressed by (8). We take as an analytical expression for the shape of deformation

$$\left.\begin{aligned} w &= A\cos\frac{\pi\phi}{\alpha}\sin\omega t, \\ v &= \left[a_1\sin\frac{2\pi\phi}{\alpha} + a_2\sin\frac{6\pi\phi}{\alpha}\right]\sin\omega t, \end{aligned}\right\} \quad . \quad . \quad (10)$$

fulfilling the boundary and symmetry conditions, but not the non-extensibility condition (2).

Here a_1 and a_2 are arbitrary constants, which will be determined so as to make the elastic energy,

$$V = \frac{ES}{R}\int_0^{\alpha/2}\left(w+\frac{\partial v}{\partial\phi}\right)^2 d\phi + \frac{EI}{R^3}\int_0^{\alpha/2}\left(w+\frac{\partial^2 w}{\partial\phi^2}\right)^2 d\phi, \quad . \quad (11)$$

a minimum *.

Fig. 2.

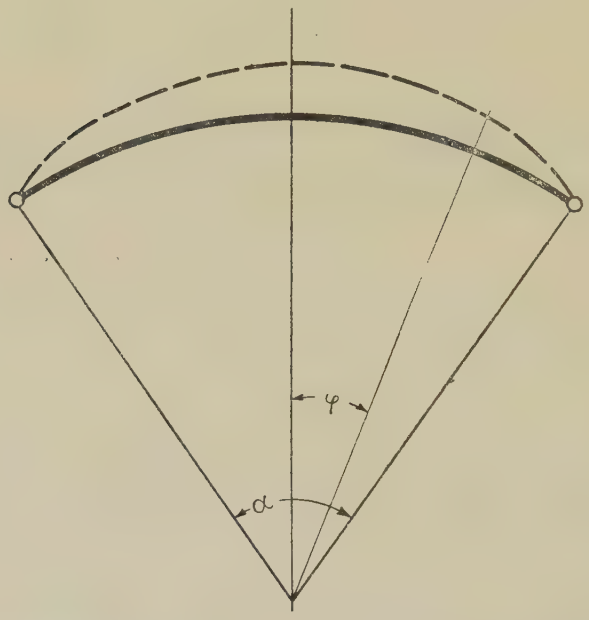

Substituting (10) in (11), a_1 and a_2 have been calculated from $\frac{\partial V}{\partial a_1}=0$; $\frac{\partial V}{\partial a_2}=0$ leading to the results :

$$a_1 = -\frac{2}{3}\cdot\frac{\alpha}{\pi^2}\cdot A,$$

$$a_2 = -\frac{2}{105}\cdot\frac{\alpha}{\pi^2}\cdot A.$$

With these values the elastic energy becomes

$$V = \frac{EIA^2\alpha}{4R^3}\left[\cdot 820\left(\frac{R}{k}\right)^2 + \left(1-\frac{\pi^2}{\alpha^2}\right)^2\right]\sin^2\omega t.$$

* This involves less calculation than determining a_1 and a_2 from the condition that ω be minimum, the result being about as accurate.

The kinetic energy from (10) and (4) is

$$T=\frac{\gamma R\omega^2 A^2\alpha}{4}[1+\cdot004\alpha^2]\cos^2\omega t.$$

For angles α not over 80° an error of less than ·3 per cent. in the frequency is made by neglecting $\cdot004\alpha^2$ with respect to 1 in the expression for T. Then it is found

$$\omega^2=\frac{EI}{\gamma R^4}\left[\cdot820\left(\frac{R}{k}\right)^2+\left(1-\frac{\pi^2}{\alpha^2}\right)^2\right]. \quad . \quad . \quad (12)$$

This can be brought to the form (9) with the constant

$$C'_2=4\sin^2\frac{\alpha}{2}\sqrt{\cdot820\left(\frac{R}{k}\right)^2+\left(\frac{\pi^2}{\alpha^2}-1\right)^2}. \quad . \quad . \quad (13)$$

Fig. 3.

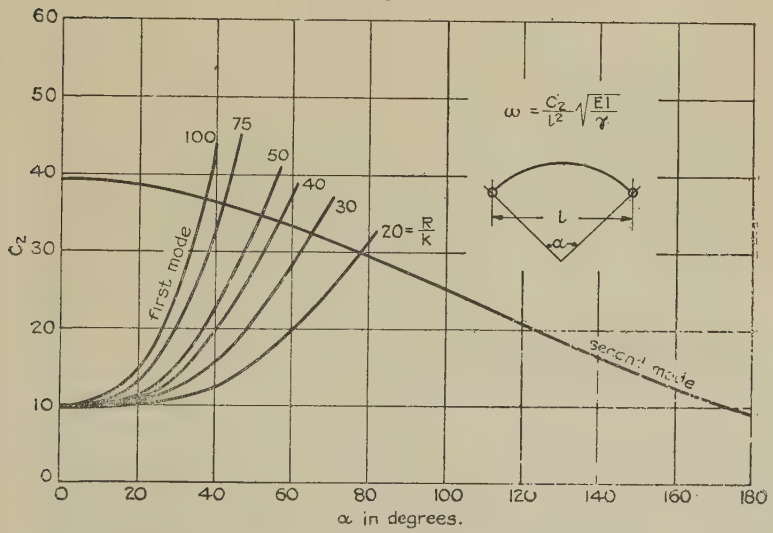

The numerical values of this constant and of the one in Table II. are shown in fig. 3.

It is seen that for angles α smaller than about 60° *the extensional mode of vibration has a lower period than the non-extensional.*

B. Clamped Ends.

The boundary conditions for clamped ends are

$$\phi=\pm\frac{\alpha}{2}, \qquad v=w=\frac{dw}{d\phi}=0. \quad . \quad . \quad . \quad (14)$$

The simplest non-extensional shape for W, fulfilling (14) and (2), has a node in the middle. Due to the tangency at the ends, however, this shape is more complicated than with hinged ends, so that an assumption, like (3), with *one* parameter does not give accurate enough results. We have to take recourse to two parameters A and B for instance:

$$\left.\begin{aligned} w &= \left(\frac{A}{8}-\frac{B}{32}\right)\frac{\phi}{\alpha}-\left(A-\frac{3B}{8}\right)\left(\frac{\phi}{\alpha}\right)^3+\left(2A-\frac{2B}{2}\right)\left(\frac{\phi}{\alpha}\right)^5 \\ &\qquad +2B\left(\frac{\phi}{\alpha}\right)^7, \\ v &= \alpha\left[\left(\frac{A}{192}-\frac{B}{1024}\right)-\left(\frac{A}{16}-\frac{B}{64}\right)\left(\frac{\phi}{\alpha}\right)^2+\left(\frac{A}{4}-\frac{3B}{32}\right)\left(\frac{\phi}{\alpha}\right)^4\right. \\ &\qquad \left.-\left(\frac{A}{3}-\frac{B}{4}\right)\left(\frac{\phi}{\alpha}\right)^6-\frac{B}{4}\left(\frac{\phi}{\alpha}\right)^8\right]. \end{aligned}\right\} \quad . \quad . \quad . \quad . \quad . \quad (15)$$

Substituting this in (4) and equating the maximum values of V and T, we arrive at an expression for ω in terms of A and B.

Determining these two parameters in such manner as to make ω a minimum, the following result is obtained:

$$\omega = \frac{C_3}{R^2}\sqrt{\frac{EI}{\gamma}}, \quad . \quad . \quad . \quad . \quad . \quad (16)$$

where C_3 is to be taken from

Table III.

α ...	0°	20	40	60	80	100	120	140	160	180
C_3...	∞	504	124	53·8	29·2	17·9	11·85	8·22	5·93	4·38
α ...	200	220	240	260	280	300	320	340	360	
C_3...	3·31	2·54	1·98	1·57	1·25	1·01	·821	·677	·567	

Again, for small angles α it is more convenient to use the chord l rather than the radius R:

$$\omega = \frac{C_4}{l^2}\sqrt{\frac{EI}{\gamma}} \quad . \quad . \quad . \quad . \quad . \quad . \quad (17)$$

with

TABLE IV.

α ...	0°	20	40	60	80	100	120	140	160	180
C_4...	61·7	60·7	58·0	53·8	48·3	42·1	35·6	29·0	23·0	17·55

For the extensional vibrations of the arc with clamped ends corresponding to the fundamental mode of the straight bar, we follow the same course as before for hinged ends, assuming

$$\left.\begin{aligned} w &= A\left(1+\cos\frac{2\pi\phi}{\alpha}\right), \\ v &= a_1 \sin\frac{2\pi\phi}{\alpha} + a_2 \sin\frac{6\pi\phi}{\alpha}. \end{aligned}\right\} \quad . \quad . \quad . \quad (18)$$

Fig. 4.

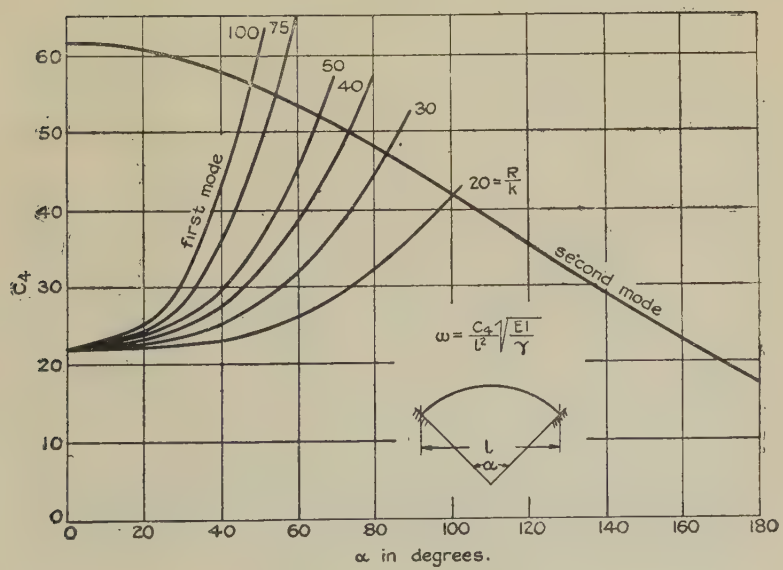

With the aid of (11) we find

$$a_1 = -\frac{\alpha}{2\pi}A, \qquad a_2 = 0.$$

The elastic energy becomes

$$\frac{EIA^2\alpha}{2R^3}\left[\frac{R^2}{k^2}+1+\frac{1}{2}\left(1-\frac{4\pi^2}{\alpha^2}\right)^2\right] \quad . \quad . \quad . \quad (19)$$

and the kinetic energy

$$\gamma RA^2\omega^2\alpha\left[\frac{3}{4}+\frac{1}{16}\frac{\alpha^2}{\pi^2}\right]. \quad . \quad . \quad . \quad . \quad (20)$$

Equating (19) and (20), making some simplifications and bringing ω in the form (17), we find for the constant:

$$C'_4=4\sin^2\frac{\alpha}{2}\sqrt{\frac{2}{3}\left(\frac{R}{k}\right)^2+\frac{1}{3}\left(\frac{4\pi^2}{\alpha^2}-1\right)^2}. \quad . \quad (21)$$

The value of this constant for various ratios R/k and various angles α can be taken from figure 4.

Research Laboratory,
Westinghouse Elec. & Mfg. Co.,
East Pittsburgh, Penna.

XLI. *The Results of Classical Wave Mechanics obtained by using the Methods of Relativity Mechanics.* *By* T. Lewis, *M.Sc., University College of Wales, Aberystwyth* *.

Introduction.

THE close similarity between the Principle of Least Action in the Maupertuis form and Fermat's Principle of Least Time led de Broglie † to associate a wave of phase with every type of energy quantum in motion. Schrödinger's ‡ "Wave Mechanics" is a development of this idea along lines slightly different from de Broglie's. He pays more attention to the amplitude of the associated wave, and practically ignores the phase. O. Klein § has interpreted Wave Mechanics from the standpoint of a five-dimensional "universe," and has shown that the path of the material particle emitting the wave is the projection in space-time of a null-geodesic in this five-fold "universe." In this paper we will show that the spatial path of a particle

* Communicated by Prof. G. A. Schott, F.R.S.

† J. Phys. t. vii. pp. 1–6 (1926): "Ondes et Mouvements," par L. de Broglie.

‡ *Ann. der Phys.* Bd. lxxix. (1926)

§ *Zeit. für Phys.* Bd. xxxvii. (1926).

moving in a conservative field according to classical laws is the projection of a null-geodesic in a certain space-time, and that this geodesic is the "track" of a ray of its associated wave. It will be seen that the equations of motion of the particle and those of a ray of its associated wave follow from the same principle of variation, thus demonstrating the close connexion between the above-named principles. These equations will then be expressed in canonic form—the same set represents the motion of the particle and the ray it follows, provided the parameters are suitably interpreted in each case. We next derive the Hamilton-Jacobi equation, and show that the phase, regarded as a function of time and position, is a solution. Finally, we derive Schrödinger's equation from a principle of variation. No new results are given. We merely apply the methods of Relativity Mechanics in order to derive the known results of Classical Mechanics, including Wave Mechanics. But, first of all, for the sake of continuity, we deduce the equations of motion of a particle from the Principle of Least Action, and those of the ray which it follows from Fermat's Principle.

§ 1. *The Principle of Least Action.*—Let a particle of mass m move in a conservative field according to classical laws. If V is its potential energy and E its total energy, its velocity u is given by

$$u=\sqrt{2(\mathrm{E}-\mathrm{V})/m}. \quad . \quad . \quad . \quad . \quad . \quad (1.1)$$

The path joining two points A and B of the field corresponds to a stationary value of the action, the total energy being kept constant for all variations considered. This is expressed mathematically by the equation

$$\delta\mathrm{A}=\delta\int_{\mathrm{A}}^{\mathrm{B}} u^2\,dt=\delta\int_{\mathrm{A}}^{\mathrm{B}} u\,d\sigma=0, \quad . \quad . \quad . \quad (1.2)$$

where $d\sigma$ is an element of the path.

Let τ be any parameter, and let differentiation with respect to it be denoted by dots. Then

$$\delta\mathrm{A}=\delta\int_{\mathrm{A}}^{\mathrm{B}} u\,\dot{\sigma}\,d\tau=0, \text{ with } \dot{\sigma}^2=\dot{x}^2+\dot{y}^2+\dot{z}^2.$$

The parameter τ can be chosen so that the values corresponding to A and B in the varied path are the same as for the actual path. Bearing this in mind, the above equation

is equivalent to three of the following type :

$$\frac{d}{d\tau}\left(\frac{u\dot{x}}{\dot{\sigma}}\right)-\dot{\sigma}\frac{\partial u}{\partial x}=0. \quad . \quad . \quad . \quad . \quad (1.3)$$

The form of this equation is invariant with respect to change of parameter ; so if τ denote the time, (1.3) becomes

$$\ddot{x}-\frac{1}{2}\frac{\partial u^2}{\partial x}=0. \quad . \quad . \quad . \quad . \quad . \quad (1.3)'$$

§ 2. *Fermat's Principle of Least Time.*—Let us regard the conservative field as an isotropic medium of refractive index β ($=u/c$, where c is a constant having the dimensions of a velocity). The velocity of light in this medium will be

$$v=\beta^{-1}c=c^2/u, \quad . \quad . \quad . \quad . \quad . \quad (2.1)$$

and the path of a ray joining two points A and B is given by

$$\delta(t_A-t_B)=\delta\int_A^B\frac{d\sigma}{v}=c^{-2}\delta\int_A^B u\,d\sigma. \quad . \quad . \quad (2.2)$$

We see that (2.2) is identical with (1.2). However, the law of description of the path is different. Proceeding as before, and this time denoting the actual time by t and differentiation with respect to it by accents, we find the equations of motion to be of the type

$$\frac{d}{dt}\left(\frac{x'}{v^2}\right)+\frac{\partial v}{\partial x}\Big/v=0. \quad . \quad . \quad . \quad . \quad (2.3)$$

§ 3. *The Geodesic Principle.*—Let us now consider the space-time characterized by the quadratic form

$$ds^2=v^2dt^2-(dx^2+dy^2+dz^2)=v^2dt^2-d\sigma^2. \quad . \quad (3.1)$$

The critical velocity in this space-time is that of the wave associated with a particle moving in the conservative field already described. The determinant of the coefficients is $-v^2$. Hence the four-dimensional element of volume is

$$d\Omega=v\,dt\,dx\,dy\,dz. \quad . \quad . \quad . \quad . \quad . \quad (3.2)$$

As before, τ is any parameter, and we write

$$2L=v^2\dot{t}^2-(\dot{x}^2+\dot{y}^2+\dot{z}^2)=v^2\dot{t}^2-\dot{\sigma}^2=\dot{S}^2. \quad . \quad (3.3)$$

A geodesic in this space-time is defined by

$$\delta\int_P^Q ds=0,$$

where P and Q are two fixed points in space-time. But

this is not the only integral which is stationary along a geodesic. If the parameter τ is chosen so that the values corresponding to P and Q in the varied curves are the same as for the geodesic joining P and Q, the integral

$$S=\int_P^Q \mathrm{L}\,d\tau \quad . \quad . \quad . \quad . \quad , \quad . \quad (3.4)$$

is stationary along the geodesic. In view of the fact that we shall be dealing with geodesics of zero length, it is more convenient to define them by the equation

$$\delta S=\delta\int_P^Q \mathrm{L}\,d\tau=0. \quad . \quad . \quad . \quad . \quad (3.5)$$

Performing the variation and bearing in mind the condition imposed on τ, we arrive at the equations

$$\frac{d}{d\tau}(v^2\dot{t})=0, \quad \ddot{x}+v\frac{\partial v}{\partial x}\dot{t}^2=0, \quad . \quad . \quad . \quad (3.6)$$

with two more of the latter type. From the first of these equations we get

$$v^2\dot{t} = \text{constant} = c^2. \quad . \quad . \quad . \quad . \quad (3.7)$$

Let c^2 have the same meaning as in (2.1), and substitute for v in terms of u. The second of equations (3.6) now becomes

$$\ddot{x}-\frac{1}{2}\frac{\partial u^2}{\partial x}=0. \quad . \quad . \quad . \quad . \quad . \quad (3.8)$$

This equation is identical with (1.3)′. So the parameter τ is the time of the material particle describing the path which is the spatial projection of the geodesic. However, it must not be thought that the track of a material particle in space-time is a geodesic. For the equations (3.6) have an integral

$$\mathrm{L} = \text{constant}. \quad . \quad . \quad . \quad . \quad . \quad (3.9)$$

This equation, together with (3.7), is inconsistent with $\dot{\sigma}=u$.

If we eliminate τ from (3.6) and denote differentiation with respect to t by accents as before, we get three equations of the type

$$\frac{d}{dt}\left(\frac{x'}{v^2}\right)+\frac{\partial v}{\partial x}\Big/v=0, \quad . \quad . \quad . \quad . \quad (3.10)$$

which is identical with (2.3), provided

$$x'^2+y'^2+z'^2=v^2;$$

i. e., provided the constant on the right-hand side of (3.9)

is zero. In other words, the track of a ray of the wave associated with the particle is a geodesic of zero length.

§ 4. *The Canonic form of the Equations of Motion.*—The covariant components of the four-vector $(\dot{t}, \dot{x}, \dot{y}, \dot{z})$ are defined in the following manner :

$$p_t = \frac{\partial \mathrm{L}}{\partial \dot{t}} = v^2 \dot{t}, \quad p_x = \frac{\partial \mathrm{L}}{\partial \dot{x}} = -\dot{x}, \quad . \quad . \quad (4.1)$$

with two more equations of the second type.

If we express L in terms of these covariant components and the coordinates, it becomes

$$\mathrm{L} = \mathrm{H}(p, x) = \tfrac{1}{2}\{v^{-2}p_t^2 - (p_x^2 + p_y^2 + p_z^2)\}, \quad . \quad (4.2)$$

and the system of equations (3.6) is equivalent to the double system

$$\frac{dt}{d\tau} = \frac{\partial \mathrm{H}}{\partial p_t}, \quad \frac{dx}{d\tau} = \frac{\partial \mathrm{H}}{\partial p_x}; \quad . \quad . \quad . \quad . \quad (4.3)$$

$$\frac{dp_t}{d\tau} = 0, \quad \frac{dp_x}{d\tau} = -\frac{\partial \mathrm{H}}{\partial x}. \quad . \quad . \quad . \quad . \quad (4.4)$$

The equations of motion of the particle, as well as of the rays of its associated wave, are contained in (4.3) and (4.4). As before, τ is the time of the particle and t the time of a ray. The double system has an integral H = constant. This constant is zero in the present case. Another integral is p_t = constant. If, as before, we put this constant equal to c^2 and substitute in H, the latter differs from the ordinary Hamiltonian function by a constant—the total energy.

§ 5. *The Hamilton-Jacobi Equation.*—This equation is obtained by assuming that the covariant components (p_t, p_x) are derivable from a scalar potential. We write

$$p_t = \frac{\partial \psi}{\partial t}, \quad p_x = \frac{\partial \psi}{dx}. \quad . \quad . \quad . \quad . \quad (5.1)$$

Substituting these values in (4.2), we get the desired equation

$$\mathrm{H} = \frac{1}{2}\left\{v^{-2}\left(\frac{\partial \psi}{\partial t}\right)^2 - \left(\frac{\partial \psi}{\partial x}\right)^2 - \left(\frac{\partial \psi}{\partial y}\right)^2 - \left(\frac{\partial \psi}{\partial z}\right)^2\right\}$$

$$\equiv \mathrm{H}\,.\,(\psi, \psi). \quad . \quad . \quad (5.2)$$

If we put $\mathrm{H} = 0$ and $\frac{\partial \psi}{\partial t} = C^2$, we arrive at the usual

Hamilton-Jacobi equation for a particle in a conservative field. However, this particular form does not correspond to de Broglie's point of view. He assumes the particle to move along a natural path (in our case, a Fermat path described according to the laws of classical mechanics) and to emit at every point of its path a disturbance ψ, which is propagated in all directions with velocity v. If the disturbance is a periodic one, the surface of constant phase (ϕ, say) is the locus of the extremities of Fermat paths (corresponding to the same time of description) which issue from the point where the particle was situated when in that phase. We will now show that ϕ, considered as a function of position and time, satisfies the Hamilton-Jacobi equation (5.2).

Write

$$\phi = 2\pi\nu(t - \chi + \text{const.}), \quad \chi(\text{A, B}) = \int_{\text{A}}^{\text{B}} \frac{d\sigma}{v}, \quad . \quad (5.3)$$

where A is the position of the particle at the time t_0 when it emitted the phase which reaches B at time t. The coordinates of A will be denoted by (x_0, y_0, z_0) and those of B by (x, y, z).

Let us consider once again the function S defined by (3.3) and (3.4). If we vary it in the most general manner possible, we get

$$\delta S = [\text{L}\,\delta t]_{\text{P}}^{\text{Q}} + [v^2\dot{t}\,\delta t - \dot{x}\,\delta x \ldots]_{\text{P}}^{\text{Q}} - \int_{\text{P}}^{\text{Q}} \left\{ \frac{d}{d\tau}(v^2\dot{t})\,\delta t - \left(\ddot{x} + v\frac{\partial v}{\partial x}\dot{t}^2\right)\delta x \ldots \right\} d\tau. \quad . \quad (5.4)$$

We now impose the condition that the varied tracks are also geodesics of zero length. (5.4) then reduces to

$$\delta S = [v^2\dot{t}\,\delta t - \dot{x}\,\delta x \ldots]_{\text{P}}^{\text{Q}} = 0.$$

Or, writing c^2 for $v^2\dot{t}$,

$$c^2\,\delta t_0 - \dot{x}\,\delta x_0 \ldots = c^2\,\delta t - \dot{x}\,\delta x \ldots . \quad . \quad . \quad . \quad (5.5)$$

The accompanying diagrams will help us to interpret (5.5). P (fig. 1) is the position of the particle in space-time when it emits a wave, a ray of which reaches the point Q in space-time. PQ is therefore a null-geodesic. PP′ is the natural track of the particle, and P′Q′ is another null-geodesic.

A (fig. 2) is the spatial position of the particle at time t_0 when it emits the disturbance which reaches the space-point B at time t. AB is therefore a Fermat path, the spatial projection of PQ. AA′ is the path of the particle and therefore the spatial projection of PP′. A′B′, the projection of P′Q′, is another Fermat path.

Fig. 1.

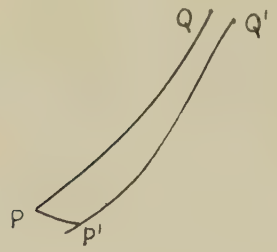

Fig. 2.

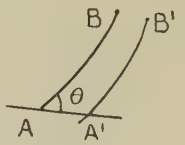

From what we have said, it follows that

$$\delta x_0 = u_x \delta t_0, \quad \delta y_0 = u_y \delta t_0, \quad \delta z_0 = u_z \delta t_0, \quad . \quad . \quad (5.6)$$

where (u_x, u_y, u_z) are the velocity components of the particle, and u_0 its resultant velocity. These components must not be confused with $(\dot{x}_0, \dot{y}_0, \dot{z}_0)$, for, although the resultant of the latter is u_0, they refer to a different direction—that of the path AB.

If we substitute the expressions (5.6) in (5.5), we get

$$c^2\left(1-\frac{{u_0}^2}{c^2}\cos\theta\right)\delta t_0 \equiv c^2\left(1-\frac{c^2}{{v_0}^2}\cos\theta\right)\delta t_0$$

$$\equiv c^2\left(1-\frac{u_0}{v_0}\cos\theta\right)\delta t_0 = c^2\,\delta t - \dot{x}\,\delta x - \ldots, \quad (5.7)$$

where θ is the angle between the path of the particle and AB. If we regard t_0 as a dependent variable and write

$$\mathrm{K} = (1-(u_0/v_0)\cos\theta), \quad . \quad . \quad . \quad . \quad (5.8)$$

we get

$$\frac{\partial t_0}{\partial t} = 1/\mathrm{K}, \quad \frac{\partial t_0}{\partial x} = -\dot{x}/\mathrm{K}c^2 \equiv -x'/\mathrm{K}v^2, \quad . \quad . \quad (5.9)$$

and we can easily verify that t_0 satisfies (5.2) with $\mathrm{H}=0$. Again from (5.3)

$$\phi = 2\pi\nu(t-\chi + \text{const.}) = 2\pi\nu(t_0 + \text{const.}).$$

It follows that ϕ satisfies the Hamilton-Jacobi equation (5.2).

On account of the motion of the particle the frequency of

the disturbance at B is not the frequency of the particle, but that multiplied by the Doppler factor 1/K.

§ 6. *Stationary States of the Atom.*—Let an electron describe a closed orbit about the nucleus, as in the case of the hydrogen atom. De Broglie imagines the electron to emit a periodic disturbance which is propagated in the manner explained. A ray of the wave of phase will describe the orbit of the electron in the same sense as the electron itself, while another will describe it in the opposite sense. A stationary state is possible only when the length of the orbit consists of an integral number of wave-length, *i. e.*

$$\oint \frac{\nu d\sigma}{v} = n.$$

But $\nu = E/h = mc^2/h$. Hence the above condition becomes

$$\oint mu\, d\sigma = nh.$$

We will now assume that the electron is a pulsating sphere—the periodic expansion and contraction being due to the pressure of the æther and some internal pressure. On account of this pulsation the surrounding æther will be subject to a periodic disturbance; and if we assume that the phase is propagated with velocity v, the velocity of transfer of energy at any point will be the group-velocity

$$u\left(=\frac{dv}{d\left(\frac{\nu}{v}\right)}\right).$$

In the vicinity of the surface of zero-velocity (in this case, the sphere $E-V=0$) the phase-velocity becomes very great and ultimately infinite. The group-velocity, on the other hand, becomes small and ultimately zero—the æther becomes rigid in this neighbourhood. Outside this surface both u and v become imaginary. It follows that the atom is a closed system in a very real sense. The electron radiates energy even when the atom is in a stationary state, but none of this energy can escape—most of it will be reabsorbed by the electron, while an infinitesimal amount may accumulate on the surface of zero-velocity. When for some reason or other the atom passes from one stationary state to another, it will radiate the quantum of energy demanded by Bohr's theory. Hence it appears that, in some respects, the Quantum Theory and the Wave Theory are not irreconcilable.

§ 7. *Schrödinger's Equation.*—If we multiply $(\mathrm{H}(\psi, \psi)$ by a scalar quantity ρ/v and integrate throughout a portion of space-time, we get an invariant integral

$$\mathrm{I}=\frac{1}{2}\iiiint\left\{v^{-2}\left(\frac{\partial\psi}{\partial t}\right)^2-\left(\frac{\partial\psi}{\partial x}\right)^2-\left(\frac{\partial\psi}{\partial y}\right)^2-\left(\frac{\partial\psi}{\partial z}\right)^2\right\}\rho\,dt\,dx\,dy\,dz. \quad (7.1)$$

The conditions that this integral should be stationary for small variations in ψ which vanish on the boundary is

$$\frac{1}{v^2}\frac{\partial}{\partial t}\left(\rho\frac{\partial\psi}{\partial t}\right)-\frac{\partial}{\partial x}\left(\rho\frac{\partial\psi}{\partial x}\right)-\frac{\partial}{\partial y}\left(\rho\frac{\partial\psi}{\partial y}\right)-\frac{\partial}{\partial z}\left(\rho\frac{\partial\psi}{\partial z}\right)=0. \quad (7.2)$$

This equation is identical with Schrödinger's when ρ is constant. In any case, it gives the ordinary Hamilton-Jacobi equation for S $(=h\log\psi/2\pi i)$, when h^{-1} is neglected in comparison with h^{-2}.

Schrödinger seeks solutions of (7.2) which are finite, continuous, and one-valued throughout the whole of physical space-time, and thereby obtains the accepted energy-levels—at least for the standard cases already worked out.

De Broglie, on the other hand, seeks a solution which has a moving singularity—the electron. His solutions are of the nature of retarded and advanced potentials for which he assumes the form

$$\psi=fe^{i\phi}. \quad (7.3)$$

If we substitute this value for ψ in (7.2) and denote by $\square$ the operator on ψ in that equation, we get the two following:

$$\square(f)-\rho f\mathrm{H}(\phi,\phi)=0, \quad 2\rho\mathrm{H}(f,\phi)+f\square(\phi)=0. \quad (7.4)$$

De Broglie does not assume $\mathrm{H}(\phi, \phi)=0$, but it is natural to do so; and since we have an extra function ρ to dispose of, we can do so here. The consequence of this is that f satisfies the same equation as the complete wave-function ψ. We can also verify the following equation:

$$\square(f\phi)=0. \quad (7.5)$$

A solution can therefore be got by assuming f to be a function of ϕ, and regarding (7.5) as a linear equation of the first order to determine the function ρ.

In conclusion, I wish to express my gratitude to Prof. Schott for his encouragement and valuable advice.

Applied Mathematics Department,
Aberystwyth.

XLII. *The Structure of Vortex Sheets.* *By* A. Fage, *A.R.C.Sc., and* F. C. Johansen, *B.Sc., of the Aerodynamics Department, The National Physical Laboratory**.

I. Introduction.

(1) THE outstanding features of the two-dimensional flow behind an infinitely long obstacle of bluff cross-section immersed in a moving fluid are now well known. Two thin bands of vorticity are shed at the after end of the obstacle, or edges in the case of an inclined flat plate, and these as they flow downstream separate the freely-moving stream from a low-pressure region of nearly motionless fluid at the back of the obstacle. At some distance behind, these sheets break up with a uniform frequency into two trails of discrete cylindrical vortices of opposite direction of rotation, to form a vortex street. The vortices are arranged alternately in the street so that each vortex in one trail is midway between two successive vortices in the other trail.

(2) In an earlier paper † the writers describe an investigation undertaken to furnish information on the flow of air behind an inclined flat plate. Experiments were then made to determine, for several angles of inclination of the plate, the frequency and speed with which the individual vortices pass downstream, the dimensions of the vortex system, the average strength of the vortices, and the rate at which vorticity was leaving the edges of the plate. The present investigation ‡ can be regarded as a continuation of this earlier work, in that it includes a more detailed examination of the structure of the vortex sheet shed from the edge of a plate set normal to an air stream. To obtain more generality, an examination has also been made of the sheets shed from other bodies of widely different forms—such as an aerofoil, a cylinder, and wedges,—and it has been possible to show how some of the characteristics of these sheets, such as the velocity distribution across a section and the rate of opening-out, depend on the form of the body. Some of the experimental results are compared with those predicted by the theory § of the rate of spread of turbulence in

* Communicated by Ernest F. Relf, A.R.C.Sc.

† Proc. Roy. Soc. A, vol. cxvi. (1927).

‡ Permission to communicate the results was kindly granted by the Aeronautical Research Committee.

§ *Zeitschrift für Angewandte Mathematik und Mechanik*, December 1926 (Tollmien) and April 1925 (Prandtl).

a vortex sheet, which has been developed by W. Tollmien on the basis of earlier work by L. Prandtl.

In addition, measurements have been made to determine the longitudinal spacing between consecutive vortices in the vortex street at some distance behind each body, and also the frequency and speed at which these vortices pass downstream. Finally, an analysis has been made to determine to what extent these characteristics of the vortex sheet are influenced by the structure of the sheets leaving the body.

(3) All the experimental work has been carried out in a wind tunnel, with each model extending between the floor and roof, and the observations have been in the median plane of the tunnel, where the flow is two-dimensional. A summary of some of the principal results obtained is given at the end of the paper.

II. List of Symbols.

V = velocity at any point in the field.

V_0 = velocity of the undisturbed air relative to model.

V_1 & V_2 = velocities at points in the outer and inner boundaries respectively.

V_3 = downstream velocity of the individual vortices.

p_0 = pressure in the undisturbed air.

p = pressure at any point in the field.

p_m = mean pressure at the back of a model.

H_0 = total head in the undisturbed wind.

H = total head at any point in the field.

α = angle of incidence of the plate or aerofoil (degrees).

θ = wind direction at any point in the field relative to undisturbed wind direction (degrees).

b = a representative dimension of a model (see figs. 7 and 8).

x & y = the longitudinal and lateral coordinates of a point in the field. They are measured along and at right angles to the undisturbed wind direction (see figs. 7 and 8).

a = longitudinal spacing between two consecutive vortices in the same row.

f = frequency per second with which the individual vortices in each row leave the model.

T = time-interval between the shedding of successive vortices in the same row.

K = total strength of vorticity leaving each side of the body in one second.

ρ = density of the air.

Δ = breadth of a vortex sheet.

s = longitudinal distance behind a body of a section of a sheet.

III. The Sheet shed from a Normal Flat Plate.

(4) *Observations of Velocity and Total Head.*—The vortex sheet selected for a detailed examination was that shed from the sharp edge of a flat plate 6 in. broad, mounted normal to the air stream and extending between the floor and roof of a 7-ft. wind-tunnel. To obtain some idea of the structure of

Fig. 1.

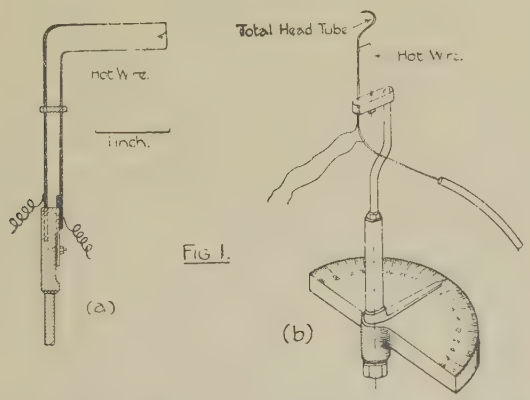

this sheet, observations of velocity and total head were taken along transverse lines parallel to the plate, $\frac{x}{b} = 0{\cdot}034$, 0·084, 0·168, 0·252, 0·336, and 0·504 respectively, and situated in the median plane of the tunnel, where the flow is two-dimensional. The observations of velocity were taken with a small hot-wire velocity meter (fig. 1 (*a*)) mounted so that the wire was parallel to the edge of the plate—that is, normal to the plane of the two-dimensional flow. The wire was of platinum 0·3 in. long and 0·001 in. diameter. A complete description of this instrument and

also of its method of use is given in the paper referred to in § (2).

The direction and total-head observations were taken with the instrument shown in fig. 1 (*b*). The principle of direction measurement is the same as that described by A. Bailey *, and depends on the fact that the shielding effect of a cylindrical rod mounted in a wind stream in front of a heated wire is a maximum when the plane passing through the axes of the rod and wire is along the local wind direction. In use the hot wire was maintained at a constant resistance (and therefore temperature) on a Wheatsone bridge. The instrument, mounted so that the hot wire was parallel to the edge of the plate, was rotated about an axis midway between those of the shield and hot wire through an angular range including the position for which the current was a minimum, and the direction of the local wind obtained from a curve showing the variation of current with angular position. To obtain compactness, the shielding cylinder was made of steel tube of outside diameter 0·032 in., and used for the measurement of total head. Fig. 1 (*b*) shows that the upper part of the tube was shaped so that its mouth, situated in the axis of rotation, pointed into the local wind when the hot wire was completely shielded by the stem. Although the direction and total head are measured at different points in the axis of rotation, no appreciable error is introduced thereby because the flow is two-dimensional. The total head (H) was measured against the total head (H_0) in the undisturbed wind. It should perhaps be mentioned that the advantage of the hot-wire direction meter over the standard pressure-direction meter † commonly used at the laboratory is that it is more suitable for use in a region of steep velocity gradient, such as that which occurs in a vortex sheet. In other regions, where the velocity changes slowly from point to point, the standard instrument is to be preferred because of its greater accuracy.

(5) The actual observations of velocity and total head taken across the several transverse lines of exploration, expressed as non-dimensional coefficients by dividing by V_0 and ρV_0^2 respectively, are plotted in figs. 2 and 3. These curves show that immediately behind the plate the total head is a minimum and the velocity is small, and

* Aeronautical Research Committee, Reports and Memoranda, No. 777.

† T. Lavender, Aeronautical Research Committee, Reports and Memoranda, No. 844.

that outward beyond this region rapid increases in both velocity and total head occur.

There is, then, a vortex sheet or band separating the freely-moving stream from the stationary air at the back of the plate. The increase in the breadth of the sheet and its lateral displacement with increasing distance behind the plate are shown in fig. 7 (*a*), where dotted lines have been drawn to represent the boundaries of the vorticity region.

Figs. 2 and 3.

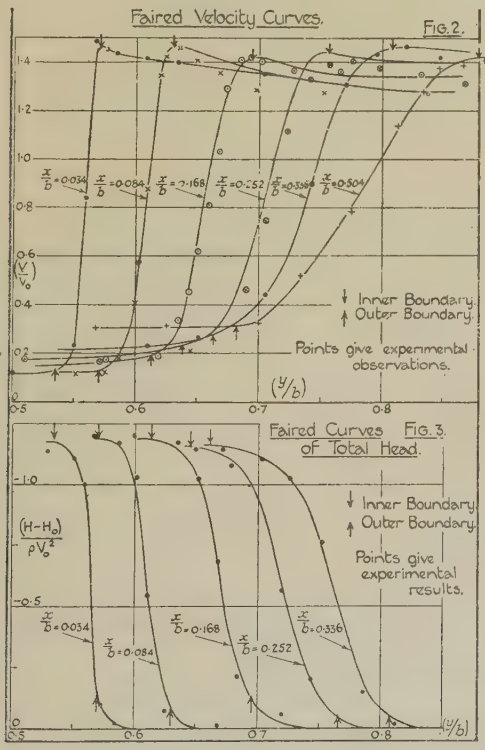

It is of course obvious that these dotted lines are not streamlines; since, as will be shown in § (14), there is a flow across them.

6. The instruments just described give average values over comparatively long intervals of time; and so the observations obtained with them can only be accepted with confidence when the flow is steady. Records of the velocity

fluctuations were accordingly taken in the region immediately behind the plate, where the explorations were made, in order to examine the steadiness of the flow. These records are analysed later in the paper (§ 12), but it is necessary to mention now that most of the observations which are about to be analysed were taken in a region where the flow was comparatively steady. Some uncertainty undoubtedly exists in a restricted region near the inner boundary of the sheet, but this does not appreciably affect the conclusions arrived at from the calculations made throughout the paper because the velocity in this region is so small.

(7) To eliminate, as far as possible, small experimental errors of observation, and also to obtain greater accuracy in

Fig. 4.

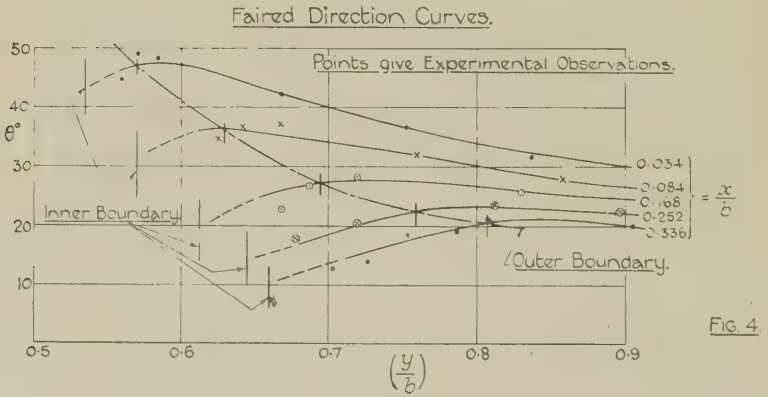

FIG. 4.

the subsequent calculations, the observed values of $\left(\frac{V}{V_0}\right)$, $\left(\frac{H-H_0}{\rho V_0}\right)$, and θ have been faired by the usual system of cross-plotting. Figs. 2–4 show that, in general, the faired curves pass closely through the actual observations. It should be noticed in fig. 4 that no direct observations of θ were taken near the inner boundary. The direction of the flow in this region of the sheet was obtained from extrapolations of the curves drawn through observations taken in the steadier region near the outer boundary.

(8) *Boundaries of the Sheet.*—Fig. 2 shows that at each

section of the sheet the velocity rises from a small to a well-marked maximum value, which is a constant $\left[\frac{V_1}{V_0} = 1{\cdot}45\right]$ within the accuracy of measurement. We shall first assume, as was done in the paper referred to in § (2), that the outer boundary of the sheet is the line passing through the points of maximum velocity (V_1), and the inner boundary is the line passing through the points of minimum velocity (V_2). If this assumption is justifiable, these boundaries should be in close agreement with those obtained from direct calculations of vorticity. It will now be shown that this is so. The time-average value of the vorticity, $\frac{b}{V_0}\left(\frac{\partial v}{\partial x} - \frac{\partial u}{\partial y}\right)$, at any point was determined from the faired observations of $\left(\frac{V_1}{V_0}\right)$ and θ given in figs. 2 and 4. The values of $\left(\frac{\partial v}{\partial x}\right)$ and $\left(\frac{\partial u}{\partial y}\right)$ were estimated graphically from the slopes of tangents drawn to the curves of v and u on x and y bases respectively, where $u = V\cos\theta$, $v = V\sin\theta$, and x and y are measured from the centre of the plate respectively, parallel to and normal to the direction of the undisturbed wind. The estimated values of $\frac{b}{V_0}\left(\frac{\partial v}{\partial x} - \frac{\partial u}{\partial y}\right)$ plotted against $\left(\frac{y}{b}\right)$ for several constant values of $\left(\frac{x}{b}\right)$ are given in fig. 5 *a*. It will be noticed that there is a progressive opening-out of the sheet, and also a progressive diminution in the value of the maximum vorticity at each section. There is therefore a lateral spreading of vorticity due to an inflow of fluid from outside.

Arrows are placed on each of the curves of fig. 5 *a* to indicate the position of the boundaries of the vortex sheet as estimated from the velocity curves of fig. 2. These arrows are seen to be in close proximity to the points of zero vorticity on the curves; so that almost all the vorticity leaving the edge is contained within the boundaries estimated from the velocity curves.

(9) The average experimental distribution of vorticity across the sheet estimated from the five curves of fig. 5 *a* is shown by a dotted line in fig. 5 *b*, where values of $\frac{\Delta}{V_1}\left(\frac{\partial v}{\partial x} - \frac{\partial u}{\partial y}\right)$—where Δ represents the breadth of the

sheet and V_1 the velocity at points in the outer boundary—are plotted on a base representing the breadth of the sheet. Included in this figure is a curve giving the theoretical distribution of vorticity which, according to the Prandtl-Tollmien * theory, is identical at all sections across the sheet. The agreement between the theoretical and experimental curves is not very close; but some discrepancy is to be

Figs. 5 *a* and 5 *b*.

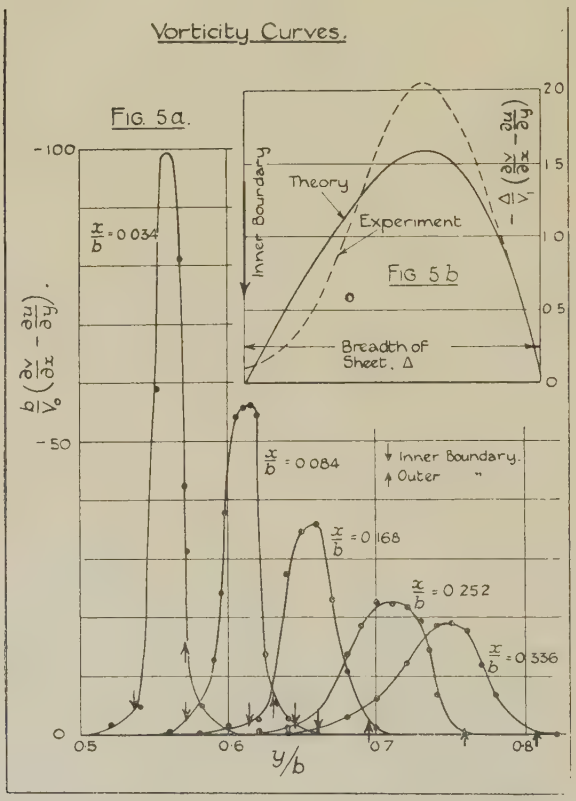

expected because, owing to the steep velocity gradient across the sheet, it is difficult to determine with good accuracy the experimental values of $\frac{\Delta}{V_1}\left(\frac{\partial v}{\partial x}-\frac{\partial u}{\partial y}\right)$. Both curves exhibit the interesting feature that the vorticity has

* See § (2).

its maximum value not at the centre of the sheet, but along a line situated about 60 per cent. of the breadth from the inner boundary.

(10) Since the values of $\left(\frac{\partial v}{\partial x} - \frac{\partial u}{\partial y}\right)$ were obtained graphically from the slopes of tangents to velocity curves, they are liable to be in error. To check the accuracy of these estimations, the cross-section of the sheet was included by several rectangular contours (see fig 7 (*a*)), and the total strength of the vorticity within each rectangle determined from the integral over the surface of the estimated values of $\left(\frac{\partial v}{\partial x} - \frac{\partial u}{\partial y}\right)$. These results are given in Table I., where they are compared with those obtained by the more simple and accurate method of finding the circulation $\int (u dx + v dy)$ around the contour of each rectangle. The agreement between the two series of results is reasonably close, from which it is inferred that the accuracy of the values of $\left(\frac{\partial v}{\partial x} - \frac{\partial u}{\partial y}\right)$ is satisfactory. It should be noted that the comparison undertaken in this section has been made on the assumption that the motion in the sheet is steady. It will be shown in § (12) that the motion is steady except near the inner boundary; but the unsteadiness in this region should not appreciably lessen the value of the work because the velocity there is very small.

Table I.

Rectangle (see fig. 7 (*a*)).	$\frac{1}{V_0 b}\iint\left(\frac{\partial v}{\partial x} - \frac{\partial u}{\partial y}\right) dx \,.\, dy$ over the area.	$\frac{1}{V_0 b}\int (u\,dx + v\,dy)$ around the contour.
I.	−0·097	−0·107
II.	−0·136	−0·139
III.	−0·125	−0·128
IV.	−0·118	−0·116

(11) The boundaries of the vortex sheet have also been marked on the curves of total head given in fig. 3. As would be expected, the total head beyond the outer boundary is approximately uniform and equal to the total head in the

undisturbed wind, H_0; and the total head in the dead-air region contained within the inner boundaries is also approximately constant. These conditions of flow provide further evidence to support the method of estimating the boundaries of the vortex sheet. This method has therefore, because of its simplicity, been used to determine the boundaries of the vortex sheets considered later in the paper.

(12) *Steadiness of Sheet.*—To examine the steadiness of the sheet, photographic records of the velocity fluctuations were taken with an Einthoven galvanometer used in conjunction with a hot wire. The method of observation was the same as that described in the paper to which reference has been made in § (2). To illustrate the general character

Figs. 6 *a* and 6 *b*.

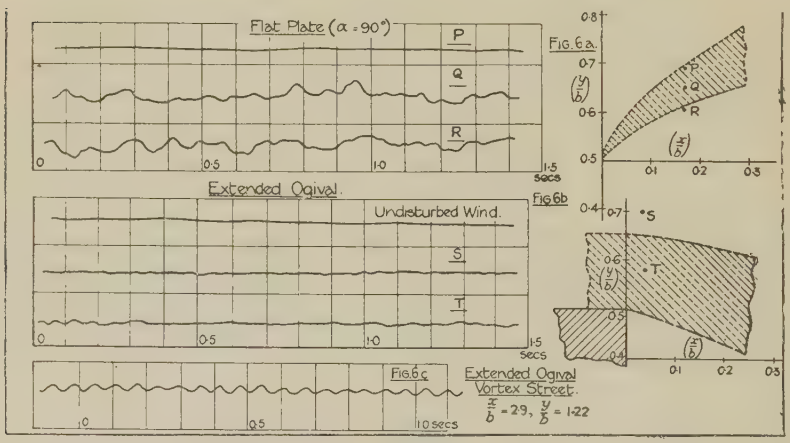

of the velocity fluctuations, three records taken in the section $\frac{x}{b} = 0{\cdot}168$, at points situated in the outer boundary, the centre of the sheet, and the inner boundary respectively, are given in fig. 6 *a*. The mean values of $\left(\frac{V}{V_0}\right)$ at these points are 1·42, 0·68, and 0·18 respectively. These records show that the velocity fluctuations near the outer boundary—where the mean velocity is a maximum—are very small, but that they become appreciable near the inner boundary, where the mean velocity is low; and also that the fluctuations at any point do not appear to be regular either in amplitude or frequency, although there is an occasional indication of a frequency

($T=0{\cdot}202$ sec., $V_0=16{\cdot}8$ ft./sec.) equal to that with which the individual vortices, arising from the rolling-up of the sheets, are shed. Other records (not included in the paper) showed that the amplitude of the velocity fluctuations tended to increase with the distance behind the plate. In all cases, therefore, velocity observations have been taken at sections as close to the body as possible, and away from the region where the sheet was rolling-up. Some evidence of a "flutter" or "whip" of the sheet, of a slow indefinite frequency, was also obtained. It was suspected from the magnitude of the angular amplitude that this disturbance was associated with the ordinary disturbances in the tunnel wind; the evidence was not, however, conclusive.

(13) *Rate at which Vorticity is shed from Edge.*—In steady motion the vorticity at any point (x, y) is given by $\left(\frac{\partial v}{\partial x}-\frac{\partial u}{\partial y}\right)$, so that the total amount of vorticity, K, passing a section of a sheet in unit time is, in non-dimensional units,

$$\frac{1}{V_0^2}\int_{y_2}^{y_1}\left(\frac{\partial v}{\partial x}-\frac{\partial u}{\partial y}\right)u dy,$$

where y_1 and y_2 are the limits of the sheet. For a theoretical sheet of infinitesimal breadth the above expression reduces to $\left(\frac{V_1^2-V_2^2}{2V_0^2}\right)$, where V_1 and V_2 are the velocities at points in the boundaries of the sheet. In the earlier paper [see § (2)] it was shown that the breadth of the sheet, although increasing with the distance downstream, is small compared with its radius of curvature, and it was assumed that the latter expression, $K=(V_1^2-V_2^2)/2V_0^2$, gave a reasonably accurate value for the amount of vorticity leaving the edge in unit time. The additional observations since taken allow an estimate to be made of the accuracy of this approximate expression for K.

Values of $\frac{1}{V_0^2}\int_{y_2}^{y_1}\left(\frac{\partial v}{\partial x}-\frac{\partial u}{\partial y}\right)u \,.\, dy$

estimated for several sections of the sheet are given in Table II. The values of u, that is $V\cos\theta$, used in these calculations were determined from values of V and θ taken from the faired curves of figs. 2 and 4. The values of $\left(\frac{\partial v}{\partial x}-\frac{\partial u}{\partial y}\right)$ were taken from the curves of fig. 5 *a*. Included in the table are the corresponding values of $\left(\frac{V_1^2-V_2^2}{2V_0^2}\right)$.

A comparison of the two series of values given in this table shows that the approximate expression $K=\left(\frac{V_1^2-V_2^2}{2V_0^2}\right)$ underestimates the amount of vorticity leaving the edge in unit time by about 9 per cent. Closer agreement between the two expressions for K is to be expected for other types of sheet, such as those considered later in the paper, for which the curvature is smaller than that for the flat plate.

TABLE II.

$\frac{x}{b}$.	$-\frac{1}{V_0^2}\int_{y_2}^{y_1}\left(\frac{\partial v}{\partial x}-\frac{\partial u}{\partial y}\right)u\,.\,dy.$	$\left(\frac{V_1^2-V_2^2}{2V_0^2}\right)$.
0·034	1·18	1·07
0·084	1·20	1·07
0·168	1·15	0·99
0·252	1·11	1·02
0·336	1·10	1·05

Fig. 7 (*a*), (*b*), (*c*), (*d*), (*e*).

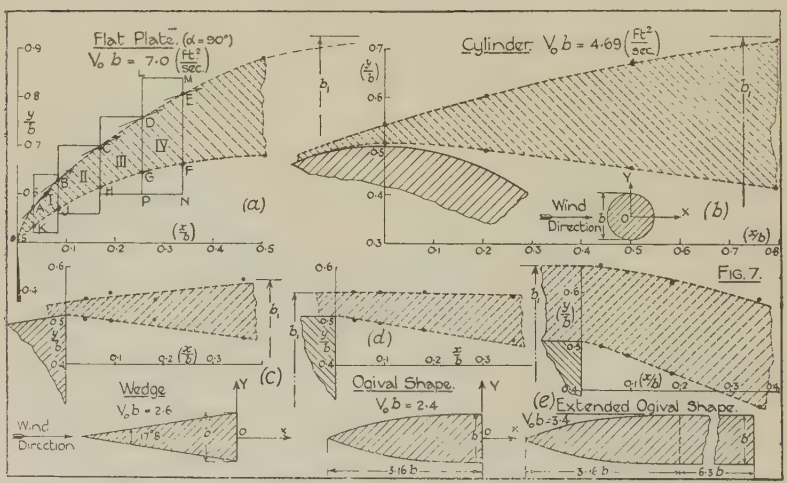

(14) *Flow across each Boundary.*—To determine these flows, the field containing the sheet was divided into rectangles by lines parallel to and normal to the section of the plate, as shown in fig. 7 (*a*). The flow through an arc of a boundary was then obtained by the evaluation of $\int(u\,dy-v\,dx)$ around the contour of that part of the rectangle cut off by the arc. For example, for the arc DE of the outer boundary,

the integration was taken around the contour DLME, and for the arc GF of the inner boundary around the contour GLMF. The results are given in Table III., and indicate that air is flowing into the sheet across both boundaries. The values in the last column of this table give the flow per sec. per unit length of each arc. The agreement between the values for the arcs of each boundary is not very close; there is, however, no indication of any systematic variation along the boundary. Average values of the flow per sec. per unit length of arc have therefore been taken for the outer boundary from A to E, and for the inner boundary from K to F. They are $0{\cdot}189\ V_0$ and $0{\cdot}083\ V_0$ respectively, the ratio being 2·3 *. This ratio on the Prandtl-Tollmien theory is 2·6. The close agreement between these two values must be regarded as partly fortuitous in view of the following discussion in § (15).

TABLE III.

	Arc of boundary (see fig. 7 (*a*)).	Flow per sec. / bV_0.		$\frac{1}{V_0}$ (flow per sec. per unit length).
Outer boundary.	AB	0·0111	0·0737	0·140
	BC	0·0220		0·204
	CD	0·0231		0·222
	DE	0·0175		0·180
Inner boundary.	KJ	−0·0050	−0·0276	−0·081
	JH	−0·0059		−0·062
	HG	−0·0058		−0·064
	GF	−0·0109		−0·128

(15) The reason why estimates of the flow across arcs of the inner boundary are included in the paper, when no measurements of the direction of flow in this region could be taken—see § (7),—is that the method of estimation is such that no exact knowledge of the direction of the flow near the inner boundary is needed. Thus the magnitude of the flow across an arc such as FG (fig. 7 (*a*)) has been determined from the fact that it must be equal and opposite to that of the flow through the contour FMLG. If, therefore, any uncertainty in the direction of flow at points situated in the sections MF and LG, and also near the inner boundary—where, it must be noted, the velocity is very small compared with that at points near the outer boundary—does not greatly modify the flow across these sections, a reasonable estimate of the flow

* Lengths of arcs AE and KF are 0·388 *b* and 0·333 *b* respectively.

across the arc FG can be obtained. To show that this is the case, the flow across the inner boundary from K to F has been determined on two assumptions: (*a*) that the unknown directions at K and F are taken from the dotted lines in fig. 4, that is, more or less tangential to the boundary; and (*b*) that the directions are normal to the boundary. The results are given below, and indicate that, although the assumptions are so different, the reduction in the flow through the inner boundary does not exceed 17 per cent. of the value given in Table III.

See fig. 7 (*a*).	(*a*). See Table III.	(*b*).
Flow across EF	−0·1156	−0·1094
,, ,, AE (outer boundary) .	0·0737	0·0737
,, ,, AK	0·0143	0·0127
Flow across KF (inner boundary) .	−0·0276	−0·0230

This percentage corresponds to an increase in the ratio of the flows across the outer and inner boundaries AE, KF from 2·3 to 2·8. It would be possible, of course, so to adjust the values of θ at points in the inner boundary that the flow calculated by an integration along its length would be exactly equal to that obtained by an integration around the contour formed by the two end sections and the outer boundary. This, however, has not been attempted, because the velocity at points in the inner boundary is too small and unsteady to be measured with reliable accuracy. In short, it follows that a reasonable estimate of the flow across the inner boundary can be made because the method adopted takes advantage of the fact that the air which is passing across this boundary at a low velocity and in an unmeasurable direction is gradually absorbed into the sheet (together, of course, with the air flowing across the outer boundary), and eventually acquires a higher velocity and a measurable direction. The direction of the flow across the outer boundary is indicated by arrows in fig. 7 (*a*).

IV. Sheets shed from Other Bodies.

(16) Attention has been centred, so far, on the sheet shed from a sharp edge of a flat plate mounted normally to the wind. To obtain more generality, the research has been extended to include an analysis of the vortex sheets shed from bodies of widely different forms. This work shows how the rate of spread of turbulence and the velocity distribution in a sheet depends on the form of the body.

(17) The sectional shapes of the models selected are shown in figs. 7 and 8. The models were :—

No. 1.—A flat plate normal to wind (fig. 7 (*a*)). Breadth, $b = 0{\cdot}5$ ft. (This model is included here for the purpose of a general comparison with the other models.)

No. 2.—Cylinder (fig. 7 (*b*)). Diameter, $b = 0{\cdot}281$ ft.

No. 3.—Flat-sided wedge with the apex pointing into the wind. Width of base, $b = 0{\cdot}232$ ft. ; apex-angle, 17°·8. (Fig. 7 (*c*).)

No. 4.—An "ogival" wedge with the apex pointing into the wind (fig. 7 (*d*)). This shape is formed by the arcs of a cubic parabola, $y = \pm \frac{b}{2}\left[1 + \frac{x^3}{h^3}\right]$, from $x = -h$ to $x = 0$. Width of base, $b = 0{\cdot}232$ ft. ; height, $h = 3{\cdot}16\, b$.

No. 5.—Ogival model, with parallel-sided extension at the back (fig. 7 (*e*)). Width of base, $b = 0{\cdot}232$ ft. ; overall length $= 9{\cdot}46\, b$.

No. 6.—An aerofoil inclined at 10°, 20°, and 45° to the undisturbed wind (fig. 8 (*a*), (*b*), (*c*)). Length of chord $= 0{\cdot}5$ ft. At the speeds of the experiment there was a pronounced dead-air region behind the aerofoil at each angle of incidence. The air-flow at 10° incidence was, however, sensitive to the wind-speed, and it was found that at this incidence the dead-air region disappeared at speeds greater than 40 ft./sec.

No. 7.—Flat plate inclined at 40° to the undisturbed wind (fig. 8 (*d*)). Breadth, $b = 0{\cdot}5$ ft.

(18) Each model had a length of 7 ft., and was mounted between the floor and the roof of a 7-ft. wind-tunnel. Observations were confined to the median section of the tunnel where the flow is two-dimensional. The product $(V_0 b)$, where V_0 is in ft./sec. and b is in feet, together with the position of the axes OX and OY in relation to each model, are given in figs. 7 and 8. The models fall into two groups : first, symmetrical models with the axes of symmetry in the direction of the wind (fig. 7), and second, asymmetric models (aerofoil and inclined flat plate, fig. 8). The sheets shed from each model of the first group are arranged symmetrically, whereas those for the second group are asymmetric both in shape and position.

(19) The boundaries of the sheets shed from each model were determined, as before, from velocity observations along several lines, taken at right angles to the undisturbed wind-direction. The lines selected were taken close to the model,

and in a region where the motion was comparatively steady. The estimated coordinates of points in the boundaries of each sheet, and also the velocity at these points, are given in Tables IV. and V. Included in these tables are the values of K estimated from the approximate expression $K = \left(\frac{V_1^2 - V_2^2}{2V_0^2}\right)$. The boundaries of the various sheets are shown by the dotted lines in figs. 7 and 8. The values given in Tables IV. and V. show that the velocity at a point on

Fig. 8 (*a*), (*b*), (*c*), (*d*).

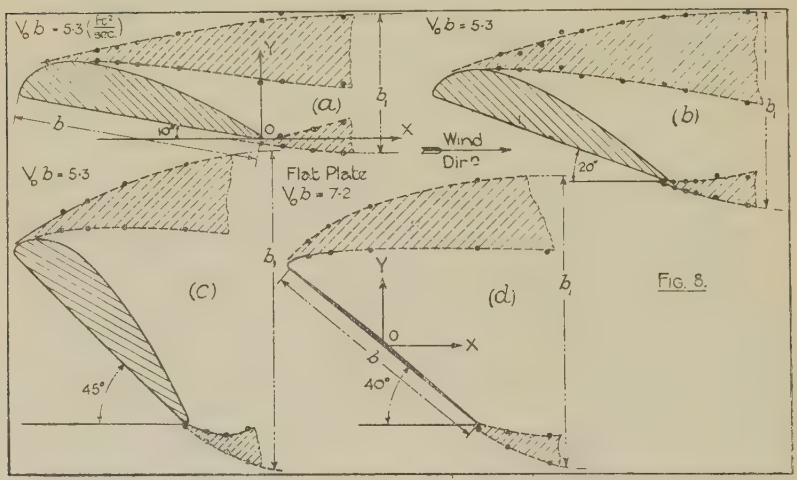

Fig. 8.

each outer boundary is uniform, within the accuracy of measurement—except for the aerofoil at $\alpha = 20°$, for which two types of flow appear possible,—and that the velocity at a point on each inner boundary, taken close behind the the model, is small. For any one sheet the values of K are also in fairly close agreement if the sections are taken near the model (V_2 small). Table V. also brings out the important fact that vorticity is shed from the upper and lower surfaces of an asymmetric model at the same rate.

(20) *Velocity Distribution in Sheets.*—The observations of Tables IV. and V. show that, although at points on the outer boundary the velocity is uniform, it slowly increases on the inner boundary with the distance of a point downstream. The velocity distribution across a section depends therefore

on its distance behind a model. To make a genuine comparison between the velocity distributions for the various sheets it is necessary, therefore, to take observations in a section close behind a model for which the value of V_2 is small. The breadth of the sheet immediately behind a model is in most cases small, and it is difficult to take observations with good accuracy. An approximation to the velocity distribution across a section of the sheet close behind each model has, however, been obtained by drawing a fair curve through observations taken in several sections near the model, the closeness of these sections being such that the velocity at the inner boundary did not exceed 0·1 V_1 approximately (V_1 = velocity at a point in the outer

TABLE IV.—Symmetrical Models.

Model.	$\left(\frac{x}{b}\right)$.	Ordinates of boundaries.		Velocity in boundaries.		K.
		$\left(\frac{y_1}{b}\right)$.	$\left(\frac{y_2}{b}\right)$.	$\left(\frac{V_1}{V_0}\right)$.	$\left(\frac{V_2}{V_0}\right)$.	
Flat plate ($\alpha = 90°$).	0·034	0·570	0·535	1·47	0·13	1·07
	0·084	0·630	0·570	1·47	0·13	1·07
	0·168	0·695	0·613	1·42	0·18	0·99 } 1·05
	0·252	0·759	0·645	1·44	0·22	1·02
	0·336	0·807	0·660	1·47	0·26	1·05
	0·504	0·880	0·680	1·43	0·31	—
Cylinder.	0	0·540	0·505	1·42	0	1·01
	0·204	0·600	0·490	1·37	0·07	0·94 } 0·96
	0·500	0·670	0·455	1·38	0·23	0·93
	0·796	0·720	0·415	1·25	0·35	—
Wedge.	−0·180	0·504	—	1·20	—	—
	0·036	0·535	0·490	1·40	0·07	0·97
	0·090	0·545	0·490	1·38	0·07	0·95 } 0·86
	0·180	0·530	0·490	1·27	0·08	0·81
	0·360	0·575	0·455	1·23	0·22	0·73
Ogival model.	0·036	0·550	0·490	1·13	0·05	0·64
	0·090	0·550	0·485	1·14	0·07	0·65 } 0·66
	0·180	0·550	0·470	1·18	0·09	0·69
	0·360	0·540	0·450	1·23	0·19	—
Extended ogival model.	−4·35	0·612	—	1·04	—	—
	0·036	0·656	0·490	1·19	0·04	0·71
	0·090	0·641	0·471	1·18	0·05	0·69 } 0·69
	0·180	0·620	0·433	1·16	0·12	0·67
	0·360	0·587	0·366	1·15	0·16	—

Table V.—Asymmetric Models.

Model.	Upper Surface.						Lower Surface.					
	Ordinates of boundaries.		Velocity in boundaries.		K.		Ordinates of boundaries.		Velocity in boundaries.		K.	
	$\left(\frac{x}{b}\right)$.	$\left(\frac{y_1}{b}\right)$.	$\left(\frac{y_2}{b}\right)$.	$\left(\frac{V_1}{V_0}\right)$.	$\left(\frac{V_2}{V_0}\right)$.		$\left(\frac{x}{b}\right)$.	$\left(\frac{y_1}{b}\right)$.	$\left(\frac{y_2}{b}\right)$.	$\left(\frac{V_1}{V_0}\right)$.	$\left(\frac{V_2}{V_0}\right)$.	
Aerofoil ($\alpha=10°$)	−0·870	0·323	—	1·27	—	—	0	−0·020	—	1·18	0	0·70 } 0·69
	−0·667	0·370	0·330	1·16	0·05	0·67	0·083	−0·030	0·009	1·19	0·14	0·70
	−0·583	0·383	0·323	1·23	0·07	0·75	0·208	−0·050	0·040	1·20	0·28	0·68
	−0·500	0·400	0·310	1·24	0·23	0·74 } 0·70	0·333	−0·060	0·065	1·19	0·36	—
	−0·333	0·435	0·295	1·20	0·24	0·69						
	0	0·494	0·230	1·15	0·19	0·64						
	+0·083	0·525	0·235	1·19	0·21	0·69						
	0·333	0·500	0·225	1·20	0·37	—						
Aerofoil ($\alpha=20°$).	−0·667	0·525	0·467	1·32	0·05	0·87	0	−0·017	—	1·20	0	0·72
	−0·583	0·527	0·458	1·24	0·11	0·76	0·042	−0·032	−0·007	1·23	0·09	0·75
	−0·500	0·560	0·453	1·33	0·17	0·87 0·87	0·083	−0·047	−0·008	1·22	0·12	0·74 } 0·75
	−0·417	0·617	0·467	1·24	0·14	0·76 } or	0·125	−0·052	−0·007	1·23	0·14	0·75
	−0·333	0·620	0·435	1·26	0·18	0·77 0·77	0·208	−0·075	+0·017	1·26	0·19	0·77
	−0·167	0·650	0·410	1·25	0·09	0·78	0·333	−0·107	0·010	1·19	0·29	0·67
	0	0·675	0·392	1·32	0·14	0·86						
	+0·083	0·675	0·367	1·30	0·15	—						
	0·333	0·690	0·320	1·19	0·23	—						
Aerofoil ($\alpha=45°$).	−0·500	0·876	0·797	1·40	0·09	0·98	0	−0·013	—	1·37	0	0·94
	−0·400	0·911	0·803	1·37	0·15	0·93	0·083	−0·077	−0·027	1·39	0·16	0·96 } 0·93
	0	1·068	0·800	1·36	0·18	0·91 0·94	0·167	−0·115	−0·050	1·37	0·22	0·92
	−0·250	0·990	0·810	1·37	0·13	0·93	0·250	−0·155	−0·020	1·36	0·19	0·91
Flat plate ($\alpha=40°$)	−0·303	0·434	0·372	1·36	0·09	0·92	0·383	−0·339	−0·321	1·35	0	0·91 } 0·92
	−0·218	0·493	0·383	1·38	0·10	0·94	0·503	−0·412	−0·348	1·37	0·17	0·93
	−0·051	0·575	0·390	1·38	0·11	0·94 0·93	0·672	−0·490	−0·367	1·35	0·35	—
	+0·383	0·682	0·403	1·36	0·19	0·90						
	0·672	0·700	0·383	1·37	0·30	—						

boundary). The curves obtained are shown in fig. 9 *a*, where values of $\left(\frac{V}{V_1}\right)$ are plotted on a base representing the breadth of the sheet. The actual observations from which these faired curves have been obtained are too numerous to be shown conveniently in the paper. An exception has, however, been made in the case of the flat plate ($\alpha = 90°$), in order to convey some idea of the accuracy of this method of estimation. These results are given in fig. 9 *b*. The agreement between the separate sets of observations for this sheet can be regarded as representative of that obtained for the other sheets, and is considered to be sufficiently close to justify the taking of a mean curve.

Figs. 9 *a* and 9 *b*.

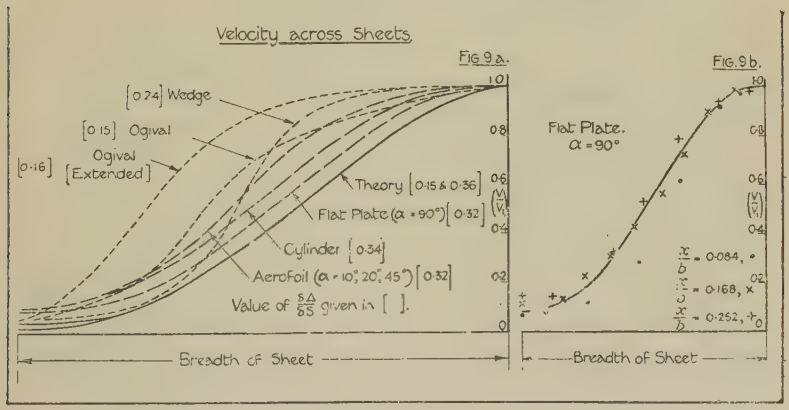

The velocity distribution in the sheets shed from the aerofoil at 10°, 20°, and 45° incidence has been represented by one curve, because although the curves for the lower surface were somewhat higher than those from the upper surface, the differences were of the same order as those obtaining between the observations in any one sheet.

(21) The rate at which the breadth of each sheet increases with the distance downstream has been determined, and was found to have a constant value throughout the length. These values, denoted by $\frac{\partial \Delta}{\partial s}$, where Δ is the breadth of a section and s is its distance downstream from the body measured along the sheet, are given on the curves of fig. 9 *a*.

They are seen to lie between the limits 0·15 and 0·36. The distributions of velocity predicted by the Prandtl-Tollmien theory for these two values of $\frac{\partial \Delta}{\partial s}$ have been determined, and they are also shown in fig. 9 *a*. They were found to be identical except near the inner boundary.

(22) The velocity curves of fig. 9 *a* show a progressive departure from the theoretical curve in the order: flat plate, cylinder, aerofoil, wedge, ogival, extended ogival. Also they appear to fall into two more or less distinct groups: (flat plate, cylinder, aerofoil) and (wedge, ogival. extended ogival). The curves of the first group resemble more closely the theoretical curve, and the values of $\frac{\partial \Delta}{\partial s}$ are in close agreement; whereas those of the second group show more marked departures from theory, and the values of $\frac{\partial \Delta}{\partial s}$ are, by comparison, distinctly lower. Another difference—exhibited in figs. 7 and 8—is that each sheet of the second group has a relatively larger breadth where it leaves the model, due to the appreciably larger surface exposed to the wind-stream, for the same area of obstruction. In this connexion it is of interest to note that the addition of the extension piece to the ogival model increases the overall length in the ratio 3:1, and also increases the breadth of the sheet, leaving the model in about the same proportion (2.8:1). The experiments demonstrate, then, how the shape of the body influences both the rate of opening-out and the velocity distribution across the vortex sheets trailing behind.

(23) One of the assumptions of the Prandtl-Tollmien theory is that the breadth of a sheet is initially zero. Of the sheets considered above, that shed from the flat plate most closely realises this condition, and it is of interest to note that it is for this case that the velocity distribution is in closest agreement with that predicted by theory.

(24) To determine whether the flow around the surface of the extended ogival model had become unsteady, records of the velocity fluctuations both within and without the vortex sheet were taken immediately behind the body. The positions at which these records were taken, and also tracings of the records, are shown in fig. 6 *b*. A comparison of these records with that taken in the undisturbed wind shows that, although there are occasional indications of a slight periodic

disturbance, the motion both within and without the sheet is comparatively steady. There does not appear in this case to have been any tendency for the creation of vortices of appreciable size, due to the coalescence of neighbouring vortices as they pass along the surface from nose to tail, as has been tentatively suggested by H. Levy * in his paper on the growth of eddies in a viscous fluid. In fact, throughout the present experiment, there appeared to be fairly definite evidence that the large vortices, which pass downstream at some distance behind a body, are created by the rolling-up of the sheets after they have left the body. A record of the velocity fluctuations due to the vortices in the *vortex street*, taken at a point $\left(\frac{x}{b}=2{\cdot}9\,\frac{y}{b}=1{\cdot}22\right)$ situated some distance behind the extended ogival model, is given in fig. 6 *c*. A comparison of this record with those given in fig. 6 *b* shows that the velocity fluctuations within the sheet are small compared with those which occur outside the street at some distance behind the body.

(25) *Relation between* p_m *and* p_1.—Table VI. gives the

Table VI.

Model.	Coordinates of point in boundary. $\left(\frac{x}{b}\right)$.	$\left(\frac{y}{b}\right)$.	$\left(\frac{p_1-p_0}{\rho V_0^2}\right)$.		$\left(\frac{p_m-p_0}{\rho V_0^2}\right)$.
Flat plate ($\alpha=90°$).	0·034	0·570	−0·71	−0·65	−0·69
	0·084	0·630	−0·66		
	0·168	0·695	−0·63		
	0·252	0·765	−0·59		
	0·336	0·807	−0·63		
Flat plate ($\alpha=40°$).	0·672	0·700	−0·49	−0·47	−0·55
	0·672	−0·490	−0·45		
	−0·218	0·493	−0·47		
Aerofoil ($\alpha=45°$).	−0·400	0·911	−0·45	−0·47	−0·51
	0·167	−0·115	−0·48		
Cylinder.	0·204	0·600	−0·45	−0·49	−0·51
	0·500	0·670	−0·52		
Ogival.	0·090	0·550	−0·170	−0·183	−0·252
	0·180	0·550	−0·196		
Extended ogival.	0·136	0·656	−0·208	−0·207	−0·225
	0·090	0·641	−0·206		

* Phil. Mag. October 1926.

relation between the pressure p_m at the back of each model (except the wedge, which has been excluded because the position of the outer boundary was not determined very exactly) and the pressure p_1 in the outer boundary of the sheet. The values of p_m were measured directly, while those of p_1 were deduced from observations of velocity and total head. A comparison of the results shows that, in general, the pressure in the outer boundary is slightly greater than that measured in the dead-air region behind a model. It should here be mentioned that it was also found for the flat plate, $\alpha=90^\circ$, that the average pressure p_2 at points in the inner boundary was equal to $(p_0-0{\cdot}69\rho V_0^2)$, that is, the pressure, p_m, measured directly behind the plate.

V. Vortex Streets behind Models.

(26) It is well known that the vortex sheets behind a body are unstable, and that at some distance behind the body they break up into two rows of discrete vortices, to form a vortex street. To determine some general characteristics of vortex streets, measurements have been made for each model of the frequency, f, with which the vortices pass downstream, and also of the longitudinal spacing, a, between consecutive vortices in the same row. The method of

Table VII.

Model.	Col. 1. $\left(\frac{V_1}{V_0}\right)$.	Col. 2. K.	Col. 3. $\left(\frac{fb}{V_0}\right)$.	Col. 4. $\left(\frac{a}{b}\right)$.	Col. 5. $\left(\frac{V_3}{V_0}\right)$.	Col. 6. $\left(\frac{b'}{b}\right)$.	Col. 7. $\left(\frac{fb'}{V_0}\right)$.	Col. 8. $\left(\frac{a}{b'}\right)$.
Flat plate ($\alpha=90^\circ$).	1·45	1·06	0·146	5·25	0·77	1·85	0·270	2·84
Flat plate ($\alpha=40^\circ$).	1·37	0·93	0·231	3·55	0·82	1·20	0·277	2·96
Cylinder.	1·39	0·96	0·187	4·27	0·80	1·45	0·271	2·95
Aerofoil ($\alpha=45^\circ$).	1·37	0·94	0·210	3·67	0·77	1·31	0·275	2·80
Aerofoil ($\alpha=10^\circ$).	1·19	0·70	0·735	1·25	0·92	0·57	0·418	2·19
Wedge...	1·32	0·86	0·238	3·45	0·82	1·15	0·273	3·00
Ogival ...	1·15	0·66	0·271	3·16	0·86	1·10	0·298	2·87
Extended ogival.	1·18	0·69	0·254	3·33*	0·81	1·31	0·332	2·54

* Value steadily increases with distance behind model.

measurement was precisely the same as that described in the paper previously mentioned (§ 2). The speed, V_3, with which the vortices in each row pass downstream has also been calculated from the product (fa). The results are given in Table VII., together with values of V_1 and K (taken from Tables IV. and V.). The values in columns 1, 2, and 5 (Table VII.) show that, in general, the speed (V_3) with which the individual vortices pass downstream decreases with an increase in (V_1) and consequently in K. The values of both $\left(\frac{f.b}{V_0}\right)$ and $\left(\frac{a}{b}\right)$ for the different models—columns 3 and 4—are seen to vary considerably. This variation is, of course, not surprising, since the values of b taken refer to a particular dimension of each model, and so are unrelated.

(27) If the sheets shed from the models were parallel bands of small breadth, and if they had the same velocity V_1 in the outer boundary, the frequency (f) would vary inversely, and the longitudinal spacing (a) directly, as the distance between the bands, at the velocity V_0. If, then, b' represented the distance between the outer boundaries of the sheets, both $\left(\frac{fb'}{V_0}\right)$ and $\left(\frac{a}{b'}\right)$ would have constant values, even although the values of $\left(\frac{fb}{V_0}\right)$ and $\left(\frac{a}{b}\right)$ varied from model to model. Calculations of $\left(\frac{fb'}{V_0}\right)$ and $\left(\frac{a}{b'}\right)$—where b' represents the maximum distance between the outer boundaries, as shown in figs. 7 and 8—have accordingly been made, and the results are given in columns 7 and 8. Except for the extreme cases of the aerofoil at 10° incidence and the extended ogival, the values of $\left(\frac{fb'}{V_0}\right)$ and also $\left(\frac{a}{b'}\right)$ are in close agreement. It appears, then, at a constant speed V_0, both the frequency (f) and the longitudinal spacing (a) of the individual vortices behind a body depend largely on the lateral spacing between the vortex sheets, and that these characteristics are influenced to a much smaller extent (except possibly in extreme cases) by the shape and structure of the sheets.

(28) The values of $\left(\frac{fb}{V_0}\right)$ measured in the vortex streets, behind the flat plate and aerofoil at several angles of incidence, are given in Table VIII. It is of interest to note that the two series of values are in close agreement, except below 30°, where the values for the plate are greater than

those for the aerofoil. The agreement at a large incidence is not unexpected, because only the flat lower surface of the aerofoil, which resembles a flat plate except for the curvature at the edges, is then exposed to the wind; at a small incidence this is not the case, as a part of the upper surface is also exposed.

TABLE VIII.

Values of $\left(\frac{fb}{V_0}\right)$.

$\alpha°$.	Flat plate (b=breadth).	Aerofoil (b=chord).
90	0·146	0·150
60	0·173	0·179
50	0·196	0·197
45	0·205	0·210
40	0·231	0·247
30	0·307	0·313
20	0·478 0·503	0·448
16	0·548 0·677	0·544
14	0·746 0·900	0·608

VI. SUMMARY.

The structure of the sheets shed from infinitely long bodies of widely different cross-section has been examined. Measurements have also been made to determine the principal characteristics of the vortex streets formed at some distance behind each body.

It is established from estimations of vorticity and also from observations of total head, that the outer boundary of a sheet can be taken as a line drawn through the points in the field of maximum velocity (V_1), and the inner boundary as the line passing through the points of minimum velocity (V_2).

The motion in a sheet is steady near the body, except possibly near the inner boundary.

The pressure at points in an outer boundary is slightly greater than that in the dead-air region behind the body.

Air flows into a sheet through both boundaries, but at a greater rate through the outer boundary.

The simple expression $\left(\frac{V_1^2-V_2^2}{2V_0^2}\right)$ gives a close estimate

of the total amount of vorticity passing a section of a sheet in unit time.

Vorticity is shed from the two sides of an asymmetric body at the same rate.

The variation of velocity across a section of a sheet, and also the rate of increase of the breadth with the distance downstream, depend on the form of the body. The velocity distribution in the sheet shed from a flat plate normal to the stream is in close agreement with that predicted by the Prandtl-Tollmien theory.

At a constant forward speed, both the frequency and the longitudinal spacing of the individual vortices in the vortex street depend largely on the lateral spacing between the sheets, and to a smaller extent on the form of the body.

In conclusion, the writers wish to acknowledge their indebtedness to Dr. H. Lamb, F.R.S., for valuable suggestions made during the preparation of the paper, and also to Mr. J. H. Warsap for assistance in carrying out the experimental work.

XLIII. *On the Geyser Theory.*

To the Editors of the Philosophical Magazine

GENTLEMEN,—

IN the August number last year of the Philosophical Magazine, p. 341, Professor J. Joly has based argumentations on the geyser theory of Bunsen. I desire, therefore, to call attention to the fact that I and other students of the geyser phenomena have come to the conclusion that this theory is inadequate to explain the geyser phenomena. Some of my arguments against Bunsen's theory are brought forward in my paper, "The Hot Springs of Iceland," pp. 54–56 (*D. Kgl. Danske Vidensk. Selsk. Skrifter*, 7. *Række. Naturvidensk. og Mathem.* Afd. viii. København, 1910, pp. 232–244).

The Bunsen theory is partly based upon incorrect measurements of the temperature in the geyser channel, and does not explain the intensity and periodicity of the eruptions. The well-known fact that soap is an efficient agent in producing eruptions cannot be brought into accordance with the theory. The heat from the surrounding strata does not enter the geyser channel, where the source of the periodicity is located. The heat conveyed by hot gases and steam from the origin of heat deeper down in

the earth is, on the contrary, liable to dissipate from the geyser channel to its surroundings.

The explanation of the geyser phenomena is to be sought in the interaction of the hot-spring gases, steam, and water in suitable channels and concavities belonging to the geyser (*loc. cit.* and my paper, "Undersögelse af nogle varme Kilder paa Nordisland," pp. 10–19, *Det Kgl. Danske Vidensk. Selsk. Mathematisk-fyskiske Meddelelser*, iii. 1, Köbenhavn, 1920). The evolution of gases is a common feature of the hot springs, and is of utmost importance for the geyser eruptions. Although there is a great variety in the manifestations of the geyser phenomena, I have in every case been able to explain them on these lines.

I take the opportunity of communicating my last experience regarding the Icelandic geysers. Two months ago I visited Reykjanes, the extreme south-western point of Iceland. There is a geyser there situated in a fissure of the rock. In the interval between the eruptions no water is to be seen in the fissure. The first sign of the approaching eruption is the low rumbling produced by the spring water as it advances up through the channel. Apparently the water is strongly agitated by penetrating gas-bubbles. As soon as the spring water reaches the surface the eruption commences. Great bubbles filled with gases and water-vapour forcing their way out of the channel throw the water columns 3–4 metres into the air. When the eruption has lasted for a time the eruptive force is apparently exhausted, and the spring water disappears, receding down into the channel.

The eruptions of this geyser occurred with great regularity, as evidenced by the following observations on August 24, 1927 :—

No.	Eruption commenced.			Eruption ended.			Period.	
	h.	m.	sec.	h.	m.	sec.	m.	sec.
1	10	16	10	10	18	40	—	—
2	10	31	10	10	33	15	15	00
3	10	45	50	10	48	05	14	40
4	11	00	45	11	03	10	14	55
5	11	15	30	11	18	05	14	45
(12)	13	00	30	13	03	25	7×(15	00)
(25)	16	15	00	16	17	45	13×(14	54)
						Mean	14	57

The temperature of the spouting spring was 99° C., the atmospheric pressure being 750 mm. The colour of the spring water during the eruption was whitish, owing to diminutive gas-bubbles dispersed throughout the fluid. The spring water turned out to be real sea-water. In connexion with this interesting fact, it is worth mentioning

that the shortest distance to the sea-shore is 1350 metres and the elevation of the geyser orifice above sea-level is 20 metres. There are hot springs in abundance in the neighbourhood. I tested the water of several springs in different places, but failed to detect sea-water anywhere.

In my opinion it is impossible to bring the above-described geyser phenomena in accordance with the theory of Bunsen. In conformity with the views set forth in my papers quoted above, I have therefore assumed a principal channel connecting the orifice of the geyser with the interior, where the steam and the hot-spring gases are produced. Through a narrow side channel the sea-water oozes into the principal channel and for a moment bars the flux of gases through the main channel. Owing both to the accumulation of the gaseous exhalations locked up in the channel and its eventual adjacent concavities, and probably also to the increasing temperature, the pressure increases, and the gases will soon be able to force their way up through the channel and expel the sea-water: the eruption takes place. When the accumulated energy in the principal channel and its concavities has spent itself, the study flux of gaseous exhalations from the interior is unable to prohibit the channel being blocked up, either by the water in the orifice or by the sea-water from the side-channel. In both cases the result will be the same. The current of steam and hot gases through the channel is checked, and consequently the water at the orifice recedes into the channel. Evidently the well is intermittent.

Among the hot springs in the neighbourhood of the geyser I observed in Reykjanes, there are two vents with powerful outflow of steam and gaseous exhalations, which fact renders still more probable my assumption of a main channel with originally steady current of gases and steam.

Yours faithfully,

THORKELL THORKELSSON,
Director of the Icelandic
Meteorological Office.

Veourstofan, Reykjavik,
Iceland.

Editorial Note.—It appears to be generally admitted that Bunsen's theory, which was based upon a study of the Great Geyser of Iceland, may not be applicable to all cases of geyser activity. Tyndall, Arrhenius, and many other authorities accept Bunsen's views as regards the Great Geyser. Bunsen's thermometric observations were confirmed by Coles in 1881. In Supan's 'Grundzuge der Physichen Erdkunde' extensive references to geyser literature will be found.

There is nothing in M. Thorkelsson's interesting letter which affects the matters discussed by Dr. Jeffreys and myself in this Journal. Our opposing deductions might be based upon the model geyser constructed by Tyndall. The teaching would be the same.—J. Joly.

XLIV. *Note on the Formation of Pleochroic Halos in Biotite.* By J. H. J. Poole, *Sc.D.**

In my paper on the Action of Heat on Pleochroic Halos, appearing in the January issue of this Journal, I refer to an alternative view of the mode of formation of the halo; *i.e.*, the direct oxidation of the ferrous iron in the biotite by the oxygen liberated by the α-ray from the water present. On the strength of an experiment showing that the darkening of the mica by heating took place even in a reducing atmosphere, I left the genesis of the halo as referable simply to the loss of water by the mica brought about by the radioactive decomposition of the former.

On reconsideration, however, the view that the actual oxidation of the ferrous iron is responsible for the halo would appear to be deserving of direct acceptance. It is plain that the presence of a reducing atmosphere would have little if any effect on changes proceeding within the mica. Now, biotite is distinguished from muscovite (which neither darkens on heating nor contains halos) by its much greater content of ferrous iron. The water present is probably loosely combined with the silica, and when oxygen is radioactively liberated by the decomposition of the water, it would be at once taken up by the ferrous iron and the highly-coloured ferric salt formed.

Coming now to the experiment showing that when biotite is heated water is given up and the mica darkens, we have to remember that here the water is liberated at a high temperature and is present in the form of a gas since it is well above its critical temperature. It seems certain that under these conditions it would oxidize some of the ferrous iron to the ferric state, thus producing the observed darkening of the mica.

Thus we seem to have a simple and consistent explanation of the mode of formation of the halo in biotite based on quite definite and well-known chemical changes attending the ionizing activity of the α-ray.

Iveagh Geological Laboratory,
January 9th, 1928.

* Communicated by Professor Joly, F.R.S.

XLV. *A Reply to the Paper "Ionization by Collision."**

To the Editors of the Philosophical Magazine.

Gentlemen,—

IN the Nov. issue of the Phil. Mag., Mr. Huxley discusses the points raised in my reply to his previous criticism of the Photoelectric Theory of Sparking Potentials which I put forward for discharges in rare gases. In the first criticism he raised objections gathered from results on active gases, and applied them to the consideration of rare gas discharges. Notwithstanding this I accepted the application, and showed that the objections raised did not invalidate the theory. Mr. Huxley apparently agrees with this.

At the same time, it was pointed out that the writer looked to a definite experimental testing of the theory to give a conclusive answer. This has been carried out for the case of helium (see 'Nature,' Oct. 1, p. 477, and *Zts. f. Phys.* xlv. 1927, "Ueber eine neue photoelektrische Theorie der Funkenspannung," Proc. Roy. Soc. A, cxvii. p. 508, 1928), and the agreement between theory and experiments was quantitatively correct. It is probable that the other rare gases—if the investigations could be carried out—would yield similar results.

With "impure" rare gases or mixtures of gases, collisions of the second order and other complications may occur to alter the conditions so that no *a priori* judgement in the matter may be pronounced, and there is, up to the present time, no quantitative experimental evidence on the matter. Nevertheless, for such cases the photoelelectric hypothesis appears to be as probable as any other.

My general ideas are given in my Utrecht Dissertation (1927), chapts. 5 and 6. Quoting from page 60:—"The initiation of the self-sustained electrical discharge will be brought about by that particular action of the positive ions that is most easily accomplished under the conditions of experiment."

Mr. Huxley is wrong in imagining that I bring up the objections against Townsend's theory of ionization by collision by electrons, to disprove the Classical Theory of Sparking Potentials—this will be evident from a consideration of the previous papers and the references given above. That the Townsend theory is not universally adopted is proved by the existence of other theories (cp. *Handbuch der Phys.* xiv. 1927, pp. 39–42, 380) and the recent controversies.

* Phil. Mag. Nov. 1927.

With regard to ionization by collision by positive ions, in addition to the objections of Sir J. J. Thomson and Horton and Davies, there are the difficulties described in Franck and Jordan's book, 'Anregung von Quantenspruengen durch Stoesse,' p. 188. The points brought forward in support of ionization by collision of positive ions in gases are all controversial ones, and it is wrong to assume that the conditions under which a positive ion can give rise to ionization by collision will be the same as those for a neutral atom or molecule (cp. Franck and Jordan, *loc. cit.* p. 190, also Bloch, 'Ionisation et Resonance des Gas et des Vapeurs,' p. 183).

That Prof. Townsend had considered alternative theories I was well aware (Taylor, Phil. Mag. iii. p. 765, 1927), but the question of cathode falls of potential does not come into considerations for sparking potential theories (though there may be a parallel variation).

So far as I can see, Mr. Huxley brings no new evidence to bear upon the problem, nor any experimental results for rare gases or discharge-tubes with electrodes of variable surface. The subject of the collisions between ions and atoms etc. is in great need of interpretation, but is one that requires experimental investigation.

Believe me,

Yours truly,

The Cavendish Laboratory,
Cambridge, November 9th, 1927.

JAMES TAYLOR.

XLVI. *Cathode Rays in the Electrodeless Ring-Discharge.*

To the Editors of the Philosophical Magazine.

GENTLEMEN,—

IN a recent publication in the Philosophical Magazine (ser. 7, ii. p. 674, 1926) which I have just received, Sir J. J. Thomson notes that the electrodeless discharge is a copious source of that radiation of very short wavelength which he has detected in discharge tubes. At very low pressure, when an ordinary discharge was no longer visible, he found a green phosphorescence of the glass walls which he believed to be caused by that radiation because it was not affected by a magnet brought near.

While investigating the electrodeless ring-discharge in hydrogen in a cylindrical quartz tube*, I also found, without being aware of Sir J. J. Thomson's experiments, a very

* A full report of these experiments will be published later on in another place. Note added in proof: Meanwhile published *Ann. d. Phys.* lxxxiv. p. 553 (1927).

brilliant phosphorescence, in this case a blue one, which here was present under various conditions of the discharge, also at relatively high pressure. Usually the walls continued phosphorescing for some time (about 15 minutes) after the discharge was stopped, a fact which seems to have not yet been recorded. With decreasing pressure the duration of this after-luminosity became remarkably less. Still, at the lowest obtainable pressures (0·0001 mm.), when a visible luminosity of the gas had already completely disappeared, the phosphorescence remained observable while the after-luminosity had nearly vanished. The same results were obtained in oxygen and air ; merely the colour of the phosphorescence seemed to be a little different.

When in hydrogen the pressure was above about 0·001 mm. Hg, but below that point at which the visible discharge disappears, the phosphorescence was very much strengthened in the middle of the plates which covered the quartz cylinder. A magnet brought near deflected these luminous spots to the border of the plates in a sense which proved them to be caused by cathode rays coming from the middle of the tube, where under ordinary conditions the discharge took place. At the same time they became more diffuse, indicating that the velocity of these cathode rays is not homogeneous. They seem to be caused in the following way :—The potential difference at the ends of the coil overlapping the high-frequency electromagnetic field, which causes the ordinary discharge, accelerates the electrons produced in the invisible ring-discharge parallel to the axis of the tube. By the magnetic field in the coil this electron current is concentrated into the axis of the tube. The spectrum of the phosphorescence caused by the cathode rays was a continuous band between $\lambda 4800$ and $\lambda 4300$. In air and oxygen the cathode rays could not be detected because the pressure which was necessary to cause the ordinary discharge to vanish was less than the pressure at which the cathode rays would appear in hydrogen. But I do not doubt that they have been present, the increased phosphorescence in the middle of the plates being hidden by the brilliant luminosity of the discharge.

Sir J. J. Thomson's failure to detect the presence of cathode rays may be caused by the special design of his apparatus. The most essential point seems to be that I used very high potentials, the spark-gap consisting of spheres of 5 cm. in diameter which were 2 cm. apart.

On account of my experiments, it is clear that at least part of the observed phosphorescence is caused by cathode rays. Whether the phosphorescence observed when a

definite cathode ray is absent is produced by diffuse electrons or by the short wave-length radiation as suggested by Sir J. J. Thomson will further be investigated; likewise the cause of the long-lasting after-luminosity. At any rate, the production of a well-defined cathode ray in the axis of an electrodeless ring-discharge tube is proved by my experiments—a fact which presumably has not yet been recorded.

Yours faithfully,

Physikalisches Institut der
Technischen Hochschule,
Darmstadt, Germany.
April 8th, 1927.

GERHARD HERZBERG.

Note added in proof (January 23rd, 1928).—In a more recent publication Sir J. J. Thomson (Phil. Mag. iv. p. 1128, 1927) has given an extensive theory of the electrodeless ring-discharge and a description of further experiments on this subject. Among others he observed, in the "sensitive state of the ring-discharge" in cyanogen, a bright line which was bent by a magnet in a sense opposite to that of the deflexion of the above-mentioned spots. Already at the time when I wrote the above I had observed such a bright line in hydrogen and nitrogen, as well as in oxygen, in a relatively wide range of pressure. I believed (*l. c.*) it to be caused by the cathode rays described above, but did not succeed in deflecting it by a magnet, because it was only as long (6 cm.) as the coil (12 turns of 1 mm. copper wire) which produced the discharge. An enumeration of the different phosphorescences in the electrodeless ring-discharge is to be found in the Appendix of a paper by the author in the *Zeitschr. f. Phys.* in print.

XLVII. *Notices respecting New Books.*

Abstracts of Theses, Science Series, Vol. III. (University of Chicago Press, Chicago, Illinois, U.S.A., and Cambridge University Press. Price 15*s.*)

BY recent regulations of the University of Chicago, candidates for the degree of Doctor of Philosophy are required to publish abstracts of their theses, between 3,000 and 1,200 words in length. This volume includes nearly sixty abstracts in the departments of the Ogden School of Science. Practically all the branches of Natural Science are represented—mathematics, physics, geology, geography, botany, and zoology, with six abstracts in the departments of anatomy, physiology, and hygiene. A number of the theses are of special interest to students in the States of America, but a considerable proportion, especially mathematical, physical, and chemical, have a wider appeal.

[*The Editors do not hold themselves responsible for the views expressed by their correspondents.*]

Fig. 5 A.

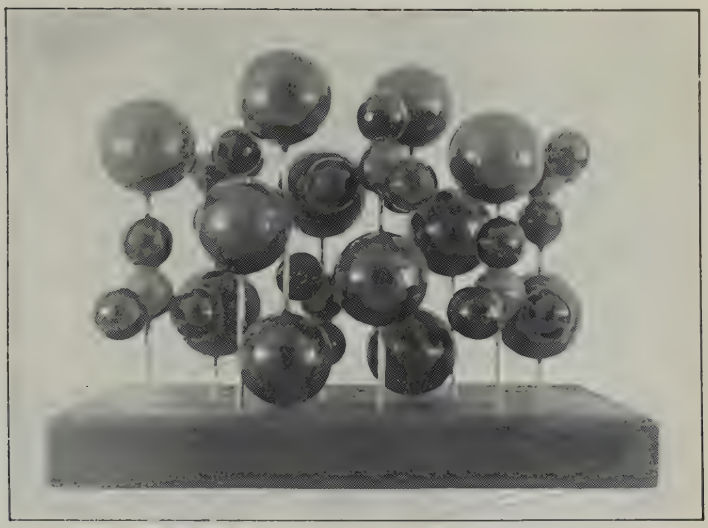

K_2SO_4 (100).

Fig. 5 B.

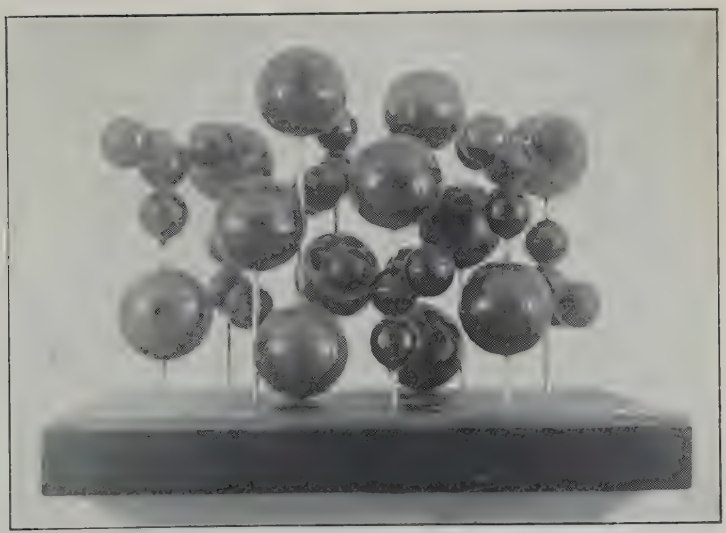

K_2SO_4 (100).

Fig. 6 A.

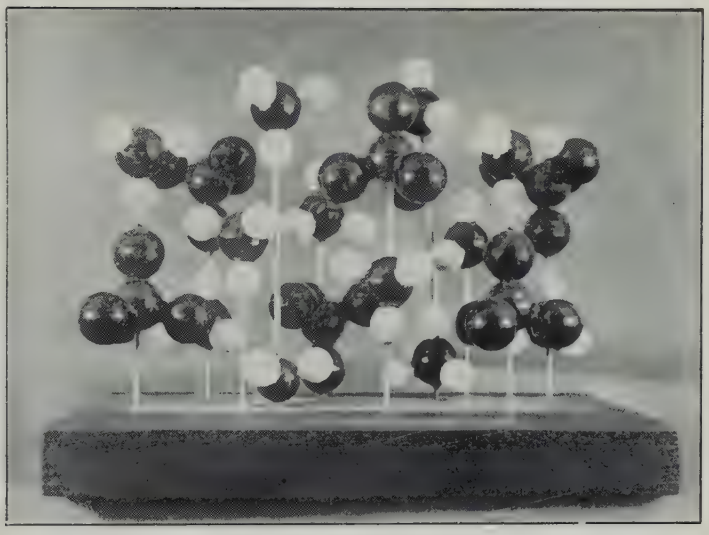

$(NH_4)_2SO_4$ (100).

Fig. 6 B.

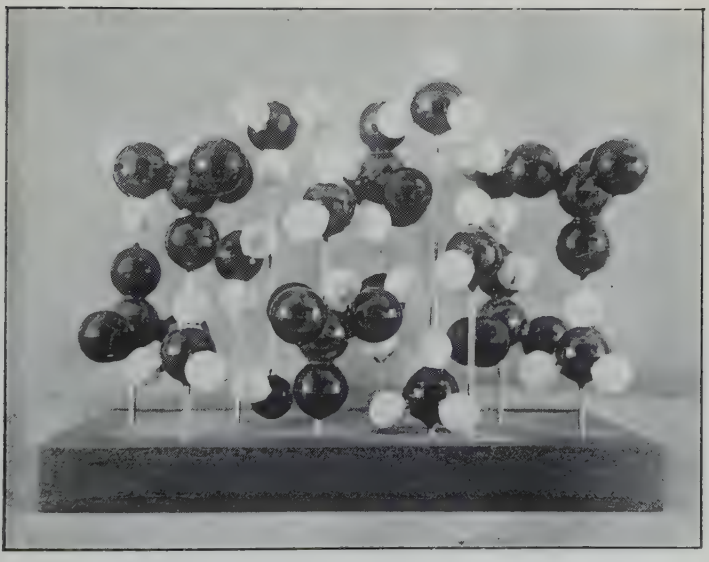

$(NH_4)_2SO_4$ (100).

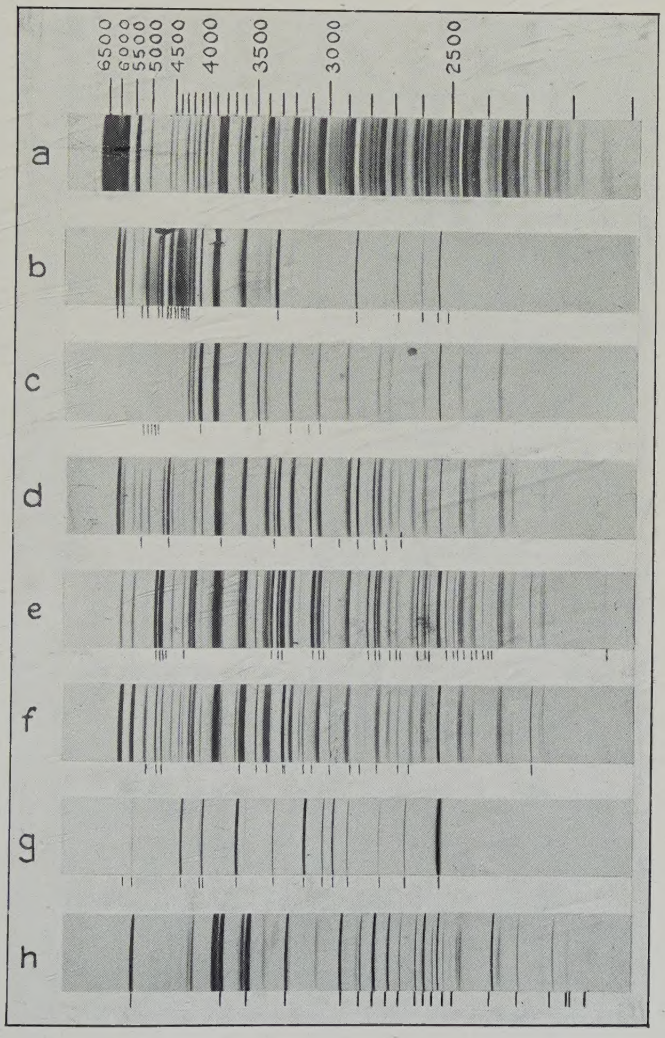

a. Active Nitrogen. *b*. Sodium. *c*. Potassium. *d*. Magnesium. *e*. Zinc. *f*. Cadmium. *g*. Mercury. *h*. Thallium.

Fig. 1.

Fig. 2.

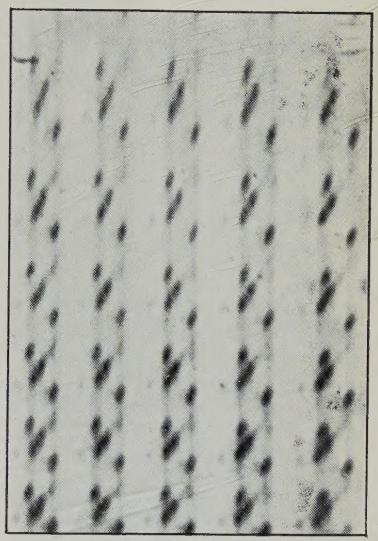

Fig. 3.

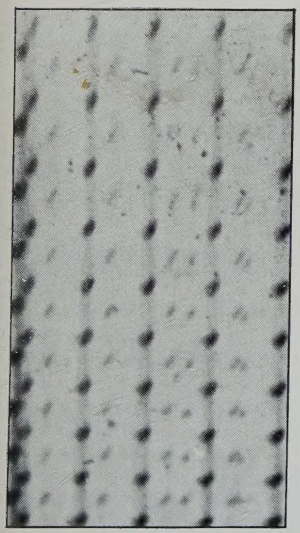

Fig. 4.

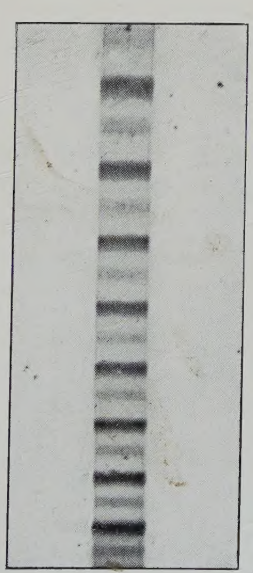

Fig. 5.